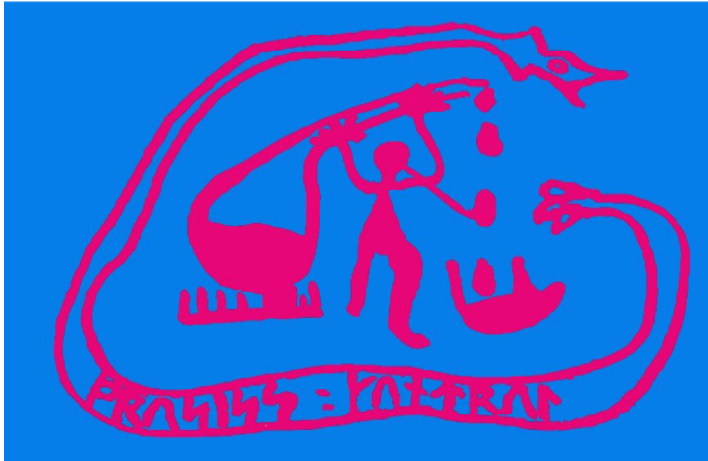


# 19th NORDIC PROCESS CONTROL WORKSHOP

On the Coastal Steamer "Richard With"  
from Trondheim to Bodø



Editor: S. Skogestad

# Proceedings of the 19th Nordic Process Control Workshop

On a Coastal Steamer from Trondheim to Bodø  
January 13–16 2015



Editor: S. Skogestad



NTNU – Trondheim  
Norwegian University of  
Science and Technology

*Proceedings booklet created by:  
Chriss Grimholt  
Vladimiro Minasidis  
Trondheim 2014*

# 19th Nordic Process Control Workshop

Welcome to the 19th Nordic Process Control (NPC) Workshop. The tutorial and workshop is held at 13–16 of January 2015. The topic of the tutorial on 13–14 January is Practical MPC and is presented by Prof. B. Wayne Bequette. This year's NPC workshop on 15–16 January is held on the Coastal Steamer "Richard With" from Trondheim to Bodø. The objective of the workshop is to bring together the NPC community, and to provide a rather informal forum for presenting recent and ongoing work in the process control area. The presentations may concern new results, ongoing research, planned research or open problems. The workshops are organized once every one and half year and the venue alternates between Denmark, Finland, Norway and Sweden.

The workshop is organized by the Nordic Working Group on Process Control which currently consists of the following members:

Prof. Sigurd Skogestad, NTNU, Norway  
Dr. Jenő Kovacs, Foster Wheeler Co., Finland  
Dr. Elling W. Jacobsen, KTH, Sweden  
Dr. John Bagterp Jørgensen, DTU, Denmark  
Prof. Sirkka-Liisa Jamsa-Jounela, Helsinki Univ. Tech., Finland  
Dr. Jan Peter Axelsson, Pfizer, Sweden  
Prof. Kurt Erik Häggblom, Åbo Akademi, Finland  
Prof. Bjarne Foss, NTNU, Norway  
Dr. Annika Leonard, Vattenfall, Sweden  
Dr. Alf Isaksson, ABB, Sweden  
Prof. Bernt Lie, Telemark Univ. College, Norway  
Dr. Hans Aalto, Neste Jacobs, Finland  
Dr. Bjørn Glemmestad, Yara, Norway  
Prof. Tore Hägglund, Sweden  
Dr. Gurkan Sin, DTU, Denmark  
Mr. Tommy Mølbak, Dong Energy, Denmark  
Docent Torsten Wik, CTH, Sweden  
Dr. Krister Forsman, Perstorp, Sweden

The NPC Working Group awards the "Nordic Process Control Award" to people who have made a lasting and significant contribution to the field of process control. The 2015 Nordic Process Control Award is given to Professor Rudolph Kalman (unfortunately, he cannot come in person, but we have made a nice interview which will be shown). The previous years recipients were,

Howard H. Rosenbrock (Aaland, Finland, August 1995)  
Karl Johan Åström (Wadahl, Norway, January 1997)  
F. Greg Shinskey (Skeviks Gård, Stockholm, 24 August 1998)  
Jens G. Balchen (Lyngby, Denmark, 14 Jan. 2000)  
Charles R. Cutler (Åbo, Finland, 23 Aug. 2001)  
Roger W. Sargent (Trondheim, Norway, 09 Jan. 2003)  
Ernst Dieter Gilles (Gothenburg, Sweden, 19 Aug. 2004)  
Manfred Morari (Lyngby, Denmark, 26 Jan. 2006)  
Jacques Richalet (Espoo, Finland, 23. Aug. 2007)  
John MacGregor (Porsgrunn, Norway, 29 Jan. 2009)  
Graham Goodwin (Lund, Sweden, 26 Aug. 2010)  
Lawrence T. Biegler (Lyngby, Denmark, 26 Jan. 2012)  
James B. Rawlings (Oulu, Finland, 22 Aug. 2013)

The Process Control Group and PROST at the Department of Chemical Engineering, Norwegian University of Science and Technology, is responsible for the local arrangement this year. The local organizing committee consists of the following members:

Sigurd Skogestad  
Johannes Jäschke  
Chriss Grimholt  
Vladimiro Minasidis  
Vinicius de Oliveira  
Adriana Reyes-Lua  
Julian Straus

On a final note, we wish you all a great workshop ☺

# Participants for the 19th Nordic Process Control Workshop

<b>Austria</b>	Martin	Mayer	evon GmbH	<i><a href="mailto:martin.mayer@evon-automation.com">martin.mayer@evon-automation.com</a></i>
<b>Denmark</b>	Thomas	Bisgaard	Technical University of Denmark	<i><a href="mailto:thbis@kt.dtu.dk">thbis@kt.dtu.dk</a></i>
	Riccardo	Boiocchi	Technical University of Denmark	<i><a href="mailto:ricca@kt.dtu.dk">ricca@kt.dtu.dk</a></i>
	Dimitri	Boiroux	Technical University of Denmark	<i><a href="mailto:dibo@dtu.dk">dibo@dtu.dk</a></i>
	Andrea	Capolei	Technical University of Denmark	<i><a href="mailto:acap@dtu.dk">acap@dtu.dk</a></i>
	Emil Schultz	Christensen	GEA Process Engineering A/S	<i><a href="mailto:emil.christensen@gea.com">emil.christensen@gea.com</a></i>
	Gianluca	Frison	Technical University of Denmark	<i><a href="mailto:giaf@dtu.dk">giaf@dtu.dk</a></i>
	Jakob K.	Huusom	Technical University of Denmark	<i><a href="mailto:jkh@kt.dtu.dk">jkh@kt.dtu.dk</a></i>
	John Bagterp	Jørgensen	Technical University of Denmark	<i><a href="mailto:jbjo@dtu.dk">jbjo@dtu.dk</a></i>
	Seyed Soheil	Mansouri	Technical University of Denmark	<i><a href="mailto:seso@kt.dtu.dk">seso@kt.dtu.dk</a></i>
	Lisa	Mears	Technical University of Denmark	<i><a href="mailto:lmea@kt.dtu.dk">lmea@kt.dtu.dk</a></i>
	Sazuan Nazrah	Mohd Azam	Technical University of Denmark	<i><a href="mailto:snaz@dtu.dk">snaz@dtu.dk</a></i>
	Lars	Petersen	Technical University of Denmark	<i><a href="mailto:lnpe@dtu.dk">lnpe@dtu.dk</a></i>
	Gurkan	Sin	Technical University of Denmark	<i><a href="mailto:gsi@kt.dtu.dk">gsi@kt.dtu.dk</a></i>
	Christer	Utzen	GEA Process Engineering A/S	<i><a href="mailto:christer.utzen@gea.com">christer.utzen@gea.com</a></i>
	Andreas	Åberg	Technical University of Denmark	<i><a href="mailto:aben@kt.dtu.dk">aben@kt.dtu.dk</a></i>
<b>Finland</b>	Alexey	Zakharov	Aalto University	<i><a href="mailto:alexey.zakharov@aalto.fi">alexey.zakharov@aalto.fi</a></i>
	Miao	Yu	Aalto University	<i><a href="mailto:miao.yu@aalto.fi">miao.yu@aalto.fi</a></i>
	Amirhossein	Shirdel	Åbo Akademi University	<i><a href="mailto:ashirdel@abo.fi">ashirdel@abo.fi</a></i>
	Palash	Sarkar	Aalto University	<i><a href="mailto:palash.sarkar@aalto.fi">palash.sarkar@aalto.fi</a></i>
	Mikael	Manngård	Åbo Akademi University	<i><a href="mailto:mmanngar@abo.fi">mmanngar@abo.fi</a></i>
	Rinat	Landman	Aalto University	<i><a href="mailto:rinat.landman@aalto.fi">rinat.landman@aalto.fi</a></i>
	Jeno	Kovacs	University of Oulu	<i><a href="mailto:jeno.kovacs@fufin.fwc.com">jeno.kovacs@fufin.fwc.com</a></i>
	Sirkka-Liisa	Jämsä-Jounela	Aalto University	<i><a href="mailto:sirkka-liisa.jamsa-jounela@aalto.fi">sirkka-liisa.jamsa-jounela@aalto.fi</a></i>
	Kortela	Jukka	Aalto University	<i><a href="mailto:jukka.kortela@aalto.fi">jukka.kortela@aalto.fi</a></i>
	Tushar	Jain	Aalto University	<i><a href="mailto:tushar.jain@aalto.fi">tushar.jain@aalto.fi</a></i>
	Kurt-Erik	Häggblo	Åbo Akademi University	<i><a href="mailto:khaggblo@abo.fi">khaggblo@abo.fi</a></i>
	Matias	Hultgren	University of Oulu	<i><a href="mailto:matias.hultgren@oulu.fi">matias.hultgren@oulu.fi</a></i>
	Ramkrishna	Ghosh	Åbo Akademi University	<i><a href="mailto:rghosh@abo.fi">rghosh@abo.fi</a></i>
	Alexandre	Boriouchkine	Aalto University	<i><a href="mailto:alezandre.boriouchkine@aalto.fi">alezandre.boriouchkine@aalto.fi</a></i>
	Pasi	Airikka	Metso Corporation	<i><a href="mailto:pasi.airikka@metso.com">pasi.airikka@metso.com</a></i>
	Hans	Aalto	Neste Jacobs Oy	<i><a href="mailto:hans.aalto@nestejacobs.com">hans.aalto@nestejacobs.com</a></i>
<b>Germany</b>	Rainer	Dittmar	West Coast Univ. of Applied Sciences	<i><a href="mailto:dittmar@fh-westkueste.de">dittmar@fh-westkueste.de</a></i>
<b>Norway</b>	Christoph Josef	Backi	NTNU	<i><a href="mailto:backi@itk.ntnu.no">backi@itk.ntnu.no</a></i>
	Nadav (Nadi)	Bar	NTNU	<i><a href="mailto:nadi.bar@ntnu.no">nadi.bar@ntnu.no</a></i>
	Bo	Sun	NTNU	<i><a href="mailto:eric_sun@sjtu.edu.cn">eric_sun@sjtu.edu.cn</a></i>
	Vinicius	de Oliveira	NTNU	<i><a href="mailto:viniciud@ntnu.no">viniciud@ntnu.no</a></i>
	Bjarne	Foss	NTNU	<i><a href="mailto:bjarne.foss@ntnu.no">bjarne.foss@ntnu.no</a></i>
	Bjørn	Glemmestad	Yara	<i><a href="mailto:bjorn.glemmestad@yara.com">bjorn.glemmestad@yara.com</a></i>
	Jan Tommy	Gravdahl	NTNU	<i><a href="mailto:tommy.gravdahl@itk.ntnu.no">tommy.gravdahl@itk.ntnu.no</a></i>
	Chriss	Grimholt	NTNU	<i><a href="mailto:chriss.grimholt@ntnu.no">chriss.grimholt@ntnu.no</a></i>
	Ivar	Halvorsen	SINTEF	<i><a href="mailto:ivar.j.halvorsen@sintef.no">ivar.j.halvorsen@sintef.no</a></i>
	Finn Aakre	Haugen	Telemark University College	<i><a href="mailto:finn.haugen@hit.no">finn.haugen@hit.no</a></i>
	Tor Aksel	Heirung	NTNU	<i><a href="mailto:heirung@itk.ntnu.no">heirung@itk.ntnu.no</a></i>
	Morten	Hovd	NTNU	<i><a href="mailto:morten.hovd@itk.ntnu.no">morten.hovd@itk.ntnu.no</a></i>
	Esmail	Jahanshahi	Siemens AS	<i><a href="mailto:esmaeil.jahanshahi@siemens.com">esmaeil.jahanshahi@siemens.com</a></i>
	Johannes	Jäschke	NTNU	<i><a href="mailto:jaschke@ntnu.no">jaschke@ntnu.no</a></i>
	Jonatan	Klemets	NTNU	<i><a href="mailto:jonatan.klemets@itk.ntnu.no">jonatan.klemets@itk.ntnu.no</a></i>

	Dinesh	Krishnamoorthy	Statoil	<i>dikr@statoil.com</i>
	D. Kwame Minde	Kufoalor	NTNU	<i>kwame.kufoalor@itk.ntnu.no</i>
	Vladimirov	Minasidis	NTNU	<i>vladimirov.minasidis@gmail.com</i>
	Adriana	Reyes Lua	NTNU	<i>adriana.r.lua@ntnu.no</i>
	Brad	Schofield	Siemens AS	<i>john.b.schofield@siemens.com</i>
	Selvanathan	Sivalingam	Siemens AS	<i>selvanathan.sivalingam@siemens.com</i>
	Sigurd	Skogestad	NTNU	<i>skoge@ntnu.no</i>
	Olav	Slupphaug	ABB	<i>olav.slupphaug@no.abb.com</i>
	Julian	Straus	NTNU	<i>julian.straus@ntnu.no</i>
<b>Slovenia</b>	Dejan	Dovžan	University of Ljubljana	<i>dejan.dovzan@fe.uni-lj.si</i>
	Igor	Škrjanc	University of Ljubljana	<i>igor.skrjanc@fe.uni-lj.si</i>
<b>Spain</b>	Miguel	Mauricio-Iglesias	University of Santiago de Compostela	<i>miguel.mauricio.iglesias@gmail.com</i>
<b>Sweden</b>	Elling	Jacobsen	KTH Royal Institute of Technology	<i>jacobsen@kth.se</i>
	Krister	Forsman	Perstorp AB	<i>krister.forsman@perstorp.com</i>
	Olle	Trollberg	KTH Royal Institute of Technology	<i>olletr@kth.se</i>
	Alfred	Theorin	Lund University	<i>alfred.theorin@control.lth.se</i>
	Olof	Garpinger	Lund University	<i>olof.garpinger@control.lth.se</i>
	Staffan	Skålén	Borealis AB	<i>staffan.skalen@borealisgroup.com</i>
	Tore	Hägglund	Lund University	<i>tore.hagglund@control.lth.se</i>
	Martin	Hast	Lund University	<i>martin.hast@control.lth.se</i>
	Josefin	Berner	Lund University	<i>josefin.berner@control.lth.se</i>
	Ola	Johnsson	Lund University	<i>ola.johnsson@control.lth.se</i>
	Torsten	Wik	Chalmers University of Technology	<i>tw@chalmers.se</i>
	Johan	Rönnerberg	Perstorp AB	<i>johan.ronnberg@perstorp.com</i>
	Linnéa	Ahlman	Chalmers University of Technology	<i>linnea.ahlman@chalmers.se</i>
	Wolfgang	Birk	Luleå University of Technology	<i>wolfgang@ltu.se</i>
	Ali	Kadhim	Luleå University of Technology	<i>alikal@ltu.se</i>
	Bengt	Lennartson	Chalmers University of Technology	<i>bengt.lennartson@chalmers.se</i>
	Patrik	Kerttu	ÅF AB	<i>patrik.kerttu@afconsult.com</i>
	Pär	Sivertsson	ÅF AB	<i>Par.Sivertsson@afconsult.com</i>
<b>USA</b>	Matthew	Titus	Rensselaer Polytechnic Institute	<i>titusm@rpi.edu</i>
	Daniel	Howsmon	Rensselaer Polytechnic Institute	<i>howsmd@rpi.edu</i>
	B. Wayne	Bequette	Rensselaer Polytechnic Institute	<i>bequette@rpi.edu</i>

# Program outline

## Tutorial: Practical Model Predictive Control by B. Wayne Bequette

### Tuesday 13/01

09:00–10:45	Theory:	<i>Introduction to Practical MPC</i>
11:00–12:30	MATLAB:	<i>Implement discrete internal model control (IMC)</i>
12:30–13:30	Lunch	
13:30–15:00	Theory:	<i>Introduction to Practical MPC (cont.)</i>
15:15–15:45	Exercise:	<i>Derive coincidence point control</i>
15:45–16:15	MATLAB:	<i>Implement co-incidence point control</i>
16:15–17:00	MPC:	<i>Disturbance Rejection</i>
20:00	Social event	<i>“Happy popsicles in Trondheim”</i>

### Wednesday 14/01

09:00–10:45	MPC:	<i>Constrained QMPC</i>
11:00–12:30	MATLAB:	<i>Implement QMPC</i>
12:30–13:30	Lunch	
13:30–17:00	MPC:	<i>Applications</i>
20:00–22:00	Social event	<i>“Informal get-together and a beer at Trondhjem Mikrobryggeri”</i>

## Workshop

### Thursday 15/01

08:40–09:00	Welcome	
09:00–10:20	Oral presentations 1:	<i>Industrial Process Control</i>
10:20–10:50	Coffee break	
10:50–12:30	Oral presentations 2:	<i>MPC and Optimization</i>
12:30–13:40	Lunch break	
13:40–15:20	Oral presentations 3:	<i>PID and Decentralized Control</i>
15:20–16:40	Poster session	
16:40–18:00	Oral presentations 4:	<i>Applications</i>
18:00–18:30	NPC award:	<i>Rudolph Kalman Interview (video)</i>
20:00	Dinner	

### Friday 16/01

08:10–10:10	Oral presentations 5:	<i>Power and Bio Applications</i>
10:10–10:40	Coffee break	
10:40–12:40	Oral presentations 6:	<i>Modelling and Identification</i>
12:40–14:40	Lunch and disembarkation	

# Technical program

**Thursday 15/01**

**08:40–09:00 Welcome and Introduction**

Chair: Sigurd Skogestad, NTNU

**09:00–10:20 Oral presentations 1: Industrial Process Control**

Chair: Bjarne Foss, NTNU

1. *The “hidden” process control discipline and its link to operational profit for oil- and gas production*  
Olav Slupphaug, ABB, Oslo, Norway
2. *Industrial control structures practice: some observations*  
Krister Forsman, Perstorp AB, Sweden
3. *Control of granulation processes*  
Bjørn Glemmestad, Vidar Alstad, Trude Odberg Nysæter  
Yara, Porsgrunn, Norway
4. *Improved Feed Control with Feed-forward for Producing Aggregates*  
Pasi Airikka, Metso Corporation, Tampere, Finland

**10:20–10:50 Coffee break**

**10:50–12:30 Oral presentations 2: MPC and Optimization**

Chair: Kurt Häggblom. Åbo Univ.

5. *Optimal control of uncertain systems using Dual Model Predictive Control (DMPC)*  
Tor Aksel N. Heirung\*, B. Erik Ydstie\*\* and Bjarne Foss\*  
\* Dept. of Chem.Eng, Carnegie Mellon University, USA  
\*\* Dept. of Engineering Cybernetics, NTNU
6. *Efficient solvers for soft-constrained MPC*  
Gianluca Frison, John Bagterp Jørgensen  
Technical University of Denmark, Denmark

7. *Sensitivity-based economic model predictive control*  
Johannes Jäschke, Xue Yang, Lorenz T. Biegler  
NTNU & Carnegie-Mellon University, Pittsburgh, USA
8. *On the Convergence Rate of Extremum Seeking Control*  
Olle Trollberg and Elling W. Jacobsen  
Automatic Control, KTH, Stockholm
9. *Model Predictive Control of Pasteurization Processes*  
Patrick Hammer and Martin Mayer  
evon GmbH, Gleisdorf, Austria

**12:30–13:40 Lunch break**

**13:40–15:20 Oral presentations 3: PID and Decentralized Control**

Chair: Elling Jacobsen, KTH

10. *Software-based optimal PID design with PI versus PID performance comparison*  
Olof Garpinger and Tore Hägglund  
Department of Automatic Control, Lund University, Lund, Sweden
11. *Industrial setup for autotuning of PID controllers in large-scale processes: Applied to Tennessee Eastman process*  
Selvanathan Sivalingam and Esmaeil Jahanshahi  
Technology & Innovation Department, Siemens AS, Trondheim, Norway
12. *Derivative Backoff: A Process Value Saturation Problem for PID Controllers*  
Alfred Theorin and Tore Hägglund  
LTH, Lund, Sweden
13. *Wireless process control - Handling of variable latency and sampling rates in PI controllers*  
Ivar J. Halvorsen, SINTEF, Applied Cybernetics, Trondheim
14. *Reconfiguration of Decentralized Controllers Using Closed-Loop Sensitivity Factorization*  
Wolfgang Birk  
Control Engineering Group, Luleå University of Technology, Sweden

**15:20–16:40 Poster session**

**16:40–18:00 Oral presentations 4: Applications**

Chair: Tore Hägglund, Lund Univ.

15. *A mid-ranging control strategy for non-stationary processes and its application to dissolved oxygen control in a bioprocess*

O. Johnsson\*, D. Sahlin\*\*, J. Linde\*\*\*\*, G. Liden\*\*\*, T. Hagglund\*

\* Department of Automatic Control, Lund University, Sweden

\*\* Novozymes A/S, Denmark

\*\*\* Department of Chemical Engineering, Lund University, Sweden

16. *Integrated Process Design and Control of Reactive Distillation Processes*

Sayed Soheil Mansouri\*, Mauricio Sales Cruz\*\*, Jakob Kjøbsted Huusom\*, John M. Woodley\*, Rafiqul Gani\*

\* DTU, Lyngby, Denmark

\*\* UAM, Mexico

17. *A Mean-Variance Objective for Robust Production Optimization in Uncertain Geological Scenarios*

Andrea Capolei<sup>a</sup>, Eka Suwartadi<sup>b</sup>, Bjarne Foss<sup>b</sup>, John Bagterp Jørgensen<sup>a</sup>

<sup>a</sup>Department of Applied Mathematics and Computer Science & Center for Energy Resources Engineering, Technical University of Denmark, Lyngby, Denmark.

<sup>b</sup>Department of Engineering Cybernetics, NTNU, Trondheim, Norway

18. *Modelling and Model Predictive Control of ESP lifted wells*

Alexey Pavlov, Dinesh Krishnamoorthy, Elvira Marie B. Aske, Kjetil Fjalestad and Morten Fredriksen. Statoil Research Centre, Norway.

**18:00–18:30 NPC award: Rudolph Kalman Interview (video)**

Chair: Sigurd Skogestad, NTNU

Interview (video) by Johannes Jäschke, NTNU

**20:00–t See Problem (Dinner)**

$$\begin{array}{ll} \underset{\text{mind \& body}}{\text{minimize}} & -(f_o(o^d) + f_u(n)) \\ \text{subject to} & t \leq 16/01 \text{ 08:10 am} \end{array} \quad (\text{Dinner})$$

☺

## Friday 16/01

### 08:10–10:10 Oral presentations 5: Power and Bio Applications

Chair: John Bagterp Jørgensen, DTU

19. *Remote light stress detection for greenhouse LED lighting control*  
Anna-Maria Carstensen, Torsten Wik and Tessa Pocock  
Department of Signals and Systems, Chalmers University of Technology, Sweden
20. *Fault tolerant model predictive control for the BioPower 5 CHP plant*  
J. Kortela and S-L. Jämsä-Jounela  
Aalto University School of Chemical Technology, Finland
21. *Relative Gain Measures for Once-through Circulating Fluidized Bed Boiler Control Design*  
Matias Hultgren\*, Jenő Kovács\*\* and Enso Ikonen\*  
\* Systems Engineering Laboratory, University of Oulu, Finland.  
\*\* Foster Wheeler Energy Ltd, Varkaus, Finland.
22. *Model-based optimal design and control of an anaerobic digestion reactor*  
Finn A. Haugen  
Telemark University College, Porsgrunn, Norway
23. *A study on the combustion dynamics of a biomass fuel bed in a BioGrate boiler*  
<sup>1</sup>A. Boriouchkine, <sup>2</sup>V. Sharifi, <sup>2</sup>J. Swithenbank and <sup>1</sup>S.-L. Jämsä-Jounela,  
<sup>1</sup> School of Chemical Technology, Aalto University, Finland;  
<sup>2</sup> University of Sheffield, Department of Chemical and Biological Engineering, UK;
24. *Investigation of tuning of a fuzzy-logic control for biological wastewater treatment systems*  
Riccardo Boiocchi, Krist V. Gernaey and Gürkan Sin  
Chemical Engineering, DTU, Lyngby, Denmark

### 10:10–10:40 Coffee break

### 10:40-12:40 Oral presentations 6: Modelling and Identification

Chair: Sirkka-Liisa Jämsä-Jounela, Aalto Univ.

25. *Dynamic modelling of a multiple hearth furnace for kaolin calcination*  
Aleksi Eskelinen, Alexey Zakharov, Sirkka-Liis and Jämsä-Jounela  
Aalto University, Research group of Process Control and Automation, Finland
26. *A Continuous-Discrete Extended Kalman Filter for State and Parameter Estimation in People with Type 1 Diabetes*  
Dimitri Boiroux<sup>1,2</sup>, Vladimír Bátorá<sup>3</sup>, Morten Hagdrup<sup>1</sup>, Tinna Björk Aradóttir<sup>1</sup>,  
Caroline Johannsen<sup>1</sup>, Marían Tárnik<sup>3</sup>, Ján Murgas<sup>3</sup>, Signe Schmidt<sup>2,4</sup>, Kirsten

Nørgaard<sup>4</sup>, Niels Kjølstad Poulsen<sup>1</sup>, Henrik Madsen<sup>1</sup> and John Bagterp Jørgensen<sup>1</sup>

<sup>1</sup> Technical University of Denmark, Kgs. Lyngby, Denmark

<sup>2</sup> Danish Diabetes Academy, Odense, Denmark

<sup>3</sup> Slovak University of Technology, Bratislava, Slovakia

<sup>4</sup> Department of Endocrinology, Hvidovre Hospital, Denmark

27. *Output-Error System Identification in the Presence of Structural Disturbances*

Amir H. Shirdel, Jari Böling, Hannu T. Toivonen

Department of Chemical Engineering, Åbo Akademi University, Finland

28. *Iterative Sub Network component analysis*

Nadav Bar, Lasse Aasgaard and Naresh D. Jayavelu

Department of Chemical Engineering, NTNU, Trondheim

29. *Balanced input excitation for identification of ill-conditioned  $n \times n$  systems with  $n > 2$*

Ramkrishna Ghosh, Kurt E. Häggblom and Jari M. Böling

Department of Chemical Engineering, Åbo Akademi University, Finland

30. *Advanced optimization of C5 and C6 fermentation by the use of state estimators with pH measurements*

Miguel Mauricio-Iglesias, Krist V. Gernaey and Jakob K. Huusom.

CAPEC-PROCESS, Department of Chemical and Biochemical Engineering, DTU. Lyngby.

**12:40–13:40 Lunch**

**13:40 Farewell and Disembarkation at Bodø**

*Thank you all  
Bon Voyage!*

## Posters (Thursday and Friday)

- P1 *Self-tuning of predictive controller based on step response model in real-time framework*  
Dejan Dovzan, Igor Skrjanc  
Faculty of Electrical Engineering, Ljubljana, Slovenia
- P2 *Modeling the Automotive SCR Catalyst*  
Andreas Åberg\*, Anders Widd\*\*, Jens Abildskov\* and Jakob Kjøbsted Huusom\*  
\* DTU, Lyngby, Denmark  
\*\* Haldor Topsøe A/S, Lyngby, Denmark
- P3 *A Trajectory-based Bumpless Switching Control of Multi-Evaporator Air-Conditioning Systems*  
Tushar Jain<sup>1</sup>, Joseph J. Yame<sup>2</sup>  
<sup>1</sup> Aalto University, School of Chemical Technology, Finland  
<sup>2</sup> Université de Lorraine, Vandoeuvre-lès-Nancy, France
- P4 *Active Disturbance Rejection Control of the Newell-Lee forced circulation evaporator – a simulation study*  
Rainer Dittmar, West Coast University of Applied Sciences at Heide, Germany
- P5 *Nonlinear Model Predictive Control of a High-Pressure Polyethylene Tubular Reactor in Stenungsund, Sweden*  
Staffan Skålén and Fredrik Josefsson  
Advanced Process Control group, Borealis AB, Stenungsund, Sweden.
- P6 *Automation experiences during projects in Abu Dhabi*  
Staffan Skålén  
Advanced Process Control group, Borealis AB, Stenungsund, Sweden.
- P7 *Enabling High-Performance Industrial Embedded Model Predictive Control using Code Generation and High-speed Solvers*  
D. K. M. Kufoalor\*, B. J. T. Binder\*, L. Imsland\*, T. A. Johansen\*, G. O. Eikrem\*\*, A. Pavlov\*  
\* Department of Engineering Cybernetics, NTNU, Trondheim, Norway  
\*\* Statoil ASA, Rotvoll & Porsgrunn.
- P8 *Model Selection and Estimation of Neural Networks by Using Weight Dropout*  
Mikael Manngård and Jari M. Böling  
Department of Chemical Engineering, Åbo Akademi University, Finland

- P9 *Using Fluorescence as Control Parameter to Decide Optimal Light Spectrum for Plant Growth*  
Linnéa Ahlman, Torsten Wik and Daniel Bånkestad  
Department of Signals and Systems, Chalmers University of Technology, Göteborg, Sweden
- P10 *Dynamic Effects of Diabatization in Distillation Columns*  
Thomas Bisgaard, Jakob K. Huusom, Jens Abildskov  
CAPEC-PROCESS, Technical University of Denmark, Lyngby, Denmark
- P11 *Fault propagation analysis by merging process causality and plant topology*  
R. Landman, J. Kortela and S-L. Jämsä-Jounela  
Aalto University, Process Control and Automation Research Group, Finland
- P12 *Relative Gain Array Estimation Based on Non-parametric Process Identification for Uncertain Systems*  
Ali M. H. Kadhim\*, Wolfgang Birk and Thomas Gustafsson  
Control Engineering Group, Luleå University of Technology, Sweden
- P13 *Convex optimization as a design tool for feedforward controllers*  
Martin Hast and Tore Hägglund  
Department of Automatic Control, Lund University, Sweden
- P14 *Autotuning Based on Asymmetric Relay*  
Josefin Berner, Karl Johan Åström and Tore Hägglund  
Department of Automatic Control, Lund University, Sweden
- P15 *A reduced observer design for a freezing process*  
Christoph Josef Backi and Jan Tommy Gravdahl  
Department of Engineering Cybernetics, NTNU, Trondheim
- P16 *Decoupling approach in fluidized bed combustor control*  
Szabó, Z.\*, Kovács, J.\*\*\*, Szentannai P.\*  
\* Budapest University of Technology and Economics, Department of Energy Engineering Budapest, Hungary  
\*\*\* University of Oulu, System Engineering Laboratory, Oulu, Finland
- P17 *A performance optimization algorithm in fault tolerant distributed model predictive control*  
Alexey Zakharov, Elena Zattoni, Miao Yu and Sirkka-Liisa Jämsä-Jounela  
Aalto University, Department of Biotechnology and Chemical Technology, Finland
- P18 *Modeling Vapor Compression Cycles for Dynamic Simulation of Supermarket Refrigeration Systems*  
S. N. Mohd. Azam <sup>a</sup>, R. Izadi-Zamanabadi <sup>b</sup>, J. B. Jørgensen <sup>a</sup>  
<sup>a</sup> Department of Applied Mathematics and Computer Science, Technical University of Denmark, Lyngby, Denmark  
<sup>b</sup> Danfoss A/S, Electronic Controllers & Services, DK-6430 Nordborg, Denmark

- P19 *Data Reconciliation method for improving performance and reliability of MPC control strategy for a BioGrate boiler*  
Palash Sarkar, Jukka Kortela, Alexandre Boriouchkine and Sirkka-Liisa Jämsä-Jounela  
Aalto University, Process Control and Automation Research Group, Finland
- P20 *An indirect fuel moisture content estimation approach for BioGrate boilers*  
Alexandre Boriouchkine\*, Miao Yu and Sirkka-Liisa Jämsä-Jounela  
Aalto University, Department of Biotechnology and Chemical Technology, FI-00076 Aalto, Finland.
- P21 *Dynamic Real-Time Optimization for a Reactor, Separator and Recycle Processes*  
Vladimiro Minasidis and Sigurd Skogestad  
Department of Chemical Engineering, NTNU, Trondheim, Norway
- P22 *Non-robustness and limitations of Smith Predictor Control*  
Chriss Grimholt and Sigurd Skogestad  
Department of Chemical Engineering, NTNU, Trondheim, Norway
- P23 *Novel strategies for control of fermentation processes*  
Lisa Mears<sup>1</sup>, Stuart Stocks<sup>2</sup>, Gürkan Sin<sup>1</sup>, Krist V. Gernaey<sup>1</sup>, Kris Villez<sup>3</sup>  
<sup>1</sup> Department of Chemical and Biochemical Engineering, DTU, Denmark  
<sup>2</sup> Novozymes A/S, Pilot plant, Denmark  
<sup>3</sup> Eawag: Swiss Federal Institute of Aquatic Science and Technology, Dübendorf, Switzerland
- P24 *From Tweets to Optimality in the Smart and Sustainable Factory*  
Bengt Lennartson  
Chalmers University of Technology, Göteborg, Sweden
- P25 *Optimal Controller Design for Balancing Input/Output Disturbance Rejection Response with Robust Stability Condition*  
Bo Sun  
School of Electronic Information and Electrical Engineering, Shanghai Jiao Tong University.

## Oral presentations 1

# Industrial process control

Chair: Bjarne Foss, NTNU

### **Presentations:**

1. *The “hidden” process control discipline and its link to operational profit for oil- and gas production*  
Olav Slupphaug, ABB, Oslo, Norway
2. *Industrial control structures practice: some observations*  
Krister Forsman, Perstorp AB, Sweden
3. *Control of granulation processes*  
Bjørn Glemmestad, Vidar Alstad, Trude Odberg Nysæter  
Yara, Porsgrunn, Norway
4. *Improved Feed Control with Feed-forward for Producing Aggregates*  
Pasi Airikka, Metso Corporation, Tampere, Finland

# The “hidden” process control discipline and its link to operational profit for oil- and gas production

Olav Slupphaug

*ABB, (e-mail: olav.slupphaug@no.abb.com)*

---

*Abstract:* The dynamic process behavior is fundamental to regularity and integrity - high level Key Performance Indicators of any production asset, including oil- and gas production assets. In other words, process behavior - or, the way flows, pressures, temperatures, levels, rpm, valves, and compositions in the production system vary as a function of time – is key to the operational profit. The process should behave in such way that the operators find it easy to operate, it causes few unnecessary alarms, a minimum of unplanned shut downs are caused, and unnecessary equipment wear is avoided. We will present a possible decomposition of the process behavior and argue that what might be seen as the process control discipline, specialized in efficiently sorting out dynamic process behavior issues, is “hidden” - at least when it comes to upstream oil- and gas. Following this, we discuss what we have experienced are key competencies when it comes to process control, and describe some typical process control activities as well as typical value creation related to process behavior improvements. Before summarizing, we present some real world example process behavior problems, solutions, and associated value creation estimates (generally the sites will be anonymous).

---

# Control structures practice: some observations

Nordic Process Control Workshop, Trondheim 2015  
Krister Forsman, Perstorp AB, 284 80 Perstorp, Sweden  
krister.forsman@perstorp.com

**Abstract.** The task of choosing the “right” control structure for a given process in a chemical industrial plant is often as interesting and creative as it is frustrating. The combinations of unit operations or apparatuses are endless, and only a few standard processes have been studied in the literature. There seems to be no general algorithmic procedure for designing a classical control structure for a given process. We review some control structures used in the process industry, relating to practical applications. The focus is on issues that are not very well known in literature, but may be handled by modifications to the classical schemes. Examples include different versions of cascade control, dual actuator control, ratio control and conditional control. We also give some advice on how to analyze these types of questions theoretically.

**Keywords:** multivariable control, cascade control, dual actuator control, ratio control

## Introduction

We consider control problems where there is not just one manipulated variable (MV, denoted  $u$ ) and one controlled variable (process value, PV, denoted  $y$ ). These can often be handled by connecting several controllers and calculations in various combinations. Many aspects of this are covered in [4], [8] and [11].

Model predictive control (MPC) is a well established and commonly used technology in parts of the process industry. So why not just use MPC for all multivariable control problems? As argued in [8], the amount of modeling work required to configure an MPC controller grows rapidly with the number of variables, whereas most classical structures do not require a full model.

However, if the suggested “classical” solution contains several non-linearities, such as limiters and selectors, it is probably a good idea to consider MPC instead. The classical solution easily becomes intransparent and hard to maintain and optimize. An example of this is so called cross-limiting, sometimes used in boiler control [10]. Furthermore, if the cross couplings in the process are very strong, and there are more than two MVs and CVs, MPC is probably superior.

## Cascade control

The cascade control structure most commonly used today is the one depicted in Figure 1. We refer to it as the “textbook” cascade controller. This structure only works well if the slave loop (controller  $C_2$ ) is significantly faster than the master. If the separation in the frequency domain is too small, the overall system typically becomes unstable.

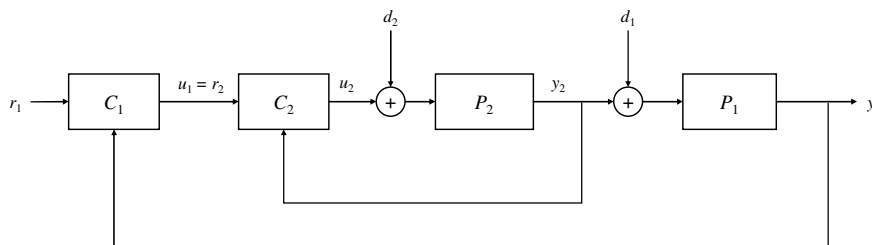


Figure 1: Textbook cascade control structure

A potential disadvantage with the textbook structure is that even if the separation between master and slave is big enough to keep the system stable, the master controller reacts to a disturbance that enters at the slave level ( $d_2$  in Figure 1). The result is an undershoot in master PV as showed in Figure 2.

If we wish to decouple the action of the master and the slave controller we can use the structure showed in Figure 3. This structure is briefly described in [4], but not analyzed in depth. Calculations of the type described in the appendix show that choosing  $F_1 = P_1$  the transfer function from  $d_2$  to  $u_1$  becomes zero, as we wanted.

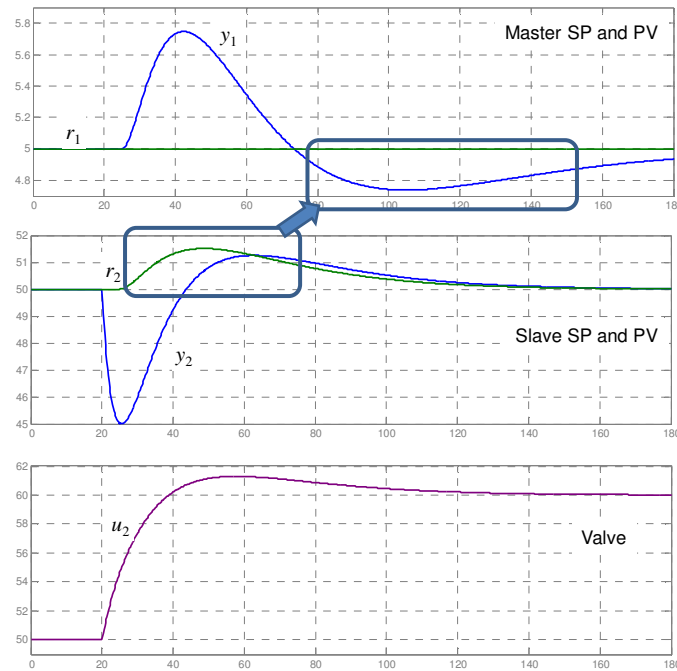


Figure 2: Cascade control. Response to a step disturbance on the slave loop MV.

This structure has some severe disadvantages, though. The transfer function from  $d_2$  to  $y_1$  is

$$\frac{P_1 P_2}{1 + C_2 P_2} \quad (1)$$

The specification for this transfer function is that it should have zero steady state gain, i.e. it should be of the type  $s^k \frac{p_1(s)}{p_2(s)}$  where  $k > 0$  and  $p_1$  and  $p_2$  are polynomials such that  $p_i(0) \neq 0$ . Now, if  $P_1$  is integrating, and  $C_2$  has one integration or less, then  $k \leq 0$ , and a step disturbance in  $d_2$  produces a steady state error in the master loop. In fact, any dynamics present in  $P_1$  will not be addressed by the master controller, if the disturbance enters as  $d_2$ . (Of course, this is what we asked for!)

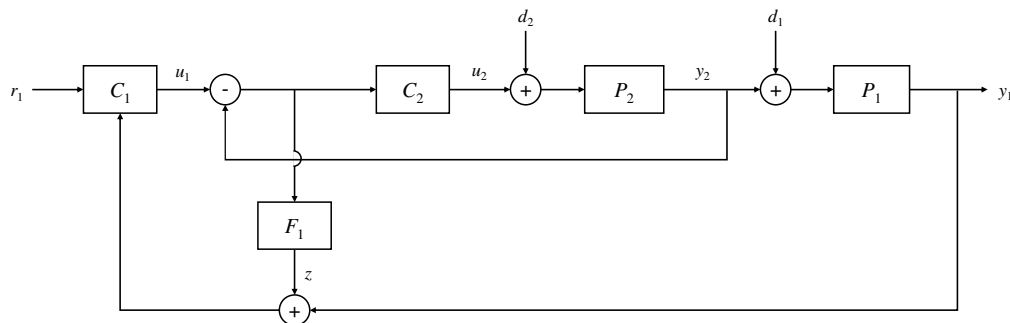


Figure 3: Cascade control with internal decoupling.

In this context we also mention a different version of cascade control, depicted in Figure 4. Here, the block  $C_2$  is a filter, and does not have a setpoint. It may be seen as a “feedforward” from the slave PV, even though that is an abuse of the term “feedforward”.

This structure seems to be older than the textbook structure. It is not internally stable if  $C_2$  has an integration, as can be seen from several of the transfer functions derived and analyzed as described in the appendix. This may be the reason why it is sometimes said that the slave controller in a cascade should not have integral action, even though that is not true for the textbook version.

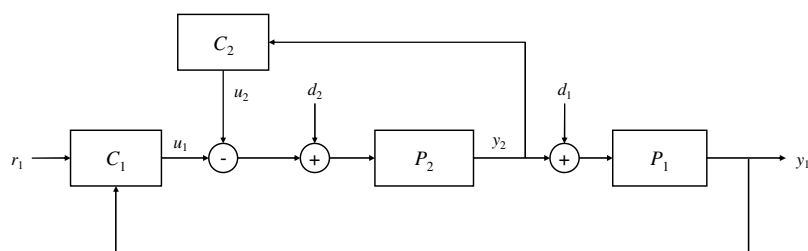


Figure 4: Cascade control without inner setpoint.

## Dual actuator control

By dual actuator control we mean control structures for processes with two MVs affecting the same PV. There are many applications where this issue may arise, e.g.

- two stage dilution processes
- pressure control in distillation columns using inert gas, with pressurization and venting
- temperature control where both the coolant flow rate and temperature can be manipulated
- some pH-control systems
- pressure control in a steam high-pressure header with shunt valve and vent valve
- heat exchanger with bypass valve
- so called maximizing control

Depending on control specifications there are different solutions to this problem. Some commonly occurring structures are

- mid-ranging, e.g. valve position control
- parallel control
- split-range control

If we have one high resolution MV and one coarse, and strive for high precision, we wish to keep the fine MV in the middle of its operating range. This can be done using valve position control (VPC), as showed in Figure 5. This is one solution to the mid-ranging problem, which is also referred to as input-resetting [8]. It has been studied in e.g. [1], [2], [7], [9], [11] and various improvements have been proposed, e.g. the internal decoupling link showed in Figure 6. Since VPC has been studied rather thoroughly, we do not discuss it further here.

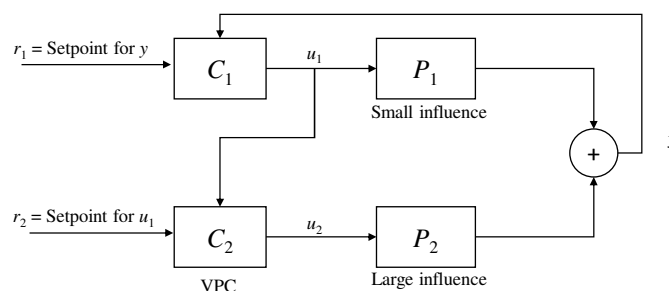


Figure 5: Valve position control (VPC).

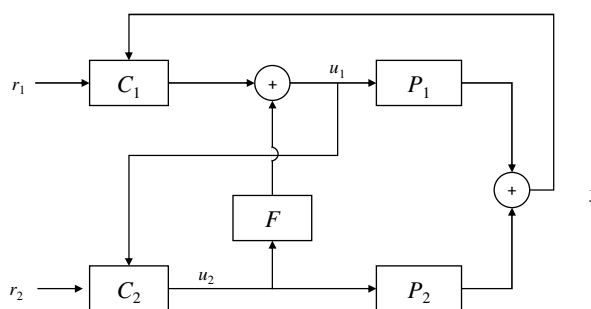


Figure 6: VPC with inner decoupling.

Another control structure that handles the extra degree of freedom in dual actuator is parallel control, which comes in a few different flavors. They have in common that each MV has a separate controller,

and both controllers have the same PV. In Figure 7 we see this, in the case where both controllers have the same setpoint. This structure is internally stable, even if both  $C_1$  and  $C_2$  are PI-controllers.

If one of them is a P-controller and the other one a PI-controller, then we get a structure that addresses the mid-ranging problem.

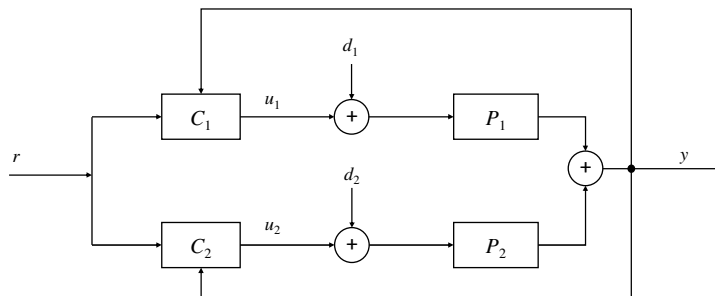


Figure 7: Parallel control with common setpoint.

In Figure 8, on the other hand, where the controllers have different setpoints ( $r_1 \neq r_2$ ), we get internal instability if both  $C_1$  and  $C_2$  has an integration. In practice this means that both controllers will drift off until one of them reaches the output saturation limit. In some applications, this is a desirable behavior. For example if one of the actuators uses a resource that is more expensive than that of the other, we want the expensive one not to be used in normal operation.

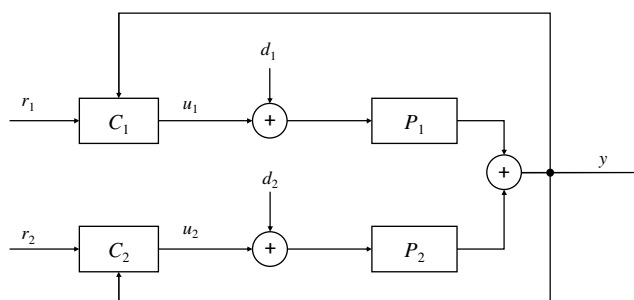


Figure 8: Parallel control with two setpoints.

Yet another solution to dual actuator control is to use split range control: there is only one controller but its output is sent through two look-up tables – one for each valve. Split-range is not discussed a lot in control literature, but in fact there are several non-trivial aspects of it, e.g. when the two subprocesses have significant differences in dynamics.

## Conditional control

In conditional control, or override control, we have two PVs but only one MV. It frequently occurs e.g. in steam systems as the one in Figure 9. The pressure reduction valve should normally be used to keep the LP-header pressure constant, but if the HP-header pressure drops below a critical limit, we should sacrifice the LP-header pressure to save the boiler from tripping.

Conditional control is usually implemented using two controllers and a minimum or maximum selector element, determining which controller output to send to the valve. In the steam system above, the SP for the HP-header PC should be set well below the normal operating pressure of that header. That PC is the limiting “rescue controller”.

However, that solution suffers from a problem that may be serious: When the rescue controller, which is normally not affecting the final control element (the valve), is to take over manipulation of the valve, there is often an undesired delay, because the rescue controller has an output that deviates substantially from that of the everyday controller normally manipulating the valve. The whole system is in “limbo”, just waiting for the rescue controller to take over. There are different ways to minimize this delay, some of which have been described in literature, e.g. [10]. The simplest solution is probably just letting the rescue controller be a proportional only controller. The rescue controller setpoint is not intended to be strictly adhered to, anyway.

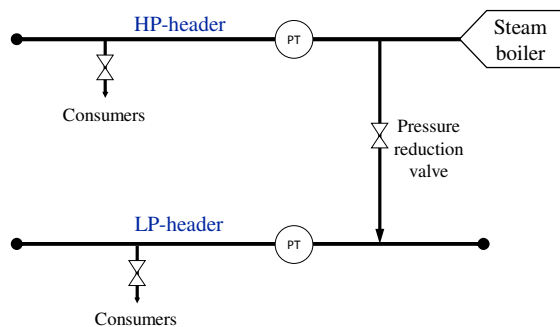


Figure 9: Steam system. Application case for conditional control.

## Ratio control

Ratio control is a classical scheme for maintaining the ratio between two process variables. If both variables are controlled, then we have a choice to let the slave controller setpoint be calculated based on the setpoint or the PV of the master, or even as a weighted sum of them [3]. In theory, it is easier to make the ratio deviations small by using the master SP rather than PV for calculating the slave SP, but there are many severe practical disadvantages with that solution.

Another way of making the slave response match that of the master without losing the monitoring of the master PV is to use PV-based ratio control, but with a feedforward from the master SP. This is illustrated in Figure 10. The filter  $F_1$  is non-standard. Often, it is sufficient to use a lead-lag compensator here. A small disadvantage is that the gain in  $F_1$  depends on the desired ratio  $\alpha$ .

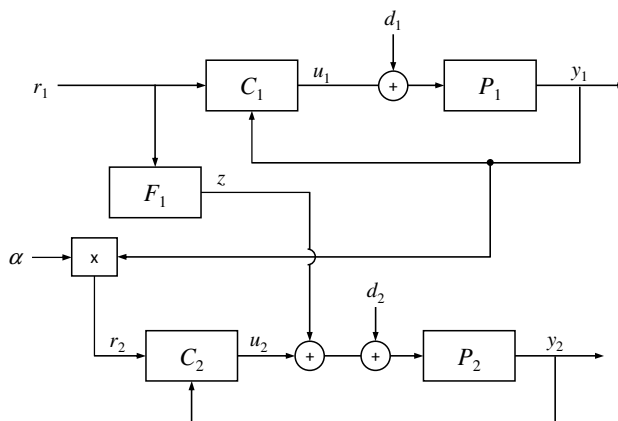


Figure 10: PV-based ratio control with additional feedforward from setpoint.

## Appendix: General analysis of multivariable control structures

The analysis of block diagrams is crucial in the study of control structures. Here we summarize some basic principles that are not new, but also not particularly well known.

In order to determine all transfer functions in a block diagram, the easiest way is probably to write down one equation for each block, considering the internal variables (outputs of the blocks) as “unknowns”, the scalar transfer functions of each block as “coefficients” and external inputs as “parameters”. In this way we get a set of linear equations represented by a square matrix. The example below shows the equation for the textbook cascade control scheme (Figure 1).

$$x = \begin{pmatrix} u_1 \\ u_2 \\ y_2 \\ y_1 \end{pmatrix} \quad x = \underbrace{\begin{pmatrix} 0 & 0 & 0 & -C_1 \\ C_2 & 0 & -C_2 & 0 \\ 0 & P_2 & 0 & 0 \\ 0 & 0 & P_1 & 0 \end{pmatrix}}_F x + \begin{pmatrix} C_1 \\ 0 \\ 0 \\ 0 \end{pmatrix} r_1 + \begin{pmatrix} 0 \\ 0 \\ P_2 \\ 0 \end{pmatrix} d_2 + \begin{pmatrix} 0 \\ 0 \\ 0 \\ P_1 \end{pmatrix} d_1$$

The solution to this equation is of course

$$x = (I - F)^{-1}(b_1 r_1 + b_2 d_2 + b_3 d_1) \quad (2)$$

which gives us all the transfer functions. The adjugate matrix expression for the matrix inverse, tells us that the denominator for all transfer functions is  $1/\det(I - F)$ , except for possible cancellations. All these calculations are easy to make using some symbolic math software. These observations are captured, in quite a different formulation, by “Mason’s rule” [6], originally stated in [5]. It is worth noticing that the  $F$ -matrix is closely related to the adjacency matrix of the block diagram considered as a directed graph.

Thus we have expressed all the system transfer functions as rational functions of the block transfer functions. We want to study what type of controllers are feasible in which position, e.g. proportional only vs PI-control, and whether integrating processes can be handled by the structure in question. To do this, write all transfer functions in the form  $s^k \frac{p_1(s)}{p_2(s)}$  where  $p_1$  and  $p_2$  are polynomials such that  $p_i(0) \neq 0$ . Then the integer  $k$  is uniquely defined. Some straight forward rules for how  $k$  behaves under multiplication, division and addition can be derived, and control specifications can be formulated in terms of  $k$  for different system transfer functions. The limited space available here does not allow for a full review of these techniques, so we just mention some caveats:

- In some cases, the conditions thus obtained are only necessary
- The behavior of the  $k$ -value under *addition* is complex, except in the “generic” case (no cancellation of coefficients can occur).
- In the above formulation, the technique only works for rational transfer functions, i.e. e.g. no time delays are allowed. This restriction can probably be overcome without too much modification.

## References

- [1] B.J. Allison and A.J. Isaksson: *Design and performance of mid-ranging controllers*. J. Process Control, Vol 8, No 5-6, pp. 469-474. 1998
- [2] S. Haugwitz and P. Hagander: *Mid-ranging control of the cooling temperature for an Open Plate Reactor*. In *Proc. 12th Nordic Process Control Workshop*. Gothenburg, 2004.
- [3] T. Hägglund: *The Blend Station – a new ratio control structure*. Control Eng. Practice, Vol 9, pp 1215-1220, 2001.
- [4] T.E. Marlin: *Process Control*. 2nd edition. McGraw Hill, 2000.
- [5] S.J. Mason: *Feedback Theory – Further Properties of Signal Flow Graphs*. Proc. Institute of Radio Engineers, pp 920–926. July, 1956
- [6] K. Ogata: *Modern Control Engineering*. Pearson, 2008.
- [7] F.G. Shinskey: *Process Control Systems*. Second Edition. McGraw-Hill, 1979.
- [8] S. Skogestad and I. Postlethwaite: *Multivariable Feedback Control: Analysis and Design*. 2nd ed. Wiley, 2005.
- [9] O. Slätteke: *Modeling and Control of the Paper Machine Drying Section*. PhD Thesis, Lund University. Sweden, January 2006.
- [10] C.A. Smith and A. Corripio: *Principles and Practice of Automatic Process Control. Third Edition*. Wiley, 2006.
- [11] K.J. Åström and T. Hägglund: *Advanced PID Control*. ISA – The Instrumentation, Systems and Automations Society, 2005.

Abstract for Nordic Process Control Workshop 2015.

Title: Control of granulation processes

Authors: Bjørn Glemmestad, Vidar Alstad, Trude Odberg Nysæter (Yara International ASA)

The purpose of granulation is to make solid particles (granules) from a slurry that is crystallizing. This presentation describes one common granulation process in the fertilizer industry, and shows a recent example where one simple additional control loop improved performance in a full-scale plant.

A simple sketch of a typical granulation process (or granulation loop) is shown in the figure below.

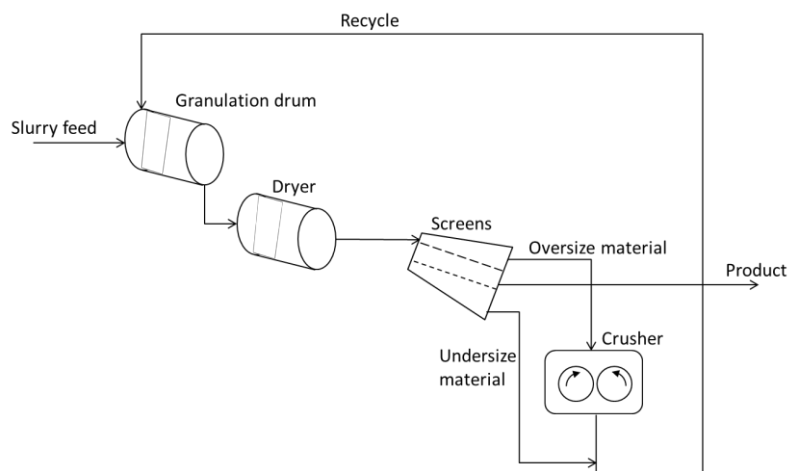


**Figure 1.** Simple sketch of typical granulation loop

A slurry with liquid ammonium nitrate and dissolved minerals is sprayed into the granulation drum together with atomizing air and recycled particles acting as seeds for new granules. The detailed chemical and physical processes in the granulator are not fully understood, but it is clear that a significant part of the slurry droplets are hitting existing particles and crystallizing so the particles are growing. Some of the slurry droplets may also form seed particles by crystallizing or by acting as 'glue' for recycled very fine particles (dust) that is agglomerating and forming new seed particles. From the granulator the granules are entering the drier to become less sticky.

The granules out of the drier have a particle size distribution that is wider than the size specification of the product. Typically, most of the product size material is taken out as product, while the granules that are too small are recycled with the crushed oversize granules. In some plants, a significant part of the product size material is also recycled. The total recycled stream can be several times larger than the product stream. Some granulation loops show oscillatory behavior (limit cycling) during operation and this may limit the production capacity. Typically the cycle time is a few hours and there are oscillations in particle size distribution of material out of the granulator.

The specific example in this presentation is a fertilizer plant in Yara where the limit cycles were a bottleneck for the production capacity for some products. This plant had a possibility to recycle product size material via the crushers (there are two crushers in parallel). This is not shown in the

sketch above. It may seem counter-productive to crush and recycle product material since this can be taken out as product and sold directly.

It was decided to implement a simple feedback controller (PI) to have stable total feed to both crushers, in order to have more stable flow of seed particles recycled to the granulator. This made the granulation loop more stable. Only two days after the test of the new controller started the production rate was increased with more than 20% compared to the highest previous production for a period of more than 24 hours.

# Improved Feed Control with Feed-forward for Producing Aggregates

Pasi Airikka

Metso Corporation, Tampere, P.O Box 237, FIN-33101  
FINLAND (Tel: +358 40 587 2730; e-mail: [pasi.airikka@metso.com](mailto:pasi.airikka@metso.com))

---

**Abstract:** An aggregate production process comprises of crushing and screening blasted rock material into several targeted end-product aggregate fractions measured in size and shape. The aggregate production process typically starts with human-based rock feeding onto a feeder. Depending on an aggregate plant layout, rock material is fed by either a dumper or an excavator operator. As soon as the rock material is spread on a feeder, the feeder starts carrying the material forward. Surprisingly, most of the feeders operate with relay-based on/off controls lacking PI(D)- or PPI(D)-controllers and good control performance. And, furthermore, there is no measured information on the volume that a feeder carries forward to the crushing and screening process. In this paper, a real implemented case is presented on improving feed control with properly designed predictive PI control with feed-forward control using the on-line measured feeder material volume.

*Keywords:* Automatic control, predictive PI, feed-forward, feeder, aggregate, crushing and screening.

---

## 1. INTRODUCTION

A typical aggregate production plant, such as a quarry, produces hundreds of thousands or millions of tons of aggregates annually. The produced aggregates are separated already in the production process resulting in different piles of aggregates measured in size (millimeters). The raw material to produce aggregates is often on-site blasted rock.

The aggregate production process is primarily crushing and screening particles of different sizes and moving them between consecutive crushing circuits (see 2. Appendix). Typically, there are two to three crushing circuits: primary, secondary and tertiary but the plant layout does not have to be limited to this plant layout structure. Typical process equipment are crushers, screens, conveyors, feeders, hoppers and silos.

One thing being in common in any aggregate production process is material (rock) feeding. To start with, there is human-based feeding by dumpers or excavators which can be instructed but not automated. An operator feeds or dumps the rock material onto a feeder which is actually the first stationary process equipment which can be controlled. And, furthermore, it is also the most important actuator in the whole aggregate production process as it also dictates the production rate measured in tons per hour.

Typically, there are only simple hardwired interlockings acting on a feeder. The triggering signal for interlocking is quite often a volume measurement taken from the first crusher after the feeder. As soon as the volume (or material height level) reaches a fixed upper limit, the interlocking is activated pausing the feeder. Once the volume decreases

below the limit, the interlocking is off and the feeder is allowed to start feeding again.

There may be also other interlockings action on a single feeder, however, all these interlockings can be considered on/off controls from a process control perspective. Occasionally, a feeder is equipped with a variable speed drive allowing smooth non-portable operation between pause/stop and full speed but, in most cases, the feeder is operated at a fixed speed, no matter if its speed is adjustable or not.

A feeder always comes with a fixed volume capacity. The instantaneous feeder volume, however, is highly dependant on the human-based feeding cycle. As soon as an empty feeder is loaded, it carries a lot of tons forward to the process and, similarly, when reaching the end of the feeding cycle (typically 2-4 minutes for dumber feeding and 20-30 seconds for excavator feeding), the feeder volume obviously decreases. Yet, by default, this information is not available in hardwired, on/off based or PI/PPI based feed controls.

By adding a sensor for measuring feeder volume on-line and taking that measurement into account, a feed-forward controller can be designed to assist a PI/PP controller in feed control. The relation between feeder volume and its manipulable speed is non-linear making the design a bit cumbersome. However, by linearising the first-principle based process model and simplifying it, the guidelines can be given for tuning the feed-forward controller.

In this paper, a real case on feed control design with implementation is presented. An existing feeder was equipped with a variable speed drive allowing smooth feeder speed control. In addition to this, an additional ultrasonic sensor was mounted onto a feeder to measure its volume (material height, to be precise). This information is extremely

useful in both ends of the human-based feeding cycle (in the beginning and at the end) providing assets to the feedback based feeder control.

Although the feed control concept contains only one actuator, feeder, there are several control loops involved if all the feed-related process variables are considered, such as primary crusher volume, secondary crusher volume and production rate (measured by a belt scale or indirectly, by measuring conveyor material height). To accomplish regulation of all these variables, parallel limiting control loops with min/max selector are required. Second, there are certain threshold values (high volumes, high crusher power draws or pressures) that must stop feeding immediately when active. Third, there is a slave controller acting on the variable speed drive receiving its setpoint from the upper master controller.

A dominant characteristic of all the control loops is a necessity to compensate dead times of the process. Due to material transportation between and through crushers and screens, there are dead times that must be considered in control design. Thus, a predictive PI controller is preferred as a controller type.

## 2. APPENDIX

An example of an aggregate production process is illustrated in figure 1. There is a dumper feeding the process by dumping the material onto a vibrating feeder. Instead of the dumper, there may be an excavator feeding the process.

The vibrating feeder is controlled in manual or in auto to feed a primary crusher where the first crushing of the process takes place. Primary crushing is about processing large particles into smaller particles for secondary crushing. Often, the primary feeder screens fine particles making them bypass the primary crusher to enter the discharging conveyor of the primary crusher. The discharging conveyor combines the crushed feeding material with the bypassed fines.

fine crushing circuit. Sometimes, there may be a re-circulation material flow after the secondary crusher back to the secondary crushing to get over-sized and non-crushed material crushed. In this paper, it is assumed that there is no such a material flow but, instead, the material coming out of the secondary crusher continues to fine-crushing.

## 3. REFERENCES

As always, there are references to be referred to but they are lacking in this abstract. However, the reference list is given in the full paper.

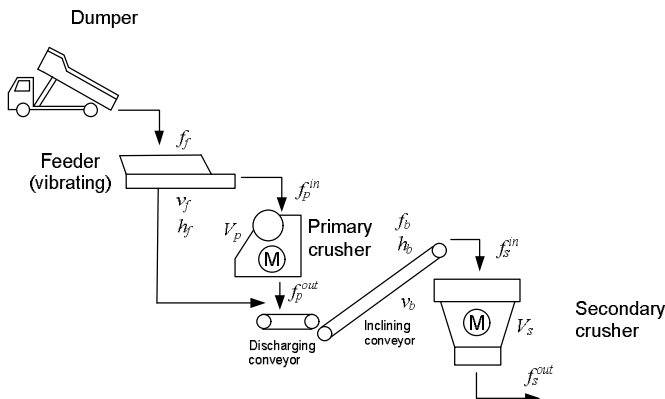


**Figure 1.** A typical crushing and screening process setup for material feeding.

Next, the crushed material enters an inclining conveyour feeding a secondary crusher. The secondary crusher crushes the material into even smaller particles which are taken to

## Oral presentations 2

# MPC and optimization

Chair: Kurt Häggblom. Åbo Univ.

### Presentations:

5. *Optimal control of uncertain systems using Dual Model Predictive Control (DMPC)*  
Tor Aksel N. Heirung\*, B. Erik Ydstie\*\* and Bjarne Foss\*  
\* Dept. of Chem.Eng, Carnegie Mellon University, USA  
\*\* Dept. of Engineering Cybernetics, NTNU
6. *Efficient solvers for soft-constrained MPC*  
Gianluca Frison, John Bagterp Jørgensen  
Technical University of Denmark, Denmark
7. *Sensitivity-based economic model predictive control*  
Johannes Jäschke, Xue Yang, Lorenz T. Biegler  
NTNU & Carnegie-Mellon University, Pittsburgh, USA
8. *On the Convergence Rate of Extremum Seeking Control*  
Olle Trollberg and Elling W. Jacobsen  
Automatic Control, KTH, Stockholm
9. *Model Predictive Control of Pasteurization Processes*  
Patrick Hammer and Martin Mayer  
evon GmbH, Gleisdorf, Austria

# Optimal control of uncertain systems using Dual Model Predictive Control (DMPC)

Tor Aksel N. Heirung\*      B. Erik Ydstie†      Bjarne Foss\*

We present an adaptive model predictive controller (MPC) for plants with uncertain model parameters. Inspection of the objective function shows that the adaptive MPC must include caution and probing in order to generate optimal controls. We propose a dual model predictive controller (DMPC) that performs better than certainty-equivalence adaptive MPC by integrating optimal plant excitation with respect to current and predicted parameter estimate errors.

We consider linear models in discrete time with Gaussian disturbances and quadratic performance cost. The least-squares estimate provides the model parameters at the current time given past data. In certainty-equivalence adaptive control these parameters are used directly to generate the controls by assuming that the estimate provides the best control. However, evaluation of our cost function shows that optimal controls are functions of the current and future parameter-estimate error covariances. The current covariance matrix provides a rationale for caution, whereas probing can reduce the future covariance matrices. Our proposed deterministic objective-function reformulation provides the optimal combination of caution, probing, and nominal control.

We demonstrate the application of DMPC to a finite impulse response (FIR) system and present the deterministic equivalent of the associated stochastic optimal control problem. The advantages of the FIR model includes the compactness of the exact objective function reformulation and that the covariance predictions are explicit functions of the decision variables. Generalizations to Laguerre and ARX formulations follow but the computational expense is higher.

In order to facilitate online solution of the DMPC problem we formulate our optimal control problem in terms of an information matrix that is the inverse of the recursive least-squares (Kalman) covariance update. We show that the nonconvex optimization problem can be solved as a quadratic program with bilinear constraints. Although optimization problems constrained by quadratic equality constraints are not trivial to solve, there exist methods for solving this class of problem to global optimality that apply to the DMPC problem. We further simplify and speed up solution by exploiting the symmetry of the information matrix, reducing the number of variables through decomposition, and using constraints for controls and outputs.

The performance of the controller is compared with adaptive MPC and fixed-parameter MPC. We discuss the online solution of the optimization problem and the use of local and global solvers. The simulation examples show that the optimal excitation strategy provides better mean-square performance than approaches that rely on persistent excitation. Our controller excites the system just enough to obtain good estimates of the unknown parameters while minimizing the resulting adverse effect on output regulation. Simulation shows that the parameter estimates converge quickly and that exact parameter estimates are obtained in the limit even though the excitation vanishes.

---

\*Dept. of Engineering Cybernetics, NTNU—Norwegian University of Science and Technology, Trondheim, Norway.

†Dept. of Chemical Engineering, Carnegie Mellon University, Pittsburgh, PA, USA.

# Efficient solvers for soft-constrained MPC

Gianluca Frison, John Bagterp Jørgensen

**Abstract**—The ability of easily and naturally handling constraints is certainly one of the winning features of Model Predictive Control (MPC). The use of hard output constraints, however, is often not physically necessary, and furthermore it can lead to unfeasible optimization problems. One way to avoid this issue is the use of soft-constraints on the outputs (and more in general on the states). In the soft-constrained formulation, the constraint may be violated, but incurring in a penalty cost: the optimization procedure thus avoid the violation of these constraints whenever possible. Soft-constraints are traditionally handled by introducing a decision variable for each slack variable associated with the soft-constraints. This increases the size of the dynamic system variables, and therefore the size of the optimization problem, and it increases remarkably the solution time. In this paper, we want to show that IP and ADMM methods for box-constrained MPC can be modified to handle the case of soft-constraints on the states, and at a similar cost-per-iteration. This is obtained by exploit the special structure of the KKT system of the soft-constrained MPC problem, avoiding the introduction of additional control variables. As a consequence, each iteration of the IP or ADMM methods requires the solution of an unconstrained MPC sub-problem with the same size as in the case of box-constrained MPC.

## I. INTRODUCTION

Model Predictive Control (MPC) is probably the most successful advance control technique in industry [6]. It makes use of a plant model to predict the future evolution of the plant dynamic and compute an input sequence optimal with respect to some cost function. At each sampling instant, only the first input of this optimal sequence is applied to the plant, before a new input sequence is computed using the latest measurements: thus, at each sampling instant an optimization problem has to be solved in real-time. This has traditionally limited the use of MPC to system with slow dynamic, as in process or chemical industry. In recent years MPC has been successfully applied to system with fast dynamic, with sampling times also in the micro-seconds range [4]: these improvements are due to both faster hardware as well as the use of structure-exploiting algorithms.

One of the winning features of MPC is certainly its ability of easily and naturally handling constraints [5]. However, the presence of constraints makes computationally-expensive the solution of optimization problems. Therefore, algorithms exploiting special constraints formulations (e.g. box constraints) have been proposed [1], [8]. One drawback of the use of hard-constraints is that they may make the optimization problem unfeasible: this is especially true in

the case of output constraints. Furthermore, often the use of hard-constraints is not physically necessary.

One way to avoid this issue is the use of soft-constraints on the outputs (and more in general on the states). In this formulation, the constraint may be violated, but incurring on a penalty cost. This is usually obtained by introducing slack variables associated with the soft constrained, and heavily penalizing them: the optimization algorithm keeps these slack variables to zero whenever possible, and violates the constraints only if necessary. Soft-constraints are usually handled by introducing a decision variable for each slack variable associated with the soft-constraints. This approach has the advantage of formulating the optimization problem in the form of an hard-constrained one. However, this comes at a cost from a computational point of view: the simple constraint structure is lost (and thus algorithms for general constraints must be employed), and furthermore the extra decision variables enter in the optimization problem as dynamic system variables, that typically contribute with a cubic term in the flop count. Recently, a different formulation has been proposed [7], avoiding the introduction of extra optimization variables: however, this comes at the cost of approximating of the soft constraint penalty

In this paper, we propose a different approach. We want to show that both IP and ADMM methods for box-constrained MPC can be modified to handle the case of soft-constraints on the states, and that the flop count increases only by a linear term. This is obtained by exploit the special structure of the KKT system associated with the soft-constrained MPC problem: new optimization variables are introduced for the slack variables, but these are not additional control variables. As a consequence, each iteration of the IP and ADMM methods requires the solution of an unconstrained MPC sub-problem (accounting for cubic and quadratic terms in the flop count) with the exact same structure and size as in the case of box-constrained MPC, and that can be solved efficiently [2], [3].

## REFERENCES

- [1] A. Domahidi, A. Zgraggen, M.N. Zeilinger, M. Morari, and C.N. Jones. Efficient interior point methods for multistage problems arising in receding horizon control. In *IEEE Conference on Decision and Control (CDC)*, pages 668 – 674, Maui, HI, USA, December 2012.
- [2] G. Frison, H.H. B. Sørensen, B. Dammann, and J.B. Jørgensen. High-performance small-scale solvers for linear model predictive control. In *IEEE European Control Conference*, pages 128–133. IEEE, 2014.
- [3] G. Frison, L.E. Sokoler, and J.B. Jørgensen. A family of high-performance solvers for linear model predictive control. In *IFAC World Congress*, pages 3074–3079. IFAC, 2014.
- [4] J. Jerez, P. Goulart, S. Richter, G. Constantinides, E. Kerrigan, and M. Morari. Embedded online optimization for model predictive control at megahertz rates. *IEEE Transactions on Automatic Control*, 2013.

Authors are with Technical University of Denmark, DTU Compute - Department of Applied Mathematics and Computer Science, DK-2800 Kgs Lyngby, Denmark. Email: {giaf, jbjjo} at dtu.dk

- [5] J.M. Maciejowski. *Predictive Control with Constraints*. Prentice Hall, 2002.
- [6] S.J. Qin and T.A. Badgwell. A survey of industrial model predictive control technology. *Control Engineering Practice*, 11:733–764, 2003.
- [7] A. Richards. Fast model predictive control with soft constraints. In *IEEE European Control Conference*, 2013.
- [8] S. Richter, C.N. Jones, and M. Morari. Real-time input-constrained MPC using fast gradient methods. In *IEEE Conference on Decision and Control*, pages 7387 – 7393, 2009.

# Sensitivity-based Economic Model Predictive Control

Johannes Jäschke, Xue Yang, Lorenz T. Biegler

In recent years, model predictive control has been successfully applied to many large-scale industrial processes. Because computational power is cheaply available, also nonlinear model predictive control with economic objective functions has become increasingly attractive (Diehl et al., 2011). Although optimization algorithms and computers are constantly improving, obtaining fast and reliable solutions to the underlying nonlinear optimization problem (NLP) remains a challenge, because models have become more complex, and long computational delays can cause instability. A popular approach for minimizing computational delays is based on sensitivity updates of the optimal NLP solution. Here we use information about how the optimal solution changes close to one optimal point in order to find an approximate solution for the NLP at another point close by. However, previous work on this approach does either not take changing constraints into account (Zavala and Biegler 2007), does it in a heuristic way (Lynn et al., 2009, Yang and Biegler 2013), or assumes very strong regularity conditions (Diehl, 2001).

In this work we first review a method for calculating the NLP sensitivity based on very weak regularity conditions (Ralph and Dempe, 1995). This result lets us compute the NLP sensitivity also in case of non-unique multipliers (MFCQ) and changing active sets. The solution point sensitivity is obtained by solving a quadratic program (QP), and the corresponding multiplier sensitivity is obtained from the solution of a linear program (LP)

Second, we use this result in a predictor path-following method, where we track the solution of the NLP along a parameter change (Jäschke et al. 2014). In a model predictive control context this parameter change generally corresponds to changes in the initial conditions from one sample time to the next. Our path-following idea is similar to an explicit Euler method, where we subsequently apply many small sensitivity updates along the path from one initial condition to the next.

At each step along the path we monitor the Lagrangian multipliers and the constraints, in order to detect changes in the active set. If an active set change is detected, we update the sensitivity calculations accordingly and continue following the path until we reach the final point.

We demonstrate our path-following method on a CSTR example (Diehl et al. 2011), which has been modified to exhibit active set changes. Our method is compared with heuristic methods for handling active set changes, and shows good performance. Directions for future work include adding a corrector step to our path-following method, and establishing convergence results in order to prove robust stability of the resulting model predictive controller.

## References

- M. Diehl (2001) *Real-Time Optimization of Large-Scale Nonlinear Processes*, PhD Thesis, Univ. Heidelberg
- M. Diehl, R. Amrit, J.B. Rawlings (2011) *A Lyapunov function for economic optimizing model predictive control*, IEEE Trans. Autom. Control, 56, pp. 703–707
- J. Jäschke, X. Yang, L.T. Biegler (2014) *Fast economic model predictive control based on NLP-sensitivities* J. Process Control 24, pp. 1260–1272
- D. Ralph, S. Dempe (1995) *Directional derivatives of the solution of a parametric nonlinear program*, Math. Program., 70, pp. 159–172
- L. Würth, R. Hannemann, W. Marquardt (2009) *Neighboring-extremal updates for nonlinear model-predictive control and dynamic real-time optimization*, J. Process Control, 19, pp. 1277–1288
- X. Yang, L.T. Biegler (2013) *Advanced-multi-step nonlinear model predictive control*, J. Process Control, 23, pp. 1116–1128
- V.M. Zavala, L.T. Biegler (2009) *The advanced-step NMPC controller: optimality, stability and robustness*, Automatica, 45, pp. 86–93

# On the Convergence Rate of Extremum Seeking Control

Olle Trollberg and Elling W. Jacobsen

**Abstract**—Extremum seeking control (ESC) is an adaptive optimization method originally proposed for static systems but later extended to Hammerstein/Wiener-like systems and more recently also to more general dynamic systems. In the latter case the focus has been on proving convergence and stability of solutions in the vicinity of the optimum. The proofs are in general based on combining asymptotic methods like singular perturbations and averaging, which leads to a three time-scale factorization of the problem where the control action is forced to be several orders of magnitude slower than the open-loop dynamics of the plant. This implies that the convergence rate will be impractically slow for many applications. In this paper, we employ Tikhonov theory and averaging to study the rate of convergence while employing only two time-scales. In particular, the analysis places no restrictions on the rate of the gradient estimation and therefore allows for significantly faster control compared to the conventional approach. The plant is approximated as a linear parameter varying system (LPV) which is then used to derive a global quantitative expression for the convergence rate in terms of the ESC parameters and the frequency response of the LPV plant. For Hammerstein/Wiener-like systems, the derived expression is used to show that the ESC loop behaves like a gradient descent method while it has a more complex behavior in the general case. Finally, an isothermal biochemical reactor is used to illustrate the results and some of the difficulties which might arise in the general case, such as the fact that the convergence rate can be low locally even if the gradient of the cost function is large.

## I. INTRODUCTION

Extremum seeking control (ESC) based on sinusoidal perturbations is a powerful adaptive method used to locate and track the optimal output of a plant, even when no plant model is available. This is achieved by utilizing feedback to force the system to a point where an estimate of the gradient of the cost function is zero. Since the method is feedback based, it inherits the robustness towards uncertainty and disturbances which are associated with such methods. Furthermore, it is also model free, which implies that the often costly and difficult step of deriving complex models can be avoided. These strengths combined with a relatively simple implementation makes ESC a prime candidate for optimizing complex plants.

ESC was introduced as early as 1922 when it was used to optimize an application with a static nonlinearity [10]. In the 50's and 60's the method gained in popularity after a monograph by Draper and Li [6], and was also extended to dynamic systems of Hammerstein/Wiener type. Over the years, the method has been implemented in numerous applications, ranging from optimization of bioreactors [5] to drag minimization in formation flight [2, Chapter 9]. It is

thus surprising to note that the field for a long time suffered from a lack of rigorous results on stability and convergence, at least for general dynamic systems. In recent years, this situation has improved significantly after a break-through stability result by Krstić and Wang [9] (2000), which has led to a revival of the field.

During the last decade, much effort has been spent on proving convergence and stability of ESC for a broad class of general nonlinear dynamic systems [9], [19], [4]. However, for ESC to be practically useful, it is not enough that it converges; it must also do so with a reasonable *convergence rate*. For Hammerstein/Wiener-like systems, this topic has been investigated in e.g., [8] and [11] where it is shown that under certain assumptions, arbitrarily fast convergence can be achieved. However, for the broader class of general dynamic systems, there exist few results on the convergence rate. The results that do exist are mainly qualitative remarks, e.g., pointing out that the convergence rate increases with the magnitude of the ESC-parameters, e.g., [9], [4]. In [19], the argument is extended to show that there is a trade-off between convergence rate and domain of attraction of the optimum in terms of the magnitude of the ESC-parameters. In [3], error bounds on the deviation from the ideal scheme approximated by the loop are derived and used as constraints in an optimization problem serving to maximize the nominal convergence rate by making the ESC-parameters as large as possible. However, the results above are mainly qualitative and valid only under rather restrictive assumptions for which most dynamic properties of the plant can be neglected.

When studying faster convergence rates, the dynamics of the plant become essential and must be taken into consideration. By using a different method of analysis where the plant dynamics are of central importance, we derive a *quantitative* expression for the convergence rate in terms of the ESC-parameters and properties of the plant's local frequency response. This gives fundamental insight into which plant properties are limiting and also how to counter such limitations. Furthermore, the derived results are globally applicable and if a model is available the results can be used to predict the convergence rate. Hence, the derived results can easily be validated by comparing the prediction with actual simulations.

The paper is organized as follows: In section II we present some general assumptions on the plant to be optimized, introduce the ESC scheme, and briefly discuss how the convergence rate usually is limited by assumptions. In section III, we derive an explicit expression for the convergence rate in terms of the ESC-parameters and properties of the plant dynamics. In section IV the results are applied to Hammerstein/Wiener systems and the effect of the plant

KTH Royal Institute of Technology, School of Electrical Engineering, Department of Automatic Control, Stockholm 100 44, Sweden (Email: olletr@kth.se, jacobsen@kth.se)

dynamics on the convergence rate is discussed further. In section V we give an example illustrating our results and some of the difficulties which may arise for general dynamic systems.

## II. BACKGROUND

In this section we state some assumptions on the plant, introduce the ESC method considered, and finally discuss briefly how various assumptions can affect the achievable convergence rate.

### A. General Assumptions Regarding the Plant

The input  $\theta$  and the output  $y$  of the plant is assumed to be related by a nonlinear state space description:

$$\begin{aligned} \dot{x} &= f(x, \theta) \\ y &= h(x, \theta), \end{aligned} \quad (1)$$

where  $x$  is the state vector, and  $f$  and  $h$  are sufficiently smooth but unknown functions. It is assumed that for each input  $\theta$ , there exists a globally stable unique steady state solution such that

$$f(x, \theta) = 0 \quad \text{if and only if} \quad x = l(\theta).$$

That is, the plant steady states are parametrized by the input  $\theta$ . The composite function

$$J(\theta) = h(l(\theta), \theta) \quad (2)$$

is the steady-state input-output map of the plant.  $J(\theta)$  is assumed to be differentiable, have a unique global maximum for  $\theta^*$  and be free from local extrema.

### B. Extremum Seeking Using Sinusoidal Perturbations

The task of ESC is to locate and track the control input  $\theta^*$  which maximizes the steady-state input-output map  $J(\theta)$ . There exists a great variety of ESC methods in the literature, e.g., ESC using sliding mode [13], adaptive ESC [7], [1] or ESC based on numerical optimization [21]. The method we consider in this paper belong to the classical and most investigated class of methods based on sinusoidal perturbations, e.g., [2], [8], [9], [4], [6], [10], [12], [17], [18]. The scheme is summarized in Fig. 1, which also serves to define the variables and parameters used in the paper. These are:

- $y$  - plant output,
- $\theta$  - actuated control input,
- $\hat{\theta}$  - nominal control input, the operating point,
- $y - \eta$  - high-pass filtered output,
- $\xi$  - estimate of the cost function's gradient,
- $\omega$  - perturbation frequency,
- $a$  - perturbation amplitude,
- $k$  - integrator gain,
- $F_H$  - linear high-pass or band-pass filter,
- $F_L$  - linear low-pass filter.

Essentially, by perturbing the plant input, an estimate of the local gradient can be extracted and used to drive a gradient descent scheme. A good introduction to the method can be found in one of the surveys [15], [16], [5], or alternatively the monographs [2], [21].

The stability and convergence properties of the loop in Fig. 1 have in recent years been the subject of numerous investigations [9], [4], [18]. The focus has mainly been

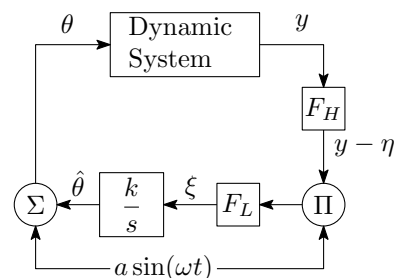


Fig. 1. Block diagram of the extremum seeking control loop based on sinusoidal perturbations.

on showing existence of and convergence to a stationary solution in the vicinity of the optimum. Such results are typically derived using a series expansion about the optimum and a combination of the two asymptotic methods singular perturbations and averaging theory. The latter combination typically establishes a three time-scale factorization of the problem. First, singular perturbations are used to substitute a static nonlinearity for the plant dynamics under the assumption that the variations in the perturbed control input are slow. This implies that the perturbation frequency  $\omega$  acts in a slow time-scale as compared to the plant dynamics. In a second step, averaging is used to get an autonomous approximation of the system. However, this requires in turn that the nominal control input varies in a slow time-scale as compared to the perturbation frequency  $\omega$ , hence a three time-scale factorization of the problem is established. This line of analysis has been successful in proving existence, convergence and stability of stationary solutions in the vicinity of the optimum [9], [4], [18]. However, from a convergence rate perspective, the three time-scale factorization is unfortunate since it also implies that the convergence rate of the nominal control input must be *several orders of magnitude* lower than the slowest dynamics of the plant if the stability results are to be valid. Hence, we would like to restrict the number of time-scales in the analysis to allow for faster convergence rates. Furthermore, the use of a series expansion about the optimum generally limits the discussion to a local neighborhood of the optimum which might be less relevant when the convergence rate is considered.

Avoiding the use of time-scale separation altogether is probably hard. The reason for this is that the steady state optimum is a property of the equilibrium manifold, and in lack of model information, this manifold needs to be explored. Hence, it is necessary to operate the plant in a neighborhood of the manifold. Without model knowledge, the easiest way to ensure that the plant operates in such a neighborhood is to move the plant slowly enough, on average, that the natural affinity of the plant for the manifold keep the states close to it. Note though that the local exploration of the manifold does not necessarily have to be slow.

## III. CONVERGENCE RATE

We here derive an explicit expression for the convergence rate in terms of the ESC loop parameters and the local

frequency response of the plant. This is done in two steps; we first reduce the plant complexity using Tikhonov time-scale arguments, then the reduced plant is used to derive an expression for the convergence rate.

In the analysis below we assume that the control action is slow with regards to both the perturbation and the plant dynamics, but, *we do not assume that the perturbation is slow with respect to the plant dynamics* as in most previous works. Hence, we use only two time-scales which allow us to consider significantly faster convergence rates. It might seem counter intuitive at first to allow high frequencies since we are looking to find a static property of the plant, but as shown in [20], the steady state optimum is in fact also reflected in the dynamic properties of the plant, hence allowing higher frequencies to be used.

### A. Reducing the Complexity of the Plant

Consider again the ESC loop in Fig.1. Assuming the control action  $d\hat{\theta}/dt = k\xi$  is slow relative to the plant dynamics, low- and high-pass filters and the perturbation frequency  $\omega$ , we can introduce two corresponding time-scales. If we also assume that the open-loop plant and filters are asymptotically stable, we can according to Tikhonov theory on time-scale separation analyze the fast and slow time-scales separately using reduced order models. In the fast time-scale one then considers the states and output of the slow system to be constant, while in the slow time-scale the fast and asymptotically stable system is assumed to exist on its equilibrium, or slow, manifold at all times.

We first consider the fast time-scale in which the control input  $\hat{\theta}$  is assumed constant and derive an expression for the output of the fast system, i.e., the output of the low-pass filter when  $\hat{\theta}$  is assumed constant. Since we are primarily interested in what happens on the slow manifold, i.e., the equilibrium manifold of the fast system, we neglect any transients and focus on the local behavior around the slow manifold. We correspondingly approximate the plant in the fast time-scale as a bias term  $J(\hat{\theta})$  combined with a linear parameter varying (LPV) system, parametrized by the current point of operation  $\hat{\theta}$ . Let  $G_{\hat{\theta}}(s)$  be the  $\hat{\theta}$ -parametrized transfer-function representation of the locally linearized plant at the corresponding point at the slow manifold, i.e.,

$$G_{\hat{\theta}}(s) = C(sI - A)^{-1}B + D$$

with

$$\begin{aligned} A &= \left. \frac{df}{dx} \right|_{x=l(\hat{\theta}), \theta=\hat{\theta}} & B &= \left. \frac{df}{d\theta} \right|_{x=l(\hat{\theta}), \theta=\hat{\theta}} \\ C &= \left. \frac{dh}{dx} \right|_{x=l(\hat{\theta}), \theta=\hat{\theta}} & D &= \left. \frac{dh}{d\theta} \right|_{x=l(\hat{\theta}), \theta=\hat{\theta}} \end{aligned}$$

Note that this LPV plant description allows fast but small amplitude variations in the actuated plant input,  $\theta$ , hence allowing for any frequency of the perturbation. The aim is next to derive the slow manifold output, which serves as the input to the slow time-scale controller, in order to determine the convergence rate of  $\hat{\theta}$  in the slow time-scale.

### B. Derivation of the Convergence Rate

Assuming  $\hat{\theta}$  constant in the fast time-scale, the plant's response to the control input  $\theta(t) = \hat{\theta} + \sin(\omega t)$  will be on the form

$$y(t) = J(\hat{\theta}) + a|G_{\hat{\theta}}(i\omega)| \sin(\omega t + \arg[G_{\hat{\theta}}(i\omega)])$$

which is the local frequency response of the perturbation at the current equilibrium on the slow manifold. The constant bias term  $J(\hat{\theta})$  is removed by high-pass filtering the output, leaving only the frequency response,

$$y(t) - \eta(t) = a|F_H(i\omega)||G_{\hat{\theta}}(i\omega)| \sin(\omega t + \varphi_{\hat{\theta}}),$$

where

$$\varphi_{\hat{\theta}} = \arg[G_{\hat{\theta}}(i\omega)] + \arg[F_H(i\omega)] \quad (3)$$

is the combined phase lag of the plant and the high-pass filter. The filtered signal is demodulated by multiplication with the original perturbation. Using a trigonometric product-to-sum identity we arrive at the following output from the demodulation

$$\begin{aligned} (y(t) - \eta(t))a \sin(\omega t) &= \\ \frac{a^2}{2}|F_H(i\omega)||G_{\hat{\theta}}(i\omega)| &[\cos(\varphi_{\hat{\theta}}) - \cos(2\omega t + \varphi_{\hat{\theta}})]. \end{aligned} \quad (4)$$

Thus, the output of the demodulator contains a static term as well as a high-frequency term. The static term carries the relevant information while the high-frequency term is an unwanted by-product of the demodulation. The low-pass filter serves to dampen the high-frequency term, leaving us with the gradient estimate

$$\begin{aligned} \xi &= \frac{a^2}{2}|F_H(i\omega)||G_{\hat{\theta}}(i\omega)| \{ |F_L(0)| \cos(\varphi_{\hat{\theta}}) \\ &\quad - |F_L(i2\omega)| \cos(2\omega t + \varphi_{\hat{\theta}} + \arg[F_L(i2\omega)]) \} \end{aligned}$$

When considering the slow time-scale, we can employ averaging to remove the time-varying effect from the high-frequency term in  $\xi$ . This is motivated by the fact that  $\cos(2\omega t)$  is fast relative to the slow control action and that its amplitude is small due to the low-pass filtering. Employing averaging over  $t \in [0, \pi/\omega]$  yields

$$\xi = \frac{a^2}{2}|F_L(0)||F_H(i\omega)||G_{\hat{\theta}}(i\omega)| \cos(\varphi_{\hat{\theta}})$$

i.e., the sinusoidal variation has an average of zero.

In the slow time-scale, the rate of change of  $\hat{\theta}$  can now be expressed as

$$\dot{\hat{\theta}} = \frac{ka^2}{2}|F_L(0)||F_H(i\omega)||G_{\hat{\theta}}(i\omega)| \cos(\varphi_{\hat{\theta}}).$$

The term  $|F_L(0)||F_H(i\omega)|$  originates from the filters and is a constant which can be freely chosen during the design of the filters. To simplify the notation we assume that this constant has been absorbed into  $k' = k|F_L(0)||F_H(i\omega)|$  which leaves us with

$$\dot{\hat{\theta}} = \frac{k'a^2}{2}|G_{\hat{\theta}}(i\omega)| \cos(\varphi_{\hat{\theta}}) = L(\hat{\theta}). \quad (5)$$

Note that this is an explicit expression for the convergence rate in terms of the ESC loop parameters and properties of

the local frequency response for the perturbation frequency used. Since we are assuming that the plant model is unknown to us, the last two terms in the product will in practice be unknown, but the expression is still useful since it can help shed light on how parameter choices and certain plant properties affect the convergence rate. If the plant model is known, expressions (5) and (2) can be combined to predict the convergence behavior of the plant under the assumptions given. Furthermore, note that equation (5) implies that we will have a stationary solution whenever  $L(\hat{\theta}) = 0$ . The stability of these stationary solutions are determined by the sign of  $dL/d\hat{\theta}$  evaluated at the stationary solution. A negative value of  $dL/d\hat{\theta}$  implies stability while a positive value implies instability. More details on stationary solutions and stability can be found in [20].

From equation (5), we see that the following parameters affect the convergence rate:

- $k$  - integrator gain. The convergence rate scales linearly with  $k$ . The user is essentially free to set this parameter as long as the time-scale separation arguments are fulfilled.
- $a$  - perturbation amplitude. The convergence rate scales quadratically with  $a$ . This parameter is small by assumption in order for the linearization to be a good approximation.
- $\omega$  - perturbation frequency. The impact of varying  $\omega$  is system dependent and discussed below. The user is essentially free to set this parameter. Note that a low choice of  $\omega$  indirectly limits the convergence rate by forcing  $k$  small in order to fulfill the separation of time-scale assumptions. On the other hand, the distance to the optimum may increase with increasing  $\omega$ , and for too large values of  $\omega$  there might not be any stationary solution close to the optimum at all. Note also that the filters,  $F_H$  and  $F_L$ , must typically be redesigned when  $\omega$  is altered.

#### IV. EFFECTS OF LOCAL SYSTEM PROPERTIES ON THE CONVERGENCE RATE

By studying the expression (5), it is clear that the convergence rate of the control input  $\hat{\theta}$  is affected by the plant dynamics through the term

$$|G_{\hat{\theta}}(i\omega)| \cos(\varphi_{\hat{\theta}}).$$

It is of interest to consider how these terms vary and the effect of such variations on the convergence rate to understand how the dynamics can cause slow convergence and to gain insight into how such problems can be countered.

##### A. Hammerstein/Wiener Systems

In the literature, Hammerstein/Wiener-like systems, i.e., systems consisting of linear dynamics in series with a static nonlinearity, have received much attention, e.g., [11], [8]. In this section we apply our framework to such a model to demonstrate the applicability of the results derived above and to show that the ESC-loop reduces to a gradient ascent method for such systems. This provides some contrast to and highlights the difficulties of the general case.

We will consider a Hammerstein system (similar results can be derived for any Wiener/Hammerstein system) on the form

$$\begin{aligned} \dot{x} &= Ax + Bg(\theta) \\ y &= Cx \end{aligned}$$

where  $g(\theta)$  is the nonlinear function acting on the input. To put this system into our framework, we linearize it about a steady-state solution to get our LPV description,

$$G_{\hat{\theta}}(s) = C(sI - A)^{-1}B \left. \frac{dg}{d\theta} \right|_{\theta=\hat{\theta}} = G(s) \left. \frac{dg}{d\theta} \right|_{\theta=\hat{\theta}}$$

which just correspond to the transfer function of the linear system,  $G(s)$ , scaled by the local gradient of the static nonlinearity. In other words, the dynamics of a Hammerstein model is essentially only "rescaled" when the point of operation  $\hat{\theta}$  moves, but unchanged otherwise. Looking at the gain for a fixed frequency  $\omega$ ,

$$|G_{\hat{\theta}}(i\omega)| = |G(i\omega)| \left. \frac{dg}{d\theta} \right|_{\theta=\hat{\theta}},$$

we realize that it is directly proportional to the size of the local gradient of the nonlinearity with the gain of the linear dynamics only acting as a fixed proportionality constant. The phase lag is given as

$$\begin{aligned} \varphi_{\hat{\theta}} &= \arg \left[ G(i\omega) \left. \frac{dg}{d\theta} \right|_{\theta=\hat{\theta}} \right] + \arg[F_H(i\omega)] = \\ &\arg[G(i\omega)] + \arg[F_H(i\omega)] + \pi \left( \frac{1}{2} - \frac{1}{2} \operatorname{sgn} \left( \left. \frac{dg}{d\theta} \right|_{\theta=\hat{\theta}} \right) \right) \end{aligned}$$

which is a piecewise constant function changed by  $\pi$  radians at the optimum  $\hat{\theta} = \theta^*$  reflecting the sign change of  $dg/d\theta$  at that point.

By inserting the gain and phase lag into (5), noting that  $dg/d\theta = |G(0)|^{-1} dJ/d\theta$ , and working out the algebra, we realize that for Hammerstein plants the convergence rate reduces to

$$\dot{\hat{\theta}} = K \frac{dJ}{d\hat{\theta}}$$

where  $K$  is a constant given by

$$K = \frac{k' a^2 |G(i\omega)| \cos(\arg[G(i\omega)] + \arg[F_H(i\omega)])}{2|G(0)|}.$$

We recognize this as a gradient descent method for which the convergence behavior is already well known. This is not surprising since the ESC loop is in fact intended to approximate gradient descent. This also perhaps explain the popularity of Hammerstein/Wiener-like models in the literature; the linear dynamics does not in any essential way change the problem compared to a static map, as long as the perturbation frequency is chosen to ensure stability.

##### B. General Dynamics

For Hammerstein/Wiener like systems, the expression for the convergence rate reduces to a simple gradient decent method, mainly due to the dynamics being independent of the point of operation. For systems where the nonlinearity is inherent in the dynamics, things are more complicated since both the gain  $|G_{\hat{\theta}}(i\omega)|$  and the phase lag  $\varphi_{\hat{\theta}}$  can vary with  $\hat{\theta}$ , often in nontrivial ways.

In [20] it is shown that the condition on the phase lag

$$\varphi_{\hat{\theta}} = \pi/2 + n\pi$$

in general determines the stationary solutions of the ESC loop for systems with the nonlinearity inherent in the dynamics. This condition is usually fulfilled close to the optimum, but can also be satisfied at steady-states arbitrarily far removed from the optimum. From expression (5) it is evident that the plant phase lag also affects the convergence. In particular, the convergence rate will be close to zero whenever

$$\varphi_{\hat{\theta}} \approx \pi/2 + n\pi,$$

irrespective of the local gradient of the cost function  $dJ/d\theta$  at the point since  $\cos \varphi_{\hat{\theta}} \approx 0$ . In particular, the convergence rate will be low in the vicinity of stationary points given that  $\varphi_{\hat{\theta}}$  is continuous with respect to  $\hat{\theta}$ . For stable stationary points, this causes the convergence to be asymptotic, as should be expected. However, it also implies that the divergence rate from unstable stationary points will be low, even for large local gradients of the cost function. Note that the phenomena is not isolated to stationary points since the phase lag can fulfill  $\varphi_{\hat{\theta}} \approx \pi/2 + n\pi$  at arbitrary points.

### V. EXAMPLE

In this section we provide an example illustrating our findings and some of the difficulties that can arise for general dynamics. The plant considered here is an isothermal tubular bioreactor with plug-flow [14], used to convert chemical  $A$  into  $B$ . However, there is also a side reaction converting  $B$  into  $C$ , implying that there is a maximum yield of  $B$  with respect to the residence time in the reactor. The total flow into the reactor can be used to control the residence time and will thus be considered as the control input in our example. The reactor model is

$$\begin{aligned} \frac{\partial \alpha}{\partial t} + \frac{1}{q} \frac{\partial \alpha}{\partial z} &= -\alpha\beta \\ \frac{\partial \beta}{\partial t} + \frac{1}{q} \frac{\partial \beta}{\partial z} &= \alpha\beta - \frac{\beta}{\phi(1 + \rho\beta)} \end{aligned}$$

where  $\alpha$  and  $\beta$  are dimensionless concentrations of  $A$  and  $B$ ,  $\phi$  and  $\rho$  are constants describing the reaction rate, and  $q$  is the total flow which will act as control input  $\theta$ . The reactor length is normalized such that the spatial coordinate  $z \in [0, 1]$ . For the analysis and simulations, we use the method of lines with Euler forward and  $N = 10$  elements to discretize the plant such that it can be written on the form (1). We use the same parameters as in [14];  $\phi = 20$ ,  $\rho = 3$ ,  $\alpha(t, 0) = 0.8$ , and  $\beta(t, 0) = 0.2$ .

The cost function  $J(\theta)$  which we want to maximize is shown in Fig. 2, i.e., the steady-state input output mapping between flow  $q$  and yield of  $B$  at the reactor output. As can be seen from the figure, the optimal input is  $q^* = 6.01$  yielding  $B = 0.91$  at the output.

Assume now that the plant model is unknown. To find the optimum we apply ESC with the nominal parameters  $a = 0.125$ ,  $k = 5$ , and  $\omega = 0.2$  and initialize the optimization from the steady state corresponding to  $q = 15.9$ . Since ESC seeks to approximate a gradient descent method, we would expect the convergence rate to be proportional to the gradient of the cost function in Fig. 2, i.e., essentially only decrease

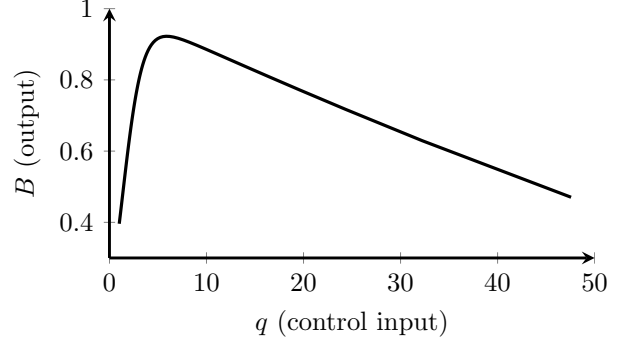


Fig. 2. The cost function  $J(\theta)$ : the steady state input output mapping between flow  $q$  and yield of  $B$  for the tubular reactor.

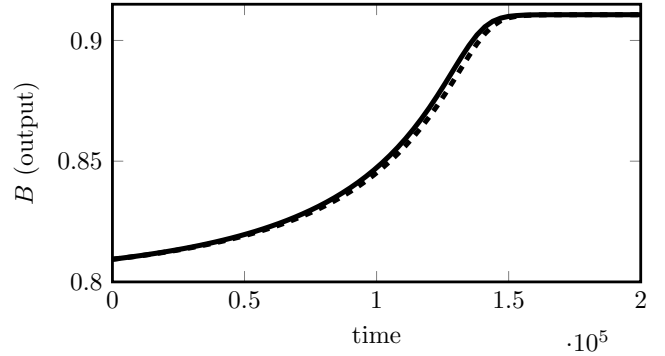


Fig. 3. Dashed: simulated convergence of the reactor output. Solid: predicted convergence using (6).

when the optimum is approached. However, as can be seen in Fig. 3, it turns out that this is not the case. Instead, the convergence rate initially increases from a very low rate, and only decrease towards the end of the optimization.

According to our results, the convergence behavior in Fig. 3 should be possible to predict by integrating the simple system

$$\begin{aligned} \dot{\hat{\theta}} &= L(\hat{\theta}) \\ y &= J(\hat{\theta}) \end{aligned} \quad (6)$$

where  $L$  is defined in (5) and  $J$  in (2). As can be seen from the dashed line in Fig. 3, the prediction is quite accurate for the chosen set of ESC parameters.

To understand the mechanisms causing the initial slow convergence in the simulation, consider Fig. 4 where the predicted convergence rate  $L(\hat{\theta})$  is plotted as a function of the point of operation. Apparently, there is an unstable stationary solution at  $\hat{\theta} = 16$  (since  $L(16) = 0$  and  $dL(16)/d\hat{\theta} > 0$ ). The slow initial convergence rate can thus be explained by the fact that the optimization was initialized close to an unstable stationary solution.

As can be seen in Fig. 3, the prediction obtained by integrating (6) is acceptable when the control parameters are chosen small. However, it is also interesting to see how well the results agree when the gain  $k$  is increased, that is, when we put strain on the time-scale separation arguments. The result of such an experiment is illustrated in Fig. 5. Note that the time-scale is logarithmic and that the gain  $k$  is increased

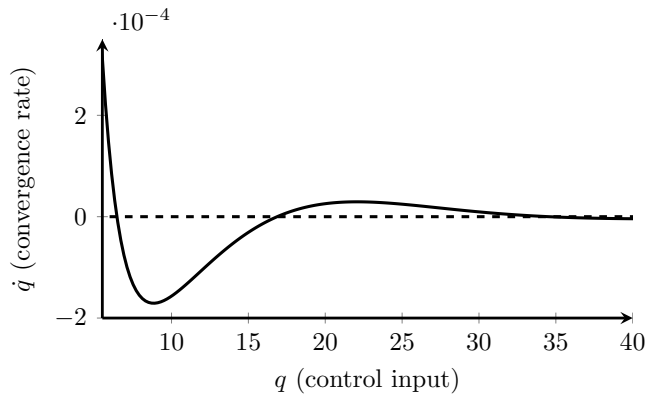


Fig. 4. Predicted convergence rate  $\dot{q} = L(q)$  of the control signal  $q$  using equation (5).

by a factor 3 between each simulation. Clearly, for low values of  $k$ , the predictions are accurate. For larger values of  $k$ , an error appears but the convergence rate is still of the same order as predicted. For all gains up to  $k = 3^5$  the qualitative behavior of the loop is well predicted, but for  $k = 3^6$  (not shown in the figure) the qualitative behavior has changed drastically and the prediction is off limited value.

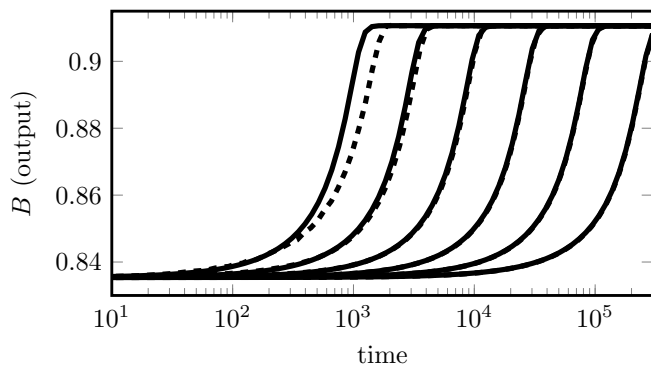


Fig. 5. Dashed: convergence of the reactor output from simulations. Solid: convergence predicted by (6). The initial conditions and all parameters except  $k$  were fixed in all simulations. The integrator gain  $k$  was increased by a factor 3 between each simulation, i.e.,  $k = 3^i$ ,  $i = 0, \dots, 5$ .

## VI. CONCLUSIONS

In this paper we have derived a quantitative expression for the convergence rate of the ESC loop. The derived expression provides insight into how the convergence is affected both by the parameter choice and by the local frequency response of the system. The local phase lag can have a major effect on the convergence rate and is a key factor in determining stationary solutions to the ESC loop. The results in the paper are confirmed and illustrated by a simple example which also demonstrate some of the difficulties that might arise for general dynamic systems. The results in this paper indicates that it may be wise to adapt the controller gain to compensate for the impact of changes in the local phase lag of the plant. However, how this should be done in a robust fashion is an open question left for future studies.

## REFERENCES

- [1] V Adetola and M Guay. Parameter convergence in adaptive extremum-seeking control. *Automatica*, 43(1):105–110, 2007.
- [2] Kartik B Ariyur and Miroslav Krstic. *Real-time optimization by extremum-seeking control*. Wiley-Interscience, 2003.
- [3] Gabriel Bousquet and Jean-Jacques Slotine. Large gain stability of extremum seeking and higher-order averaging theory. *arXiv preprint arXiv:1303.4474*, 2013.
- [4] Moncef Chioua, Bala Srinivasan, Martin Guay, and Michel Perrier. Dependence of the error in the optimal solution of perturbation-based extremum seeking methods on the excitation frequency. *The Canadian Journal of Chemical Engineering*, 85(4):447–453, 2007.
- [5] Denis Dochain, Michel Perrier, and Martin Guay. Extremum seeking control and its application to process and reaction systems: A survey. *Mathematics and Computers in Simulation*, 82(3):369–380, 2011.
- [6] Charles Stark Draper and Yao Tzu Li. *Principles of optimizing control systems and an application to the internal combustion engine*. American Society of Mechanical Engineers, 1951.
- [7] M Guay and T Zhang. Adaptive extremum seeking control of nonlinear dynamic systems with parametric uncertainties. *Automatica*, 39(7):1283–1293, 2003.
- [8] Miroslav Krstić. Performance improvement and limitations in extremum seeking control. *Systems & Control Letters*, 39(5):313–326, 2000.
- [9] Miroslav Krstić and Hsin-Hsiung Wang. Stability of extremum seeking feedback for general nonlinear dynamic systems. *Automatica*, 36(4):595–601, 2000.
- [10] M Leblanc. Sur l’électrification des chemins de fer au moyen de courants alternatifs de fréquence élevée. *Revue générale de l’électricité*, 12(8):275–277, 1922.
- [11] William H Moase and Chris Manzie. Fast extremum-seeking for wiener-hammerstein plants. *Automatica*, 2012.
- [12] D Nesić, Y Tan, WH Moase, and C Manzie. A unifying approach to extremum seeking: Adaptive schemes based on estimation of derivatives. In *Decision and Control (CDC), 2010 49th IEEE Conference on*, pages 4625–4630. IEEE, 2010.
- [13] Yaodong Pan, Ümit Özgüner, and Tankut Acarman. Stability and performance improvement of extremum seeking control with sliding mode. *International Journal of Control*, 76(9-10):968–985, 2003.
- [14] G Roopsingh and M Chidambaram. Periodic operation of bioreactors for autocatalytic reactions with Michaelis-Menten kinetics. *Bioprocess Engineering*, 20, 1999.
- [15] Jan Sternby. *A review of extremum control*. 1979.
- [16] Y Tan, WH Moase, C Manzie, D Nesić, and IMY Mareels. Extremum seeking from 1922 to 2010. In *Control Conference (CCC), 2010 29th Chinese*, pages 14–26. IEEE, 2010.
- [17] Y Tan, D Nešić, IMY Mareels, and Alessandro Astolfi. On global extremum seeking in the presence of local extrema. *Automatica*, 45(1):245–251, 2009.
- [18] Ying Tan, Dragan Nešić, and Iven Mareels. On non-local stability properties of extremum seeking control. *Automatica*, 42(6):889–903, 2006.
- [19] Ying Tan, Dragan Nesić, and Iven Mareels. On stability properties of a simple extremum seeking scheme. In *Decision and Control, 2006 45th IEEE Conference on*, pages 2807–2812. IEEE, 2006.
- [20] Olle Trollberg and Elling W. Jacobsen. Multiple stationary solutions to the extremum seeking control problem. In *European Control Conference (ECC), 2013*, pages 376–381. IEEE, 2013.
- [21] Chunlei Zhang and Raúl Ordóñez. *Extremum-Seeking Control and Applications: A Numerical Optimization-Based Approach*. London: Springer London, 2012.

# Model Predictive Control of Pasteurization Processes

Patrick Hammer\*, Martin Mayer\*

\*evon GmbH, Gleisdorf, Austria

**Abstract**—A methodology for optimizing distributed parameter systems (non-linear energy intensive processes) by the use of Model Predictive control (MPC) is shown. The approach is to represent the process as a parabolic Partial Differential Equations (PDEs), compare the application of explicit and implicit numerical algorithms (Crank Nicolson scheme, Euler scheme) for receiving a state space model to be applied in a linear MPC. The results are analyzed concerning the accuracy and stability of the numerical discretization of the PDEs as well as the control and optimization results.

## I. INTRODUCTION

Globally, energy consumption is one main topic of interest. Since 65% of the total consumption are caused by the process industry, optimization approaches within this industry are highly valuable, [2]. Since European legacy claims continuous improvement of energy efficiency, the goal is a reduction of 20% by 2020 compared to 2010, [6]. In the field of energy consumption/efficiency automation systems, in combination with control theory, can deliver great support for energy and cost reduction.

Within the process industry drying, evaporating and heating are the most energy demanding processes, with limited technical opportunities for energy recovery. Due to their non-linearity, these processes are complex in terms of control design, and their system dynamics require fast control cycles. For this study, the process of pasteurizing food is investigated. Its high energy demand occurs due to hygienic issues. For canned or bottled liquid products, the heat treatment is done in large scale equipment, so called tunnel pasteurizers. These plants are tunneled conveyer belts, that are sprinkled with hot water for heating and with cold water for re-cooling the products on the belt. The dimension of these plants exceed 50m in length and 2.5m in width, pasteurizing up to 50.000 products per hour. From the process point of view, it is a complex combination of multiple coupled heat transfer systems with constraints. From the mathematical point of view, it is a distributed parameter system.

Optimization of energy consumption can be done in three phases of a project: designing of the plant, production planning and the online control, where this study will focus on. Studies in the field of MPC have shown promising results for constraint optimization tasks in industrial real-time environment, [5]. Identifying the model is a crucial point since it might be very time and costs demanding in order to achieving an acceptable result for the use within an MPC. This work shows a modeling approach, where the process is described by PDEs. Furthermore, it is demonstrated how to

transform PDEs by numerical discretization into State Space Models used within an MPC.

## II. PROCESS MODELING-TUNNEL PASTEURIZER

The model has to cover the parameters like conveyer speed, zone temperature, product temperature at inlet, temperature of environment, and their impacts on the quality parameters like pasteurization units (PU) and time above temperature (TAT). Scientific work was successfully done in the field of modeling and simulation of the tunnel pasteurizer. These models are used for offline optimization as well as online condition monitoring. Concerning online control, these simulation models contribute to PID cascade loops, to control the process in a conservative single-input single-output (SISO) approach without gaining an optimal solution. The basic idea of above concepts is to pursue the division of the problem into smaller sub problems, to model each of them separately, and to connect them in the environment of a flowchart oriented simulation, [3]. Nevertheless, models of this type are focused on simulation only, and are not in the form needed by an MPC to optimally control the process. Another work focuses on approximating the PDEs by time-varying linear ODEs with an explicit Runge-Kutta scheme in order to solve the optimization problem by a  $H_\infty$  approach, [4]. This approach is only stable for small discretization steps which leads to high computation load. Furthermore the  $H_\infty$  controller is not flexible in respect to different optimization criteria, for example constraints are not considered although they are crucial.

This work focuses on modeling the tunnel pasteurizer by using PDEs. For the numerical solution, the implicit Crank Nicolson scheme, [1], as well as the explicit Euler approach is considered. For Crank Nicolson guaranteed numerical stability  $\forall \Delta t \in \mathbb{R}^+$  was applied. Furthermore the approach transfers the PDEs, with high accuracy, into a state space model. The design of the PDE includes several additive terms, the first describing the diffusion of the heat between the products, the second describing the impact of the water spray temperature in the different zones to the products on the band.  $r_C$  represents the temperature in the current zone,  $D$  the diffusion coefficient,  $\gamma$  the zone temperature gain, and  $u$  the product temperature,  $\partial x$  represents the the conveyer direction:

$$\frac{\partial u}{\partial t} = D \frac{\partial^2 u}{\partial x^2} - \gamma(u - r_C)$$

### III. PDE TO STATE SPACE MODEL BY CRANK NICOLSON

On this, we apply the Crank Nicolson finite-difference scheme, [1], where  $i \in \mathbb{N}$  represents the position in the tunnel and  $j \in \mathbb{N}$  the time:

$$\begin{aligned} \frac{\partial u}{\partial t} &= \frac{u_i^{j+1} - u_i^j}{\Delta t} \\ &= \frac{1}{2} \left[ F_i^{j+1} \left( u, x, t, \frac{\partial u}{\partial x}, \frac{\partial^2 u}{\partial x^2} \right) \right] + \\ &+ \frac{1}{2} \left[ F_i^j \left( u, x, t, \frac{\partial u}{\partial x}, \frac{\partial^2 u}{\partial x^2} \right) \right] \end{aligned}$$

$$\begin{aligned} \frac{\partial^2 u}{\partial x^2} &= \frac{1}{2(\Delta x)^2} \left( (u_{i+1}^{j+1} - 2u_i^{j+1} + u_{i-1}^{j+1}) \right) + \\ &+ \frac{1}{2(\Delta x)^2} \left( (u_{i+1}^j - 2u_i^j + u_{i-1}^j) \right) \\ u &= \frac{1}{2} (u_i^{j+1} + u_i^j) \end{aligned}$$

By creating the following constants the next following algebra is simplified:

$$\alpha = \frac{D\Delta t}{2\Delta x^2} \quad \beta = \gamma * \Delta t$$

Now we substitute into the first equation, also we distinguish between last and next step by putting them on different sides:

$$\begin{aligned} &- \alpha u_{i-1}^{j+1} + (1 + 2\alpha + \frac{\beta}{2}) u_i^{j+1} - \alpha u_{i+1}^{j+1} \\ &= \alpha u_{i-1}^j + (1 - 2\alpha - \frac{\beta}{2}) u_i^j + \alpha u_{i+1}^j \end{aligned}$$

Let's express it as linear system:

$$A_2 u^{j+1} = B_2 u^j + d$$

with

$$A_2 = \begin{bmatrix} 1 + 2\alpha + \frac{\beta}{2} & -\alpha & 0 & \dots & 0 & 0 & 0 \\ -\alpha & 1 + 2\alpha + \frac{\beta}{2} & -\alpha & \dots & 0 & 0 & 0 \\ \dots & \dots & \dots & \dots & \dots & \dots & \dots \\ 0 & 0 & 0 & \dots & 0 & -\alpha & 1 + 2\alpha + \frac{\beta}{2} \end{bmatrix}$$

$$B_2 = \begin{bmatrix} 1 - 2\alpha - \frac{\beta}{2} & \alpha & 0 & \dots & 0 & 0 & 0 \\ \alpha & 1 - 2\alpha - \frac{\beta}{2} & \alpha & \dots & 0 & 0 & 0 \\ \dots & \dots & \dots & \dots & \dots & \dots & \dots \\ 0 & 0 & 0 & \dots & 0 & \alpha & 1 - 2\alpha - \frac{\beta}{2} \end{bmatrix}$$

The  $d$  vector represents the zone temperature impact at the specific position.

$$d = \begin{bmatrix} \beta r_1^j \\ \dots \\ \beta r_{n_z * n_p}^j \end{bmatrix}$$

With regard to an additional shift matrix  $S_1$  the band movement is taken into account, different speeds can then be achieved by taking  $S_1$  to the specific power:

$$S = S_1^v$$

The state space model,

$$u^{j+1} = Au^j + Bd$$

can then be obtained by setting  $A = SA_2^{-1}B_2$  and  $B = SA_2^{-1}$  which can then be used by a MPC for control issues. Also this model can easily be extended to calculate characteristic values like pasteurization units which are directly dependent of the product temperatures the model already provides.

### IV. RESULTS

The presented approach was realized for a tunnel pasteurizer with 12 coupled heating zones. The discretization in conveyor direction was set to 50, representing one meter of the physical plant length. The discretization in time was varied between 0,05 and 0,5. The implicit Crank Nicolson scheme delivered more robust and accurate results for larger  $\partial t$  compared to explicit Euler approach, becoming unstable solving the PDEs numerically.

### V. CONCLUSION

The shown approach delivers good results for online optimization of distributed parameter systems, representable as parabolic PDEs. Applying Crank Nicolson for discretization of the PDEs delivers State Space Models with high mathematical accuracy. The use of these State Space Models within the framework of MPC allows the application of both Input- and Output-constraints and guarantees low calculation load needed for online closed loop control.

### REFERENCES

- [1] J. Crank, P. Nicolson (1947) - A practical method for numerical evaluation of solutions of partial differential equations of the heat-conduction type, *Proc. Cambridge Philos. Soc.* 43 (1947), 50
- [2] U.S. Energy Information Administration (2013) - International Energy Outlook 2013, web site <http://www.eia.gov/forecasts/ieo/industrial.cfm>
- [3] Pavel Jonas (2009) - Modelling and Control of Tunnel Pasteurizers. *Diploma Thesis*, Czech Technical University Prague, Fac. Electr. Engineering.
- [4] Mikael Larsen (1997) -  $H_\infty$  Tracking Problems for a Distributed Parameter System. *PhD Thesis*, Technical University of Denmark, Department of Applied Mathematics and Computer Science
- [5] Jan M. Maciejowski (2002) - Predictive Control with Constraints, *Englewood Cliffs, NJ*. Prentice Hall, 2002
- [6] European Commission (2012), Energy efficiency directive 2012/27/EG, web site <http://eur-lex.europa.eu/LexUriServ/LexUriServ.do?uri=OJ:L:2012:315:0001:0056:EN:PDF>

## Oral presentations 3

# PID and decentralized control

Chair: Elling Jacobsen, KTH

### **Presentations:**

10. *Software-based optimal PID design with PI versus PID performance comparison*  
Olof Garpinger and Tore Hägglund  
Department of Automatic Control, Lund University, Lund, Sweden
11. *Industrial setup for autotuning of PID controllers in large-scale processes: Applied to Tennessee Eastman process*  
Selvanathan Sivalingam and Esmail Jahanshahi  
Technology & Innovation Department, Siemens AS, Trondheim, Norway
12. *Derivative Backoff: A Process Value Saturation Problem for PID Controllers*  
Alfred Theorin and Tore Hägglund  
LTH, Lund, Sweden
13. *Wireless process control - Handling of variable latency and sampling rates in PI controllers*  
Ivar J. Halvorsen, SINTEF, Applied Cybernetics, Trondheim
14. *Reconfiguration of Decentralized Controllers Using Closed-Loop Sensitivity Factorization*  
Wolfgang Birk  
Control Engineering Group, Luleå University of Technology, Sweden

# Software-based optimal PID design with PI versus PID performance comparison

Olof Garpinger \* Tore Hägglund \*

*\* Department of Automatic Control, Lund University, Lund, Sweden  
(e-mail: [olof,tore]@control.lth.se).*

---

**Abstract:** This work proposes a new PID design method that automatically picks the best controller from a set of PID, PI and I controllers. It uses a Matlab-based software to find controllers with optimal or near optimal load disturbance response subject to robustness and noise sensitivity constraints. The optimal controller type depends on the maximum allowed noise sensitivity as well as the process dynamics. The software is also used to compare PI and PID control performance with equivalent noise sensitivity and robustness over a large batch of processes representative for the process industry. This is used to show how much a particular process benefits from using the derivative part.

*Keywords:* Control system design; Measurement noise; Optimization; PID control; Software tools

---

# Derivative Backoff: A Process Value Saturation Problem for PID Controllers

Alfred Theorin (alfred.theorin@control.lth.se), Tore Hägglund

The PID controller is by far the most commonly used controller. To ensure good behavior under all circumstances, a PID implementation must consider many aspects. In particular, physical limits of signals must be considered. If physical limits for the control signal are not considered, there is integrator windup when the control signal saturates. An analogous issue has been discovered and named derivative backoff. If physical limits for the process value are not considered, there is derivative backoff when the process value saturates.

The derivative part of PID controllers predicts future process values by estimating the process value derivative. With a saturated process value there is no information about the process value derivative and thus the derivative part breaks down. At saturation, the derivative of the measured process value is 0 and, consequently, there is no derivative action. This makes sense as there is no information about future process values. However, the behavior when the process value saturates makes less sense, see Figure 1. Here, the process is controlled close to a physical limit (100) when a large load disturbance occurs. Just before the process value saturates, the process value derivative is positive, which means that the derivative action is negative. Shortly after the process value saturates, the derivative part is 0, that is, there is no derivative action. Together, this means that when the process value reaches its maximum, the negative derivative action backs off and thus the control signal increases. This is not a desirable behavior.

In Figure 1, the process  $P = \frac{1}{(s+1)^4}$  and its corresponding MIGO design method parameters have been used. Note that MIGO produces a robust controller with optimal load disturbance handling. The example shows what derivative backoff looks like and demonstrates that it is an issue for industrially relevant processes with well tuned PID controllers.

To implement anti-backoff, that is, to avoid derivative backoff, the derivative action needs to be kept when the process value saturates. Different anti-backoff approaches have been evaluated and the proposed solution is to disable and immediately re-enable the derivative part bumplessly when the process value saturates. This requires that the process value limits are known, which is true for most control loops. The PID controller must also have integral action, since it is otherwise not possible to bumplessly disable the derivative part. This is also true for most PID controllers with derivative action. Further investigation is needed to find a good solution for controllers without integral action.

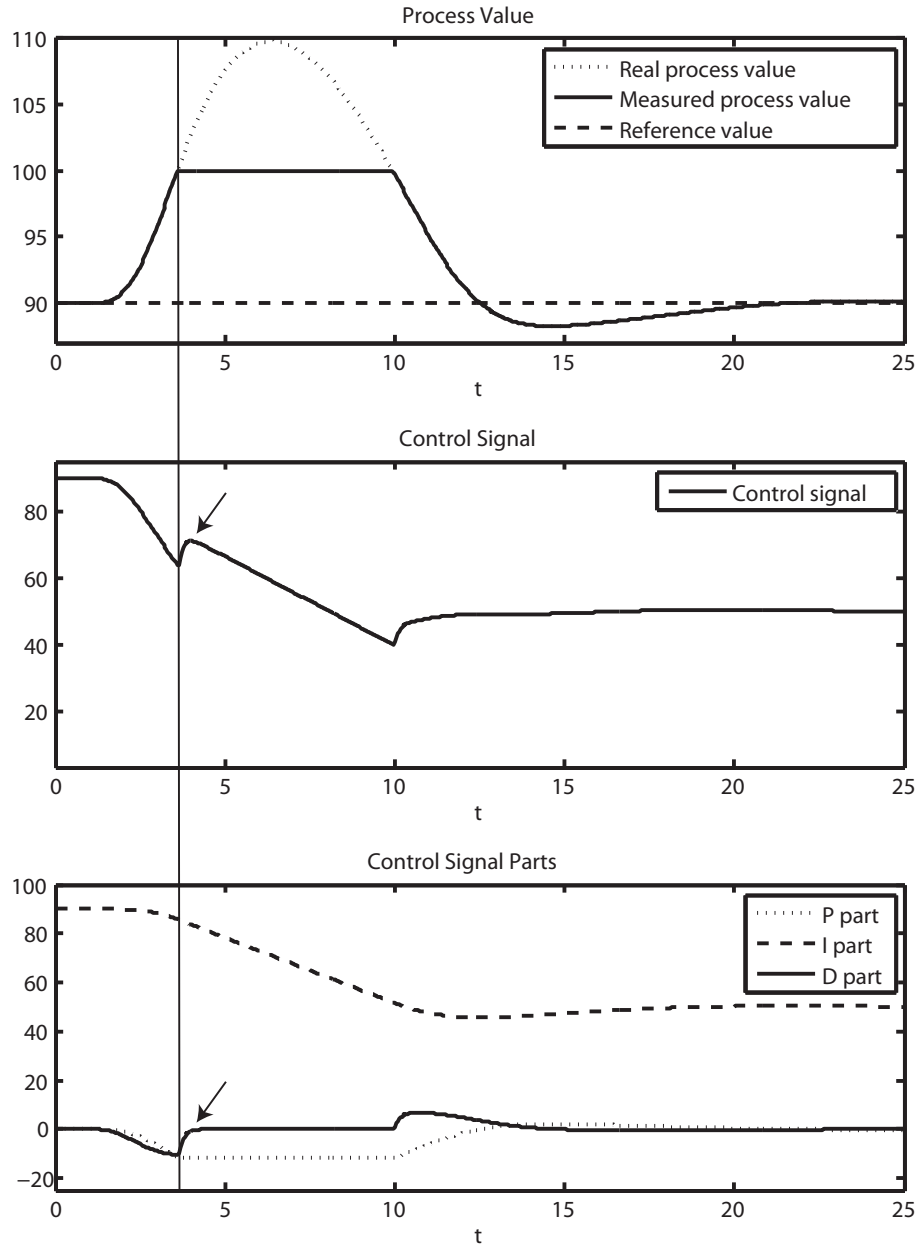


Figure 1: A large load disturbance occurs. When the process value saturates, the derivative part backs off and thus the control signal increases. The process value is thus pushed further away from the measurement range.

# **Industrial setup for autotuning of PID controllers in large-scale processes: Applied to Tennessee Eastman process**

**Selvanathan Sivalingam, Esmaeil Jahanshahi**

*Technology & Innovation Department, Siemens AS, Bratsbergvegen 5, 7037  
Trondheim, Norway (E-mail: selvanathan.sivalingam@siemens.com).*

Although many PID tuning approaches are available, it is not easy to find a method that does not require any engineer's / operator's interference. In this work, we present a fully automated method for PID tuning based on relay feedback. This work involves sending the relay feedback test data (from PLCs) into a historian, analyzing the test data using a tuning application to generate a tuning report that contains PID parameters and sending the report back to operator station to retune control loops in PLCs.

The relay-feedback method provides two pieces of information, namely ultimate gain and ultimate period which are used by for Ziegler–Nichols PI and PID tuning rules. However, these tuning rules do not provide a good trade-off between robustness and performance of control loops. On the other hand, PI and PID tuning rules based on IMC (Internal Model Control) design are preferred because of their Pareto-optimality between performance and robustness. The tuning test based on relay feedback can easily be automated which we use for model identification.

In this paper, we present an approach that contains three key steps: 1) Development of a method to identify persistent steady-state conditions in a control loop using routine operating data (Any tuning test is performed when the process is operating at steady state), 2) Development of a novel procedure to implement relay based tuning test, 3) Development of a combination of two model identification methods (frequency domain and time domain) to find the plant model using the test data. Subsequently, the identified plant model is used to obtain PI and PID tuning parameters based on IMC design.

The method for implementing the relay test also incorporates a logic to reject any external disturbance when the control loop is put into tune-mode. The approach has been tested on an industrial test setup in which all the control loops of the Tennessee Eastman process are controlled by a Siemens PLC (Programmable Logic Controller). The necessary relay parameters, the hysteresis and relay amplitude for the test are estimated automatically where interference by an engineer or an operator is not required. In addition, a new method for model identification is used which is robust against measurement noises. The proposed method is able to tune all the control loops in the Tennessee Eastman process successfully.

## Derivative Backoff: A Process Value Saturation Problem for PID Controllers

Alfred Theorin (alfred.theorin@control.lth.se), Tore Hägglund

The PID controller is by far the most commonly used controller. To ensure good behavior under all circumstances, a PID implementation must consider many aspects. In particular, physical limits of signals must be considered. If physical limits for the control signal are not considered, there is integrator windup when the control signal saturates. An analogous issue has been discovered and named derivative backoff. If physical limits for the process value are not considered, there is derivative backoff when the process value saturates.

The derivative part of PID controllers predicts future process values by estimating the process value derivative. With a saturated process value there is no information about the process value derivative and thus the derivative part breaks down. At saturation, the derivative of the measured process value is 0 and, consequently, there is no derivative action. This makes sense as there is no information about future process values. However, the behavior when the process value saturates makes less sense, see Figure 1. Here, the process is controlled close to a physical limit (100) when a large load disturbance occurs. Just before the process value saturates, the process value derivative is positive, which means that the derivative action is negative. Shortly after the process value saturates, the derivative part is 0, that is, there is no derivative action. Together, this means that when the process value reaches its maximum, the negative derivative action backs off and thus the control signal increases. This is not a desirable behavior.

In Figure 1, the process  $P = \frac{1}{(s+1)^4}$  and its corresponding MIGO design method parameters have been used. Note that MIGO produces a robust controller with optimal load disturbance handling. The example shows what derivative backoff looks like and demonstrates that it is an issue for industrially relevant processes with well tuned PID controllers.

To implement anti-backoff, that is, to avoid derivative backoff, the derivative action needs to be kept when the process value saturates. Different anti-backoff approaches have been evaluated and the proposed solution is to disable and immediately re-enable the derivative part bumplessly when the process value saturates. This requires that the process value limits are known, which is true for most control loops. The PID controller must also have integral action, since it is otherwise not possible to bumplessly disable the derivative part. This is also true for most PID controllers with derivative action. Further investigation is needed to find a good solution for controllers without integral action.

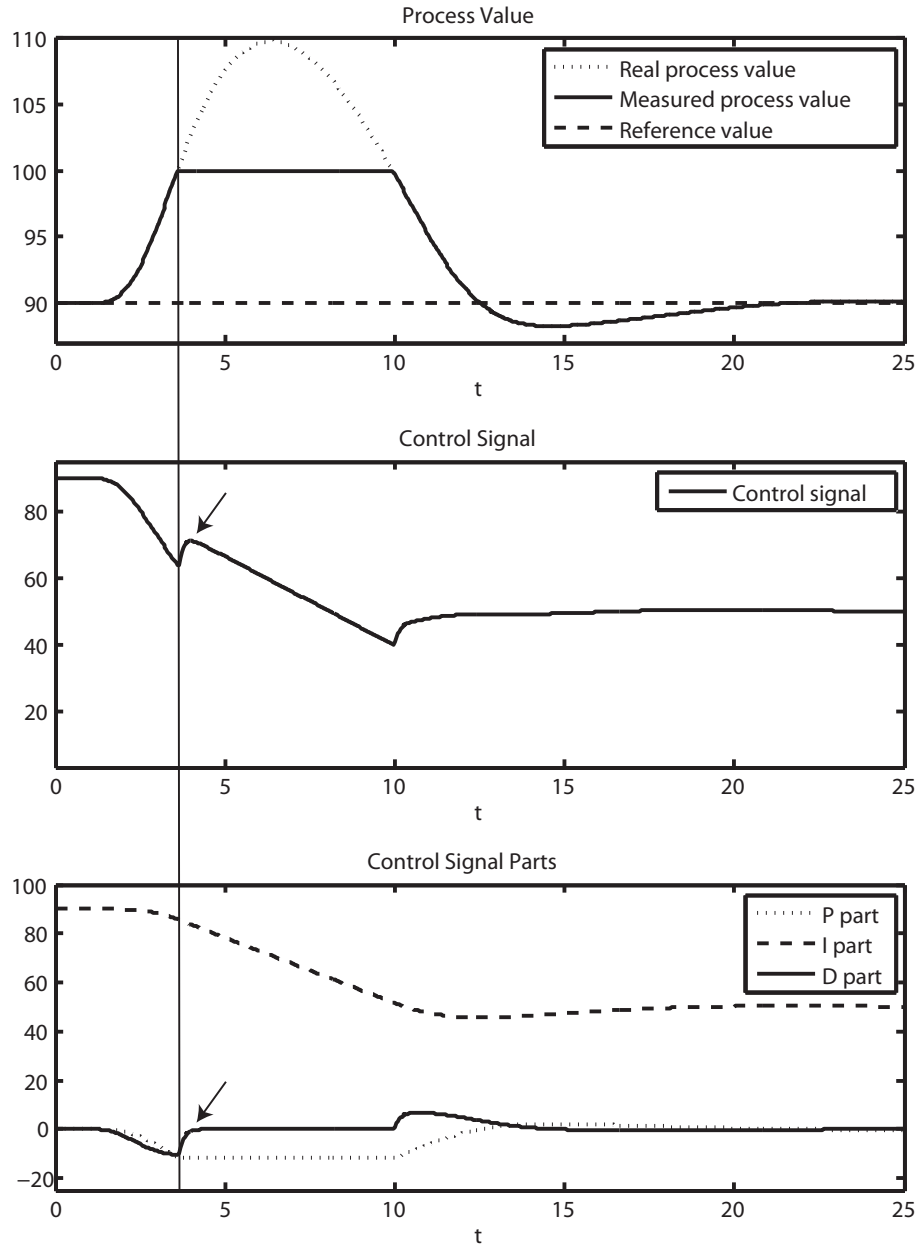


Figure 1: A large load disturbance occurs. When the process value saturates, the derivative part backs off and thus the control signal increases. The process value is thus pushed further away from the measurement range.

## Wireless process control - Handling of variable latency and sampling rates in PI controllers

Ivar J. Halvorsen, SINTEF ICT, Applied Cybernetics, Trondheim

### Abstract

When wireless instrumentation is included in process control loops, there are some properties that bring back the need for closer consideration of the sampling rates and the impact from the properties of the communication channel on the control performance. First, the wireless sampling rates are normally desired to be as slow as possible. This is both for the energy savings perspective (battery lifetime in the transmitter) and also to minimize the total radio traffic. There may also be irregularities and errors in the communication such as dropouts of measurement signals and transport delay or latency due to hops between nodes etc.

When looking into the control theory there will be a certain lower limit of the sample rate before the loop is degraded. The only way to get around this is to trade performance for stability margin and relax the controller settings in order to obtain sufficient stability margin, but reduce the speed and magnitude of the control actions. The need for feedback control actions is mainly determined by the magnitude and frequencies of the process disturbances. Thus, for the same loop, the need for actions will be different when there are little or slow acting disturbances compared to situations when there are large and fast acting disturbances. However, this can be exploited to relax control and reduce the sampling rates in calm periods.

A procedure for handling variable sample rates and latency in PI-control loops is presented. In addition, the sampling rate may be altered deliberately dependent on the actual process disturbance level. The key to a robust and safe operation is to adjust the controller parameters automatically in order to maintaining maximum performance with acceptable control loop behavior and stability margins for all expected situations. The presented procedure is based on well-known basic control theory and in particular the SIMC tuning method for PI and PID controllers (Skogestad 2003). The new contribution is how to use this to realize a gain scheduling based on knowledge of the actual transport delays or latency in the communication system.

The gain scheduling procedure is developed and the procedure is tested on two types of situations in a simulator:

1. Operation on variable sampling rates
2. Stochastic variations in dropouts and latency

### Acknowledgement:

The support of the WiCon project, funded by the Research Council of Norway (grant 201376/S10).

### References:

Waqas Ikram, Niklas Jansson, Trygve Harvei, Niels Aakvaag, Ivar Halvorsen, Stig Petersen, Simon Carlsen, Nina F. Thornhill, *Wireless Communication in Process Control Loop: Requirements Analysis, Industry Practices and Experimental Evaluation*, 19th IEEE International Conference on Emerging Technologies and Factory Automation (ETFA'2014), Barcelona (Spain) 16-19. September 2014.

S. Skogestad, "Simple rules for model reduction and PID controller tuning", *J. Process Control*, 13, 291-309 (2003).

# Reconfiguration of Decentralized Controllers Using Closed-Loop Sensitivity Factorization

Wolfgang Birk

**Abstract**—Reconfiguration of Decentralized Controllers in order to improve closed loop performance when there is no apparent fault has not received much attention. This paper discusses how a multivariable decentralized control scheme can be analyzed from the perspective of the performance loss and how the performance loss relates to a factorization of the closed loop sensitivity function. Some properties of the methods are shown, like e.g. the effect of model uncertainties and falsely tuned controller on the decision making. In the final paper an example will be used illustrate the results.

**Keywords**—interaction measures, control configuration, multi-variable control, process control

## I. INTRODUCTION

In a complex process, many process variables interact due to the process characteristics. It is also a well-known fact that the selected control configuration limits the achievable performance of a process control system. In turn, the potential improvement in performance is limited by the achievable performance. A general solution to the quantification of these performance bounds in face of structural constraints on the controller is an active area of research, see e.g. [1] and [2]. When it comes to the reconfiguration of controllers due to performance issues, it is the belief of the author that there is a lack of procedures that support control engineers to systematically reconfigure controller configurations and quantify the performance improvement a-priori. Nevertheless, there is a vast bulk of methods from controller configuration selection and performance assessment that could be combined.

Traditionally, interaction measures are used for control configuration selection of multivariable processes. The relative gain array (RGA) [3] and its dynamic version [4] are popular for the control configuration selection of decentralized controllers. Based on these concepts a host of tools has been created and a good overview is given in [5]. The advantages of RGA and its dynamic counterpart were combined and the effective relative gain array (ERGA) was suggested [6] to provide integral indications of loop interactions. More recently, gramian based interaction measure were proposed [7], [8] and [9], which support the selection of controllers, that are less sparse.

---

W. Birk is with the Control Engineering Group, Department of Computer Science, Electrical and Space Engineering, Luleå University of Technology, SE-971 87 Luleå, SWEDEN

The work has been conducted within the MeSTA and EQoRef project that is hosted at ProcessIT Innovations at Luleå University of Technology and run within the branch framework SCOPE. Funding provided by VINNOVA, Hjalmar Lundbohm Research Centre and the participants of the SCOPE consortium, is hereby gratefully acknowledged.

A drawback of the above interaction measures is that stability of the closed loop system is not guaranteed and that neither performance of the closed loop system nor the current controller configuration is considered. In [10] a factorization of the closed loop sensitivity function is proposed, where the relative model error is used. Based on this result, [11] and [12] derive a quantification of the performance loss due to neglected dynamics. The block relative gain (BRG) [13], [14] was performed like an extension of RGA to analyse block pairing and estimate the performance and stability of decentralized control structure. Another useful addition to RGA is the partial relative gain (PRG) [15]. The PRG is calculated for the relevant subsystems and points to infeasible control structures. It is also possible to compare feasible control structures with each other using PRG.

Despite the fact that there is a huge bulk of publications in the area of control configuration selection, rather little is published on the assessment of control configurations and their reconfiguration. Recently, [16] and [17] used the difference between the complementary sensitivity functions of the ideal and the actual closed loop system to provide a performance based structure selection process. In [18], it is shown how the performance difference between desired and achieved performance is related to the relative model error and how it can be used to reconfigure the currently used control scheme.

Therefore, the aim of this paper is to investigate the properties of a reconfiguration procedure which is based the factorization of the closed loop sensitivity functions.

## II. METHODS FOR CONTROLLER RECONFIGURATION

Reconfiguration of a multivariable controller means that the current controller  $K^{(n)}$  is reconfigured into the controller  $K^{(n+1)}$ . Here, it is important to note the reconfigured controller contains the structure of  $K^{(n)}$  or not. In this paper it is assumed that  $K^{(n+1)}$  builds upon  $K^{(n)}$  and increases the complexity of the control scheme incrementally.

Quantification of the structural mismatch of a multivariable decentralized control system can be based on the factorization of the closed loop sensitivity transfer function matrices and was first presented in [10] and restated in [18]. There, a method was proposed to derive indications on how a control system could be improved.

When a decentralized controller  $K$  is applied to a multivariable process  $G$  as depicted in Fig. 1 the controller design is usually based on the model

$$\hat{G} \triangleq \text{diag}(G_{11}, \dots, G_{nn})$$

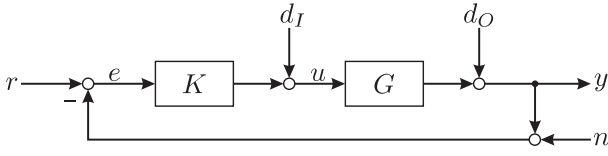


Fig. 1. Block diagram of a 1-DOF closed loop system

where the neglected dynamics between  $G$  and  $\hat{G}$  is given by

$$\tilde{G} \triangleq G - \hat{G}$$

The sensitivity transfer function matrices for the closed loop system in Fig. 1 with and without neglected dynamics are  $S = (I + GK)^{-1}$  and  $\hat{S} = (I + \hat{G}K)^{-1}$ , respectively. Moreover, the complementary sensitivity transfer function matrices are easily derived from  $T = I - S$  and  $\hat{T} = I - \hat{S}$ .

$\hat{T}$  and  $\hat{S}$  are a function of  $K$  and  $\hat{G}$ . Clearly,  $\hat{T}$  and  $\hat{S}$  coincide with  $T$  and  $S$  only if  $\tilde{G} = 0$ . Moreover,  $\hat{T}$  and  $\hat{S}$  can be interpreted as the performance requirements for the closed loop system and the controller  $K$  is designed according to them.

In [18], the following important relationships have been shown for the factorization:

$$\Delta = \hat{S}\tilde{G}K \quad (1)$$

$$\Delta S = \hat{T} - T \quad (2)$$

Clearly,  $\Delta$  is a description of the mismatch between  $T$ ,  $S$  and  $\hat{T}$ ,  $\hat{S}$ , respectively. Moreover,  $\Delta$  has the same structure as  $\tilde{G}$ , which is due to the special structure of  $\hat{S}$ ,  $\tilde{G}$  and  $K$ .

Since both  $\hat{S}$  and  $K$  are diagonal transfer function matrices and  $\tilde{G}$  has zero diagonal elements, it can be shown that  $\Delta$  has the same structure as  $\tilde{G}$ . The elements of  $\Delta$  are given by

$$[\Delta]_{ij} = \begin{cases} 0, & i = j \\ \hat{S}_{ii}G_{ij}K_{jj}, & \text{otherwise} \end{cases} \quad (3)$$

Hence, each off-diagonal element in  $\Delta$  is a filtered version of the corresponding off-diagonal element in  $G$

$$[\Delta]_{ij} = G_{ij} \frac{K_{jj}}{1 + G_{ii}K_{ii}}, \quad \text{with } i \neq j \quad (4)$$

Furthermore, the following relationship holds

$$\Delta S = \hat{T} - T \quad (5)$$

and can be interpreted that the deviation of the desired output  $\hat{y}$  and achieved output  $y$  due to a reference input  $r$  depends on  $\Delta$ . In fact, by denoting the output deviation  $\tilde{y} = \hat{y} - y$  and the control error as  $e = r - y$ ,  $\Delta$  represents the transfer function matrix from the control error  $e$  to the deviation  $\tilde{y}$ .

Most importantly, (5) gives as factorization of the performance deviation in terms of the closed loop sensitivity transfer function matrix  $S$  and  $\Delta$ . Deriving the maximum singular value  $\bar{\sigma}(\Delta S)$  yields a quantification of the deviation for different frequencies and thus, a quantification of the performance degradation for different frequencies.

The magnitude of the non-zero elements of  $\Delta$  indicate the contribution of the associated element in the neglected

dynamics to the performance degradation. Instead of directly assessing the magnitude, an index array can be used, [9], [19]. The elements of an  $\mathcal{H}_\infty$ - or  $\mathcal{H}_2$ -based index array are given by

$$[\Sigma_\bullet(\Delta)]_{ij} = \frac{\|\Delta_{ij}\|_\bullet}{\sum_{ij} \|\Delta_{ij}\|_\bullet} \quad (6)$$

where  $\bullet$  indicates the used norm.

### III. PROPERTIES OF THE METHOD

The following properties of the reconfiguration procedure will be shown in the final paper:

- Model uncertainties in the process matrix  $\hat{G}$  are reflected on the diagonal of the transfer matrix  $\Delta$ . As a result the magnitude of the diagonal elements can be used as a minimal decision threshold for the reconfiguration.
- Similarly, it can be shown that tuning deficiencies of the decentralized controller are reflected on the diagonal of  $\Delta$ . The cause for performance loss can therefore be narrowed down to either uncertainties in the process model or problems in the controller tuning. As a result unnecessary controller tuning can be avoided.
- Depends on the scaling of the controlled variables  $y$ .
- For a block diagonal controller  $K$ ,  $\Delta$  becomes block diagonal with zeroes on the block diagonal.

### IV. CONCLUSIONS

A method for the reconfiguration of multivariable decentralized controllers is proposed. In the final version of the paper several properties of the method are proven and exemplified on an example.

### REFERENCES

- [1] M. Salgado, E. Silva *et al.*, "Achievable performance bounds for tall mimo systems (brief papers)," *IET control theory & applications*, vol. 5, no. 5, pp. 736–743, 2011.
- [2] M. Cea and M. Salgado, "Performance bounds on the control of highly sparse discrete-time multivariable systems," *Control Theory & Applications, IET*, vol. 4, no. 8, pp. 1319–1329, 2010.
- [3] E. Bristol, "On a new measure of interaction for multivariable process control," *IEEE Transactions on Automatic Control*, vol. 11, pp. 133–134, January 1966.
- [4] M. Hovd and S. Skogestad, "Simple frequency-dependent tools for control systems analysis, structure selection and design," *Automatica*, vol. 28, no. 5, pp. 989–996, 1992.
- [5] A. Khaki-Sedigh and B. Moaveni, *Control Configuration Selection for Multivariable Plants*, ser. Lecture Notes in Control and Information Sciences, M. Thomas, F. Allgöwer, and M. Morari, Eds. Springer, 2009.
- [6] W.-J. C. Xiong Qiang and M.-J. He, "A practical loop pairing criterion for multivariable processes," *Journal of Process Control* 15.7, pp. 741–747, 2005.
- [7] B. Wittenmark and M. E. Salgado, "Hankel-norm based interaction measure for input-output pairing," in *Proc. of the 2002 IFAC World Congress, Barcelona*, 2002.
- [8] M. E. Salgado and A. Conley, "MIMO interaction measure and controller structure selection," *International Journal of Control*, vol. 77, no. 4, pp. 367–383, 2004.

- [9] W. Birk and A. Medvedev, "A note on gramian-based interaction measures," in *Proc. of European Control Conference ECC, Cambridge, UK*, 2003, pp. 2660–5.
- [10] G. Zames and D. Bensoussan, "Multivariable Feedback , Sensitivity , and Decentralized Control," *IEEE Transactions on Automatic Control*, vol. 28, no. 11, pp. 1030–1035, 1983.
- [11] Y. Arkun, "Relative sensitivity: a dynamic closed-loop interaction measure and design tool," *American Institute of Chemical Engineers Journal*, 34, 1988.
- [12] P. Grosdidier and M. Morari, "The  $\mu$  interaction measure," *Ind. Eng. Chem Res.*, vol. 26, pp. 1193–1202, 1987.
- [13] V. Manousiouthakis, R. Savage, and Y. Arkun, "Synthesis of decentralized process control structures using the concept of block relative gain," *AIChE Journal*, vol. 32, no. 6, pp. 991–1003, 1986.
- [14] Y. Arkun, "Dynamic block relative gain and its connection with the performance and stability of decentralized control structure," *International Journal of Control*, 1987.
- [15] K. E. Häggblom, "Control structure analysis by partial relative gains," in *Proc. of the 36th Conference on Decision & Control, San Diego, USA*, December 1997, pp. 2623–2624.
- [16] J. Lee and T. F. Edgar, "Dynamic interaction measures for decentralized control of multivariable processes," *Ind. Eng. Chem. Res.*, vol. 43, pp. 283–287, 2004.
- [17] H. Schmidt and E. W. Jacobsen, "Selecting control configurations for performance with independent design," *Computers & chemical engineering*, vol. 27, no. 1, pp. 101–109, 2003.
- [18] W. Birk, "Towards incremental control structure improvement," in *Proc of 46th IEEE Conference on Decision and Control, New Orleans, USA*, 2007.
- [19] B. Wittenmark and M. E. Salgado, "Hankel-norm based interaction measure for input-output pairing," in *Proc. of the 2002 IFAC World Congress, Barcelona*, 2002.

## Oral presentations 4

# Applications

Chair: Tore Hägglund, Lund Univ.

### Presentations:

15. *A mid-ranging control strategy for non-stationary processes and its application to dissolved oxygen control in a bioprocess*  
O. Johnsson\*, D. Sahlin\*\*, J. Linde\*\*\*\*, G. Liden\*\*\*, T. Hägglund\*  
\* Department of Automatic Control, Lund University, Sweden  
\*\* Novozymes A/S, Denmark  
\*\*\* Department of Chemical Engineering, Lund University, Sweden
16. *Integrated Process Design and Control of Reactive Distillation Processes*  
Seyed Soheil Mansouri\*, Mauricio Sales Cruz\*\*, Jakob Kjøbsted Huusom\*, John M. Woodley\*, Rafiqul Gani\*  
\* DTU, Lyngby, Denmark  
\*\* UAM, Mexico
17. *A Mean-Variance Objective for Robust Production Optimization in Uncertain Geological Scenarios*  
Andrea Capolei<sup>a</sup>, Eka Suwartadi<sup>b</sup>, Bjarne Foss<sup>b</sup>, John Bagterp Jørgensen<sup>a</sup>  
<sup>a</sup>Department of Applied Mathematics and Computer Science & Center for Energy Resources Engineering, Technical University of Denmark, Lyngby, Denmark.  
<sup>b</sup>Department of Engineering Cybernetics, NTNU, Trondheim, Norway
18. *Modelling and Model Predictive Control of ESP lifted wells*  
Alexey Pavlov, Dinesh Krishnamoorthy, Elvira Marie B. Aske, Kjetil Fjalestad and Morten Fredriksen. Statoil Research Centre, Norway.

# A mid-ranging control strategy for non-stationary processes and its application to dissolved oxygen control in a bioprocess

O. Johnsson\* D. Sahlin\*\* J. Linde\*\*\* G. Lidén\*\*\*  
T. Hägglund\*

\* *Department of Automatic Control, Faculty of Engineering LTH,  
Lund University, Sweden*

\*\* *Novozymes A/S, Hallas Alle 1, 4400 Kalundborg Denmark*

\*\*\* *Department of Chemical Engineering, Faculty of Engineering LTH,  
Lund University, Sweden*

---

**Abstract:** In this study we propose a modified mid-ranging strategy where the controller for the secondary manipulated variable uses its own output as its setpoint, possibly with an offset and/or re-scaling. This modification allows the manipulated variables to increase in unison so that the mid-ranging advantage of utilizing the fast dynamics of the primary controller to regulate the process can be achieved also in non-stationary processes, while not adding complexity to the controller. The proposed control strategy has been implemented in pilot-scale (500 l) industrial bioprocesses where it is used to control the dissolved oxygen level by manipulating agitator speed and aeration rate. The controller is demonstrated to perform well in these, outperforming a reference controller which has previously been shown to give satisfactory control performance. It is also shown in similar experiments that the strategy can easily be adapted to control dissolved oxygen in bioprocesses where the feed rate is controlled using an extremum-seeking controller. The proposed strategy is generally applicable to non-stationary processes where a mid-ranging approach is suitable.

Keywords: mid-ranging control, process control, control architecture, industrial bioprocess, dissolved oxygen control

---

# Integrated Process Design and Control of Reactive Distillation Processes

Seyed Soheil Mansouri\*, Mauricio Sales Cruz\*\*, Jakob Kjøbsted Huusom\*, John M. Woodley\*, Rafiqul Gani\*

\*CAPEC-PROCESS, Department of Chemical and Biochemical Engineering,  
Technical University of Denmark, Lyngby, Denmark

\*\*Departamento de Procesos y Tecnología,

Universidad Autónoma Metropolitana-Cuajimalpa, México D.F., Mexico

(e-mail: seso@kt.dtu.dk, asales@correo.cua.uam.mx, jkh@kt.dtu.dk, jw@kt.dtu.dk, rag@kt.dtu.dk)

---

**Abstract:** In this work, integrated design and control of reactive distillation processes is presented. Simple graphical design methods that are similar in concept to non-reactive distillation processes are used, such as reactive McCabe-Thiele method and driving force approach. The methods are based on the element concept, which is used to translate a system of compounds into elements. The operation of the reactive distillation column at the highest driving force and other candidate points is analyzed through analytical solution as well as rigorous open-loop and closed-loop simulations. By application of this approach, it is shown that designing the reactive distillation process at the maximum driving force results in an optimal design in terms of controllability and operability. It is verified that the reactive distillation design option is less sensitive to the disturbances in the feed at the highest driving force and has the inherent ability to reject disturbances.

**Keywords:** Process design, Process control, Driving force, Reactive distillation, Element-based method

---

## 1. INTRODUCTION

Traditionally, process design and process control are considered as independent problems, that is, a sequential approach is used where the process is designed first, followed by the control design. The limitations with the sequential approach are related to dynamic constraint violations, for example, infeasible operating points, process overdesign or under performance. Therefore, this approach does not guarantee robust performance (Seferlis and Georgiadis, 2004). Furthermore, process design decisions can influence process control and operation. To overcome the limitations associated with the sequential approach, operability and controllability are considered simultaneously with process design, in order to assure that design decisions give the optimum operational and economic performance. In control design, operability addresses stability and reliability of the process using *a priori* operational conditions and controllability addresses maintaining desired operating points of the process subject to disturbances.

A number of methodologies and tools have been proposed for addressing the interactions between process design and control, and they range from optimization-based approaches to model-based methods (Luyben and Floudas, 1994; Nikacevic *et al.*, 2012).

In this work, integrated design and control of reactive distillation processes is considered, since process design decisions will influence process operability and controllability. Numerous design algorithms for multi-component separation systems with reactions have accompanied the increasing interest in reactive distillation

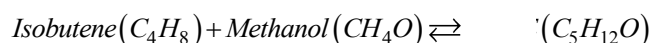
processes. In design, the input and (selected) output variables are specified and the task is to determine the optimal reactive distillation process configuration (for example, minimum number of stages), and the optimal design parameters (for example, optimum reflux ratio, optimal feed location) that achieve the given product specification. It is intended to achieve the optimal design in such way that it is also an operable process at pre-defined conditions under presence of disturbances.

Pérez-Cisneros *et al.* (1997) have proposed an element mass balance approach to design the reactive distillation processes, which employs the traditional graphical tools similar in concept to design of non-reactive distillation columns, such as McCabe-Thiele method and driving force approach of Bek-Pedersen and Gani (2004). Moreover, Hamid *et al.* (2010) have proposed an integrated process design and controller design methodology. However, their methodology covers the aspects related to design and control of non-reactive binary distillation processes. In this work, the method of Hamid *et al.* (2010) is extended to also cover a ternary compound reactive distillation process (using element-based approach) and criteria of selecting the optimal design and the controller structure selection will be presented. In order to demonstrate the application of the aforementioned approach, production of methyl-tert-butyl-ether (MTBE) from methanol and isobutene using a reactive distillation column is considered.

## 2. REACTIVE DISTILLATION COLUMN DESIGN

The computation of simultaneous chemical and physical equilibrium plays an important role in the prediction of the

limits for conversion and separation of a specific reactive separation process, particularly for the reactive distillation systems. Using the Gibbs free energy minimisation approach, Pérez-Cisneros *et al.* (1997) proposed solution procedures where the multicomponent chemical and physical equilibrium is posed as an “element phase” equilibrium problem. This transformation is based on the concept of chemical model as proposed by Michelsen (1989). This concept is derived from chemical model theory, where, the equations of chemical equilibrium together with any appropriate physical model yielding the chemical potentials are incorporated into an element-based model (called the chemical model). The main difference between the chemical model algorithm and those developed earlier, is the use of the chemical models in a way that renders the chemical and physical equilibrium problem formally identical to the physical equilibrium problem for a mixture of element (representing the system). Further details can be found in (Pérez-Cisneros, 1997; Daza *et al.*, 2003). The reaction for MTBE synthesis is given as follows:



It is evident that the selection of the elements has an important role in the present formulation. They are traditionally chosen as the “natural” chemical elements present in the reaction mixture, but, indeed, one is free to select any reaction invariant fragment of the reactants. The element matrix is constructed based on the rules provided by Pérez-Cisneros *et al.* (1997) and it is as follows:

Element	Component		
	C <sub>4</sub> H <sub>8</sub> (1)	CH <sub>4</sub> O (2)	C <sub>5</sub> H <sub>12</sub> O (3)
A	1	0	1
B	0	1	1

Therefore, the ternary system of compounds can be reduced into a binary system of elements *A* and *B* and the reaction can be rewritten as:  $A + B \rightleftharpoons AB$ . The first component (element *A*) and the second component (element *B*) form the third component (element *AB*). Having the ternary system of compounds represented in form of a binary element system, similar graphical design methods, that are applied to non-reactive binary distillation column design, such as McCabe-Thiele method can be used. However, in order to use the McCabe-Thiele method, a reactive equilibrium curve is required. The reactive equilibrium curve is constructed through sequential computation of reactive bubble points (Pérez-Cisneros, 1997). In order to generate the reactive dataset, Wilson thermodynamic model for prediction of the liquid phase behaviour and SRK equation of state for prediction of vapour phase behaviour were used. Note that the calculation of reactive vapour-liquid equilibrium (VLE) data set is in terms of compounds. Therefore, a ternary compound data set is obtained. To convert this data set to be represented in form of a binary element system the following expressions are used where mole fractions of elements *A* and *B* are calculated in the liquid phase:

$$W_A^l = \frac{x_1 + x_3}{x_1 + x_2 + 2 \cdot x_3} \quad (1)$$

$$W_B^l = \frac{x_2 + x_3}{x_1 + x_2 + 2 \cdot x_3} \quad (2)$$

In the above equations  $W_A^l$  and  $W_B^l$  are the liquid mole fractions of elements *A* and *B*, respectively. For calculation of the element mole fractions in vapour phase ( $W_A^v$  and  $W_B^v$ ), the equations used are the same as (1) and (2) where instead of liquid molar fraction ( $x_i$ ), the vapour molar fraction ( $y_i$ ) is used. Fig. 1 depicts the temperature (*T*)- $W_A$  diagram for MTBE reactive system.

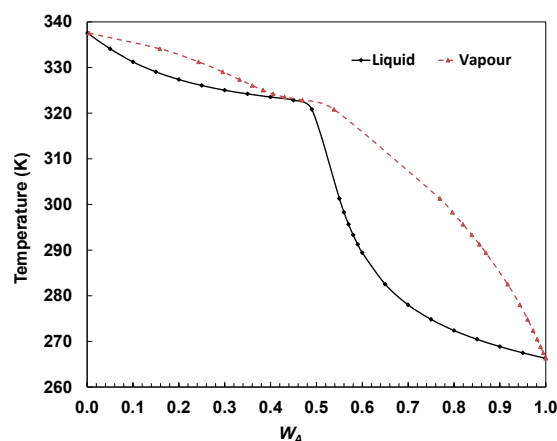


Fig. 1.  $T$ - $W_A^v$ - $W_A^l$  diagram for MTBE reactive system ( $P = 1$  atm).

The design task is to separate a binary element mixture that is 70 mole percent element *A* ( $z_{W_Af} = 0.7$ ,  $z_{W_Bf} = 0.3$ ) into 50 element mole percent bottoms product ( $W_{AB}^l = 0.50$ ) and 99 element mole percent distillate ( $W_{A,d}^l = 0.99$ ) product. Note that based on the binary element reaction matrix, element *A* and *B* correspond to isobutene and methanol, respectively. The element feed flow rate is 100 Kg-mole element/hr at 300K and 1 atm. The operating pressure of the reactive distillation column is 1 atm and pressure drop across the column is assumed to be negligible. The reflux element ratio (RR) is 2. The physical and chemical equilibrium curve is constructed using the data set presented in Fig. 1. Theoretical reactive stages are calculated from the reactive McCabe-Thiele method. A partial reboiler, total condenser and chemically saturated liquid reflux are set for the column. In order to design the described reactive distillation column for MTBE synthesis, McCabe-Thiele method is used. Fig. 2 depicts the reactive distillation column design using reactive McCabe-Thiele method. As it is shown in Fig. 2, the reactive distillation column has five reactive stages.

Daza *et al.* (2003) have extended the driving force (DF<sub>*i*</sub>) method for non-reactive systems (Bek-Pedersen and Gani, 2004) to include reactive systems. Similar in concept to non-reactive systems, the driving force is defined as the difference in composition between two coexisting phases. The driving-force design method for reactive as well as non-reactive distillation systems is based on the availability of data for the vapour-liquid behaviour. In the case of reactive systems, the vapour-liquid equilibrium data must be based on the elements (see Fig. 1).

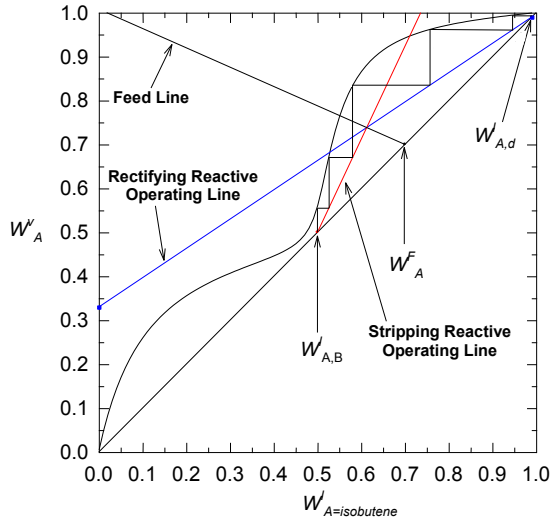


Fig. 2. Reactive distillation column design. Reactive McCabe-Thiele method for the MTBE reactive system.

The driving-force diagram can only exploit binary interaction between compounds or elements in two coexisting phases, or two compounds on a solvent-free basis. Note that the element-based driving-force diagram fully incorporates the extent of reaction on an element basis, and, therefore, it can be applied in the design of reactive distillation columns. Provided the element vapour-liquid behaviour data exist, or can be computed (which is the case in this study, see Fig. 1), the reactive driving-force diagram can be obtained using (3) with respect to the elements.

$$DF_i = W_i^v - W_i^l = \frac{W_i^l \alpha_{ij}}{1 + W_i^l (\alpha_{ij} - 1)} - W_i^l \quad (3)$$

The driving force concept is used to find the optimal (design target) values of the process variables for separation systems. Based on identification of the largest driving force (see Fig. 3), defined as the difference in composition of a component  $i$  between the vapour phase and the liquid phase, which is caused by the difference in the volatilities of component  $i$  and all other components in the system. Fig. 3 shows the driving force diagram for MTBE reactive system at 1 atm. As the driving force decreases, separation becomes difficult and may become infeasible when the driving force approaches zero. On the other hand, as the driving force approaches its maximum value, the separation becomes easier. Therefore, from a process design point of view, a separation process should be designed/selected at the highest possible driving force, which will naturally lead to the optimal design with respect to the energy consumption (Bek-Pedersen and Gani (2004)).

In this work, the optimal feed location of the reactive distillation column is determined using the driving force diagram. Reactive McCabe-Thiele method has been only used to determine the number of stages. The feed and product specifications are already known since they were used in the reactive McCabe-Thiele method. The optimal feed location at the maximum driving force can be found using (4).

$$N_F = N(1 - D_x) \quad (4)$$

In (4),  $N$  is the number of stages which was obtained from the reactive McCabe-Thiele method (was found to be 5);  $D_x$  is the value corresponding to the maximum driving force on the  $x$ -axis ( $D_x = 0.61$ ). The optimal feed location is identified using the additional rules for driving force (Bek-Pedersen and Gani, 2004) and therefore it is stage 1 from the top of the column.

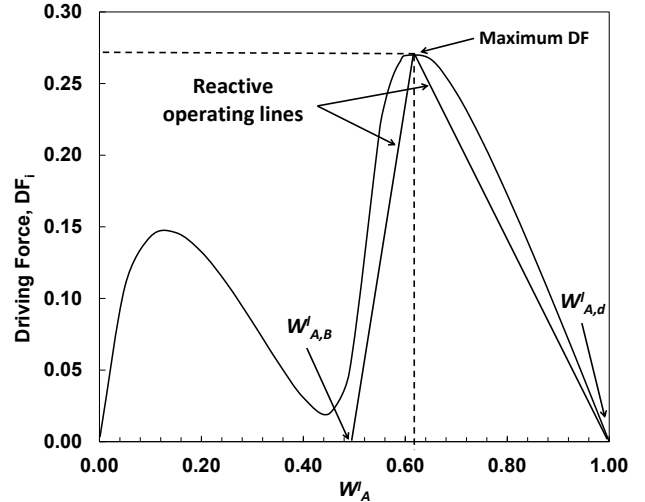


Fig. 3. Reactive driving force diagram for MTBE reactive system).

### 3. OPTIMAL DESIGN-CONTROL SOLUTIONS

From a process design point of view, for specified inputs,  $u$ , and disturbances,  $d$ , values for states,  $x$ , and outputs,  $y$ , that satisfy a set of design specifications (process design objectives) are determined. In this case,  $x$  and  $y$  also define some of the operational conditions for the process. From a controller design point of view, for any changes in  $d$  and/or set point values in  $y$ , values of  $u$  that restores the process to its optimal designed condition are determined. It should be noted that the solution for  $x$  and  $y$  is directly influenced by  $\theta$  (the constitutive variables such as reaction rate or equilibrium constant). For example, the optimal solution for  $x$  and  $y$  can be obtained at the maximum point of the reactive driving force (for reactive systems, see Fig. 3) diagrams which are based on  $\theta$ . By using model analysis, the corresponding derivative information with respect to  $x$ ,  $y$ ,  $u$ ,  $d$  and  $\theta$  can be obtained (to satisfy controller design objectives).

For each reactive distillation column design problem, the driving force diagram is drawn and the design target is selected at the highest driving force (see Fig. 3). From a process design point of view, at these targets, the optimal design objectives can be obtained. From a controller design point of view, at these design targets the controllability and operability of the process is best satisfied. The value of the derivative of controlled variables  $y$  with respect to disturbances in the feed,  $d$ ,  $dy/dd$  and manipulated variables,  $u$ ,  $dy/du$  will determine the process sensitivity and influence the controller structure selection. Accordingly,  $dy/dd$  and  $dy/du$  are defined as (Russel et al., 2002):

$$\frac{dy}{dd} = \left( \frac{dy}{d\theta} \right) \left( \frac{d\theta}{dx} \right) \left( \frac{dx}{dd} \right) \quad (5)$$

$$\frac{dy}{du} = \left( \frac{dy}{d\theta} \right) \left( \frac{d\theta}{dx} \right) \left( \frac{dx}{du} \right) \quad (6)$$

The values for  $d\theta/dx$  can be obtained from the process (dynamic and/or steady state) constraints:

$$\frac{dx}{dt} = f(x, y, u, d, \theta, Y, t) \quad (7)$$

and values for  $dy/d\theta$ ,  $dx/dd$  and  $dx/du$  can be obtained from constitutive (thermodynamic) constraints:

$$0 = g_1(v, x, y) - \theta \quad (8)$$

### 3.1. Selection of Controlled Variables

The primary controlled variable is  $D_{x_{max}}$ , which is the  $x$ -axis value corresponding to the maximum driving force ( $DF_i$ ). This resembles the purity of element A at the maximum driving force. The secondary controlled variables are the product purities, which are the desired product composition at the top and bottom of the column,  $W_A^d$  and  $W_A^B$ . The reason behind this selection is that by controlling  $W_A^d$  and  $W_A^B$  at the maximum point of the driving force will require less control effort in terms of reflux ratio (RR), and reboil ratio (RB) in the presence of disturbances in the feed compared to any other candidate point.

### 3.2. Sensitivity of Controlled Variables to Disturbances

There are several key concepts in analyzing the sensitivity of controlled variables to the disturbances in the feed which are outlined as follows:

- The desired element product at the top and the bottom is  $W_A^d$  (product element composition at the top, distillate product) and  $W_A^B$  (element composition at the bottom, bottom product).
- At the maximum point of the driving force diagram,  $W_A^d$  and  $W_A^B$  (controlled variables) are the least sensitive to the imposed disturbances in the feed.
- The design variables vector is  $y = [W_A^d \quad W_A^B]$ ,  $x = DF_i$ , is selected on the  $y$ -axis of the driving force diagram.
- The disturbances vector is,  $d = [F_f \quad z_{W_{Af}}]$  (feed flowrate and feed composition of element A).

Using the above key concepts, the sensitivity of variable  $y$  with respect to variable  $d$  can be expressed as follows:

$$\frac{dy}{dd} = \begin{bmatrix} \frac{dW_A^d}{dF_f} & \frac{dW_A^d}{dz_{W_{Af}}} \\ \frac{dW_A^B}{dF_f} & \frac{dW_A^B}{dz_{W_{Af}}} \end{bmatrix} = \begin{bmatrix} \left( \frac{dW_A^d}{dDF_i} \right) \left( \frac{dDF_i}{dW_A^d} \right) \left( \frac{dW_A^d}{dF_f} \right) & \left( \frac{dW_A^d}{dDF_i} \right) \left( \frac{dDF_i}{dW_A^d} \right) \left( \frac{dW_A^d}{dz_{W_{Af}}} \right) \\ \left( \frac{dW_A^B}{dDF_i} \right) \left( \frac{dDF_i}{dW_A^B} \right) \left( \frac{dW_A^B}{dF_f} \right) & \left( \frac{dW_A^B}{dDF_i} \right) \left( \frac{dDF_i}{dW_A^B} \right) \left( \frac{dW_A^B}{dz_{W_{Af}}} \right) \end{bmatrix} \quad (9)$$

The reactive element operating lines for the rectifying section and stripping sections are given in (10) and (11). RR is the element reflux ratio, and RB is the element reboil ratio.

$$W_A^v = \frac{RR}{RR+1} W_A^l + \frac{1}{RR+1} W_A^d \quad (10)$$

$$W_A^v = \frac{RB+1}{RB} W_A^l - \frac{1}{RB} W_A^B \quad (11)$$

Substituting (10) and (11) in (3) for  $W_A^v$  gives the top and bottom element product composition with respect to the driving force in (12) and (13) which is:

$$W_A^d = DF_i (RR+1) + W_A^l \quad (12)$$

$$W_A^B = W_A^l - DF_i RB \quad (13)$$

Equations (12) and (13) are differentiated with respect to  $DF_i$  and result in the following expressions:

$$\frac{dW_A^d}{dDF_i} = (RR+1) + \frac{dW_A^l}{dDF_i} = (RR+1) + \left( \frac{dDF_i}{W_A^l} \right)^{-1} \quad (14)$$

$$\frac{dW_A^B}{dDF_i} = \frac{dW_A^l}{dDF_i} - RB = \left( \frac{dDF_i}{W_A^l} \right)^{-1} - RB \quad (15)$$

The total element A mass balance is written as follows:

$$F_f \cdot z_{W_{Af}} = W_A^d b^d + W_A^B b^B \quad (16)$$

Where,  $b^d$  and  $b^B$  are element A mass flows in top and bottom of the column, respectively. Substituting (12) and (13), one at the time, into (16) for  $W_A^d$  and  $W_A^B$ , the total element A mass balance in terms of driving force is expressed as:

$$F_f \cdot z_{W_{Af}} = DF_i (RR+1) b^d + W_A^l b^d + W_A^B b^B \quad (17)$$

or

$$F_f \cdot z_{W_{Af}} = W_A^d b^d + W_A^l b^B - b^B DF_i RB \quad (18)$$

Differentiating (17) and (18) with respect to the  $F_f$  and  $z_{W_{Af}}$  (assuming that the changes in composition, and, top and bottom element flowrates ( $b^d$  and  $b^B$ ) with respect to the feed flowrate is negligible), the expressions for  $dW_A^l/dF_f$ ,  $dW_A^l/dz_{W_{Af}}$  are obtained. Having these derivatives, the solution to (9) is expressed by (19). Note that in (19),  $a_1, \dots, a_8$  are constants.

Values of  $dDF_i/dW_A^l$  are calculated and shown in Fig. 4. Note that in Fig. 4, two other points (points II and III) which are not at the maximum are identified as candidate alternative designs for a distillation column, which will be used for verification purposes.

It must be noted that the expressions for  $(dW_A^d/dDF_i)(dDF_i/dW_A^l)$  and  $(dW_A^B/dDF_i)(dDF_i/dW_A^l)$  in (19) are equal to 1 at point (I) in Fig. 4 (maximum driving force) and greater than 1 in any other point.

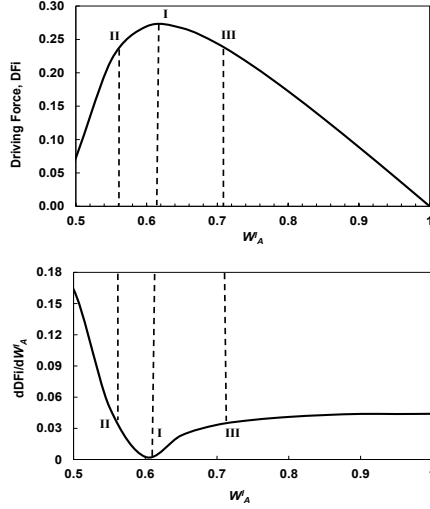


Fig. 4. Driving force diagram for  $W_A$ – $W_B$  separation (reactive zone only – top figure) and its corresponding derivative of  $DF_i$  with respect to  $W_A^I$  (bottom figure).

$$\begin{bmatrix} \frac{dW_A^d}{dF_f} \\ \frac{dW_A^B}{dF_f} \\ \frac{dW_A^d}{dz_{w_{sf}}} \\ \frac{dW_A^B}{dz_{w_{sf}}} \end{bmatrix} = \begin{bmatrix} \left( (RR+1) + \left( \frac{dDF_i}{dW_A^I} \right)^{-1} \right) \left( \frac{dDF_i}{dW_A^I} \right) \left[ \frac{a_1}{a_2 \frac{dDF_i}{dW_A^I} + a_3 + \left( \frac{dW_A^d}{dDF_i} \right) \left( \frac{dDF_i}{dW_A^I} \right)} \right] \\ \left( \left( \frac{dDF_i}{dW_A^I} \right)^{-1} - RB \right) \left( \frac{dDF_i}{dW_A^I} \right) \left[ \frac{a_4}{a_5 \frac{dDF_i}{dW_A^I} + a_6 + \left( \frac{dW_A^B}{dDF_i} \right) \left( \frac{dDF_i}{dW_A^I} \right)} \right] \\ \left( (RR+1) + \left( \frac{dDF_i}{dW_A^I} \right)^{-1} \right) \left( \frac{dDF_i}{dW_A^I} \right) \left[ \frac{a_7}{a_2 \frac{dDF_i}{dW_A^I} + a_3 + \left( \frac{dW_A^d}{dDF_i} \right) \left( \frac{dDF_i}{dW_A^I} \right)} \right] \\ \left( \left( \frac{dDF_i}{dW_A^I} \right)^{-1} - RB \right) \left( \frac{dDF_i}{dW_A^I} \right) \left[ \frac{a_8}{a_5 \frac{dDF_i}{dW_A^I} + a_6 + \left( \frac{dW_A^B}{dDF_i} \right) \left( \frac{dDF_i}{dW_A^I} \right)} \right] \end{bmatrix} \quad (19)$$

Furthermore, at point A the value of  $dDF_i/dW_A^I$  is equal to zero. Therefore, equation (19) at Point A (maximum driving force) can be expressed as:

$$\frac{dy}{dd} = \begin{bmatrix} \frac{dW_A^d}{dF_f} & \frac{dW_A^B}{dF_f} \\ \frac{dW_A^d}{dz_{w_{sf}}} & \frac{dW_A^B}{dz_{w_{sf}}} \end{bmatrix} \approx \begin{bmatrix} (0) \left( \frac{a_1}{a_3+1} \right) & (0) \left( \frac{a_4}{a_6+1} \right) \\ (0) \left( \frac{a_7}{a_3+1} \right) & (0) \left( \frac{a_8}{a_6+1} \right) \end{bmatrix} \approx \begin{bmatrix} 0 & 0 \\ 0 & 0 \end{bmatrix} \quad (20)$$

Equation (20) reveals that the sensitivity of controlled variables to disturbances in the feed is minimum at the maximum driving force.

### 3.3. Selection of the Controller Structure

The controlled variables are defined as top and bottom element A composition  $W_A^d$  and  $W_A^B$ . In this case, the potential manipulated variables are reflux ratio (RR) and reboil ratio (RB). (12) and (13) give the top and bottom product compositions with respect to the driving force.

Hence, they are differentiated with respect to  $RR$  and  $RB$ . Therefore, (6) can now be expressed as:

$$\frac{dy}{du} = \begin{bmatrix} \frac{dW_A^d}{dRR} & \frac{dW_A^d}{dRB} \\ \frac{dW_A^B}{dRR} & \frac{dW_A^B}{dRB} \end{bmatrix} = \begin{bmatrix} DF_i + (RR+1) \left( \frac{dDF_i}{dW_A^I} \right) \left( \frac{dW_A^I}{dRR} \right) + \frac{dW_A^d}{dRR} & (RR+1) \left( \frac{dDF_i}{dW_A^I} \right) \left( \frac{dW_A^I}{dRB} \right) + \frac{dW_A^d}{dRB} \\ \frac{dW_A^B}{dRR} - \left( \frac{dDF_i}{dW_A^I} \right) \left( \frac{dW_A^I}{dRR} \right) RB & \frac{dW_A^B}{dRB} - DF_i \end{bmatrix} \quad (21)$$

From Fig. 4, it is known that  $dDF_i/dW_A^I$  at the maximum driving force is equal to zero. Furthermore, assuming that  $dW_A^I/dRR = dW_A^I/dRB = 0$ , (22) is obtained. The best controller structure can easily be determined by looking at the value of  $dy/du$ . It can be noted from (22) that since the values of  $dW_A^d/dRR$  and  $dW_A^B/dRB$  are bigger, controlling  $W_A^d$  by manipulating  $RR$  and controlling  $W_A^B$  by manipulating  $RB$  will require less control action.

$$\frac{dy}{du} = \begin{bmatrix} \frac{dW_A^d}{dRR} & \frac{dW_A^d}{dRB} \\ \frac{dW_A^B}{dRR} & \frac{dW_A^B}{dRB} \end{bmatrix} = \begin{bmatrix} DF_i & 0 \\ 0 & -DF_i \end{bmatrix} \quad (22)$$

This is because only small changes in  $RR$  and  $RB$  are required to move  $W_A^d$  and  $W_A^B$  in a bigger direction. This pairing between controlled-manipulated variables is also further verified by obtaining the transfer functions between the pairs using a reactive distillation dynamic model based on elements (Pérez Cisneros, 1997). Note that most of the modelling of dynamic reactive distillation operations has been done by introducing a rate of reaction expression in the component mass balances. However, when the chemical reactions occurring are fast enough to reach the equilibrium (for example, MTBE reactive system) chemical equilibrium condition is implicitly incorporated into the element mass balances through the functionality of the phase compositions on the element chemical potentials (Pérez-Cisneros, 1997).

The next natural step to verify the pairing in (22) is calculating the relative gain array (RGA) for the design at the optimal feed location (Design (I) –  $N_F = 1$ ) and two other alternative designs (Design (II) –  $N_F = 2$ ; and Design (III) –  $N_F = 3$ ). Note that in calculating RGA,  $RB$  is represented by heat addition to the reboiler duty instead of reboil ratio; and, MTBE top and bottom compositions represent  $W_A^d$  and  $W_A^B$ , respectively. The transfer functions have the form as equation (23) with one zero and two poles.

$$G(s) = K \frac{1 + \tau_z s}{(1 + \tau_{p1} s)(1 + \tau_{p2} s)} \quad (23)$$

Using the transfer functions, RGA matrix for design B (at the maximum driving force) and designs A and C is calculated and they are as follows:

$$RGA_{(I)} = \begin{bmatrix} 0.93 & 0.07 \\ 0.07 & 0.93 \end{bmatrix}, RGA_{(II)} = \begin{bmatrix} 9.06 & -8.06 \\ -8.06 & 9.06 \end{bmatrix}, RGA_{(III)} = \begin{bmatrix} -0.28 & 1.28 \\ 1.28 & -0.28 \end{bmatrix}$$

As it can be seen the pairing at the maximum driving force (design (I), feed location 1) has the closest values on the diagonal to unity. Therefore, it has the least interaction between the loops. Furthermore, the suggested pairing by RGA for design (I) matches the pairing that was obtained from the driving force. Furthermore, singular value analysis

(SVA) was performed. However, very large condition numbers (CN) were obtained with no specific trend. Thus, no particular conclusion can be made based on them.

The open-loop and closed-loop performance of the system has been tested with the Proportional-Integral (PI) controller in a discrete-time manner. The rigorous dynamic reactive distillation model (Pérez Cisneros, 1997) was used. The controller implementation is visualized in Fig. 5. Note, however, any other control strategy can be applied to perform closed-loop simulations.

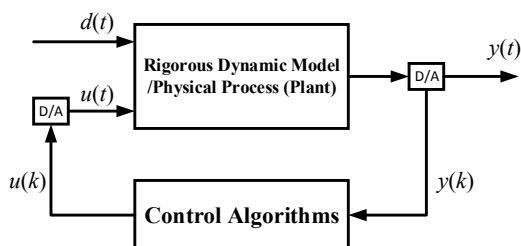


Fig. 5. Discrete-time controller structure implementation.

Fig. 6 and Fig. 7 show the open-loop and closed-loop performance of the system at maximum driving force (Design (I)), respectively. The disturbance scenario is that after 15 samples, the feed flowrate of element A (isobutene) is increased from 70 kg-mole to 85 kg-mole (~12% step change in composition of isobutene). This disturbance results in a change in total feed flowrate by +15% and also a change in the feed composition. As it can be seen in Fig. 6, as a result of an increased isobutene flowrate, its recovery in the top has increased which results in a lower MTBE composition in the top. Furthermore, because of excess isobutene in the system and thereby shifting the reaction equilibrium, MTBE composition has increased in the bottom.

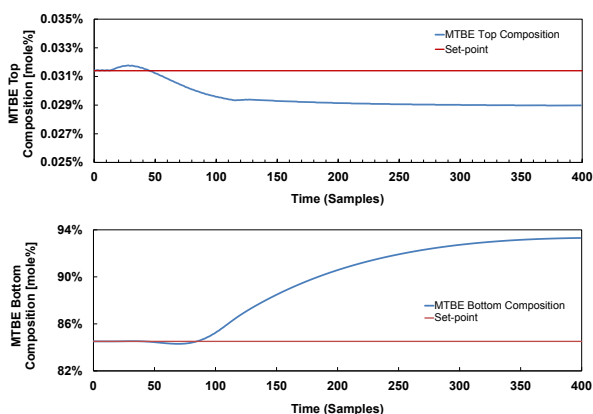


Fig. 6. Open-loop performance of Design B to a disturbance in the feed.

It can be seen in Fig. 7 that disturbance has been rejected with least interaction between the loops and both top and bottom compositions are well controlled using the selected pairing obtained from the driving force. Note that the control of the MTBE top composition is achieved with very small changes in  $RR$ .

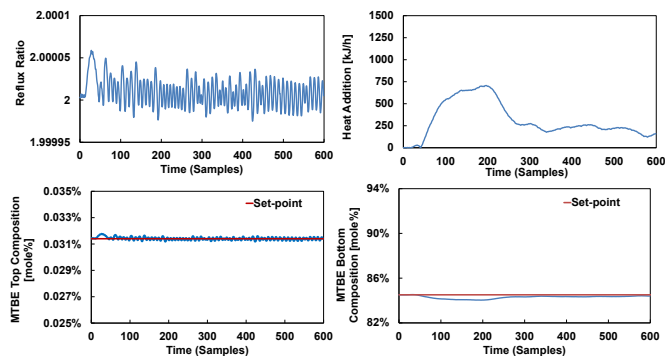


Fig. 7. Closed-loop performance of the control structure for Design B to a disturbance in the feed.

#### 4. CONCLUSIONS

Integrated process design and control of a ternary compound reactive distillation process was investigated in this work. The optimal design-control solutions were obtained analytically and verified through rigorous dynamic simulations. It is verified that the reactive distillation design option is less sensitive to the disturbances in the feed at the highest driving force and has the inherent ability to reject disturbances. Furthermore, it is advantageous to employ the element-based method for designing multicomponent and complex reacting systems.

#### REFERENCES

- Bek-Pedersen, E., Gani, R. (2004). Design and synthesis of distillation systems using a driving-force-based approach, *Chem. Eng. Process.*, 43, 251–262
- Daza, O.S., Pérez Cisneros, E.S., Gani, R. (2003). Graphical and stage-to-stage methods for reactive distillation column design, *AIChE J.*, 49, 2822–2841.
- Hamid, M. K. A., Sin, G., and Gani, R. (2010). Integration of process design and controller design for chemical processes using model-based methodology. *Comput. Chem. Eng.*, 34, 683–699.
- Luyben, M. L., Floudas, C. A. (1994). Analyzing the interaction of design and control – 2. Reactor-Separator-Recycle system, *Comput. Chem. Eng.* 18, 971–994.
- Michelsen, M.L. (1989). Calculation of Multiphase Ideal Solution Chemical Equilibrium, *Fluid Phase Equilib.*, 53, 73–80.
- Nikacevica, N.M., Huesman, A.E.M., Van den Hof, P.M.J., Stankiewicz, A.I. (2012). Opportunities and challenges for process control in process intensification, *Chem. Eng. Process.*, 52, 1–15.
- Pérez Cisneros, E.S., Gani, R., Michelsen, M.L. (1997). Reactive separation systems—I. Computation of physical and chemical equilibrium, *Chem. Eng. Sci.*, 52, 527–543.
- Pérez Cisneros, E.S. (1997). *Modelling, design and analysis of reactive separation processes*, Ph.D. Thesis, Technical University of Denmark, Lyngby.
- Russel, B. M., Henriksen, J. P., Jørgensen, S. B., Gani, R. (2002). Integration of design and control through model analysis. *Comput. Chem. Eng.*, 26, 213–225.
- Seferlis, P., Georgiadis, M. C. (2004). *The integration of process design and control*, Elsevier B. V., Amsterdam.

# A Mean-Variance Objective for Robust Production Optimization in Uncertain Geological Scenarios

Andrea Capolei<sup>a</sup>, Eka Suwartadi<sup>b</sup>, Bjarne Foss<sup>b</sup>, John Bagterp Jørgensen<sup>a</sup>,

<sup>a</sup>Department of Applied Mathematics and Computer Science & Center for Energy Resources Engineering Technical University of Denmark, DK-2800 Kgs. Lyngby, Denmark.

<sup>b</sup>Department of Engineering Cybernetics, Norwegian University of Science and Technology (NTNU), 7491 Trondheim, Norway.

Email addresses:

acap@dtu.dk (Andrea Capolei), eka.suwartadi@ieee.org (Eka Suwartadi), Bjarne.Foss@itk.ntnu.no (Bjarne Foss), jbj@dtu.dk (John Bagterp Jørgensen)

## Abstract

We introduce a mean-variance criterion for production optimization of oil reservoirs and suggest the Sharpe ratio as a systematic procedure to optimally trade-off risk and return. We demonstrate by open-loop simulations of a two-phase synthetic oil field that the mean-variance criterion is able to mitigate the significant inherent geological uncertainties better than the alternative certainty equivalent and robust optimization strategies that have been suggested for production optimization. In production optimization, the optimal water injection profiles and the production borehole pressures are computed by solution of an optimal control problem that maximizes a financial measure such as the Net Present Value (NPV). The NPV is a stochastic variable as the reservoir parameters such as the permeability field is stochastic. In certainty equivalent optimization the mean value of the permeability field is used in the maximization of the NPV of the reservoir over its lifetime. This approach neglects the significant uncertainty in the NPV. Robust optimization maximizes the expected NPV over an ensemble of permeability fields to overcome this shortcoming of certainty equivalent optimization. Robust optimization reduces the risk compared to certainty equivalent optimization because it considers an ensemble of permeability fields instead of just the mean permeability field. This is an indirect mechanism for risk mitigation as the risk does not enter the objective function directly. In the mean-variance bi-criterion objective function risk appears directly, it also considers an ensemble of reservoir models, and has robust optimization as a special extreme case. The mean-variance objective is common for portfolio optimization problems in finance. The Markowitz portfolio optimization problem is the original and simplest example of a mean-variance criterion for mitigating risk. Risk is mitigated in oil production by including both the expected NPV (mean of NPV) and the risk (variance of NPV) for the ensemble of possible reservoir models. With the inclusion of the risk in the objective function, the Sharpe ratio can be used to compute the optimal water injection and production borehole pressure trajectories that give the optimal return-risk ratio. By simulation, we investigate and compare the performance of production optimization by mean-variance optimization, robust optimization, certainty equivalent optimization, and the reactive strategy. The optimization strategies are simulated in open-loop without feedback while the reactive strategy is based on feedback. The simulations demonstrate that certainty equivalent optimization and robust optimization are risky strategies. At the same computational effort as robust optimization, mean-variance optimization is able to reduce risk significantly at the cost of slightly smaller return. In this way, mean-variance optimization is a powerful tool for risk management and uncertainty mitigation in production optimization.

# Modelling and Model Predictive Control of ESP lifted wells

Alexey Pavlov, Dinesh Krishnamoorthy, Elvira Marie.B Aske, Kjetil Fjalestad, Morten Fredriksen

*Statoil RDI*

---

*Abstract:* In this presentation, we describe control challenges related to operation of oil wells equipped with Electric Submersible Pumps (ESP) and formalize them in a control problem setting in the language of control system engineers. Then we present a simple dynamic model of an oil well equipped with ESP. This model can be used for controller development. To solve this problem, we propose a Model Predictive Control (MPC) strategy and present experimental results of an MPC controller successfully tested in a large scale test facility with a full scale ESP, live crude oil in an emulated oil well.

---

## Oral presentations 4

# Power and bio applications

Chair: John Bagterp Jørgensen, DTU

### Presentations:

19. *Remote light stress detection for greenhouse LED lighting control*  
Anna-Maria Carstensen, Torsten Wik and Tessa Pocock  
Department of Signals and Systems, Chalmers University of Technology, Sweden
20. *Fault tolerant model predictive control for the BioPower 5 CHP plant*  
J. Kortela and S-L. Jämsä-Jounela  
Aalto University School of Chemical Technology, Finland
21. *Relative Gain Measures for Once-through Circulating Fluidized Bed Boiler Control Design*  
Matias Hultgren\*, Jenő Kovács\*\* and Enso Ikonen\*  
\* Systems Engineering Laboratory, University of Oulu, Finland.  
\*\* Foster Wheeler Energy Ltd, Varkaus, Finland.
22. *Model-based optimal design and control of an anaerobic digestion reactor*  
Finn A. Haugen  
Telemark University College, Porsgrunn, Norway
23. *A study on the combustion dynamics of a biomass fuel bed in a BioGrate boiler*  
<sup>1</sup>A. Boriouchkine, <sup>2</sup>V. Sharifi, <sup>2</sup>J. Swithenbank and <sup>1</sup>S.-L. Jämsä-Jounela,  
<sup>1</sup> School of Chemical Technology, Aalto University, Finland;  
<sup>2</sup> University of Sheffield, Department of Chemical and Biological Engineering, UK;
24. *Investigation of tuning of a fuzzy-logic control for biological wastewater treatment systems*  
Riccardo Boiocchi, Krist V. Gernaey and Gürkan Sin  
Chemical Engineering, DTU, Lyngby, Denmark

# Remote Light Stress Detection for Greenhouse LED Lighting Control

Anna-Maria Carstensen\* Torsten Wik\* Tessa Pocock\*\*

\* *Department of Signals and Systems, Chalmers University of Technology, Göteborg, Sweden*

\*\* *Smart Lighting Engineering Research Center, Rensselaer Polytechnic Institute, Troy, NY, USA*

---

**Abstract:** The illumination in greenhouses is in general still controlled manually by on/off control because of the type of lamps (High Pressure Sodium) that are traditionally used. With High Brightness LEDs being introduced on the market today, sufficiently high power for greenhouse grown crops can be achieved, which opens up for advanced lighting control since both light spectrum and intensity can be controlled then. For the growers, maximizing production in order to meet customer demand and economically optimize the production, often imply a high light intensity and a high level of artificial light complementing the natural sunlight. However, a too high intensity causes light stress and a photo inhibition that can significantly reduce the photosynthetic yield and hence, production. A key issue to address is therefore to detect when this level is reached. Here we present new results on how to diagnose the plants remotely based on transient and frequency analysis, system identification and frequency function properties.

---

## 1. INTRODUCTION

Industrial scale green houses are enormous consumers of electricity. In Europe alone consumption is estimated to be around 150 TWh per year, which is about the same as the total electricity consumption in Sweden. Clearly, a reduced electricity consumption would have a significant environmental impact.

Greenhouse lamps using High Brightness LEDs are currently being introduced on the market. These lamps have several important advantages compared to the traditionally used High Pressure Sodium (HPS) lamps. The HPS lamps have a significant part of the irradiance in the far red being outside the absorption spectrum of the photosynthesis. By combining several different groups of LEDs having different colors the emitted spectrum of a LED lamp can be made to better fit the photosynthesis. Contrary to the HPS lamps, which generally allow only on-off control, LEDs are easily adjustable in power and this opens up for advanced lighting control since both light spectrum and intensity can be controlled then. Such a control applied to planning, spectrum optimization and photo inhibition, as presented in the 17th NPCW Wik et al. (2012), may potentially give both energy savings and increased production (Baker and Rosenqvist, 2004). In this work we focus on one of the mechanisms; photo inhibition. Excess light causes plant stress and the induction of protective mechanisms that lower the yield in tens of percent, even at a level where the human eye cannot detect any change. If too severe, the process is no longer reversible and the plants become damaged with a permanently decreased growth rate.

Plants are fluorescent in that they re-emit absorbed light, of any wavelength, in wavelengths around 685 and 740 nm. The emission of chlorophyll fluorescence (CF) varies depending on photosynthetic yield and plant stress. Chloro-

phyll fluorescence is therefore widely used as a non-destructive probe of physiology in photosynthetic organisms (Krause and Weis, 1991).

Although the production in greenhouses potentially could benefit a lot from using CF measurements for the control of supplementary lighting, this is rarely done today. During the last decade attempts to introduce CF measurements in commercial greenhouses have been done. However, on-line CF measurements have, to the best of our knowledge, yet not been used for automatic and closed loop control of climate and illumination in greenhouses. One of the most important reason is that it is difficult to get measurement indices that are sufficiently robust. Standard methods, such as PAM (Pulse Amplitude Modulated) techniques, were derived for on-leaf measurements, though equipment is now available for measurements at some distance (Ounis et al., 2001; Moya and Cerovic, 2004). If CF measurements should be used for automatic control, however, the measurement technique must give a representative measurement for the entire area to be controlled and, hence, a remote sensing method is more or less required. Furthermore, the measurement technique must be robust to disturbances, such as variations in incident light. Traditional techniques for stress detection, such as  $F_v/F_m$  and corresponding measures, have been tested remotely but near plants (as opposed to on-leaf) but requires dark adapted plants, which excludes them from on-line control in green houses (Takayama et al., 2011).

This research project focuses on developing a remote sensing technique based on CF to be used for the automatic control of illumination in greenhouses. The sensor measures, at a distance of 1-2 meters, the CF from the whole region of the plant canopy illuminated by the lamp, thus giving an aggregated measure. The method is based on that the dynamics of the induced fluorescence signal

reveals information on photosynthetic yield as well as stress mechanisms in the plants. The dynamics of the photosynthesis and the heat dissipation processes induced by stress, is studied as an input output relation, where the input is emitted light from the lamp and the output is re-emitted fluorescence. Here we present a first approach in studying this input output relation, using frequency and transient analysis.

The experiments and more analysis and results will be available in (Carstensen et al., Manuscript).

## 2. MATERIALS AND METHODS

In order to investigate how the dynamics is affected, plants acclimated to different conditions were exposed to light ranging from low intensity to increasing inhibiting intensity, and then low intensities again for the plants to recover. The plants used in the experiments were sweet basil Nufar (*Ocimum Basilicum*) grown in growth chambers in four different growth conditions:

- (1) LED light, 80  $\mu E$  intensity
- (2) LED light, 500  $\mu E$  intensity
- (3) HPS light, 80  $\mu E$  intensity
- (4) HPS light, 500  $\mu E$  intensity

where the notation  $\mu E$  is  $\mu\text{mol}$  of photons per  $m^2$  and  $s$ .

The light in each experiment consisted of two parts; an excitation light signal (sinusoid or step) and a background light going through four phases:

- (1) 110  $\mu E$  for 2.5 h
- (2) 530  $\mu E$  for 1 h
- (3) 1750  $\mu E$  for 2 h
- (4) 110  $\mu E$  for 3-6 h

Analysis of fluorescence from plants, using fluorescence indices such as  $F_v/F_m$ , is a well established method for detecting plant stress. However, such standard methods require on-leaf measures and a completely controlled environment. As already mentioned, to be used in practice for automatic control, the stress has to be sensed remotely. As an indication of light stress level, the maximum efficiency of PSII photochemistry can be used, through the ratio  $F_v/F_m$ . How  $F_v/F_m$  evolved during the experiments is shown in Fig. 1.

The curves in Fig. 1 also illustrates the difficulty of getting robust measures without remote sensing, though the expected trends during the four phases can be identified. Decreasing levels during Phase 2 and 3 illustrates an increasing level of stress, and the measurements during Phase 4 displays a recovery phase. It is also evident that the behaviour is different depending on the light the plants have been acclimated to. The lower the acclimation light the more stressed the plants are. Also, it appears clear that acclimation to HPS spectrum makes the plants more susceptible to light stress than acclimation to the LED spectrum. They also appear to have a slower recovery during the last phase.

Two different excitation signals were employed: (1) light varying between two levels, forming step increases and step decreases and (2) sinusoidal varying light. The step length was chosen to be 300s, since that was the time it took for

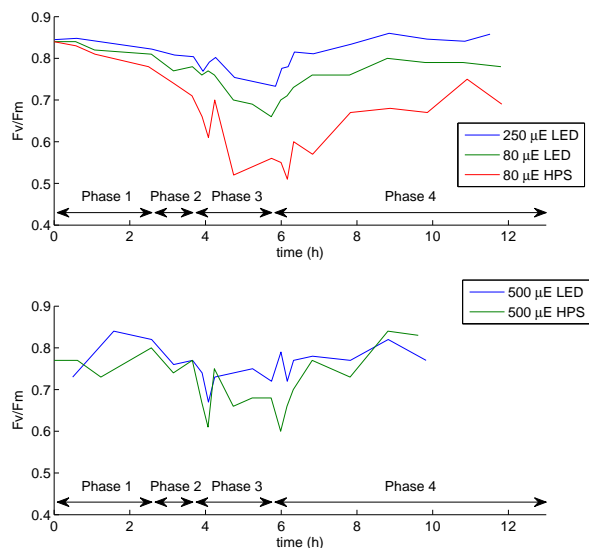


Fig. 1.  $F_v/F_m$  measured during experiments with sinusoids as excitation signal.  $F_v/F_m$  measured on plant material acclimated to different light intensities and spectrum as indicated in the graph. The figure shows the mean value of four leaves.

the transient fluorescence response to settle, and the slow kinetics of the fluorescence has been reported to contain specific information on stress (Strasser 2004). The sinusoid period was selected because this frequency ( $\omega \approx 0.1$  rad/s) has been reported to reveal interesting dynamical features in plants by Nedbal (2003), and was also believed to catch dynamic features observed in previous experiments (Wik et al., 2012). Both a resonance peak and strong upper harmonic oscillations are reported to occur, not only in fluorescence but also in  $CO_2$  capture, upon harmonically modulated light at this frequency.

The chlorophyll fluorescence is emitted with two peaks; one centered around 685 nm and one around 740 nm. The former one is within the absorption spectrum of the photosynthesis and is therefore to a large extent reabsorbed. Absolute irradiance, measured with a spectrometer facing the plants and integrated over the interval 700-780nm, thus representing the fluorescence signal with maximum at 740nm, was therefore used as system output in the analysis.

The intensity of the excitation signal (blue LEDs) at each time instance was also calculated as the integrated absolute irradiance ( $\mu E$ ) in the wavelength interval 380-480nm, based on data collected with a spectrometer facing the lamp.

In the analysis of the sinusoid experiments, sinus signals (for the known frequency) were first fitted to the measured input and output by least square fitting of amplitude, phase and mean level. The fit of the sinusoids were all over high to both the excitation signal and the fluorescence signal, which motivated a linear analysis in terms of gain and phase shifts. The *fluorescence gain* was then simply determined as the ratio of the output and input

amplitudes, and the phase shift as the difference between the estimated phases.

The step responses were different for step increases and step decreases, implying that the system is actually nonlinear. This motivated a separate estimation of models to step increases and step decreases, while keeping the modelling linear. Hence, prior to the modeling, data was cut into step increases and step decreases, with 60s of data included before each change in level. The dynamics of the responses to the step increases exhibited stronger dynamic features than those for step decreases. Therefore, we choose to focus only on the step increases in this work.

The linear modeling was performed by estimation of one model to each step to let the model parameters, within one selected model structure and order, adapt as the dynamics in the photosynthesis are changed due to altered physiology. Hence, the first part in the identification procedure was to find a model structure and model order applicable to all the four different phases in the experiment. Since the step responses under low light intensity, during Phase 1 and 4 of the experiment, exhibited the most complex transients, the model structure and order was selected based on its suitability for modeling step responses for these experimental phases. After standard testing of ARX, ARMAX, Output Error (OE) and Box Jenkins (BJ) models (Ljung, 2007), it was found that OE models with 3 poles and 4 zeros gave the best results in simulation on both estimation data and validation data, independently of the prefiltering of the data.

### 3. RESULTS

*Fluorescence gain* The fluorescence gains for the five set of plants grown under different light treatments are shown together with the Fv/Fm in Figure 2. Within each phase of the experiment the fluorescence gain exhibits slow continuous changes, whereas in the transition between the phases the gains respond instantly to the changed background light intensity. The slow continuous changes in the fluorescence gain clearly agree with the changes in the Fv/Fm and are therefore interpreted as changes in photoinhibition and heat dissipation processes. The instant changes in the fluorescence gain upon changes in the background light intensity have no counterpart in the Fv/Fm and are likely related to changes in the photosynthetic yield or to saturation effects.

*Phase shifts* Figure 3 shows how the phase shifts vary during the experiment. The relation between the phase shifts and the Fv/Fm apparently depends on both acclimation and background light intensity in an intricate way, which will be explained and discussed in relation to the results of the step responses. However, some observations can be made here.

Whether the phase shifts are positive or negative is determined by the background light intensity in relation to what light intensity the plants are acclimated to. Negative phase shifts were only observed for plants facing a lower light intensity than they were grown under. For plants facing the light intensity they were grown under, or higher intensities, the phase shifts were positive. Furthermore, a decrease in the absolute value of the phase shifts was related to a

decrease in Fv/Fm, whereas an increase in the absolute value of the phase shifts was related to an increase in the Fv/Fm.

It should be noted that, as a stress indicator, the phase shift has an important advantage over the fluorescence gain since it is basically independent of the amplitude and, thus, robust with respect to changes in leaf area, morphology and distance for example.

*Results with step excitation* In Figure 4 step responses from the four phases are shown. As can be seen, the fluorescence transients differ between different phases of the experiments and also between plants acclimated to different light intensities.

The original hypothesis of the approach in this work was that changes in model parameter values could be used to track stress levels in plants. It turned out though that both light intensity and stress level not only affected the parameter values but also the complexity of the dynamics. For plants under low light a model order with 3 poles and 4 zeros was motivated, whereas under higher light intensity this model order gave rise to cancellations between poles and zeros, implying that a lower model order was more suitable. The loss of complexity due to stress or increased light intensity made it inconvenient to track plant stress through these values. This is not only because the loss of complexity gave rise to jumps in these values but also because their uncertainties increased.

Instead of tracking parameters or combinations thereof a better approach appears to be to base the analysis on information in the frequency plane. In fact, the identified frequency functions proved to converge with increasing model order. A study of the fluorescence transients in the frequency domain revealed three main features relating to acclimation, light intensity and stress respectively.

Acclimation to different light intensities affected how fast the dynamics of the fluorescence response was. The step responses from plants acclimated to  $80\mu E$  and  $500\mu E$  were similar in shape, but the step responses from plants grown under  $80\mu E$  were faster. In the frequency domain the faster dynamics exhibited by the low light acclimated plants corresponds to a shift of the frequency function towards higher frequencies (see Fig. 5). Light intensity also affected the fluorescence dynamics such that it became faster when the intensity was increased, shifting the frequency function towards higher frequencies as shown in Figure 5. Furthermore increased light intensity led to more trivial dynamics as already discussed.

Decreased Fv/Fm made the dynamics less complex in the frequency range studied here. Figure 6 shows how the frequency function was changed during recovery of Fv/Fm under  $80\mu E$ . During recovery the complexity of the dynamics was successively increased, which could be seen through an increased resonance peak and increased phase shifts. The increased complexity of the dynamics gained during recovery of Fv/Fm could also be seen through the pole-zero placements of the modeled step responses. During recovery, poles and zeros lying close to each other were moved further away from each other.

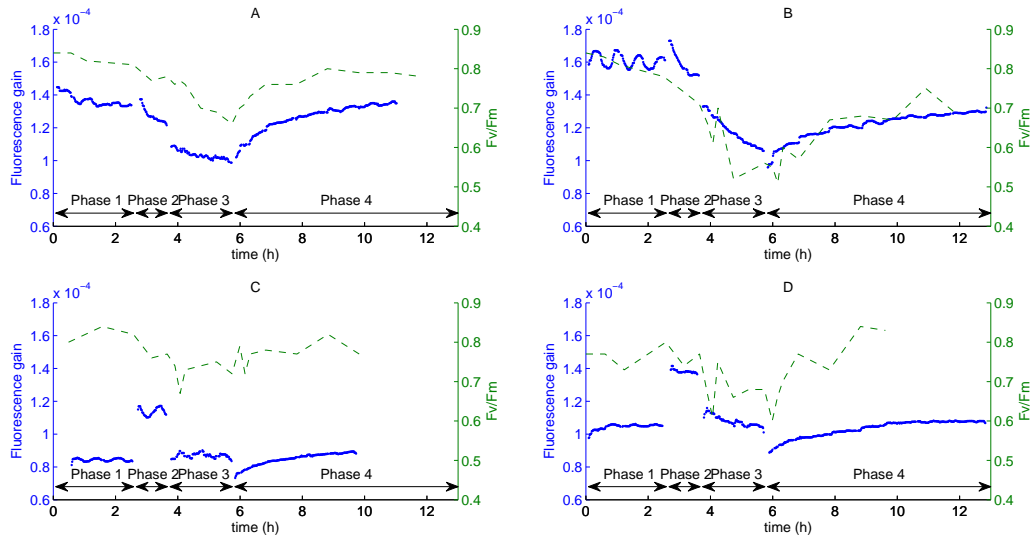


Fig. 2. Fluorescence gain and  $F_v/F_m$  from plants acclimated to  $80\mu E$  and the LED spectrum (A),  $80\mu E$  and the HPS spectrum (B),  $500\mu E$  and the LED spectrum (C) and  $500\mu E$  and the HPS spectrum (D). The oscillations in the fluorescence gain are due to temperature variations in the lab.

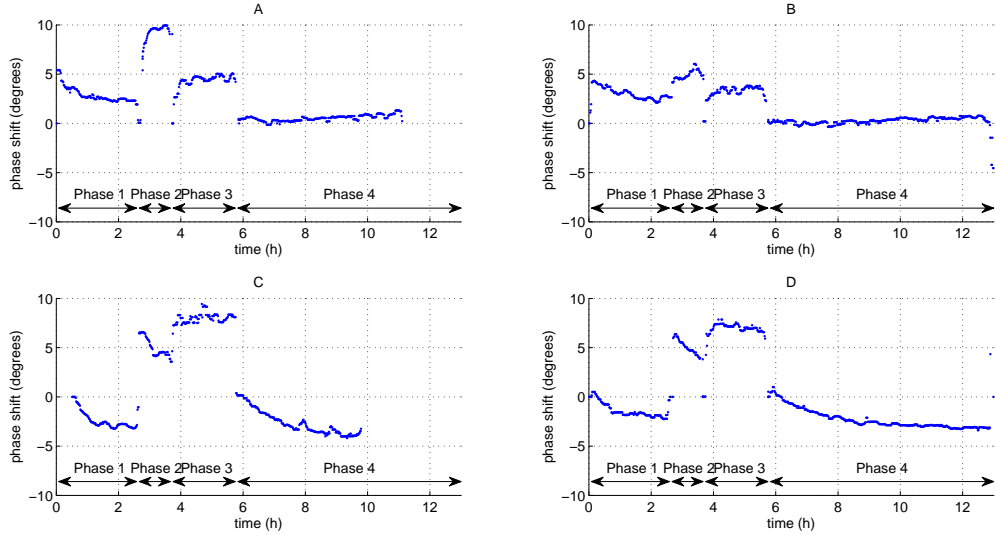


Fig. 3. Phase shifts in the fluorescence signal for plants acclimated to  $80\mu E$  and the LED spectrum (A),  $80\mu E$  and the HPS spectrum (B),  $500\mu E$  and the LED spectrum (C) and  $500\mu E$  and the HPS spectrum (D).

The observed behaviour, where the light flux (energy) in relation to the capacity of utilising energy (due to acclimation) determines how fast the system responds to an input signal, is coherent with a system of flows and buffers. For such systems, the response to an input change is faster the smaller the buffer volume, and the higher the flow is. Furthermore, as the capacity of a buffer is reached the system will lose a dynamic state, which corresponds to a loss in complexity and system order. This is also the phenomena observed here, when pole-zero cancellations occurred as the light intensity became too high compared to the plants capacity. Although a buffer-flow system alone would not give rise to any resonance, this can be caused by feedback mechanisms in the system.

*Comparing step and sinusoid excitation results* The results from the experiments with sinusoidal varying light alone were somehow hard to interpret. Especially the phase shifts appeared complex. Fortunately, the frequency domain results from the step responses provides an explanation. The frequency functions presented in Figure 5 showed that the background light intensity in relation to the light intensity the plants are acclimated to determined the position of the frequency function. This clearly explains why the phase shift and the amplification of an input signal of a fixed angular frequency ( $\omega = 0.1 \text{ rad/s}$ ) could vary significantly depending on the plant material and background light intensity. According to the Bode plots for the plants acclimated to  $500\mu E$  and Phase 1 of the experiment (see Figure 5), an input signal of frequency

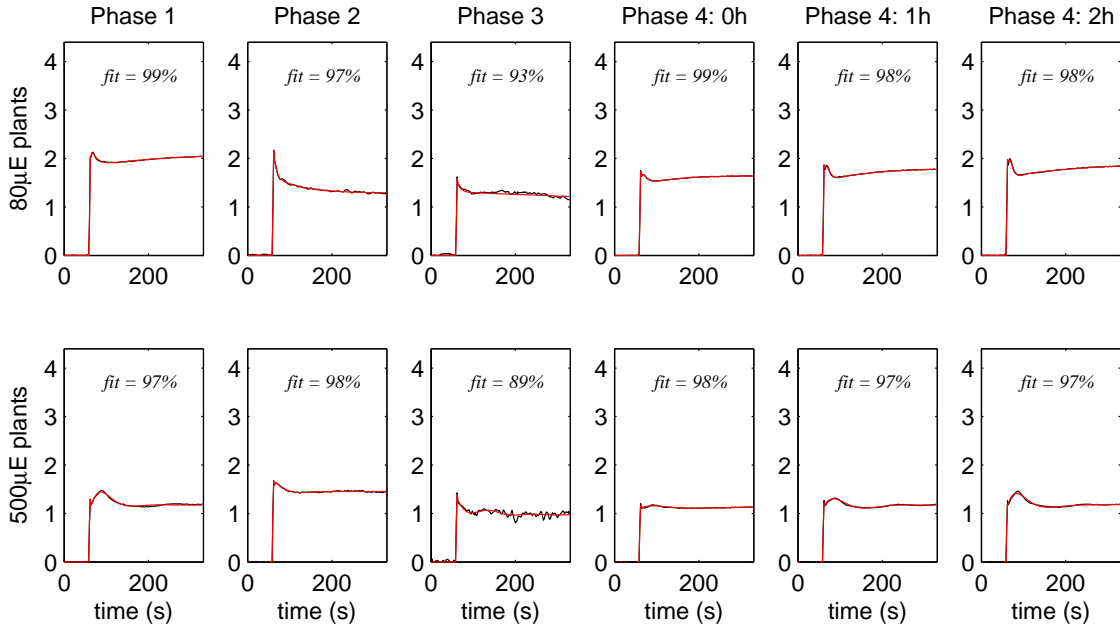


Fig. 4. Fluorescence responses to step increases; from left to right one step from each of Phase 1, Phase 2 and Phase 3, and 3 steps from Phase 4: first step during recovery, after 1h of recovery and after 2 hours of recovery. Filtered raw data (black) and simulated data (red) in the same graph.

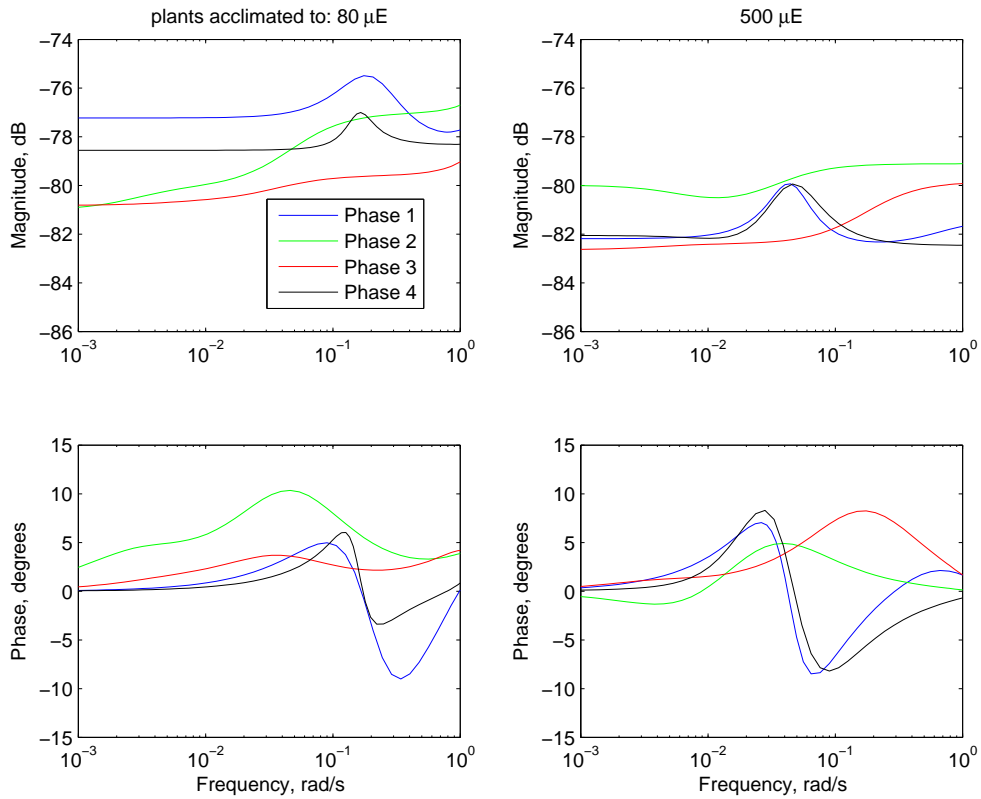


Fig. 5. Bode diagrams showing the mean value of the frequency functions from the different phases (Phase 1, blue, Phase 2 green, Phase 3, red and Phase 4, black) of the experiments. From left to right, plants acclimated to  $80\mu E$  and  $500\mu E$ .

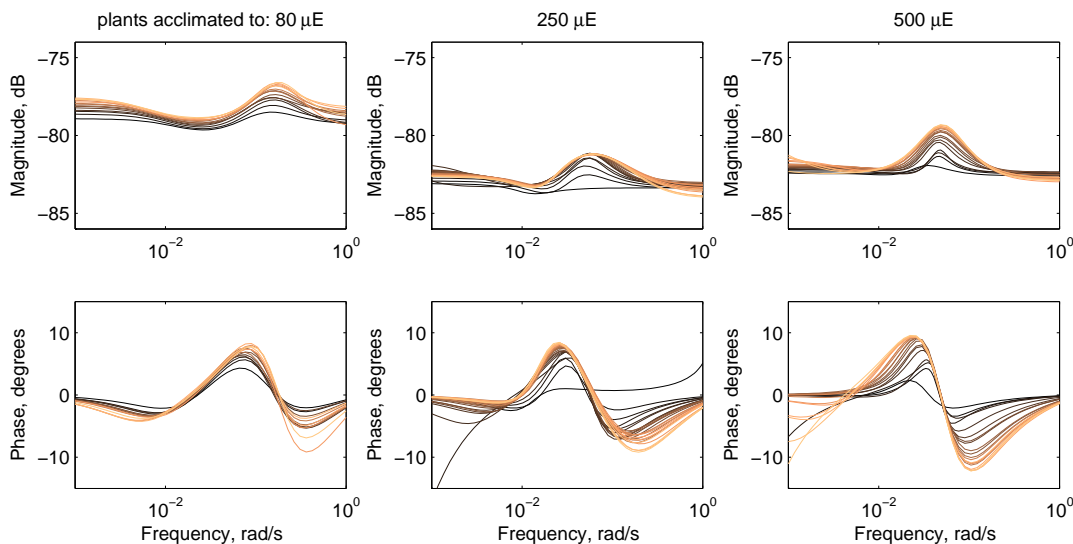


Fig. 6. Bode diagrams showing recovery from stress under  $80\mu E$  in Phase 4 of the experiments. From left to right plants acclimated to  $80\mu E$ ,  $250\mu E$  and  $500\mu E$ . The color-scale goes from black to yellow with black indicating the beginning of Phase 4 and yellow the end.

$\omega = 0.1 \text{ rad/s}$  will get a negative phase shift. However, the corresponding Bode plot for the plants acclimated to  $80\mu E$  is shifted towards higher frequencies, resulting in a positive phase shift for an input signal of  $\omega = 0.1 \text{ rad/s}$ . This is in agreement with the phase shifts presented in Figure 3. When the light intensity is increased, also the Bode plots for the plants acclimated to  $500\mu E$  moved towards higher frequencies and consequently, the sinusoid of frequency  $\omega = 0.1 \text{ rad/s}$  becomes positively phase shifted. Moreover, the discontinuities in the fluorescence gain upon changed background light intensity (see Figure 2) could to some extent be explained by movements of the position of the resonance peak in the Bode diagrams.

#### 4. CONCLUSIONS

The dynamics of plant chlorophyll fluorescence was studied through frequency- and transient- analysis in experiments where plants acclimated to different light intensities and spectra were exposed to low light, high light and excess light. One of the key findings was that the background light intensity in relation to the light intensity that the plants were acclimated to determined how fast the plants responded to a light excitation. Hence, light intensity shifted the plants dynamic behaviour in the frequency domain. Perhaps even more interesting was that the complexity of the dynamics was decreased upon increased light intensity above the light intensity of acclimation. The complexity of the dynamics was also affected by light induced stress. The mechanisms behind these observations have the character of a flow-system with buffer volumes and feedback, where the buffers likely are metabolite pools. These results were obtained from the analysis of black-box models of step responses. Interestingly, these results were also in agreement with the gain and phase shifts obtained with sinusoid excitation.

#### REFERENCES

Neil R Baker and Eva Rosenqvist. Applications of chlorophyll fluorescence can improve crop production strate-

gies: an examination of future possibilities. *Journal of experimental botany*, 55(403):1607–21, August 2004.

- A.M. Carstensen, T. Wik, T. Pocock, and D. Bånkestad. Remote detection of light induced stress in basil through the dynamic behaviour of light induced fluorescence. *Remote sensing of environment*, Manuscript.
- G H Krause and E Weis. Chlorophyll Fluorescence and Photosynthesis: The Basics. *Annual Review of Plant Physiology and Plant Molecular Biology*, 42(1):313–349, June 1991.
- Lennart Ljung. *System Identification Toolbox for Use with Matlab*. The MathWorks, Inc., 2007.
- Ismael Moya and Zoran G. Cerovic. Remote sensing of chlorophyll fluorescence: Instrumentation and analysis. In George Christos Papageorgiou and Govindjee, editors, *Chlorophyll a Fluorescence*, volume 19 of *Advances in Photosynthesis and Respiration*, pages 429–445. Springer Netherlands, 2004.
- L Nedbal. Negative feedback regulation is responsible for the non-linear modulation of photosynthetic activity in plants and cyanobacteria exposed to a dynamic light environment. *Biochimica et Biophysica Acta (BBA) - Bioenergetics*, 1607(1):5–17, October 2003.
- A Ounis, S Evain, J Flexas, S Tosti, and I Moya. Adaptation of a PAM-fluorometer for remote sensing of chlorophyll fluorescence. *Photosynthesis research*, 68(2):113–20, January 2001.
- K. Takayama, H. Nishina, S. Iyoki, S. Arima, K. Hatou, Y. Ueka, and Y. Miyoshi. Early detection of drought stress in tomato plants with chlorophyll fluorescence imaging-practical application of the speaking plant approach in a greenhouse. In *18th IFAC World Congress*, pages 1785–1790, Milano, Italy, Aug. 28 - Sep. 2 2011.
- T. Wik, A.M. Carstensen, and T. Pocock. Greenhouse LED lighting control. In *17th Nordic Process Control Workshop*, Lyngby, Danmark, Jan. 25 - 27 2012.

# Fault-tolerant model predictive control (FTMPC) for the BioGrate boiler

Jukka Kortela\* Sirkka-Liisa Jämsä-Jounela\*\*

\* *Aalto University School of Chemical Technology, PL 16100, FI-00076*

*Aalto (e-mail: jukka.kortela@aalto.fi).*

\*\* *(e-mail: sirkka-liisa.jamsa-jounela@aalto.fi)*

---

**Abstract:** The fuel bed height sensor is a critical element in the control of the BioGrate boiler. A fault appearing in this sensor greatly affects the control performance in the sense that air distribution in the BioGrate boiler deviates from its nominal distribution. To address this problem, a fault tolerant model predictive control (FTMPC) has been developed to accommodate the fault in this fuel bed height sensor by the active controller reconfiguration. In this fault tolerant strategy, water evaporation in the furnace is estimated by fuel moisture soft-sensor, and thermal decomposition of dry fuel is estimated by utilizing oxygen consumption. This renders the power output of the boiler to be accurately predicted and controlled. The proposed FTMPC is successfully tested with the BioPower 5 CHP plant data and the results are presented, analyzed, and discussed.

*Keywords:* fault-tolerant control, model predictive control, biomass, moisture, BioGrate boiler

---

## 1. INTRODUCTION

The utilization of biomass fuel for heat and power production is growing due to an increasing demand for the replacement of fossil energy sources with renewable energy. As a result, the fast and the efficient control of power producing units becomes increasingly important in combustion of biomass (Edlund et al., 2011). However, the main challenges in biomass combustion control are caused by the unpredictable variability of the fuel quality, which results in disturbances, faults, and failures in the plant behavior and operations. In particular, this is true for the grate firing that is one of the main technologies currently used in biomass combustion (Leão et al., 2011).

Several different control strategies have been developed to control the combustion. The combustion power method developed by Kortela and Lautala (1982) was employed by many control strategies to compensate variations in the fuel quality. Based on the combustion power method, in the same publication Kortela and Lautala (1982) suggested a feed-forward control: adjusting the fuel feed flow according to the thermal decomposition rate to stabilize the amount of the fuel in the furnace. As a result, the effect of the feed disturbance on the generated steam pressure decreased to about one third of the original value, and the settling time decreased from 45 min to only 13 min. The same method has later been applied to a grate boiler (Kortela and Marttinen, 1985).

Recently, the model predictive control has proven to be a successful method for controlling renewable fuel power plants. In particular, the benefits of MPC-based control over conventional multivariable control have been demonstrated by Leskens et al. (2005) at a grate boiler combusting municipal solid waste. Göllés et al. (2011); Göllés et al. (2014) implemented and experimentally verified a

model based control in a commercially available small-scale biomass boiler using the simplified first-principle model. In more details, the mass of water in the water evaporation zone and the mass of dry fuel in the thermal decomposition zone on the grate are considered as the states of the simplified model and are estimated by an extended Kalman filter. Test results showed that the control was always able to provide the required power whereas the conventional control (PID control based on standard control strategies) could not tolerate a feed water temperature drop of more than 7 °C. In addition, the control was able to operate the plant with a lower excess oxygen content during the load drop and especially under partial load conditions. The better control of the residual oxygen and the control of the air ratio led to lower emissions and higher efficiencies. In addition, the model-based control was able to handle without difficulties a step-wise change in the fuel moisture content from 26% to 38% and vice versa. However, in addition to controlling the power production, the plant control has to maintain the optimal operating conditions in the furnace. According to the boiler design, for the complete combustion of biomass, the fuel bed height should be kept at the level to achieve the specified ratio between the primary and secondary air, and the amount of fuel in the furnace (Yin et al., 2008).

In this paper a FTMPC strategy is proposed to accommodate the fault in fuel bed height sensor by active controller reconfiguration. The paper is organized as follows: Section 2 presents the BioPower 5 CHP process. The FTMPC strategy is presented in Section 3. The test results are given in Section 4, followed by the conclusions in Section 5.

## 2. DESCRIPTION OF THE BIOPOWER 5 CHP PROCESS

The BioPower 5 CHP process consists of two main parts: the furnace and the steam-water circuit. The heat used for steam generation is obtained by burning solid biomass fuel – consisting of bark, sawdust, and pellets – which is fed into the furnace together with combustion air. The heat of the flue gas is transferred by the heat exchangers to the steam-water circulation, where superheated steam is generated (Boriouchkine et al., 2012).

In the BioGrate system, the fuel is fed onto the center of a grate from below through a stoker screw, as shown in Fig. 1. The grate consists of alternate rotating and stationary concentric rings with the rotating rings alternately rotated clockwise and counter-clockwise by hydraulics. This design distributes the fuel evenly over the entire grate, with the burning fuel forming an even layer of the required thickness.

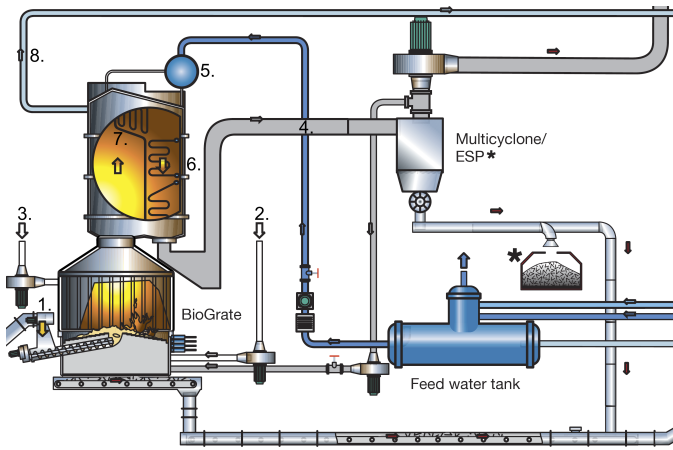


Fig. 1. 1. Fuel, 2. Primary air, 3. Secondary air, 4. Economizer, 5. Drum, 6. Evaporator, 7. Superheaters, 8. Superheated steam

The moisture content of the wet fuel in the centre of the grate evaporates rapidly due to the heat of the surrounding burning fuel and the thermal radiation coming from the brick walls. The gasification and visible combustion of the gases and solid carbon takes place as the fuel moves to the periphery of the circular grate. At the edge of the grate, ash finally falls into a water-filled ash basin underneath the grate.

The primary air for combustion and the recirculation flue gas are fed from underneath the grate and they penetrate the fuel through the slots in the concentric rings. The secondary air is fed directly into the flame above the grate and the air distribution is controlled by dampers and speed-controlled fans. The gases released from biomass conversion on the grate and a small number of entrained fuel particles continue to combust in the freeboard, in which the secondary air supply plays a significant role in the mixing, burnout, and the formation of emissions. The design of the air supply system, the ratio between primary and secondary air, plays a key role in the efficient and complete combustion of biomass (Yin et al., 2008). In modern grate-fired boilers burning biomass, the split ratio of primary to secondary air is 40/60, which should

be followed by a control design for the most efficient energy production. The overall excess air for most biomass fuels is normally set at 25% or above.

The essential components of the water-steam circuit are an economizer, a drum, an evaporator, and superheaters. Feed water is pumped from a feed water tank into the boiler. First the water is led into the economizer (4), which is the last heat exchanger extracting the energy from the flue gas, and thus, improving the efficiency of the boiler. From the economizer, the heated feed water is transferred into the drum (5) and along downcomers into the bottom of the evaporator (6) through tubes that surround the boiler. From the evaporator tubes, the heated water and steam return back into the steam drum, where they are separated. The steam rises to the top of the steam drum and flows into the superheaters (7) where it heats up further and superheats. The superheated high-pressure steam (8) is then passed into the steam turbine, where electricity is generated.

## 3. FTMPC FOR THE BIOGRATE BOILER

The overall structure of the FTMPC follows the active FTC scheme, adjusting the plant control according to the fault diagnosis results. In more detail, two different MPC configurations have been developed for the cases of normal and faulty operations of the fuel bed height sensor. In the faultless mode, the MPC configuration is as follows: the primary air flow rate and the stoker speed are the manipulated variables ( $u$ ); the moisture content in the fuel feed and the steam demand are the measured disturbances ( $d$ ); and the fuel bed height and the steam pressure are the controlled variables ( $y$ ). The fault is accommodated by employing an alternative estimation of the fuel bed height, which is based on the thermal decomposition rate. However, as the alternative estimation is less accurate, the control reconfiguration is also needed, shifting its focus to the combustion power control while the fuel height is given a low priority. Additionally, the fuel bed height is kept within the security limits in both configurations in order to avoid plant shutdowns.

In more details, the FTC scheme is presented in Fig. 2. The combustion power and fuel moisture soft-sensors are used to compensate the effect of the fuel quality variations (Kortela and Jämsä-Jounela, 2013). In particular, the fuel moisture estimation is considered by the MPC as a measured disturbance and is also used to estimate the amount of water in the furnace. Considering the combustion power as a model state enables rapid energy production level changes and improves the control performance during the transitions. In addition, the thermal decomposition rate is used in the calculations of the fuel bed height (estimator 2 in Fig. 2), which makes the fault detection and accommodation possible. According to the fault detection results, the decision on the control reconfiguration is made, which is then communicated to the fault accommodation and the FTMPC. Depending on the  $r_p$  value, the fault accommodation employs either the fuel bed height measurement or the thermal decomposition rate and the primary air flow for the MPC state estimation. Also, FTMPC is switched between the normal and the faulty configurations according to the  $r_p$  signal.

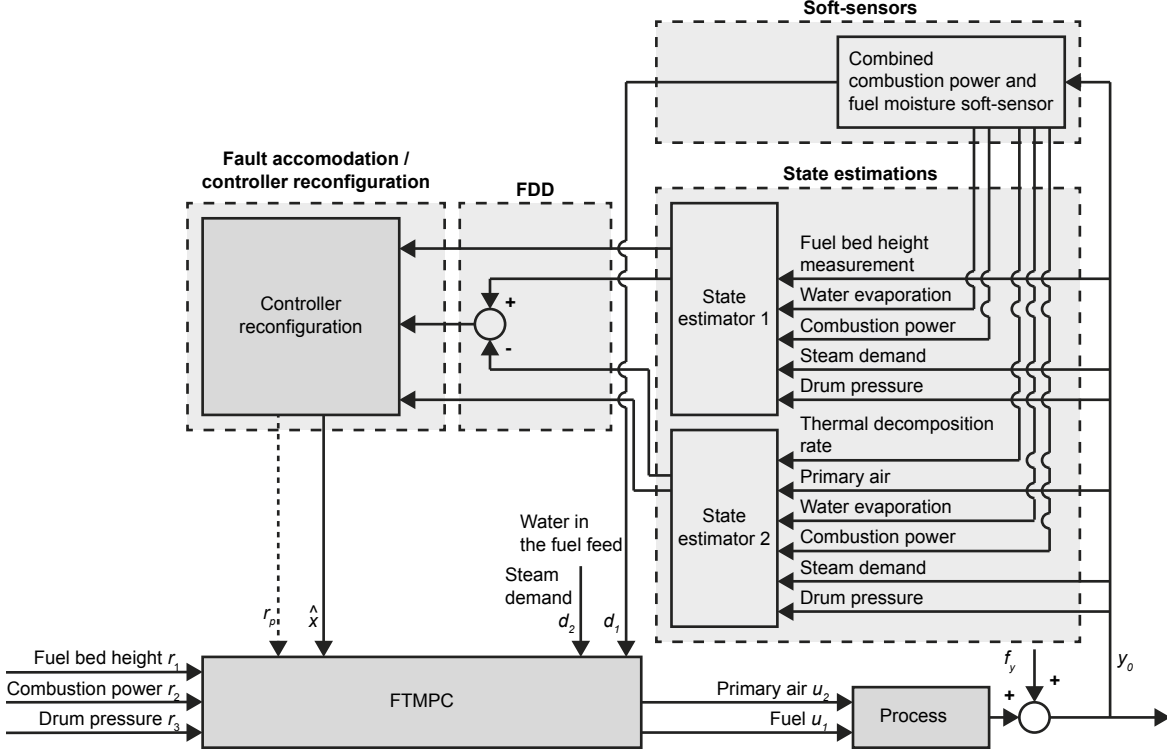


Fig. 2. FTMPC of the BioGrate boiler

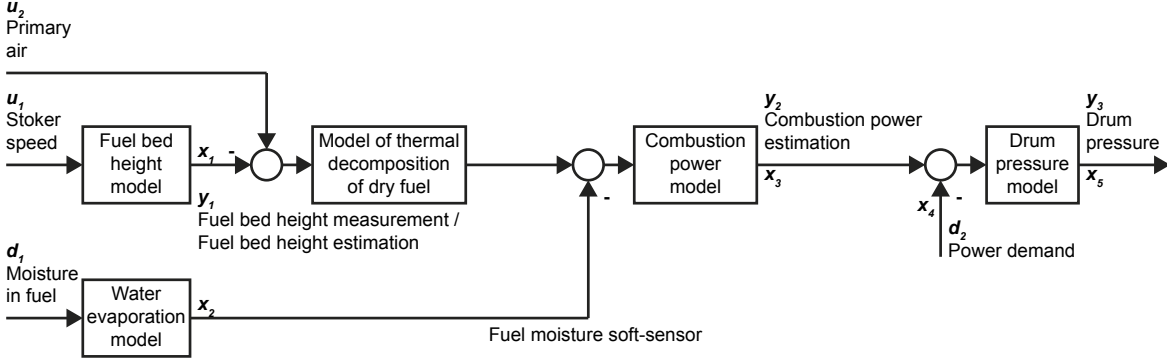


Fig. 3. The models of the BioGrate boiler

### 3.1 Controller reconfiguration

*Detection of faults in the fuel bed height sensor* Two state estimators in Fig. 2 utilize fuel moisture soft-sensor and combustion power estimations, steam, temperature, drum pressure measurements, and alternatively fuel bed height measurement and calculated fuel bed height to filter the states of the system, Fig. 3. In order to detect faults in the fuel bed height sensor, its filtered calculated value is compared with the filtered measurement. The fuel bed height can be expressed from the primary air flow rate and the thermal decomposition rate as follows:

$$m_{ds} = \frac{c_{thd} \cdot \dot{m}_{pa} \cdot \beta_{thd} - \dot{m}_{gf}}{c_{ds}} \quad (1)$$

where  $c_{thd}$  is the thermal decomposition rate coefficient,  $\dot{m}_{pa}$  is the primary air flow rate ( $\text{m}^3/\text{s}$ ),  $\beta_{thd}$  is the coefficient for a dependence on the position of the moving

grate,  $\dot{m}_{gf}$  is the thermal decomposition rate of the fuel,  $c_{ds}$  is the fuel bed height coefficient, describing the mass of the fuel proportional to the density of the fuel. If a bias of magnitude  $b_{y,i}$  occurs at time instant  $t$  in the  $i$ th sensor, then the measurement output for this sensor is given by (Prakash et al., 2002)

$$y(k) = Cx(k) + v(k) + b_{y,i}e_{y,i}\sigma(k-t) \quad (2)$$

Furthermore, when a fuel bed height sensor fault occurs, the residual  $\nu(k)$  and the two state fuel bed height estimates  $\hat{x}(k|k)$  start to diverge from each other.

$$\nu(k) = y(k) - C\hat{x}(k|k-1) \quad (3)$$

$$\hat{x}(k|k) = \hat{x}(k|k-1) + K(k)\nu(k); \hat{x}(0|0) = \hat{x}(0) \quad (4)$$

The failure of the fuel bed height measurement is detected if the *RMSEP* exceeds the detection threshold:

$$RMSEP = \sqrt{\frac{\sum_{i=1}^n |\hat{x}(i)_{1,1} - \hat{x}(i)_{1,2}|^2}{n}} \quad (5)$$

where  $n$  is the number of the samples in the test data set,  $\hat{x}(i)_{1,1}$  is the estimated fuel bed height of the first MPC configuration, and  $\hat{x}(i)_{1,2}$  the estimated fuel bed height of the second MPC configuration. The limit of detecting the faults is set above the normal disturbances of the states. Note that the fault isolation is implicitly done in the above fault detection procedure.

*MPC of the BioGrate boiler* The MPC utilizes the linear state space system (Maciejowski, 2002):

$$\begin{aligned} x(k+1) &= Ax(k) + Bu(k) + Ed(k) \\ y(k) &= Cx(k) \end{aligned} \quad (6)$$

where  $A$  is the state matrix,  $B$  is the input matrix,  $E$  is the matrix for the measured disturbances, and  $C$  is the output matrix. According to (6), the  $k$ -step ahead prediction is formulated as:

$$y(k) = CA^k x(0) + \sum_{j=0}^{k-1} H(k-j)u(j) \quad (7)$$

where  $\mathbf{H}(k-j)$  contains the impulse response coefficients. Therefore, using the Equation (7), the MPC optimization problem is:

$$\begin{aligned} \min \phi &= \frac{1}{2} \sum_{k=1}^{N_p} \|y(k) - r(k)\|_{Q_z}^2 + \frac{1}{2} \|\Delta u(k)\|_{Q_u}^2 \\ \text{s.t. } x(k+1) &= Ax(k) + Bu(k) + Ed(k), \\ &k = 0, 1, \dots, N_p - 1 \\ y(k) &= Cx(k), k = 0, 1, \dots, N_p \\ u_{\min} &\leq u(k) \leq u_{\max}, k = 0, 1, \dots, N_p - 1 \\ \Delta u_{\min} &\leq \Delta u(k) \leq \Delta u_{\max}, k = 0, 1, \dots, N_p - 1 \\ y_{\min} &\leq y(k) \leq y_{\max}, k = 1, 2, \dots, N_p \end{aligned} \quad (8)$$

where  $r$  is the target value and  $\Delta u(k) = u(k) - u(k-1)$ .

The process models of the BioGrate boiler have been developed in Kortela and Jämsä-Jounela (2014) and Kortela and Jämsä-Jounela (2015). Defining the inputs  $u$ , states  $x$ , outputs  $y$  and the measured disturbances  $d$  according to Fig. 3, the process models of the BioGrate are as follows:

$$\frac{dx_1}{dt} = c_{ds}x_1 - c_{thd}\beta_{thd}u_2 + c_{ds,in}u_1 + w_2 \quad (9)$$

$$\frac{dx_2}{dt} = -c_{wev}\beta_{wev}x_2 + c_{w,in}d_1 + w_1 \quad (10)$$

$$\frac{dx_3}{dt} = -x_3 + q_{wf}(c_{thd}\beta_{thd}u_2 - c_{ds}x_1) \quad (11)$$

$$-0.0244c_{wev}\beta_{wev}x_2 + w_3 \quad (12)$$

$$\frac{dx_4}{dt} = -x_4 + d_2 \quad (13)$$

$$\frac{dx_5}{dt} = \frac{1}{e}(x_3 - x_4) + w_4 \quad (14)$$

$$y_1 = x_1 + v_1 \quad (15)$$

$$y_2 = x_3 + v_2 \quad (16)$$

$$y_3 = x_5 + v_3 \quad (17)$$

where  $c_{ds,in}$  is the correction coefficient identified from the data,  $\beta_{wev}$  is the coefficient for a dependence on the position from the center to the periphery of the moving grate,  $c_{wev}$  and  $c_{w,in}$  are the model parameters estimated from the process data,  $q_{wf}$  is the effective heat value of the fuel (higher heat value) and 0.0244 the heat of vaporization of water.

The set points  $r_2$  and  $r_3$  for the combustion power and the drum pressure directly result from procedural considerations. The set point for the combustion power is calculated according to the steam demand and the drum pressure is kept constant. An important process parameter is  $\lambda_{fb}$  describing the ratio of primary air fed to the fuel bed and minimum amount of the air necessary for a complete combustion of fuel. From the amount of dry fuel in the thermal decomposition zone, the input variable  $\dot{m}_{pa}$  and the constant parameters ( $c_{thd}$ ,  $\beta_{thd}$ ,  $c_{ds}$ ), the set point  $r_1$  for the mass of dry fuel in the thermal decomposition zone is calculated.

$$m_{ds} = \frac{c_{thd} \cdot \dot{m}_{pa} \cdot \beta_{thd} - \dot{m}_{gf}}{c_{ds}} \quad (18)$$

Two different MPC configurations are developed for the process operating in two different modes, i.e. faultless or healthy mode and faulty mode. In the faultless mode, the primary air flow rate and the stoker speed are the manipulated variables ( $u$ ); the moisture content in the fuel feed and the steam demand are the measured disturbances ( $d$ ); and the fuel bed height and the steam pressure are the controlled variables ( $y$ ). While for the faulty mode, the controlled variables are modified: i.e. the output  $y$  is composed of the fuel bed height, the combustion power and the steam pressure. Once the fault is detected and isolated using the scheme described in Section 3.1.1, the controller is reconfigured from the healthy mode to the faulty mode.

## 4. TEST RESULTS OF THE FTMPC STRATEGY

### 4.1 Description of the simulation and testing environment

A simulation model of the BioPower 5 CHP plant was built in the MATLAB environment and additionally, the code for the FTMPC was developed. Parameters of the models of the water evaporation, the thermal decomposition of the dry fuel, and the drum were identified by using the data from the BioPower 5 CHP plant. Moreover, to identify the fuel bed height model, the plant was further modified by installing 8 pressure sensors for the BioGrate to measure the fuel bed height pressure.

### 4.2 Test results of the FTMPC strategy

To demonstrate the effectiveness of the proposed FTMPC strategy, the performance of the FTMPC was evaluated using the BioGrate boiler simulator in a MATLAB environment.

The input limits were  $u_{1,min} = 0$ ,  $u_{1,max} = 4$ ,  $\Delta u_{1,min} = -0.03$ , and  $\Delta u_{1,max} = 0.03$  [kg/s] for the stoker speed;  $u_{2,min} = 0$ ,  $u_{2,max} = 4$ ,  $\Delta u_{2,min} = -0.03$ , and  $\Delta u_{2,max} = 0.03$  [kg/s] for the primary air.

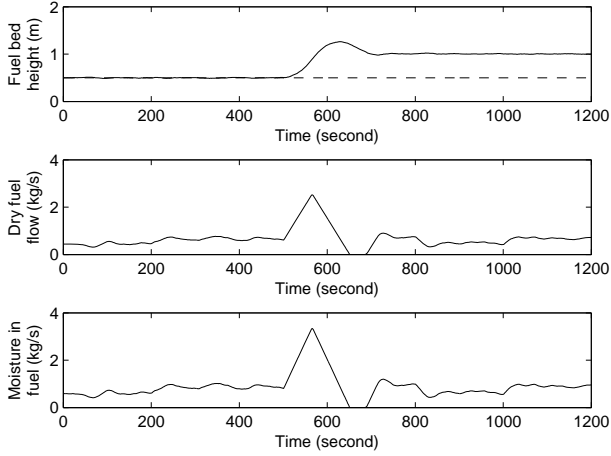


Fig. 4. Responses of the moisture in fuel, dry fuel flow, and fuel bed height to 100% bias fault in the fuel bed height sensor without the FTMPC active.

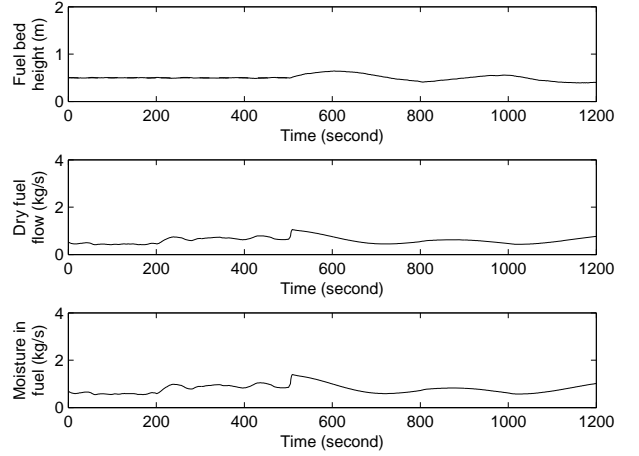


Fig. 6. Responses of the moisture in fuel, dry fuel flow, and fuel bed height to 100% bias fault in the fuel bed height sensor with the FTMPC active.

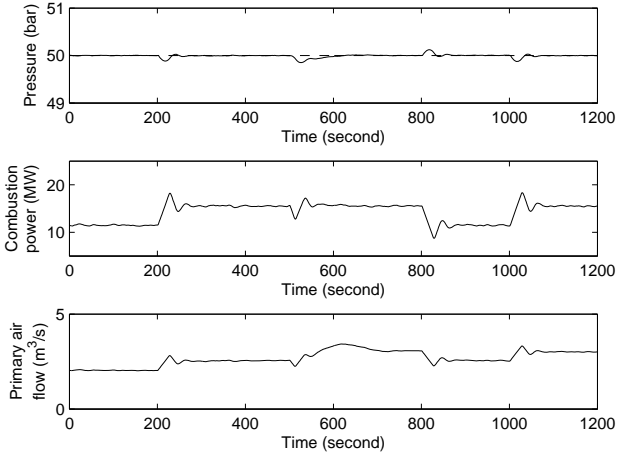


Fig. 5. Responses of the pressure, combustion power, and primary air flow to 100% bias fault in the fuel bed height sensor without the FTMPC active.

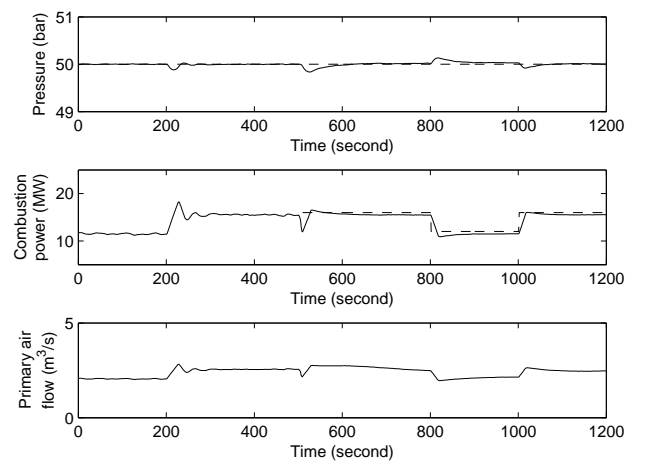


Fig. 7. Responses of the pressure, combustion power, and primary air flow to 100% bias fault in the fuel bed height sensor with the FTMPC active.

In the nominal case, the output limits were  $y_{1,min} = 0.2$ ,  $y_{1,max} = 1$  [m] for the fuel bed height; and  $y_{2,min} = 0$ ,  $y_{2,max} = 55$  [bar] for the drum pressure.

$$\mathbf{Q}_{z,1} = \begin{bmatrix} 0.1 & 0 \\ 0 & 0.1 \end{bmatrix} \quad \text{and} \quad \mathbf{Q}_{u,1} = \begin{bmatrix} 0.1 & 0 \\ 0 & 0.1 \end{bmatrix}$$

In the reconfiguration, the output limits were  $y_{1,min} = 0.2$ ,  $y_{1,max} = 1$  [m] for the fuel bed height;  $y_{2,min} = 0$ ,  $y_{2,max} = 30$  [MW] for the combustion power; and  $y_{3,min} = 0$ ,  $y_{3,max} = 55$  [bar] for the drum pressure.

$$\mathbf{Q}_{z,2} = \begin{bmatrix} 0.001 & 0 & 0 \\ 0 & 0.001 & 0 \\ 0 & 0 & 0.1 \end{bmatrix} \quad \text{and} \quad \mathbf{Q}_{u,2} = \begin{bmatrix} 0.1 & 0 \\ 0 & 0.1 \end{bmatrix}$$

The test scenario had a downward step-shaped fault in the fuel bed height measurement of 100% of the nominal value and the power demand was changed from 12 MW to 16 MW after 200 seconds. The fault was introduced into the fuel bed height measurement after 500 seconds. Then,

the power demand was changed from 16 MW to 12 MW during the time period of 800 - 1000 seconds. As it can be seen from the Figs. 4-7, the fault resulted in the extremely high values of the primary air and the fuel bed height. Fig. 8 shows the RMSEP index of the different fuel bed height state of MPC 1 and MPC 2.

## 5. CONCLUSIONS

A fuel bed height sensor is a critical element in the control of the BioGrate boiler and for optimal energy production its faulty operation should thus be avoided. In this paper a FTMPC strategy was proposed to accommodate the fault in the fuel bed height sensor by active controller reconfiguration where two different control configurations are run in parallel. In these configurations, two alternative control variables, fuel bed height and combustion power, were utilized.

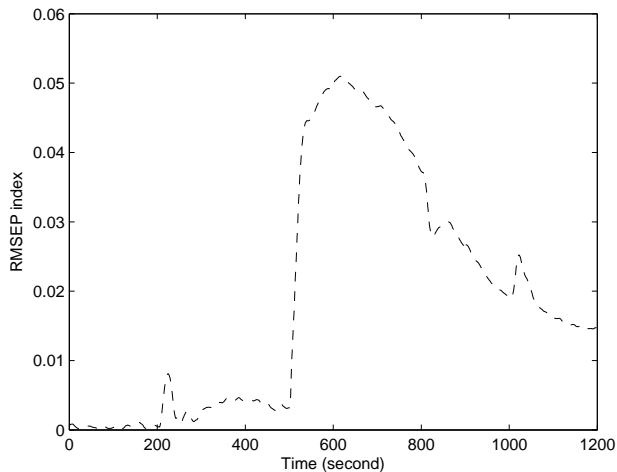


Fig. 8. Scenario 1: RMSEP index of fuel bed height state of MPC 1 and MPC 2.

The FTMPC was tested with the simulated BioPower 5 CHP plant. On the basis of the simulation results, the proposed FTMPC was able to counter the most typical fault in the BioPower 5 CHP plant caused by the unknown fuel quality and the status of the furnace (amount of fuel in the furnace). Therefore, the performance and the profitability of the BioPower 5 CHP plant would be significantly enhanced if such an FTMPC strategy is implemented.

#### REFERENCES

- Boriouchkine, A., Zakharov, A., Jämsä-Jounela, S.-L. (2012). Dynamic modeling of combustion in a BioGrate furnace: The effect of operation parameters on biomass firing. *Chemical Engineering Science*, 69(1), 669–678.
- Edlund, K., Bendtsen, J.D., Jørgensen, J.B. (2011). Hierarchical model-based predictive control of a power plant portfolio. *Control Engineering Practice*, 19(10), 1126–1136.
- Gölles, M., Bauer, R., Brunner, T., Dourdoumas, N., Obernberger, I. (2011). Model based control of a biomass grate furnace. In *Proceedings of the 9th European conference on industrial furnaces and boilers*. Estoril, 26-29 April 2011, pp. 1–10.
- Gölles, M., Reiter, S., Brunner, T., Dourdoumas, N., Obernberger, I. (2014). Model based control of a small-scale biomass boiler. *Control Engineering Practice*, 22, 94–102.
- Kortela, J., Jämsä-Jounela, S.-L. (2013). Fuel moisture soft-sensor and its validation for the industrial BioPower 5 CHP plant. *Applied Energy*, 105, 66–74.
- Kortela, J., Jämsä-Jounela, S.-L. (2014). Model predictive control utilizing fuel and moisture soft-sensors for the BioPower 5 combined heat and power (CHP) plant. *Applied Energy*, 131, 189–200.
- Kortela, J., Jämsä-Jounela, S.-L. (2015). Modeling and model predictive control of the BioPower combined heat and power (CHP) plant. *International Journal of Electrical Power & Energy Systems*, 65, 453–462.
- Kortela, U., Lautala, P. (1982). A new control concept for a coal power plant. *Control Science and Technology for the Progress of Society*, 6, 3017–3023.
- Kortela, U., Marttinen, A. (1985). Modelling, Identification and Control of a Grate Boiler. In *Proceedings of the 1985 American Control Conference*. Boston, 19-21 June 1985, pp. 544–549.
- Leão, R.P.S., Barroso, G.C., Sampaio, R.F., Almada, J.B., Lima, C.F.P., Rego, M.C.O., Antunes, F.L.M. (2011). The future of low voltage networks: Moving from passive to active. *International Journal of Electrical Power & Energy Systems*, 33(8), 1506–1512.
- Leskens, M., van Kessel, L.B.M., Bosgra, O.H. (2005). Model predictive control as a tool for improving the process operation of MSW combustion plants. *Waste Management*, 25(8), 788–798.
- Maciejowski, J.M. (2000). *Predictive Control with Constraints*. Prentice Hall, Harlow, pp. 36–150.
- Prakash, J., Patwardhan, S.C., Narasimhan, S. (2002). A Supervisory Approach to Fault-Tolerant Control of Linear Multivariable Systems. *Industrial & Engineering Chemistry Research*, 41(9), 2270–2281.
- Yin, C., Rosendahl, L.A., and Kær, S.K. (2008). Grate-firing of biomass for heat and power production. *Progress in Energy and Combustion Science*, 34(6), 725–754.

# Relative Gain Measures for Once-through Circulating Fluidized Bed Boiler Control Design

Matias Hultgren\*. Jenő Kovács\*\*. Enso Ikonen\*

\* *Systems Engineering Laboratory, University of Oulu, POB 4300, 90014 Oulu, Finland. firstname.lastname@oulu.fi*

\*\* *Foster Wheeler Energy Ltd, Varkaus, Finland. jeno.kovacs@fwfin.fwc.com.*

---

**Abstract:** The present work describes the use of relative gain based measures for pairing manipulated and controlled variables in circulating fluidized bed (CFB) power plant control design. Combustion power plant control has become challenging during recent years due to increasingly fast load change demands, the need to constantly improve the boiler efficiency, the interconnected and cyclic nature of the flowsheet and the extreme operating conditions in the process, especially when the once-through (OTU) steam cycle is considered. These challenges call for a deeper interaction between control and process design, which can be performed in various ways through process characterization techniques or mathematical programming design frameworks. The topic of integrated control and process design is currently being investigated by the authors, and a part of this work is the definition of criteria for desirable control performance. Integrated design often requires a plantwide focus, and plantwide control can be considered as one of the research directions within this topic.

One central question for plantwide control is the pairing of manipulated (MV) and controlled variables (CV) to form the control system topology. One popular tool for this purpose is the relative gain array (RGA), which utilizes open-loop steady-state gain information. As a pairing based on the RGA alone might produce misleading results for larger MIMO systems and disregard gain effects in partially controlled systems, the partial relative gain (PRG) metric has been proposed in literature to provide an improved MV-CV pairing. Loop selection with the PRG is performed to ensure integral controllability with integrity (ICI), where the system remains unconditionally stable with any combination of controllers in or out of service. ICI is achieved with positive RGA and Niederlinski index (NI) values for the open-loop system pairings, and positive PRG values for the pairings of any partially controlled subsystem.

This work investigated the proposed PRG controllability measure and determined its suitability for CFB boiler control structure design. After initial testing with steam cycle and combustion side models from literature, the PRG pairing was applied to a complete industrial OTU-CFB power plant model of Foster Wheeler. The model was a fully validated APROS software simulator, which contained both the OTU water-steam cycle and a 1-D Matlab/Simulink combustion side model. The simulator was utilized to generate the steady-state gain matrix of the system by performing step changes close to the nominal operating point for the main process inputs (load, turbine valve, feedwater flow, fuel flow, air flows, desuperheater spray flows). The RGA, NI and PRG metrics were then used for the gains in order to generate the MV-CV pairings. The results showed that the PRG was able to form feasible control structures for the OTU-CFB, and many of the suggested pairings confirmed the validity of existing boiler control design practices. The PRG metric proved to be more effective for solution candidate screening than the more commonly used RGA, which suggested more solutions with limited practical applicability.

The testing showed that relative gain analysis could be applied to yield a limited amount of satisfactory OTU-CFB control structure candidates, utilizing only steady-state gains to reach the final solution. Consequently, the PRG showed potential as an easily applicable tool for the early stages of control and process design. However, the work also disclosed shortcomings of the PRG analysis in the generation of boiler control strategies, as the tight ICI requirements ruled out some control options that are known to be preferable in real life due to their dynamic properties. This applied especially to the so called unit master configuration between output MW and steam pressure control (“turbine-following” or “boiler-following” control), and the “boiler-following” configuration with its fast MW responses was rarely deemed as ICI or suggested as a solution by the PRG. Therefore, steady-state analysis and the specified MV-CV pairing rules alone might not form a sufficient basis for selecting the final plantwide control design for the CFB.

*Keywords:* CFB, power plant control, relative gain analysis, integral controllability with integrity, plantwide control.

---

# ***Model-based optimal design and control of an anaerobic digestion reactor***

Results are presented from a research project involving theoretical and experimental work based on a real pilot UASB type AD reactor fed with animal waste (cow manure) at Foss dairy farm, Skien, Telemark, Norway. The main results from this project are:

- A mechanistic dynamic AD model, named the modified Hill model, has been adapted to the pilot reactor using steady-state and dynamic data from on-line sensors and laboratory analysis. A dynamic model for the reactor temperature based on an energy balance of the liquid is adapted to the pilot reactor.
- Both simulations and practical experiments show that the produced CH<sub>4</sub> gas flow depends on the reactor temperature, indicating a need for feedback temperature control. Both on-off control and industry-standard PI control are shown appropriate as controllers. The Skogestad PI controller tuning method for "integrator with time-delay" process dynamics with parameters estimated from the process step response is identified as the favoured tuning method. A novel closed loop tuning method, named Relaxed Ziegler-Nichols tuning method, which is based on a combination of the Skogestad method and the original Ziegler-Nichols closed-loop tuning method, compares favourably with both the Ziegler-Nichols method and the Tyreus-Luyben tuning method.
- The produced power is proportional to the produced CH<sub>4</sub> gas flow, at fixed conditions. Therefore, a constant power production may be obtained by controlling the CH<sub>4</sub> flow control to a setpoint. Conditions for safe reactor operation are found using steady-state responses of dynamic simulations, taking into account an upper limit of the reactor VFA concentration recommended in the literature. Both simulations and practical experiments indicate that both an on-off controller and the industrial-standard PI controller are viable for CH<sub>4</sub> gas flow control. The Skogestad method is (again) identified as the favoured controller tuning method.
- A state estimator, or a soft sensor, is implemented in the form of the Unscented Kalman Filter (UKF) algorithm based on the modified Hill model and using continuous measurement of CH<sub>4</sub> gas flow. The UKF estimates continuously the four model state variables of the modified Hill model, and an augmented state variable which is the concentration of volatile solids of the influent. The estimates are verified against laboratory analyses. (Contrary to the common Extended Kalman Filter, the UKF avoids model linearization.)
- Various model-based control systems have been designed using the modified Hill model and the UKF: A model-based predictive controller (MPC) is designed for controlling the methane gas flow to a setpoint which may be varied, e.g. due to changing produced power demands. Simulations indicate that, with a known setpoint profile, the setpoint tracking with MPC is considerably better than with PI control. For unknown disturbance changes, the disturbance compensation is not much better with MPC than with PI control, as expected. The MPC is applied successfully to the real pilot reactor with known CH<sub>4</sub> gas flow setpoint profile. An MPC aiming at retaining the reactor at an operating point with maximum allowable VFA concentration, is compared with PI control based on feedback from VFA estimated with the UKF, on a simulator (no practical experiments). Here, MPC and PI control have similar performance, but PI control being much simpler, of course.
- Optimal design and operation, regarding e.g. reactor volume and temperature, of the planned full-scale reactor are determined using simple brute-force optimization based on steady state simulations of the modified Hill AD model combined with models of the reactor temperature and heat exchanger temperatures based on energy balances. Various optimization criteria are considered.

The above results are reported in detail in the author's PhD thesis entitled *Optimal Design, Operation and Control of an Anaerobic Digestion Reactor*, Telemark University College, Norway, 2014.

# A study on the combustion dynamics of a biomass fuel bed in a BioGrate boiler

Alexandre Boriouchkine<sup>\*a</sup>, Vida Sharifi<sup>b</sup>, Jim Swithenbank<sup>b</sup>, Sirkka-Liisa Jämsä-Jounela<sup>a</sup>

<sup>a</sup>School of Chemical Technology, Aalto University, P.O. Box 16100, 00076 Aalto, Finland  
alexandre.boriouchkine@aalto.fi

<sup>b</sup>Department of Chemical and Biological Engineering, The University of Sheffield, Mappin Street, Sheffield, S1 3JD, UK

---

## Abstract

The main objective of this research was to study fuel bed combustion dynamics of a BioGrate boiler with a mechanistic model. First, the fuel specific pyrolysis reaction rates were experimentally determined for the model. Second, the model was validated and finally, it was used to investigate the effects of the primary air flows on drying, pyrolysis and char consumption rates occurring inside the fuel bed. The research results are presented and the role of the dynamic behavior of the reactions on improving the efficiency of the biomass combustion process discussed.

---

## 1. Introduction

Biomass is receiving increasing attention as an alternative energy resource to fossil fuels due to increasing environmental concerns related to energy production. However, biomass is associated with varying fuel composition; in addition, it is highly dependent on storing conditions as well as on local and seasonal factors. Such variations affect power production efficiency and increased pollution. As a consequence a fuller understanding of the factors which affect the efficiency of power production is particularly important for the further development of these types of energy systems. Mathematical models have shown to be an excellent tool in assessing the complex physical phenomena of biomass combustion.

Shin and Choi (2000) utilized modeling to determine the effect of process parameters on the combustion of municipal waste. The results indicated that a low air flow rate limits the combustion rate, whereas, an excessively high flow rate results in flame extinction. Van der Lans et al. (2000) described straw combustion with a two dimensional steady-state model and studied the effect of the combustion parameters on the burning of the fuel bed. Goh et al. (2000) have developed a model to simulate an incinerator bed; the results from the study indicated that fuel mixing can be modelled with swap probability method. The model developed by Yang et al. (2002) showed that air channelling can increase the concentrations of hydrocarbons in flue gas due to poor mixing. Similarly, a study by Kær (2004) suggested that poor mixing of flue gases and secondary air results in high CO concentrations and in unburnt carbon in fly ash. Miljkovic et al. (2013) constructed a model for straw bale combustion to obtain information such as a temperature profile of the fuel bed, a combustion rate and the produced chemical species. Hallett et al. (2013) found through experimental and modelling work that a volume-surface mean diameter can be used to describe non-uniformly sized particles. Combustion in a conical grate boiler was described mathematically by Boriouchkine et al. (2012) to provide information on the combustion characteristics of woody biomass, with specific emphasis on the effects of moisture content, particle size and air flow on the combustion in a BioGrate boiler.

To summarize, these studies focused solely on combustion under steady-state conditions to evaluate the effect of several parameters, like the fuel moisture content and the air flow on the burning behavior of the biomass fuel bed. However, very little research has been done on the dynamics of the burning fuel bed which is a particularly important issue, as during the operation, a boiler is subject to several dynamic disturbances (Kortela and Jämsä-Jounela, 2012), such as changes in a power demand. Consequently, the performance of a boiler is largely dependent on the behavior of a burning fuel bed under changing conditions.

Due to the importance of fuel bed combustion dynamics, this paper focuses on studying the local and furnace wide dynamic model of fuel combustion and, especially, the model of drying, pyrolysis and char combustion reactions as well as the temperature inside the bed. The analysis is done by inducing

changes to the primary air flow of different magnitudes and amplitudes, and at different conversion stages to gain insight into the time-dependent combustion modelled. The simulations considered fuel combustion in a BioGrate boiler which is a conical grate boiler that operates under concurrent combustion conditions.

## 2. Dynamic Model of a BioGrate boiler furnace

In a BioGrate boiler, biomass reacts through three main reaction pathways which can occur either in parallel or sequentially with respect to each other: drying, pyrolysis and char conversion and the mechanistic model of the BioGrate boiler considers these three stages of the biomass combustion. The burning fuel bed in a BioGrate boiler is modelled in one dimension using the walking grate assumption, since temperature gradients are more significant in a vertical than in a horizontal direction. Furthermore, since BioGrate boilers operate under concurrent combustion the combustion front propagates upward in the direction of the airflow.

### 2.1 Modelling of the solid phase mass conservation

The solid phase reactions considered by the model include drying, pyrolysis as well as char oxidation and gasification which in general can be described by Eq. (1).

$$\frac{\partial \rho_{s,j}}{\partial t} = -r_{s,j} \quad (1)$$

where  $\rho_{s,j}$  is the mass concentration of each solid component (moisture, volatiles and char) while  $r_{s,j}$  is the reaction rate of a respective component.

The rate of drying, Eq. (2), is defined by the energy available for evaporation. For numerical stability, the evaporation rate is multiplied by a conversion factor  $\rho_{s,H_2O}/\max(\rho_{s,H_2O})$ . Although this lowers the maximum local evaporation rates, as more energy is transferred to the consequent layers, the overall evaporation in the fuel bed rate remains the same as without the factor.

$$r_{s,H_2O} = \max(0, (\rho_{s,H_2O}/\max(\rho_{s,H_2O})) C_p (T_s - 373.15K) / dt) / \Delta H_{vap} \quad (2)$$

where  $T_s$  is the temperature of the solid phase and  $\Delta H_{vap}$  is the vaporization enthalpy.

The accurate modelling of fuel combustion requires that pyrolysis rate equations are determined for the simulated fuel. In this study, pyrolysis rate equations were estimated for debarking residue produced from Norway spruce. The equations were estimated from mass loss curves obtained from thermogravimetric analysis (TGA) performed in a Perkin Elmer TGA 4000 apparatus under nitrogen atmosphere (20 ml/min) and with the heating rate of 80 K/min. The rate equations were then estimated by fitting the simulated mass loss curve to the one obtained from TGA with sequential quadratic programming. The fitting results suggested that in order to obtain satisfactory fit, the pyrolysis had to be described by two parallel subreactions with the assumption of first-order kinetics. This suggested that a fuel sample comprises two components with distinct decomposition behaviors which are likely to be lignin and holocellulose. The initial mass of each component was estimated along with the rate equations and for the first volatile component it was 15.39 w% and for the second one 84.61 w% of the initial fuel sample. The obtained reaction rate constants are given in Eq. (3) and (4).

$$k_{1,pyr} = 3.16 \cdot 10^2 \exp(-1.37 \cdot 10^5 / (RT_s)) \quad (3)$$

$$k_{2,pyr} = 2.21 \cdot 10^4 \exp(-7.84 \cdot 10^4 / (RT_s)) \quad (4)$$

Char is consumed in three different chemical reactions: oxidation, Eq. (5), (Branca and Di Blasi, 2003) with the associated CO/CO<sub>2</sub> ratio, Eq. (6), (Evans and Emmons, 1977) and reduction with H<sub>2</sub>O, Eq. (7) (Senneca, 2007) and CO<sub>2</sub>, Eq. (8) (Matsumoto et al., 2009).

$$k_{s,C} = 1.1 \cdot 10^6 \cdot \exp(-114.5 \cdot 10^3 / (RT_s)) \quad (5)$$

$$CO/CO_2 = 4.3 \exp(-3390 / T_s) \quad (6)$$

$$k_{s,H_2O} = 9.99 \cdot 10^4 \cdot \exp(-136 \cdot 10^3 / (RT_s)) (1-X) \sqrt{1-10 \ln(1-X)} \quad (7)$$

$$k_{s,CO_2} = 1.1 \cdot 10^9 \exp(-260 \cdot 10^3 / (RT_s)) X \quad (8)$$

where  $X$  is the conversion stage of char.

For each heterogeneous char reaction, an effective reaction constant - given by Eq. (9) - is then calculated as follows:

$$k_{eff,i} = v_p k_{c,i} k_{r,i} / (v_p k_{c,i} + k_{r,i}) \quad (9)$$

where  $v_p$  is the area to volume ratio of a particle,  $k_{r,i}$  is the reaction constant and  $k_{c,i}$  is the mass transfer coefficient.

## 2.2 Modelling of the gas phase mass conservation

The gas phase modelling, presented in Eq. (10), describes convection of each gaseous specie ( $O_2, N_2, CH_4, H_2, CO, CO_2, Tar, H_2O$ ), combustion of CO (Eq. (11)) (Babushok and Dakdancha, 1993),  $H_2$  (Eq. (12)) (Pomerantsev, 1986) and  $CH_4$  (Eq. (13)) (Pomerantsev, 1986), and gas formation in the pyrolysis reaction,  $Y_{g,i} r_{s,pyr}$ .

$$\partial(\rho_{g,i} \varepsilon_b) / \partial t - \partial(v_g \rho_{g,i} \varepsilon_b) / \partial x = -r_{g,i} + Y_{g,i} r_{s,pyr} \quad (10)$$

where  $\rho_{g,i}$  is the mass concentration of a gaseous specie,  $\varepsilon_b$  is the bed porosity,  $v_g$  is the velocity of the gas,  $r_{s,pyr}$  is the pyrolysis reaction rate, while  $Y_{g,i}$  is the mass fraction of the forming gaseous pyrolysis product.

$$r_{g,CO} = 1.3 \cdot 10^{14} \exp(-125.5 \cdot 10^3 / (RT_g)) C_{CO} C_{O_2}^{0.5} C_{H_2O}^{0.5} \quad (11)$$

$$r_{g,H_2} = 2.14 \cdot 10^{14} \exp(-129 / (RT_g)) C_{O_2} \quad (12)$$

$$r_{g,CH_4} = 5.6 \cdot 10^{12} \exp(-103.8 / (RT_g)) C_{O_2} \quad (13)$$

## 2.3 Modelling of the solid phase energy conservation

The energy equation for the solid phase describes heat conduction, heat exchange between the phases, energy consumed in the drying and pyrolysis reactions and energy gained in char combustion (Eq. (14)):

$$C_s \rho_s \partial T_s / \partial t = \partial(k_{s,eff} \partial T_s / \partial x) / \partial x + k_{conv} v_p (T_g - T_s) + \sum Q_{reactions,solid} + k_a (I^+ + I^-) - k_a \sigma T_s^4 \quad (14)$$

where  $k_{conv}$  is the convective heat transfer coefficient,  $k_{s,eff}$  is the effective heat conduction coefficient of the solid phase,  $k_a$  is the absorption coefficient,  $I^+$  is the radiative flux in the direction of the fuel layer surface,  $I^-$  is the flux in the direction of the grate,  $T_g$  is the gas phase temperature,  $T_s$  is the solid temperature and  $Q_{reactions,solid}$  is the energy produced or consumed in the solid phase reactions (drying, pyrolysis and char reactions),  $\sigma$  is Stefan-Boltzmann constant.

The radiative heat transfer inside the bed is described with a two-flux model given by Eq. (15) and (16), where the absorption and scattering coefficients are given by Eq. (17) (Shin and Choi, 2000) where  $d_p$  is the fuel particle diameter.

$$dI^+ / dx = -(k_a + k_s) I^+ + k_s I^- + 1/2 k_a \sigma T_s^4 \quad (15)$$

$$-dI^- / dx = -(k_a + k_s) I^- + k_s I^+ + 1/2 k_a \sigma T_s^4 \quad (16)$$

$$k_a = -1/d_p \ln(\varepsilon_b), \quad k_s = 0 \quad (17)$$

## 2.4 Modelling of the gas phase energy conservation

The energy continuity equation, Eq. (18) of the gas phase considers the heat exchange between the gas and solid phases, the energy received through gas convection, and the energy gained from carbon monoxide, methane and hydrogen oxidation.

$$\rho_g \partial(H_g \varepsilon) / \partial t + \partial(\varepsilon v_g H_g) / \partial x = \sum Q_{\text{reactions, gas}} - k_{\text{conv}} v_p (T_g - T_s) \quad (18)$$

where  $H_g$  is the overall enthalpy of the gas phase and  $Q_{\text{reactions, gas}}$  is the energy released in the oxidation of CO, CH<sub>4</sub> and H<sub>2</sub>.

## 3. Model validation with the estimated kinetic parameters

The model with the estimated kinetic parameters was evaluated against ignition front propagation velocities presented in Saastamoinen et al. (2000) for fixed bed combustion of spruce wood chips. The validation showed that the model predictions were similar to the measured values presented in Saastamoinen et al. (2000) (Table 1). This shows that the model predictions are valid in a range of moisture contents and airflows. The model was also validated against the gas concentrations measured in the study by Girgis and Hallett (2010). The results, Figure 1, show acceptable accuracy of the model.

Table 1. Comparison between the measured combustion front propagation velocities and the ones predicted by the model

Moisture content, w%	Air flow	Saastamoinen et al. (2000) mm/s	Model prediction mm/s 20 mm/ 12.5 mm
10.8	0.07	0.42	0.468/0.476
	0.15	0.58	0.519/0.571
	0.23	0.47	0.476/0.529
18.8	0.07	0.34	0.380/0.391
	0.15	0.47	0.420/0.484
	0.23	0.39	0.414/0.426
33.4	0.07	0.28	0.257/0.244
	0.15	0.25	0.268/0.292
	0.23	0.27	0.277/0.260

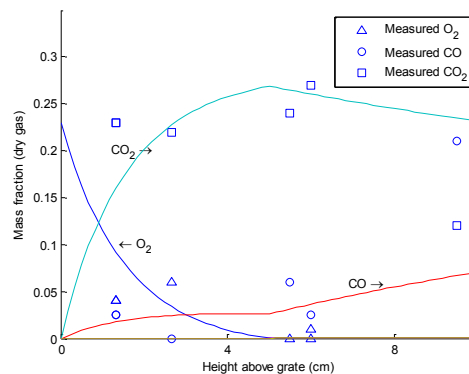


Figure 1. Gas phase composition during the simulation with steps in the airflow

## 4. Combustion dynamics of a fuel bed

### 4.1 Local combustion dynamics

Combustion of a biomass fuel bed provides energy for boiler operation and thus boiler dynamics depend to a large extent on the fuel combustion dynamics. In this study, the combustion dynamics were analyzed

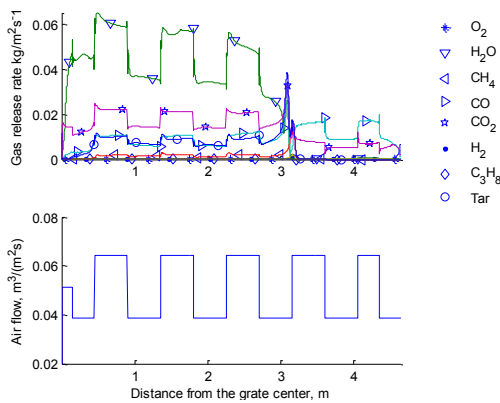


Figure 2. Gas phase composition during the simulation with steps in the airflow

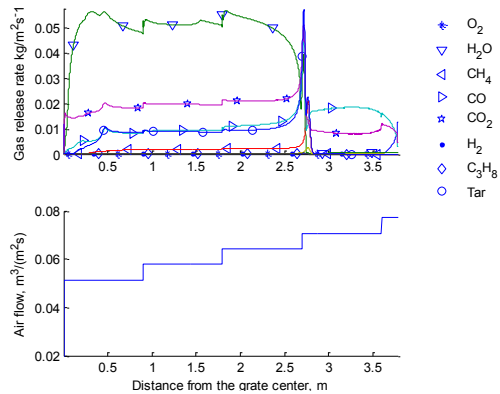


Figure 3. Gas phase composition during the simulation with a gradual increase in the airflow

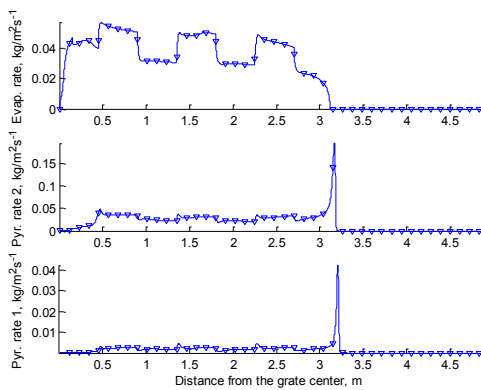


Figure 4. Reaction dynamics during the simulation with steps in the airflow

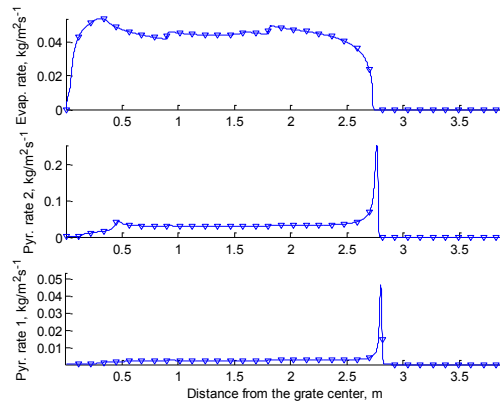


Figure 5. Reaction dynamics during the simulation with a gradual increase in the airflow

with the mechanistic model by changing the rate of primary air flow fed into the burning fuel bed and by analyzing the effects on drying, pyrolysis and char combustion. In simulations, the bed density was  $150 \text{ kg/m}^3$  on a dry basis, moisture content 55 w%, the fuel layer was 0.5 m high, the freeboard temperature  $900 \text{ }^\circ\text{C}$  and the fuel speed 1.5 mm/s. The air flows were varied between  $3 \text{ m}^3/\text{s}$  and  $5 \text{ m}^3/\text{s}$  which is the nominal air flow range used in BioGrate boilers.

The dynamic responses shown in Figures 2 and 3 indicate a significant effect of the air flow on the amount of the released gas and especially on the amount of released water. The effect of the air flow on the drying rate is also confirmed by the reaction rates presented in Figures 4 and 5 which show that the increase in the air flow notably increases the drying rate. Furthermore, the results suggest that water evaporation is only affected by the current air flow rate and not by the previously used flows as the simulations with two different air flows indicate that evaporation rate dependent only on the air flow rate, but not on the pattern of changes in the flow. The dependence of drying on the air flow was particularly well demonstrated by the simulation with a gradually increasing air feed which showed that the combustion time was significantly shortened compared to the other cases. Such behavior indicates that the increase in the gas flow also improves the overall heat exchange due to increased convection which, in turn, enhances drying.

Similar to drying, the pyrolysis reaction rates also showed the dependence on the air flow, however, the influence was slightly smaller. For instance, the decrease in the air flow from  $5$  to  $3 \text{ m}^3/\text{s}$ , which occurred between 0.5 and 1 m from the grate center (Figure 4), decreased the drying rate by 40% whereas the pyrolysis of the first component was decreased by 30%.

## 4.2 Furnace wide combustion dynamics

Furnace wide combustion dynamics were investigated by switching fuel moisture content at time instance  $t = 0$  s from 55 w% to 20 w%. Due to the higher heating value of the drier fuel and in order to maintain the constant power output, the control system gradually decreases the fuel feed rate and air supply. This control action was reproduced in the simulations by decreasing the fuel speed in proportion to the air supply (Figure 7).

The results demonstrated (Figure 7) that the release rate of each combustion product ( $H_2O$ , CO,  $CO_2$ ,  $CH_4$  and Tar) had a unique behavior. Similar to the local combustion dynamics the water evaporation had the most dependence on the air supply rate. Furthermore, the release rate of water vapor reached the new steady state quicker compared to the other components. In addition, the decrease in air flow velocity below 0.025 m/s did not decrease the evaporation rate further as was observed in the release of other components. In case of the carbon dioxide, its release rate stabilized, although not completely, before that of carbon monoxide. In addition, the amount of produced carbon monoxide was less affected by the change in the air supply than the amount of carbon dioxide. This suggests that oxygen is mostly consumed in char oxidation reaction to form CO and that at the combustion temperature of the drier fuel, carbon monoxide is the main product of char combustion. In general, only the carbon dioxide formation reached its new steady state with the air flow while other gases, except  $H_2O$ , reached it only after 300 s.

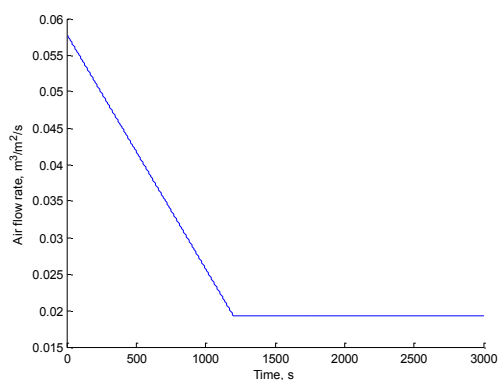


Figure 6. Air flow rate used for simulations

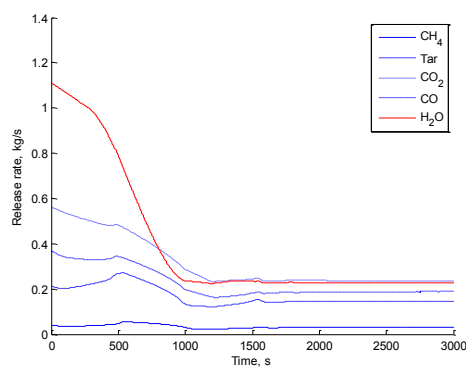


Figure 7. Gas release rate from the furnace

## 5. Conclusions

Simulations showed that combustion dynamics are largely dependent on the air flow. All reactions demonstrated a quick local response to the changed conditions. In the furnace wide investigation, the major changes in gas formation occurred quite rapidly, although the final settling time for the release rates of some components was several minutes. This implies that boilers which operate under concurrent combustion conditions can relatively quickly respond to changes in the power production demand. Furthermore, the dynamics of the system results in a quick response to the fuel bed combustion on the control actions.

Based on the simulated behavior of drying, pyrolysis and char reactions, it can be argued that moisture evaporation controls the pyrolysis rate by absorbing most of the energy produced by char combustion thus preventing the temperature from reaching the point where pyrolysis could start. Furthermore, the increased air flow influences the pyrolysis rate less significantly since drying consumes most of the extra energy generated by char oxidation. However, the results indicated that drying rate can be effectively controlled by the air flow and thus the combustion of fuels with high moisture content, which are extensively used in BioGrate boilers, can be intensified by using higher air flow rates.

## References

1. Babushok V.I., Dakdancha A.N., 1993, Global kinetic parameters for high-temperature gas-phase reactions, *Combust. Explo. Shock+* 29, 464–489
2. Boriouchkine A., Zakharov A., Jämsä-Jounela S.-L., 2012, Dynamic modeling of combustion in a BioGrate furnace: The effect of operation parameters on biomass firing, *Chem. Eng. Sci.* 69, 669-678
3. Branca C., Di Blasi C., 2003, Global Kinetics of Wood Char Devolatilization and Combustion, *Energ. Fuel.* 17, 1609-1615
4. Evans D.D., Emmons H.W., 1977, Combustion of wood charcoal, *Fire Safety J.* 1, 57-66
5. Girgis E., Hallett W. L. H., 2010, Wood Combustion in an Overfeed Packed Bed, Including Detailed Measurements within the Bed, *Energy Fuels* 24, 1584-1591
6. Goh Y.R., Lim C.N., Zakaria R., Chan K.H., Reynolds G., Yang Y.B., Siddall R.G., Nasserzadeh V., Swithenbank J., 2000, Mixing, Modelling and Measurements of Incinerator Bed Combustion, *Process Saf. Environ.* 78, 21-32
7. Hallett W., Green B., Machula T., Yang Y., 2013, Packed bed combustion of non-uniformly sized char particles, *Chem. Eng. Sci.* 96, 1-9
8. Kær S.K., 2005, Straw combustion on slow moving grates a comparison of model predictions with experimental data, *Biomass Bioenerg.* 28, 307–320
9. Kortela J., Jämsä-Jounela S.-L., 2012, Fuel-quality soft sensor using the dynamic superheater model for control strategy improvement of the BioPower 5 CHP plant, *Int. J. Electr. Power Energy Syst.* 42, 38-48
10. Matsumoto K., Takeno K., Ichinose T., Ogi T., Nakanishi M., 2009, Gasification reaction kinetics on biomass char obtained as a by-product of gasification in an entrained-flow gasifier with steam and oxygen at 900–1000 °C, *Fuel* 88, 519–527
11. Miljković B., Pešenjanski I., Vićević M., 2013, Mathematical modelling of straw combustion in a moving bed combustor: A two dimensional approach, *Fuel* 104, 351-364
12. Pomerantsev V., Ed., 1986, *Fundamentals of applied combustion theory*, Energoatomizdat Publishing House, Leningrad, USSR. (in Russian)
13. Saastamoinen J.J., Taipale R., Horttanainen M., Sarkomaa P., 2000, Propagation of the ignition front in beds of wood particles, *Combust. Flame* 123, 214-226
14. Senneca O., 2007, Kinetics of pyrolysis, combustion and gasification of three biomass fuels, *Fuel Process. Technol.* 88, 87–97
15. Shin D., Choi S., 2000, The combustion of simulated waste particles in a fixed bed, *Combust. Flame* 121, 167–180
16. van der Lans R.P, Pedersen L.T, Jensen A., Glarborg P., Dam-Johansen K., 2000, Modelling and experiments of straw combustion in a grate furnace, *Biomass Bioenerg.* 19, 199-208
17. Yang Y.B., Goh Y.R., Zakaria R., Nasserzadeh V., Swithenbank J., 2002, Mathematical modelling of MSW incineration on a travelling bed, *Waste Manage.* 22, 369-380

# Investigation of tuning of a fuzzy-logic control for biological wastewater treatment systems

*Riccardo Boiocchi, Krist V. Gernaey and Gürkan Sin*

*CAPEC-PROCESS, DTU Chemical Engineering, Technical University of Denmark, DK-2800 Lyngby, Denmark.*

Wastewater treatment plants (WWTPs) are required to meet the effluent quality limits such as total nitrogen, total phosphorus and chemical oxygen demand before discharging to receiving water sinks. To fulfil these requirements, a relatively high process performance needs to be ensured at WWTPs despite severe influent disturbances, which can be achieved by means of properly-designed controllers. In WWTP control, classical control such as Proportional Integrative Derivative (PID) control is one of the typical strategies used. However, the performance of these controllers relies on the approximation that the controlled processes are linear. Hence it may happen that PID controllers do not represent the best tools to enable achieving high WWT process performance, as these processes are always non-linear. On the contrary, the performance of Fuzzy Logic Controllers (FLCs) is independent from the linear nature of the process system itself. FLCs are designed on the basis of the knowledge acquired during operational experiences with the process system to be controlled. Their design allows the integration of quantitative mechanistic knowledge with qualitative knowledge, which could improve the overall controller performance. On the other hand, the FLCs typically have a large number of design parameters, which are usually defined ad hoc on the basis of process engineering insights. This makes them very flexible and adaptable to changes in function of specific requirements. However, unlike the PID where a large body of work about optimal design and tuning rules is already established, a straightforward mechanistic methodology describing the proper way to choose the design of a FLC in function of the desired control performance does not exist yet. Although the choice of some parameters is more intuitive and experience-based than mechanistic, it is important to note that wrong design decisions can lead to instances of low sensitivity or instability of the control system itself. For this reason, in order to improve the awareness of FLC designers regarding the impact of their decisions on the control response to disturbances, a study based on a control system applied to a Complete Autotrophic Nitrogen Removal (CANR) reactor is here carried out. CANR is a novel process designed for the side-stream treatment of the concentrated reject water produced from the dewatering unit of anaerobically-digested sludge. This process consists of an overall autotrophic conversion of ammonium into nitrogen gas. This treatment unit is increasingly integrated within existing WWTPs in order to achieve high nitrogen removal along with convenient operating costs. However, in order to take real advantage from this integration, it is important to operate the CANR reactor at a very high performance (i.e. high nitrogen removal). A control strategy designed with this aim for a sequencing batch CANR reactor was already developed by Boiocchi *et al.* [1]. Using this FLC as a starting point, the FLC design parameters are systematically modified in order to address how they affect the response of the controller. In particular, an investigation regarding the parameters which can affect the control system response time to influent disturbances will be carried out. The results of this study will provide the FLC designers with relevant instructions regarding the decisions that need to be taken on certain parameters in order to achieve the desired control system response.

- [1] R. Boiocchi, M. Mauricio-Iglesias, A. K. Vangsgaard, Krist V. Gernaey and G. Sin, Aeration control by monitoring the microbiological activity using fuzzy logic diagnosis and control. Application to a complete autotrophic nitrogen removal reactor, *J. Process Control* (2014), *in press*, <http://dx.doi.org/10.1016/j.jprocont.2014.10.011>.

## Oral presentations 6

# Modelling and identification

Chair: Sirkka-Liisa Jämsä-Jounela, Aalto Univ.

### Presentations:

16. *Dynamic modelling of a multiple hearth furnace for kaolin calcination*  
Aleksi Eskelinen, Alexey Zakharov, Sirkka-Liis and Jämsä-Jounela  
Aalto University, Research group of Process Control and Automation, Finland
17. *A Continuous-Discrete Extended Kalman Filter for State and Parameter Estimation in People with Type 1 Diabetes*  
Dimitri Boiroux<sup>1,2</sup>, Vladimír Bátorá<sup>3</sup>, Morten Hagdrup<sup>1</sup>, Tinna Björk Aradóttir<sup>1</sup>, Caroline Johannsen<sup>1</sup>, Marían Tárnik<sup>3</sup>, Ján Murgáš<sup>3</sup>, Signe Schmidt<sup>2,4</sup>, Kirsten Nørgaard<sup>4</sup>, Niels Kjølstad Poulsen<sup>1</sup>, Henrik Madsen<sup>1</sup> and John Bagterp Jørgensen<sup>1</sup>  
<sup>1</sup> Technical University of Denmark, Kgs. Lyngby, Denmark  
<sup>2</sup> Danish Diabetes Academy, Odense, Denmark  
<sup>3</sup> Slovak University of Technology, Bratislava, Slovakia  
<sup>4</sup> Department of Endocrinology, Hvidovre Hospital, Denmark
18. *Output-Error System Identification in the Presence of Structural Disturbances*  
Amir H. Shirdel, Jari Böling, Hannu T. Toivonen  
Department of Chemical Engineering, Åbo Akademi University, Finland
19. *Iterative Sub Network component analysis*  
Nadav Bar, Lasse Aasgaard and Naresh D. Jayavelu  
Department of Chemical Engineering, NTNU, Trondheim
20. *Balanced input excitation for identification of ill-conditioned  $n \times n$  systems with  $n > 2$*   
Ramkrishna Ghosh, Kurt E. Häggblom and Jari M. Böling  
Department of Chemical Engineering, Åbo Akademi University, Finland
21. *Advanced optimization of C5 and C6 fermentation by the use of state estimators with pH measurements*  
Miguel Mauricio-Iglesias, Krist V. Gernaey and Jakob K. Huusom.  
CAPEC-PROCESS, Department of Chemical and Biochemical Engineering, DTU.  
Lyngby.

# Dynamic modelling of a multiple hearth furnace for kaolin calcination

Aleksi Eskelinen<sup>a</sup>, Alexey Zakharov<sup>\*a</sup>, Sirkka-Liisa Jämsä-Jounela<sup>a</sup>

<sup>a</sup> Aalto University, School of Chemical Technology, Research group of Process Control and Automation, P.O. Box 16100, FI-00076 Espoo, Finland (\* corresponding author; email: alexey.zakharov@aalto.fi)

---

**Abstract:** A dynamic model of a multiple hearth kaolin calciner has been developed and is presented in this paper. This model describes the physical-chemical phenomena taking place in the six furnace parts: the solid phase, gas phase, walls, cooling air, rabble arms and the central shaft. The solid phase movement, in particular, is described by a novel mixing model. The mixing model divides the solid bed in a hearth into volumes and the distribution of their contents, after one full central shaft rotation, is identified by the pilot experiments. The dynamics of the multiple hearth furnace (MHF) is studied by introducing step changes to the feed rate. The responses of the gas phase temperature and solid bed component profiles are analyzed and the results are discussed.

**Keywords:** Multiple hearth furnace (MHF), dynamic modelling, kaolin calcination, pilot experiments, industrial application, parameter estimation.

---

## 1. INTRODUCTION

Multiple hearth furnaces (MHF) are widely used in industry for the calcination of clay minerals, such as kaolin<sup>1</sup>. Calcination enhances the properties of kaolin ensuring its applicability for a wide variety of products, such as paper, rubber, paint and refractory items<sup>2</sup>. However, mineral processing continues to provide challenges particularly in the area of maintaining efficient process operations<sup>3</sup>. Specifically, growing global competition in the mineral processing industry has increased the need for higher grade products. To improve the quality of calcined kaolin, more knowledge is needed on the solid temperature profile inside the furnace<sup>4</sup> and on the physico-chemical phenomena occurring during calcination. Mechanistic models have proven to be an excellent tool for gaining deeper understanding of processes and their behaviour. The development of mechanistic models is supported by the numerous studies of the reactions related to kaolin calcination. For example, the fundamentals of kaolin calcination and classification of different calcined kaolin grades have been previously introduced in Murray<sup>2, 5</sup>. Furthermore, the kinetics of kaolin calcination was examined by Ptacek et al.<sup>6,7</sup>, whilst both Langer<sup>8</sup> and Castelein et al.<sup>9</sup> have analysed the influence of the heating rate on the properties of calcined kaolin. Additionally, industrial experiments with tracer materials were used to study the residence time distribution in the MHF furnace used for calcination<sup>1</sup>.

Despite the abundance of research examining the calcination reactions, significant research is still required to quantitatively describe the phenomena occurring in the MHF calciner. In the literature, several mathematical models with necessary elements have been reported. Meisingset and Balchen<sup>10</sup> developed a steady-state mechanistic model for a single hearth rotary coke calciner, which outlined mass and energy balance equations for the coke bed, gas phase and the

lining. Martins et al.<sup>11</sup> described a one-dimensional steady-state model of the petroleum coke calcination in a rotary kiln that predicts the temperature profiles for the bed, gas phase and the kiln wall in the axial direction. Additionally, it also predicted the composition profiles for the gas and solid phase. The model included rheological characteristics of the system of particles for modelling the axial flow of the bed. Voglauer and Jörgl<sup>12</sup> presented a dynamic model of a multiple hearth furnace used for the roast process to recover vanadium consisting of a mass transfer model, thermodynamic model and a chemical model for the characterization of decisive states like mass, temperatures and the concentrations of sodium, and soluble and insoluble vanadium, respectively. Liu and Jiang<sup>13</sup> have also developed a mathematical model involving the mass and heat transfer in a continuous plate dryer. The authors presented equations to calculate the key parameters of the solid mass transfer model, such as the height and the volume of each granular heap, and retention time in the dryer. The study showed that the optimization of a plate dryer should concentrate on maximizing the effective covering ratio of the plates. More recently, Ginsberg and Modigell<sup>14</sup> developed a dynamic model of a rotary kiln used for the calcination of titanium dioxide. The overall heat transfer phenomena and the reactions occurring in the process were described. The model was validated by a dynamic test case representing a 15-day period of plant operation and the work succeeded in proving that the dynamic behaviour of a furnace can be modelled with quantitative accuracy.

The aim of this paper is to present the development of the dynamic model describing kaolin calcination in a MHF operated by a UK plant. In the model, the solid bed in a hearth is divided into volumes, as presented earlier by Meisingset and Balchen<sup>10</sup>, as the temperature difference through a solid bed in a hearth is over 150 °C. The solid phase movement, particularly, is described by a novel mixing model. In addition to dividing the solid bed in a hearth into

volumes, the mixing model provides the distribution of their contents, after one full central shaft rotation, identified by the pilot experiments.

This paper comprises of the following. First, the kaolin calcination process in a MHF is described in Section 2, whilst Section 3 presents the physical and chemical relationships for the calcination reactions, and the equations for the heat and mass transfer phenomena within the furnace. Section 4 introduces the experimental work used to determine the parameters of the calcination reactions and the mixing model. In Section 5, the dynamic behaviour of the MHF model is analysed and finally, Section 6 concludes the paper.

## 2. DESCRIPTION OF THE MULTIPLE HEARTH FURNACE

The MHF studied in this paper consists of eight hearths and it has counter-current solid and gas flows. The heat required for calcination is supplied to the furnace through four tangentially aligned methane burners located on Hearths 4 and 6. The temperature in the ‘fired hearths’ is controlled by varying the fuel gas flow, which determines the amount of combustion air. The furnace walls are constructed of bricks and enclosed by a cylindrical steel shell with refractory lining. Figure 1 presents the cross-sectional view of the furnace.

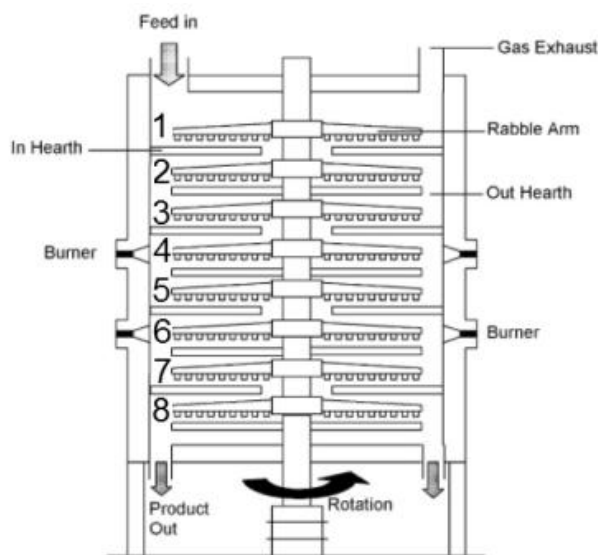


Fig. 1. Cross-sectional picture of the multiple hearth furnace with direct fire burners.

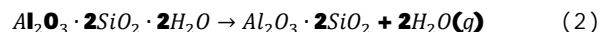
The material flow through the furnace is stirred spirally and moved across the hearths by a centrally located vertical rotating shaft carrying arms with rabble blades. Four arms are used on each hearth, and each arm carries three to five rabble blades, whilst material is fed into the top hearth through a single inlet from the weigh feed hopper to the periphery of the hearth. On the odd numbered hearths, the material is stirred by the rabble blades towards the centre of the hearth, and the material drops down to the next hearth from the centre through a single annulus around the shaft. In contrast, the material on the even numbered hearths is moved outwards

to be dropped through the drop holes at the periphery of the hearth to the following hearth. The stirring pattern is repeated until the lowest hearth is reached, from which the calcined product is extracted through the two exit holes.

During calcination, kaolin undergoes four physical-chemical processes<sup>6</sup>. First the evaporation of the free moisture occurs ( $T \leq 100^\circ\text{C}$ ).



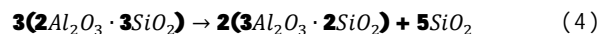
Next, kaolin undergoes a dehydroxylation reaction, in which the chemically bound water is removed and amorphous metakaolin is formed at  $450 - 700^\circ\text{C}$ .



The third physical-chemical process involves a reaction leading to the transformation of metakaolin to the ‘spinel phase’ by exothermic re-crystallization at  $925-1050^\circ\text{C}$ .



In the fourth and final process, the nucleation of the spinel phase occurs and the material transforms into mullite at temperatures above  $1050^\circ\text{C}$ .



Mullite is hard and abrasive, and as a result it can cause damage to process equipment<sup>4</sup>. The desired final consistent product which is within the specification limits has both a low mullite and metakaolin content. The differential scanning calorimetry (DSC) and thermo gravimetric (TGA) curves presenting the kaolin calcination are given in Figure 2.

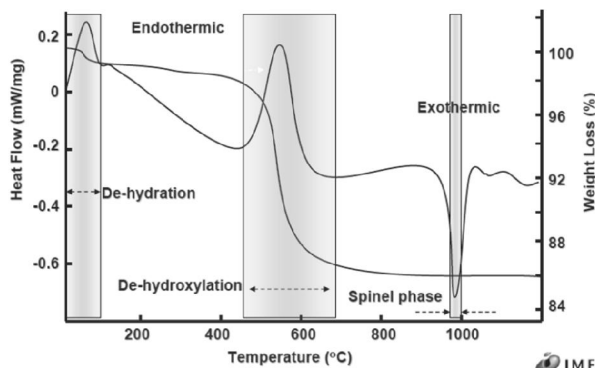


Fig. 2. DSC and TG curves of kaolin

## 3. DYNAMIC MODEL OF A MULTIPLE HEARTH FURNACE

In this modelling work, the MHF is divided to six parts: the solid bed, gas phase, walls, central shaft, rabble arms, and the cooling air. The overall mathematical model of the furnace includes the reaction kinetics for the four reactions outlined earlier, as well as models for the mass transfer and heat transfer mechanisms for each of six parts. In addition, equations for calculating the temperature dependent parameters, such as the heat capacities of the gas components, the gas emissivities and the solid bed

emissivities, are incorporated in the model. The solid bed and the gas phase both have five components: the solid bed includes kaolin, water, metakaolin, spinel phase (product), and mullite (offspec), whereas the gas phase includes methane, oxygen, nitrogen, water and carbon dioxide. The first two subsections present the main modelling equations and then Subsection 3.3 introduces a summary of the solving procedure.

### 3.1 Modelling of solids and gas phase mass transfer

A few simplifying assumptions have to be made in order to model the mass transfer inside the furnace. Firstly, the solid bed on each hearth is split into 4 (Hearths 3 to 8) or 5 (Hearths 1 and 2) homogenous annular volumes according to the furnace rabble arm configuration. Secondly, the volumes are assumed to be identical in width in the radial direction and the mass content. Thirdly, the mixing model assumes that one full shaft rotation distributes the contents of a volume between the original volume and its neighbour volumes (one of which is the next and the other is the previous). The distribution of solid among the three volumes is determined by the experimental tests which are described in Section 4. Under these assumptions, the solid mass distribution after one time step (representing a full central shaft rotation) is calculated with Equation 5:

$$m_{t+1}^j = D_j \cdot (m_t^j - R_{r,t}^j) + m_{feed,t}^j \quad (5)$$

where the mass movement matrix  $D_j$  describes the distribution of the contents of each compartment after one central shaft rotation in the hearth  $j$ . Specifically, the column  $i$  represents the distribution of volume  $i$  between the volumes of the hearth. Thus, the columns of the matrix sum up to unity, except the column representing the exit volume of the hearth. Moreover, because of the assumption that solids in a certain volume are distributed between the current volume and its neighbour volumes after one rotation, the matrix  $D$  has three nonzero central diagonals. Thus, the central diagonal represents the contents staying in the same volume, whereas the upper and lower diagonals indicate the proportion of solid moving inwards and outwards respectively. In the mixing model (Equation 5), the feed to a hearth can be found as the exit from the previous one:

$$m_{feed,t}^j = (1 - \sum D_{j-1}^K)(m_t^{j-1,K} - R_{r,t}^{j-1,K}), \quad (6)$$

where  $K$  is the exit volume of hearth  $j - 1$  and  $D_{j-1}^K$  is the column  $K$  of matrix  $D_{j-1}$ .

The solid bed movement matrix is generated for each hearth individually. As an example, Equation 7 presents the solid bed movement matrix of the upmost hearth. The parameter  $\alpha$  is introduced to describe the net forward flow through a hearth, which is the feed rate minus the mass loss caused by evaporation and dehydroxylation reactions. The upper diagonal matrix elements  $a_j$  present the full forward flow from the current volume to the next volume during one full central shaft rotation. Thus, the lower diagonal matrix elements  $(a_i - \alpha)$  present the backward flow equal to the difference of the full forward and the net forward flows. In Equation 7, the parameter  $\alpha$  is only present in the second and

third volume since the feed is introduced to volume 4 and the direction of flow is in the descending order of volumes on the first hearth.

$$D_1 = \begin{pmatrix} 1 - a_1 & a_1 & 0 & 0 & 0 \\ a_1 - \alpha & 1 - 2a_1 + \alpha & a_1 & 0 & 0 \\ 0 & a_1 - \alpha & 1 - 2a_1 + \alpha & a_1 & 0 \\ 0 & 0 & a_1 - \alpha & 1 - 2a_1 & a_1 \\ 0 & 0 & 0 & a_1 & 1 - a_1 \end{pmatrix} \quad (7)$$

The gas phase in the model is assumed to be ideal and the pressure inside the furnace atmospheric. As was the case with the solid bed, also the gas phase on a specific hearth is divided into 4 or 5 homogenous annular volumes, with the number of gas phase volumes in the hearth the same as the corresponding number of solid volumes in the hearth. Additionally, the gas phase volumes are assumed to be uniform regarding composition and temperature. The gas phase has a very short residence time in the furnace, and its temperature follows the steady-state values defined by the temperature profiles of the other model parts, allowing, the gas phase to be described with a steady-state model.

The gas phase mass balance equation (Equation 8) is derived for each primary gas component:

$$\dot{n}_{i,in} - \dot{n}_{i,out} - R_i = 0. \quad (8)$$

where  $n_{i,in}$ , denoting the incoming moles of component  $i$ , is obtained from Equation 9:

$$n_{i,in}^j = c_i^{j+1} F^j \quad (9)$$

where  $j$  is the number of the hearth.

### 3.2 Modelling of energy balances

In the model the heat exchange is described between solid and gas, solid and wall, gas and wall, wall and environment, and gas and arms. In addition, heat is conducted inside the walls in the radial horizontal direction and heat exchange exists between the cooling air, the central shaft and the rabble arms. In the model, heat exchange between the hearth bottom surface and the solid bed, and heat conduction inside the solid bed are neglected. Furthermore, the bed volumes are assumed to be homogenous in temperature. The model considers energy balances for the gas phase, walls, the central shaft, rabble arms, cooling air, and for the solid bed. The energy balance equations, containing the heat flows, are first resolved after which the temperature values can be acquired. The energy balance equation for the gas phase is:

$$\begin{aligned} \dot{Q}_{gas,in} - \dot{Q}_{gas,out} + \dot{Q}_{combustion} + \dot{Q}_{gs} + \dot{Q}_{gw} \\ + \dot{Q}_{gshaft} + \dot{Q}_{garms} = 0 \end{aligned} \quad (10)$$

The molar heat capacities of the incoming and exiting gas components are calculated as a function of temperature as previously outlined in<sup>15</sup>. The combustion energy is calculated using Equation 11:

$$\dot{Q}_{combustion} = b_i \dot{n}_{methane} \Delta H_{combust} \quad (11)$$

where  $b_i$  is an estimated combustion ratio.

The direct heat transfer between the solid bed and the gas phase occurs by both radiation and convection:

$$Q_{gs} = \sigma X_s A_{gs} \varepsilon_s \varepsilon_g (T_g^4 - T_s^4) + h_{cgs} X_s A_{gs} (T_g - T_s) \quad (12)$$

where  $X_s$  is an estimated surface view factor. Heat transfer between the inner walls and the gas phase occurs by convection and radiation and the heat flux can be written as:

$$Q_{gw} = \sigma A_{gw} \frac{(\varepsilon_w + 1)}{2} \varepsilon_g (T_g^4 - T_w^4) + h_{cgw} A_{wg} (T_g - T_w) \quad (13)$$

The radiation term is written as described in<sup>15</sup> and the effective emissivity as presented in<sup>16</sup> that can be used if the emissivity of the material is above 0.7.

To calculate the heat transfer between the gas, the central shaft and the rabble arms, the central shaft is divided into eight sections according to the hearths, so that each section has a fixed temperature and there is no vertical heat exchange in the shaft. The heat exchange flux between the gas phase and the central shaft, and between the gas phase and rabble arms consist of the radiative and the convective heat transfer terms respectively:

$$Q_{gshaft} = \sigma Z A_{gshaft} \varepsilon_{shaft} \varepsilon_g (T_{gas}^4 - T_{shaft}^4) + h_{cgshaft} Z A_{gshaft} (T_{gas} - T_{shaft}) \quad (14)$$

$$Q_{garms} = \sigma A_{garms} \varepsilon_{arms} \varepsilon_g (T_{gas}^4 - T_{arms}^4) + h_{cgarms} A_{garms} (T_{gas} - T_{arms}) \quad (15)$$

where  $Z$  is an estimated constant describing the insulation of the central shaft.

The energy balance equation for the walls is given by:

$$\frac{\partial Q_w}{\partial t} = \dot{Q}_{wg} - \dot{Q}_{ws} - \dot{Q}_{wa} \quad (16)$$

where the heat transfer between the solid bed and the walls occurs only by radiation since the two surfaces are not connected to each other. The radiative heat flux is:

$$Q_{ws} = \sigma X_s A_{sw} \varepsilon_{sw} (T_w^4 - T_s^4) \quad (17)$$

where the emissivity between the solid bed and the walls is affected by the gas phase emissivity. The heat transfer between the outer wall and the ambient air consists only of a convective term as the radiative term is neglected due to the relatively low outer wall temperature:

$$Q_{wa} = h_{cwa} A_{wa} (T_{ambient} - T_{outer\ wall}) \quad (18)$$

In order to describe the conductive heat transfer inside the wall and to calculate its temperature profile, the furnace wall is divided into eight sections according to the hearths, so that each section has a fixed temperature and there is no vertical heat exchange in the wall.

The energy balance equation for the central shaft and the rabble arms are provided by:

$$\frac{\partial Q_{shaft}}{\partial t} = \dot{Q}_{gshaft} - \dot{Q}_{shaft,cool} \quad (19)$$

$$\frac{\partial Q_{arms}}{\partial t} = \dot{Q}_{garms} - \dot{Q}_{arms,cool} \quad (20)$$

where the heat transfer between cooling air and the central shaft and the rabble arms consist of the radiative and the convective heat transfer terms respectively:

$$Q_{shaft,cool} = \sigma A_{shaft,cool} \varepsilon_{shaft} (T_{shaft}^4 - T_{cool}^4) + h_{cshaft,cool} A_{shaft,cool} (T_{shaft} - T_{cool}) \quad (21)$$

$$Q_{arms,cool} = \sigma A_{arms,cool} \varepsilon_{arms} (T_{arms}^4 - T_{cool}^4) + h_{carms,cool} A_{arms,cool} (T_{arms} - T_{cool}) \quad (22)$$

The energy balance of the cooling air is described by Equation 23:

$$\frac{\partial Q_{cooling\ air}}{\partial t} = \dot{Q}_{cooling\ air, in} + \dot{Q}_{arms,cool} + \dot{Q}_{shaft,cool} - \dot{Q}_{cooling\ air, out} \quad (23)$$

Finally, the solid phase energy balance equation is written as:

$$\frac{\partial Q}{\partial t} = \dot{Q}_{mass, in} - \dot{Q}_{mass, out} - \dot{Q}_{reactions} - \dot{Q}_{evaporation} + \dot{Q}_{sw} + \dot{Q}_{sg} \quad (24)$$

When considering the solid bed movement during one time step (one central shaft rotation), the energy in each solid bed compartment can be calculated using Equation 25:

$$Q_{t+1}^{j,k} = D_j \cdot Q_t^{j,k} + Q_{feed,t} \quad (25)$$

### 3.3 Solution procedure for the MHF model

The solution procedure for the MHF model consists of five main steps. Firstly, the reaction rates are calculated using the reaction parameters obtained from the experimental data. Secondly, the solid mass balance is computed, which requires the mixing model. Thirdly, the mass and energy balances of the gas phase are solved using the estimated parameters, such as the burning ratios, solid bed surface view factors and the extraneous air flow to Hearth 8. The next step consists of energy balance calculations for the walls, cooling air, central shaft and the rabble arms. The fifth and final step solves the energy balance of the solid bed by combining the heat fluxes determined in the previous steps by utilizing the mixing model. The model solution cycle is presented in Figure 3, summarizing the mass and energy flows between the model parts and the usage of the current model states. In addition, Figure 3 shows in which step the experimentally determined and the estimated parameters are used in the calculations.

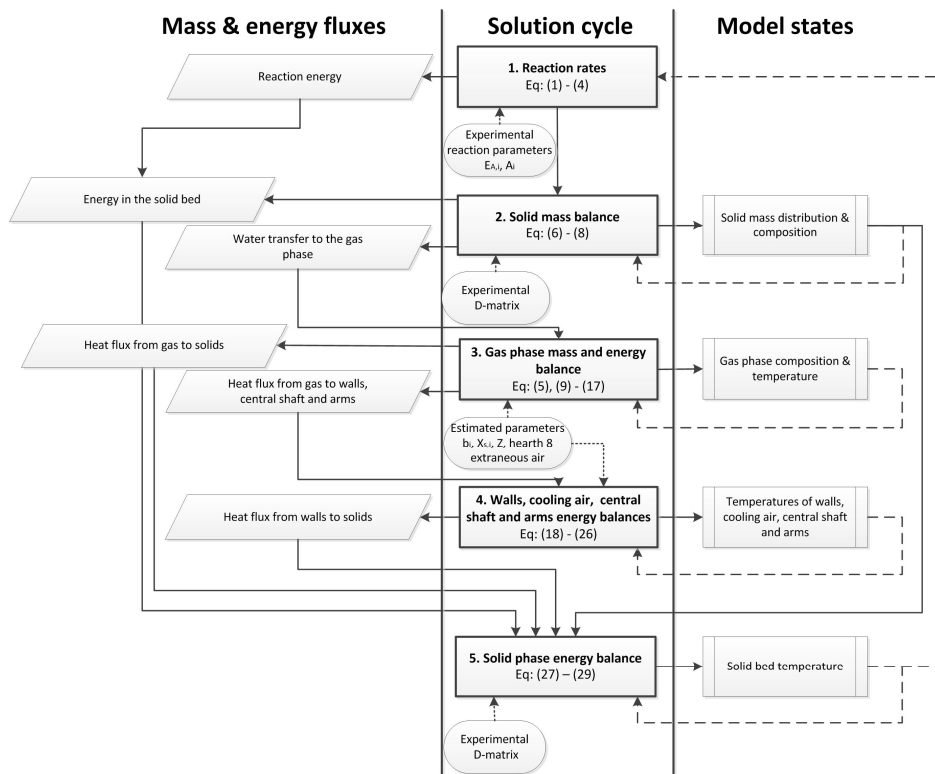


Fig.3 Scheme of the solution procedure for the MHF model.

During one solution cycle, representing one full rotation of the central shaft, the solving procedure calculates the current states of the six model parts (the solid phase, gas phase, walls, cooling air, rabble arms and the central shaft). The first step, the computation of the reaction rates in the solid phase, is done by direct calculations using the current temperature profile distribution. In the second step, the solid bed mass balance is solved using the computed reaction rates and the experimentally determined mixing model. After the first two steps, the energy produced by the reactions in the solid bed, the energy flows caused by the convection in the solid bed and the water transferred to the gas phase are available. In the next step, the water transferred to the gas phase is first used to calculate the mass balance, and subsequently the energy balance of the gas phase is determined. Specifically, the steady-state values of the heat fluxes between the gas phase and other model parts are calculated by solving algebraic equations achieved by an interval division method. Subsequently, the fourth step involves solving the temperature profiles of the walls, central shaft, rabble arms and the cooling air using the obtained heat fluxes. Finally, the last step of the solution cycle combines the heat fluxes in the solid bed, the heat exchange between the solid bed and other model parts, and the composition of the solid bed to calculate its energy balance and temperature profile through the furnace. In these last two steps, Euler's method is employed. The solving algorithms have been implemented in MATLAB environment.

The solving procedure is developed to compute the mass and energy flows between the model parts once during a solution cycle. Thus, while resolving the balance equations of two model parts, the same value of the mass and heat flow between them is used. A conservative solution scheme is attained and the mass and energy conservation is achieved in the solution.

#### 4. DETERMINATION OF MATRIX D

The movement of the solid bed was studied to determine the residence time of every hearth. The mass distribution between the hearths was studied with a pilot furnace. The residence time distribution through the whole furnace was taken from industrial experiments<sup>F</sup> utilizing tracer material to determine the residence time distribution. Subsequently, these results were combined, the residence time for each hearth was obtained, and the solid movement matrices were defined.

The main equipment used for the testing includes a pilot scale furnace and a continuous weight proportioner. The pilot scale multiple hearth furnace is a 1:12 ratio replica of the industrial furnace (without the heating equipment) having the same rabble arm configuration as the industrial size MHF. The mass distribution experiments were executed using a feed rate of 70 g/min corresponding to the real feed rate of 120 kg/min. The rotation speed of the central shaft was 3 RPM. After the mass profile inside the pilot had achieved its steady state, the mass of the kaolin on each hearth was weighted.

The mass distributions obtained in the four experiments performed are shown in Figure 4. Clearly, Hearths 3 and 7 have the largest portions of kaolin, whereas Hearths 1 and 2 have the smallest portions indicating that the material spends a relatively short time on the first two hearths and a much longer time on Hearths 3 and 7. The results of the four tests showed a good correlation and are shown in Figure 4.

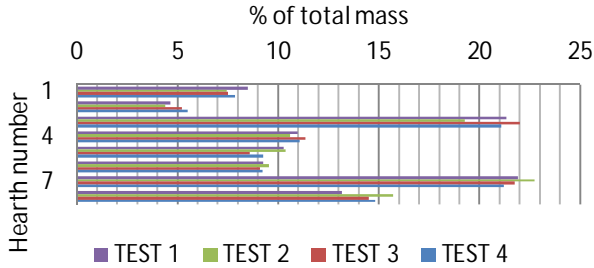


Fig. 4. Mass distribution between the hearths from the tests

The net forward flow coefficients  $\alpha_j$ , used in the solid bed movement matrix, were chosen to achieve consistency between the experimental results and the mixing model prediction of the mass distribution between the hearths and the residence time distribution. The backward flow parameters  $a_j$  were selected to be 5 percent of the total net flow for Hearths 1 and 2, and 10 percent for the rest of the other hearths, since higher values of the backward flow in the first two hearths are inconsistent with the short residence time in these particular hearths.

Figure 5 presents the resulting residence time distribution according to the identified solid movement model and shows the residence time distribution curve of the industrial experiment. Comparison between the model and the industrial setting shows that both of the curves are consistent. Additionally, in both cases, the tracer starts reaching the outlet approximately 20 minutes after introduction into the system and the last particles leave the furnace within 80 minutes.

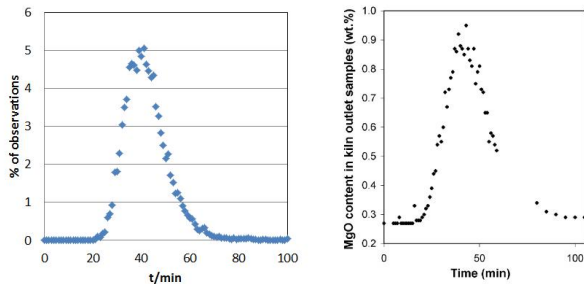


Fig. 5. The residence time distribution in the pilot plant experiments (left) and in the industrial experiments<sup>1</sup> (right).

## 5. DYNAMIC BEHAVIOR OF THE MHF

The dynamic behaviour of the model was investigated to study the effect of the process inputs on the reactions occurring in the solid bed and the process outputs. Feed rate

was chosen as manipulated variables while studying changes in the gas temperature profile through the furnace, and the quality variables: product and offspec mass-percentage in the lower hearths. The model response was studied by introducing a step change at 833 minutes in the input variables when the model had settled into a steady operation mode.

The model behaviour was first studied by introducing a 2.4 kg/min (2 percent) step increase in the feed rate. At the beginning, the mullite formation in Hearth 7 slows down, which can be observed as the slight increase in the amount of the spinel phase in the final product, see Figure 7.

As the product formation reaction is not receiving enough heat, it moves from Hearth 6 to the entrance of Hearth 7 at around 1200 minutes, as can be seen in the product content dynamics displayed in Figure 7. The shift of product formation to the beginning of Hearth 7 also affects the gas temperature profile in Hearths 5, 6 and 7 in Figure 6. However, the final product is still composed almost entirely of the spinel phase.

After 1560 minutes of the simulation time, the spinel formation partly moves to the middle of Hearth 7, which is confirmed by Figure 7. As a result, the metakaolin conversion to the spinel phase is not complete and the gas temperature in Hearth 7 decreases rapidly. During the whole test, the temperatures of the exhaust and the gas phases on Hearths 2 to 4 decrease steadily until settling to a new steady state, as Figure 6 shows. In contrast, the gas temperature in Hearth 8 slowly increases as a result of the rising temperature of the solid that enters to the last hearth.

Next, a step decrease of 2.4 kg/min (2 percent) was introduced to the feed rate and the model response is shown in Figure 8 and Figure 9. At the beginning, the mullite formation is activated in Hearth 7 due to the temperature rise, which can be seen as a decrease of the spinel phase contents in Figure 9.

After 1260 minute of the simulation time, the spinel formation partly moves towards the middle of Hearth 6, as demonstrated by Figure 9. Simultaneously, the mullite formation in Hearth 7 increases rapidly and the share of off-spec in the final product rises above 5%, which is demonstrated in Figure 9. As a result, the gas temperature in Hearths 6 and 7 changes its dynamics as it is seen in Figure 8.

In this case study, the temperatures of the exhaust and the gas temperatures of Hearths 2 to 5 increase steadily until reaching a new steady state, since more specific energy is supplied to the furnace.

## 6. CONCLUSIONS

A dynamic model of kaolin calcination in a Multi Hearth Furnace (MHF) was developed in this paper. This model describes the physical-chemical phenomena taking place in the six furnace parts: the solid phase, gas phase, walls, cooling air, rabble arms and the central shaft. A simple mixing model was proposed to describe the dynamics of the solid phase, and experiments with a pilot plant have been conducted to estimate the parameters of the mixing model.

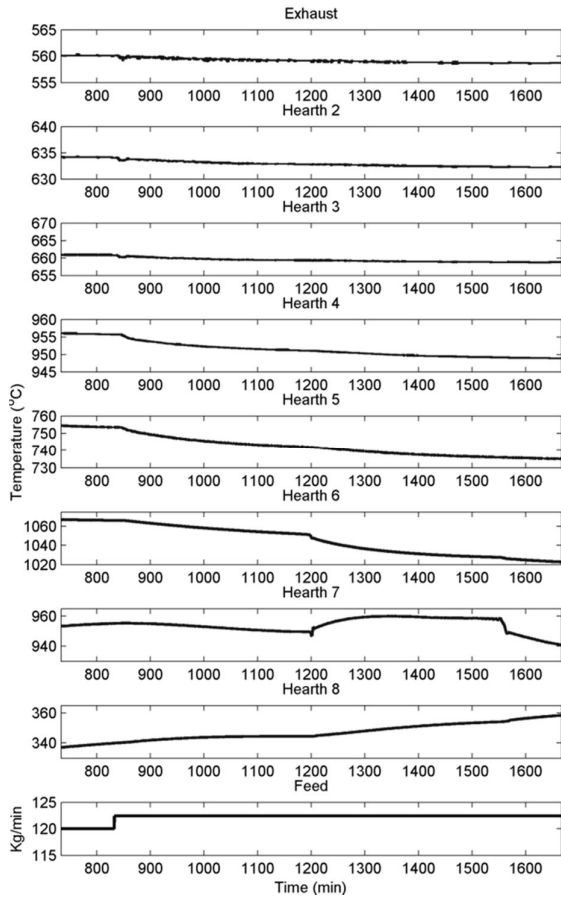


Fig. 6. The response of the gas phase temperature next to the wall in the feed rate increase test.

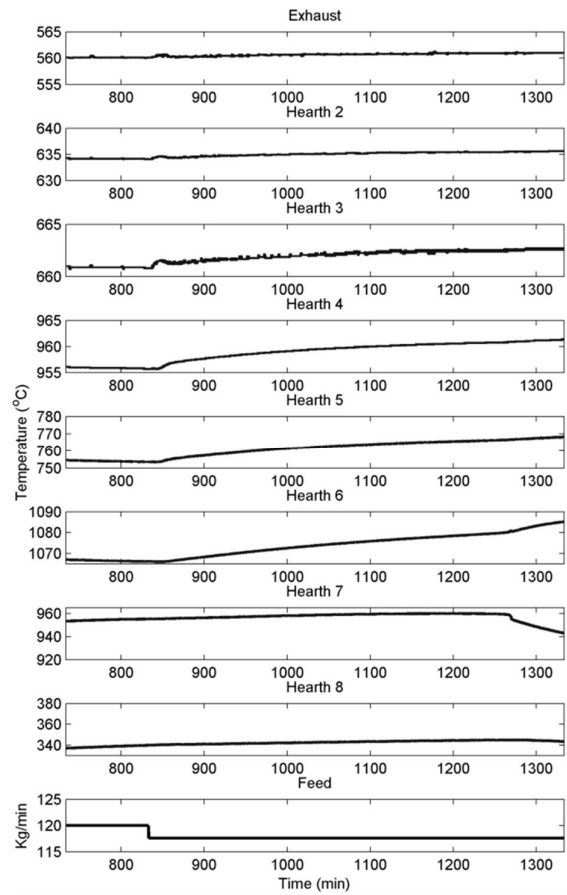


Figure 8. The response of the gas phase temperature next to the wall in the feed rate decrease test.

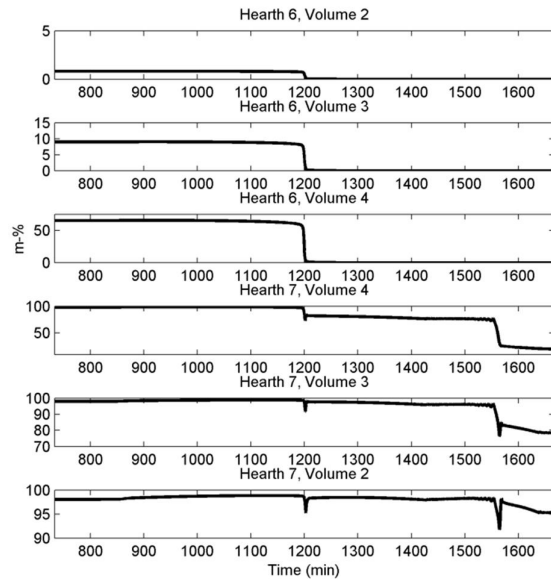


Figure 7. The response of the product content of the solid bed in Hearths 6 and 7 during the feed rate increase test.

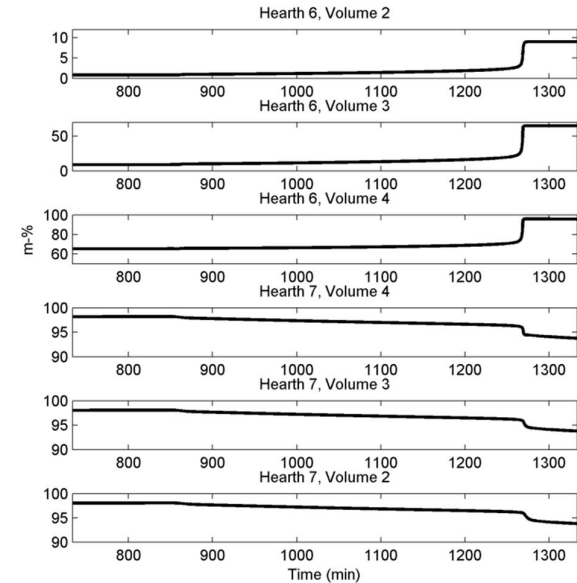


Figure 9. The response of the product content of the solid bed in Hearths 6 and 7 during the feed rate decrease test.

The performed tests have demonstrated that the model outcomes are adequate. In particular, the spinel phase formation takes place in the last two volumes of Hearth 6 and first two volumes of Hearth 7, which agrees with the process knowledge. More specifically, the reaction moves towards the entrance of Hearth 6 when higher specific energy is supplied to the furnace, and the reaction shifts towards Hearth 7 as the amount of the supplied energy decreases. In the former case, higher temperature is reached in the solid phase which activates the mullite formation reaction in Hearth 7. On the other hand, if the specific energy is decreased too much, the temperature in the solid phase drops below the temperature required for spinel formation, and the reaction collapses. In this case, the output of the furnace consists of pure metakaolin. Thus, it can be concluded that the furnace must be controlled such a way as to direct the spinel formation at the end of Hearth 6 and the first volume of Hearth 7, which would deliver both highest content of the spinel phase in the product and stable operating conditions.

Simulation studies have confirmed that the outcomes of the developed model are qualitatively adequate and its performance can be evaluated as fairly good. The developed model has proven to give valuable information about the calcination reactions which can be utilized to design an enhanced control of furnace operations. In addition, as the simulation results have demonstrated, the conditions in different volumes in a hearth vary greatly, a conclusion can be made that introducing the division into volumes is required to properly represent the actual chemical-physical phenomena.

#### ACKNOWLEDGEMENT

The research leading to these results has received funding from the European Union Seventh Framework Programme (FP7/2013-2016) under Grant Agreement No. 310645.

#### NOMENCLATURE

##### Roman letters

A	Area (m <sup>2</sup> )
A <sub>i</sub>	Frequency factor for reaction i (1/s)
C <sub>i</sub>	Concentration of solid component i (kg)
c <sub>i</sub>	Concentration of gas component (mol/m <sup>3</sup> )
D <sub>i</sub>	Solid bed movement matrix of hearth i
F	Total gas flow (m <sup>3</sup> )
h	Heat transfer coefficient (W/m <sup>2</sup> K)
j	Number of the current hearth
k	Number of the volume
m	Mass (kg)
n <sub>i</sub>	Moles of gas component i (mol)
Q	Heat (kJ)
R	Gas constant (=8.3145 J/molK)
R <sub>i</sub>	Reaction rate for reaction i (kg/s)
R <sub>r</sub>	Mass transfer rate from solids to gas phase (kg/s)
T	Temperature (K)
t	Time (s)

##### Greek letters

ε	Emissivity, radiative exchange ratio
σ	Stefan-Boltzmann-constant (=5.67·10 <sup>-8</sup> W/(m <sup>2</sup> K <sup>4</sup> ))

##### Indices

g	Gas
---	-----

s	Solid
w	Wall
gs	Gas-solid
gw	Gas-wall
gshaft	Gas-shaft
garms	Gas-arms
sg	Solid-gas
sw	Solid-wall
wa	Wall-ambient
wg	Wall-gas
ws	Wall-solid
shaft,cool	Central shaft-cooling air
arms, cool	Rabble arms-cooling air
c	Convective heat transfer

#### REFERENCES

1. Thomas R, Grose D, Obaje G, Taylor R, Rowson N, Blackburn S. Residence time investigation of a multiple hearth kiln using mineral tracers. *Chem. Eng. Process.* 2009; 48 :950-954.
2. Murray HH. Clays. In: *Ullmann's encyclopedia of industrial chemistry*. Weinheim: Wiley-VCH Verlag, 2005: 203-235.
3. Jämsä-Jounela S-L. Current status and future trends in the automation of mineral and metal processing. *Control Eng. Pract.* 2001; 9: 1021-1035.
4. Thomas R. High temperature processing of kaolinitic materials. PhD Thesis, University of Birmingham, 2010.
5. Murray HH, Kogel JE. Engineered clay products for the paper industry. *Appl. Clay Sci.* 2007; 29:199-206.
6. Ptacek P, Soukal F, Opravil T, Noskova M, Havlica J, Brandstetr J. The kinetics of Al-Si spinel phase crystallization from calcined kaolin. *J. Solid State Chem.* 2010; 183:2565-2569.
7. Ptacek P, Soukal F, Opravil T, Halvica J, Brandstetr J. The kinetic analysis of the thermal decomposition of kaolinite by DTG technique. *Powder Technol.* 2011; 208: 20-25.
8. Langer AM. Evaluation of kaolinite and quartz differential thermal curves with a new high temperature cell. *Am. Mineral.* 1967; 52:509-23.
9. Castelein O, Soulestin B, Bonnet JP, Blanchart P. The influence of heating rate on the thermal behavior and mullite formation from a kaolin raw material. *Ceram. Int.* 2001; 27: 517-22.
10. Meisingset HC, Balchen JG. Mathematical modelling of a rotary hearth coke calciner. *Modeling, identification and control.* 1995; 16:193-212.
11. Martins MA, Oliveira LS, Franca AS. Modeling and simulation of petroleum coke calcination in rotary kilns. *Fuel.* 2001; 80:1611-1622.
12. Voglauer B, Jörgl HP. Dynamic model of a roast process for simulation and control. *Mathematical and computer modelling of dynamical systems.* 2004; 10:217-230.
13. Liu X, Jiang J. Mass and heat transfer in a continuous plate dryer. *Drying Technol.* 2004; 22:1621-1635.
14. Ginsberg T, Modigell M. Dynamic modelling of a rotary kiln for calcination of titanium dioxide white pigment. *Comput. Chem. Eng.* 2011; 35:2437-2446.
15. DIPPR-801. Project 801, Evaluated Process Design Data, Design Institute for Physical Properties (DIPPR), American Institute of Chemical Engineers, AIChE, 2012.
16. Perry RH, Green DW. *Perry's chemical engineering handbook*. New York: McGraw-Hill, 1997.

# A Continuous-Discrete Extended Kalman Filter for State and Parameter Estimation in People with Type 1 Diabetes

Dimitri Boiroux<sup>1,2</sup>, Vladimír Bátorá<sup>3</sup>, Morten Hagdrup<sup>1</sup>, Tinna Björk Aradóttir<sup>1</sup>, Caroline Johannsen<sup>1</sup>, Marían Tárnik<sup>3</sup>, Ján Murgaš<sup>3</sup>, Signe Schmidt<sup>2,4</sup>, Kirsten Nørgaard<sup>4</sup>, Niels Kjølstad Poulsen<sup>1</sup>, Henrik Madsen<sup>1</sup> and John Bagterp Jørgensen<sup>1</sup>

<sup>1</sup> DTU Compute, Technical University of Denmark, Kgs. Lyngby, Denmark

<sup>2</sup> Danish Diabetes Academy, Odense, Denmark

<sup>3</sup> Faculty of Electrical Engineering and Information Technology, Slovak University of Technology, Bratislava, Slovakia

<sup>4</sup> Department of Endocrinology, Hvidovre Hospital, Denmark

## Abstract

Closed-loop control of blood glucose, also called an artificial pancreas (AP), can free people with type 1 diabetes from the burden of managing their insulin therapy. In addition, it has the potential to provide tighter blood glucose control while reducing the risk of short- and long-term diabetes complications. Currently, linear model predictive control (MPC) algorithms are being tested for the AP and show promising results. However, the insulin-glucose dynamics are highly nonlinear, and would require advanced techniques for more accurate state and parameter estimation.

Here, we apply MPC to an AP for people with type 1 diabetes. We use a minimal identifiable physiological model for simulation. In particular, we estimate the model states and parameters using a continuous-discrete extended Kalman filter (EKF). The filter should be able handle uncertainties associated with meal intake and changes in insulin sensitivity. We describe the key aspects of the numerical implementation and provide quantitative insights into the factors limiting the achievement of acceptable AP performance.

## Acknowledgements

Funded by the Danish Diabetes Academy supported by the Novo Nordisk Foundation.

# Output-Error System Identification in the Presence of Structural Disturbances

Amir H. Shirdel\*, Jari Böling, Hannu T. Toivonen  
Department of Chemical Engineering, Åbo Akademi University  
FIN-20500 Åbo, Finland

## Abstract

In experimental system identification, disturbances can affect destructively estimation of the system parameters. Therefore, finding and eliminating these disturbances can increase significantly the accuracy of system identification. In our approach, by using orthogonal Laguerre or Kautz basis functions along with sparse optimization and  $l_1$ -relaxation, the basis function parameters and structural disturbances are identified simultaneously. Important properties of using Laguerre or Kautz basis functions are to cover system delays and reduce the model complexity compared to finite impulse response models. The output-error identification models are more reliable and robust for multi-step prediction than other model structures. Using nonlinear kernel methods, such as radial basis functions, some nonlinear cases, like Wiener model, can be identified. In addition, sparse optimization with  $l_1$ -regularization can give simpler solutions and simpler kernel models. In this contribution we present the method and demonstrate it on simulated linear and nonlinear examples, and on real distillation column data. The results show that with the proposed method accurate system models can be identified using experimental data containing unknown trends and outliers.

---

\*Corresponding author. Email: ashirdel@abo.fi

# Iterative Sub Network Component Analysis

Nadav Bar, Lasse Aasgaard, Naresh D. Jayavelu

*Department of Chemical Engineering,  
Norwegian University of Science and Technology (NTNU),  
Trondheim, Norway*

---

*Abstract:* The genes of biological organisms are regulated at several stages, mostly in their expression stage. The relationship between the genes (TG) and their regulators, the transcription factors (TF) forms highly complex networks and even simple gene expression studies incorporate large number (often thousands) of components and connections. Several statistical methods, such as principal component analysis (PCA), singular value decomposition (SVD) and partial least squares regression (PLSR) were successfully applied on microarray data to extract biologically significant knowledge. Network component analysis (NCA) is another statistical method similar to PCA, but uses gene expression data and a priori known network topology to reconstruct transcription factor activity profiles. Currently, NCA algorithms are constrained by necessary conditions posed on the network topology that guarantee a unique solution. Networks with topology that satisfy the conditions are called compliant networks. To satisfy these conditions, it is common to reduce the network size, by removing potentially important components.

We developed a novel, Iterative Subnetwork Component Analysis (ISNCA) in order to reconstruct large sized networks. We divide the initial non-compliant network into two smaller, compliant sub-networks that share several components. The ISNCA first predicts the reconstruction of each compliant subnetwork. It then update the reconstruction of the other subnetwork by subtracting the contribution of their shared components. We tested the ISNCA on synthetic and real, large datasets using various NCA algorithms. We managed to increase the size of the networks substantially. Moreover, we demonstrated that the reconstruction of the entire incompliant network was more accurate. This framework enables us to reconstruct networks that fail to satisfy the NCA criteria without reducing their sizes or eliminating essential components. We propose that the ISNCA approach can be applied to any network reconstruction method such as PLS, PCA.

---

## Balanced input excitation for identification of ill-conditioned $n \times n$ systems with $n > 2$

Ramkrishna Ghosh<sup>†</sup>, Kurt E. Häggblom, Jari M. Böling

*Department of Chemical Engineering, Åbo Akademi University  
Biskopsgatan 8, FI-20500 Turku, Finland*

Typically, 75% of the cost associated with an advanced control project goes into model development (Gevers 2005). Hence, efficient modeling and system identification techniques suited for industrial use and tailored for control design applications are crucial (Hjalmarsson 2005). For an ill-conditioned system, the identification input design is sensitive to the distribution of the singular values of the system gain matrix. The construction of input excitations in smart way is crucial for a successful identification. Excitations can introduce one direction at a time or all directions simultaneously. Consider a singular value decomposition of the steady-state gain matrix, i.e.  $G(0) = W\Sigma V^T$  where  $V$  and  $W$  are unitary matrices and  $\Sigma$  is a diagonal matrix of singular values,  $\sigma_1 \geq \sigma_2 \geq \dots \sigma_n \geq 0$ . An input  $u^i = V_i \sigma_i^{-1}$  will then produce the output  $y^i = V_i$ , with  $\|y^i\| = 1$ . To properly excite all directions  $i = 1, 2, \dots, n$ , we need to apply inputs  $u^i$  that vary between  $u_-^i = -\sigma_i^{-1} V_i$  and  $u_+^i = +\sigma_i^{-1} V_i$  (Koung and MacGregor, 1993). This can be achieved by any kind of input signals (step sequence, PRBS or multi-sinusoidal). Furthermore, this excitations can be added one direction at a time or simultaneously.

The effectiveness of various input excitation methods for ill-conditioned MIMO systems is studied. Three types of perturbations are used: step, PRBS (pseudo-random binary sequence) and multi-sine inputs. The methods are evaluated for a distillation column stripper system with four-inputs and four-outputs described by a transfer function model. Various plant-friendliness measures (e.g. crest factor, PIPS, peak factor etc.) are considered in input excitation design. The relation between the phase and the crest factor of a multisine is quite complicated and cost function contains number of local minima. A plant friendly multisine signal is generated through Polya's best approximation of Chebyshev norm and crest factor optimization (Guillaume et al. 1991, Pintelon and Schoukens 2004). A Guillaume phase modified zippered signal was found to be the best option among the studied excitation signals. The distribution of the output signal over the gain directions is good for this signal. This is in agreement with a previous study of a  $2 \times 2$  system (Rivera et al. 2009). Projections of the outputs from all experiments onto the high- and low-gain are compared. This projections are obtained by using the  $W$ -matrix from the SVD of gain matrix  $G(0) = W\Sigma V^T$  and work as a measure for how well a certain direction is excited. As expected, all the experiments that not specifically excite the low-gain direction do excite the low-gain direction much less than the high-gain direction.

---

<sup>†</sup> Corresponding author, e-mail: rghosh@abo.fi

# Advanced optimization of C5 and C6 fermentation by the use of state estimators with pH measurements

Miguel Mauricio-Iglesias<sup>a,b</sup>, Krist V. Gernaey<sup>a</sup>  
Jakob K. Huusom<sup>a</sup>

<sup>a</sup> CAPEC-PROCESS, Dep. of Chemical and Biochemical Engineering, Technical University of Denmark, Søltofts Plads, Lyngby, 2800, Denmark

<sup>b</sup> Chemical Engineering Department, School of Engineering, University of Santiago de Compostela, Campus Sur, E-15782 Santiago de Compostela, Spain

---

**Abstract:** The application of the continuous-discrete extended Kalman filter (CD-EKF) as a powerful tool for state estimation in biochemical systems is assessed here. Using a fermentation process for ethanol production as a case study, the CD-EKF can effectively estimate the model states even when highly non-linear measurements such as pH are included. Several configurations of the CD-EKF are proposed using the commonly used measurements and sampling rates. Testing those configurations with two scenarios considering perfect model information and severe model mismatch (simulation of lactic acid bacteria contamination) it is seen that including pH, which is a readily available measurement in virtually every biochemical process, provides information that significantly improves the performance of the filter

*Keywords:* state estimation; non-linear filtering; fermentation; lignocellulosic ethanol

---

## 1. INTRODUCTION

Monitoring of biochemical processes is essential for fault-diagnosis, control and optimisation. However, a number of factors have hindered the development of advanced monitoring techniques, especially in comparison with standard chemical processes. Lack of appropriate sensors and the high non-linearity inherent to biochemical processes are some of the main obstacles among these factors. In this context, the continuous-discrete extended Kalman filter (CD-EKF) is an appropriate tool for state estimation in biochemical processes. The non-linearity of the model can be efficiently tackled by the CD-EKF since the sensitivity of the dynamic model is updated at each sampling time via ODE integration. Commonly this step consumes a non-negligible computation time. However, the sampling time in biochemical processes is usually relatively slow ( $\gg 1$  min) and computation time is rarely an issue. Another consequence of the slow sampling is that non-linearity between samples may be significant; other EKF formulations using linear approximations for the forecasting step are then unsuitable.

In this contribution we present the application of the CD-EKF to the monitoring of a fermentation process aimed at producing ethanol from C6 and C5 sugars. The focus is specifically on the use of pH as this is a variable that correlates well with the yeast catabolism ( $\text{CO}_2$  is co-produced with ethanol, leading to acidification of the medium) and that can be easily measured online. Several configurations of the CD-EKF are presented and it is concluded that using pH measurements is 1) a suitable means to monitor the process if a good prediction model is available; and, 2) a good

complement to other measurements if model mismatch is more severe.

## 2. PROCESS DESCRIPTION AND MODELLING

The process studied here corresponds to the production of second generation bioethanol by fermentation by *Saccharomyces cerevisiae* of C6 and C5 monosaccharides (mainly glucose and xylose respectively), obtained from lignocellulosic biomass. One of the specific challenges of this operation is to minimise the effect of the inhibitory compounds that are produced during biomass hydrolysis such as furfural, 5-hydroxymethylfurfural (HMF) and acetate. Besides, in the case of organic acids, there is evidence that only the unionized form of the acid (e.g. acetic acid and not acetate) is responsible for the inhibition (Casey et al. 2010) and pH must be taken into account.

This simulation case study is based on common configurations for fermentation found in the literature. It is carried out in a  $100 \text{ m}^3$  reactor and is run in fed-batch mode as follows: 1) first a batch phase with the inoculum ( $0.2 \text{ m}^3$ ) during 1 h; 2) a feeding phase for 7 h with a flowrate of  $4 \cdot 10^{-3} \text{ m}^3 \text{ s}^{-1}$ ; 3) finally a batch phase during 92 h. The composition of the inflow, which includes a strong base for pH regulation, is assumed to be known.

The model of the process is composed of 11 states: reactor holdup (M), cell biomass ( $X_{\text{bio}}$ ), glucose (Glu), xylose (Xyl), ethanol (Eth), furfural (Fur), total acetate (Ac), 5-hydroxymethylfurfural (HMF), furfuryl alcohol (FA), base conjugated cations (K) and total inorganic carbon (TIC), which includes several species in equilibrium ( $\text{CO}_2$ ,  $\text{H}_2\text{CO}_3$ ,  $\text{HCO}_3^-$  and  $\text{CO}_3^{2-}$ ). Of these, only M is routinely measured at

a relatively fast sampling time; Glu, Xyl and Eth are often measured but at slow sampling times. As in virtually every other fermentation, pH is measured at a relatively fast sampling time but it does not correspond directly or linearly to any state.

The total mass balance is expressed as:

$$\frac{dM}{dt} = F_{in} \rho_{in} \quad (1)$$

where  $F_{in}$  is the feed flowrate ( $\text{m}^3/\text{s}$ ) and  $\rho_{in}$  is the feed density ( $\text{kg}/\text{m}^3$ ). As the reactor is modelled as a stirred tank, the partial mass balances are generically expressed as:

$$\frac{dC_i}{dt} = \frac{F_{in}}{V} (C_{i,in} - C_i) + r_i \quad (2)$$

In (2),  $V$  represents the volumetric holdup of the reactor,  $C_i$  represents the concentration of component  $i$  in the reactor ( $\text{kg}/\text{m}^3$ ) and  $r_i$  is a lumped term representing the reaction and gas-liquid transfer of compound  $i$ .

The reactions describe the fermentation of the C6 and C5 sugars by a generic strain of *Saccharomyces cerevisiae*; it has not been attempted to model any particular strain but to build a multi-purpose model that takes into account the phenomena that impact the fermentation of lignocellulosic ethanol. Hence, several references have been used to describe the consumption of glucose and xylose (Krishnan et al. 1999), the effect of pH on metabolism (Nielsen et al. 2003), and the effect of inhibitors (Hanly and Henson, 2014). The stoichiometric matrix and the process rates description are provided in tables A1-A2.

The gas-liquid mass transfer, which in this case is only relevant to  $\text{CO}_2$  is described as:

$$J_{\text{CO}_2} = k_L a (P_{\text{CO}_2} - H_{\text{CO}_2} C_{\text{CO}_2}) \quad (3)$$

where  $k_L a$  is the volumetric mass transfer coefficient,  $P_{\text{CO}_2}$  is the partial pressure of  $\text{CO}_2$  in the headspace,  $H_{\text{CO}_2}$  is the Henry's constant and  $C_{\text{CO}_2}$  is the liquid concentration of  $\text{CO}_2$  which can be obtained from the concentration of TIC and the pH in the liquid.

Finally, pH is calculated as the solution, at every time step, of the algebraic equation accounting for the charge balance.

$$\begin{aligned} & C_{\text{H}^+} + K^+ - \frac{K_w}{C_{\text{H}^+}} - \frac{K_{\text{Ac}} C_{\text{Ac}}}{C_{\text{H}^+} + K_{\text{Ac}}} - \\ & \frac{K_{1,C} C_{\text{TIC}} C_{\text{H}^+}^2 + K^2_{1,C} C_{\text{TIC}} C_{\text{H}^+}}{\left( C_{\text{H}^+} + K_{1,C} \right) \left( C_{\text{H}^+}^2 + K_{1,C} C_{\text{H}^+} + K_{1,C} K_{2,C} \right)} = 0 \end{aligned} \quad (4)$$

where  $K_w$  is the ionic product of water,  $K_{\text{Ac}}$  is the acid constant of acetic acid,  $K_{1,C}$  is the pseudo-acid constant between carbon dioxide and the bicarbonate anion and  $K_{2,C}$  is the acid constant between the bicarbonate and carbonate anions. The kinetic models for lactic acid bacteria (LAB), used to simulate contamination in scenario 2 were modelled according to Pinelli et al (1997).

### 3. STATE ESTIMATION AND FILTER CONFIGURATION

The system described by (1-4) can be written in a general non-linear state-space form using the reactor volume as system boundary.

$$\frac{dx}{dt} = f(x(t), u(t), d(t)) \quad (5a)$$

where the states ( $x$ ), inputs ( $u$ ) and disturbances ( $d$ ) represent:

$$x = [M \ C_i]^T \quad u = [F_{in}] \quad d = [C_{i,in}] \quad (5b)$$

The estimation is indeed computed at discrete time step based on the sample rate in the control or monitoring system. The system (5) takes the following discrete step form:

$$x_{k+1} = F(x_k, u_k, d_k) = x_k + \int_{t_k}^{t_{k+1}} f(x(\tau), u(\tau), d(\tau)) d\tau \quad (6a)$$

$$y_k = G(x_k) + v_k, \quad v_k \in N_{iid}(0, R_v) \quad (6b)$$

The observer is formulated as a CD-EKF filter as described by Jørgensen et al (2007) and recently applied in a biochemical reactor by Price et al. (In Press). To determine the discrete time state evolution, the continuous time process model is used for the state integration as:

$$x_{k+1} = F(x_k, u_k, d_k) + w_k = x_k + \int_{t_k}^{t_{k+1}} f(x(\tau), u_k, d_k) d\tau + w_k \quad (7)$$

where the distribution of the process noise term  $w_k$  can be chosen to tune the filter relative to the measurement noise. The filter equations for the measurement update are:

$$e_k = y_k - C_k \hat{x}_{k|k-1} \quad (8a)$$

$$K_{f,k} = P_{k|k-1} C_k^T \left[ C_k P_{k|k-1} C_k^T + R_v \right]^{-1} \quad (8b)$$

$$\hat{x}_{k|k} = \hat{x}_{k|k-1} + K_{f,k} e_k \quad (8c)$$

$$P_{k|k} = P_{k|k-1} - K_{f,k} \left[ C_k P_{k|k-1} C_k^T + R_v \right]^{-1} K_{f,k}^T \quad (8d)$$

And the one step ahead prediction is

$$\hat{x}_{k+1|k} = \hat{x}_{k|k} + \int_{t_k}^{t_{k+1}} f(x(\tau), u_k, d_k) d\tau \quad (8e)$$

$$\bar{A}_k = I + \int_{t_k}^{t_{k+1}} \frac{\partial f}{\partial x} (x(\tau), u_k, d_k) S_{\hat{x}_{k|k}} d\tau \quad (8f)$$

$$P_{k+1|k} = \bar{A}_k P_{k|k} \bar{A}_k^T + R_w \quad (8g)$$

In this formulation, the matrices  $A_k$  and  $C_k$  are not time invariant. The main particularity of the CD-EKF in the

present work is that output matrix  $C_k$  is not time invariant.  $C_k$  is the partial derivative of the output function  $G(x_k, u_k, d_k)$  with respect to the states. Commonly,  $C_k$  is time invariant as it represents the relation between the measurements and the states.

In this case, as pH is one of the outputs:

$$C_k = \left. \frac{\partial G(x_k)}{\partial x} \right|_{\hat{x}_{k|k-1}} \quad (9)$$

$A_k$  represents the Jacobian matrix of the process model over the time interval  $k$  to  $k+1$ . It is calculated as the solution of the sensitivity equation

$$\dot{S}_{\hat{x}_{k|k}} = \frac{\partial f}{\partial x}(x(t), u_k, d_k) S_{\hat{x}_{k|k}} \quad (10)$$

integrated from time instant  $k$  to  $k+1$  with  $I$  (the identity matrix) as the initial condition. The system of differential equations from the sensitivity equation is conveniently solved together with the integration of the process model when calculating the prediction one step ahead.

Three possible configurations of the CD-EKF were tested considering different measurements and sampling rates, chosen following realistic implementation (Table 1). It is considered that the total holdup and the pH can be followed on-line and hence to a fast sampling rate. On the contrary, measuring glucose, xylose and ethanol content requires sample preparation and off-line analyses; the sampling rate is necessarily slow.

Table 1. Measured variables for three configurations of the CD-EKF

Configuration	Measurements	Sampling rate (Ts, min)
1	M, pH	20
2	M, Glu, Xyl, Eth	240
3	M, Glu, Xyl, Eth, pH	240

#### 4. SIMULATION RESULTS

A first scenario was defined where the filter is assumed to dispose of perfect knowledge of the plant model (the only difference between the model and the plant is introduced by sensor noise). The performance of the three configurations is very similar when the performance metrics are compared (Table A3). As the space of this contribution is limited, we have decided to focus on the unmeasured states that have the highest influence on the plant evolution:  $X_{\text{bio}}$ , Fur, Ac and TIC. It can be seen (Table A3) that configurations 2 and 3 outperform configuration 1, as more information is available from the measurements.

A second simulation scenario was set where a certain and realistic model mismatch is assumed: contamination in the media by lactic acid bacteria (LAB), simulated by including 0.2% w/w of the yeast biomass in the inflow. The

performance of the filter with the three configurations is compared to a simulation that does not take into account the LAB contamination. In this scenario (Figure 2), configuration 1 and 2 present a severe bias, in particular for  $X_{\text{bio}}$  and Ac. In contrast,  $X_{\text{bio}}$  is accurately estimated by configuration 3, demonstrating the importance of the information provided by pH. In general, configuration 3 presents the smallest error of all the filter configurations and the system simulations except for Ac (probably because of the presence of lactic acid produced by the LAB). The performance metrics (Table A3) confirm these results. Additionally, the variance is smallest for configuration 3, showing that a good compromise between the use of measurements and model information was reached.

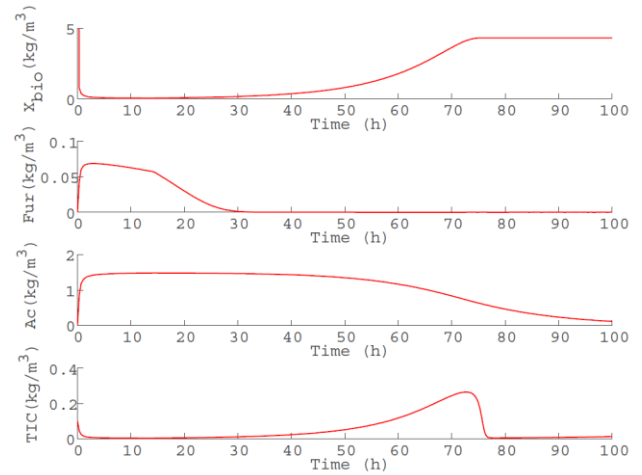


Fig. 1. Simulation of the process with LAB contamination. Selection of key states.

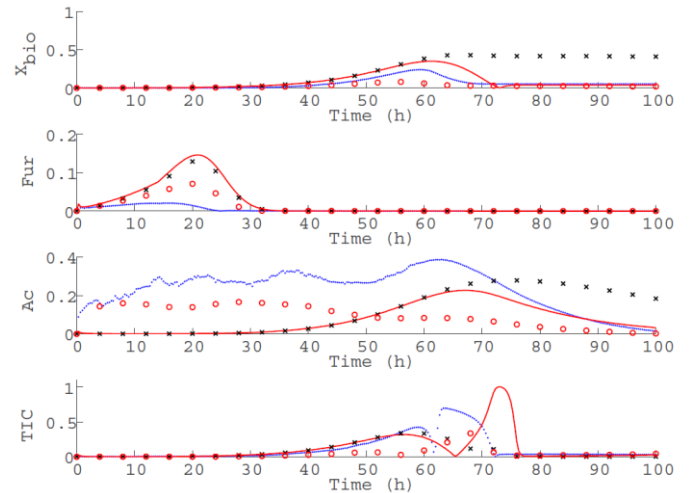


Fig. 2. Absolute normalized prediction error of the CD-EKF in scenario 2 (LAB contamination) for pure simulation (line), configuration 1 (dots), configuration 2 (crosses) and configuration 3 (empty circles)

#### 5. CONCLUSIONS

The CD-EKF was proven as a suitable tool for monitoring of biochemical processes. Its main drawback, i.e. requirement of significant computational resources, is of little relevance in these processes as sampling is relatively slow. Providing pH

helps improving the prediction of the filter when comparing several configurations. The use of pH is of great interest for such processes since it is a ubiquitous measurement in biochemical processes, in particular in fermentation. Further application in contamination detection and real time optimisation will follow this study.

## ACKNOWLEDGEMENTS

This work is partially financed by BIOPRO. BIOPRO is a collaboration between partners from companies (Novo Nordisk, Novozymes, DONG Energy and CP Kelco), universities (DTU and Copenhagen university) and the investment and innovation institution CAPNOVA. BIOPRO is financed by the European Regional Development Fund (ERDF), Region Zealand (Denmark) and BIOPRO partners.

## REFERENCES

- Casey, E., Sedlak, M., Ho, N.W.Y., Mosier, N.S. 2010, Effect of acetic acid and pH on the cofermentation of glucose and xylose to ethanol by a genetically engineered strain of *Saccharomyces cerevisiae*, FEMS Yeast Research, **10**(4):385–393.
- Hanly, T.J., Henson, M.A. 2014. Dynamic model-based analysis of furfural and hmf detoxification by pure and mixed batch cultures of *S. cerevisiae* and *S. stipitis*, Biotechnology and Bioengineering, **111**(2):272–284.
- Jørgensen, J.B., Thomsen, P.G., Madsen, H. and Kristensen, M.R. (2007) A computationally efficient and robust implementation of the continuous-discrete extended Kalman filter. in Proceedings of the American Control Conference ACC, 2468–2474.
- Krishnan, M.S., Ho, N.W.Y., Tsao, G.T. 1999, Fermentation kinetics of ethanol production from glucose and xylose by recombinant *Saccharomyces* 1400(plnh33), Applied Biochemistry and Biotechnology, **77–79**:373–388.
- Nielsen, J., Villadsen, J., Liden, G. 2011, Bioreaction engineering principles. 3<sup>rd</sup> Ed, Springer.
- Pinelli, D., González-Vara, A., Matteuzzi, D. Magelli, F. 1997, Assessment of kinetic models for the production of L- and D-Lactic Acid Isomers by *Lactobacillus casei* DMS 20011 and *Lactobacillus coryniformis* DMS 20004 in continuous fermentation, Journal of Fermentation and Bioengineering, **83** (2), 209-212
- Price, J. Nordblad, M., Woodley, J.M., Huusom, J.K. Real-Time Model Based Process Monitoring of Enzymatic Biodiesel Production, (In Press), Biotechnology Progress

## A. APPENDIX.: KINETIC MODEL DESCRIPTION AND RESULTS

Table A1. Stoichiometric matrix for the fermentation process

Compound → Process ↓	$X_{bio}$	Glucose	Xylose	Ethanol	Furfural	Acetate	HMF	FA	TIC
Glucose uptake	$Y_{X/Glu}$	-1	0	$Y_{Eth/Glu}$	0	0	0	0	$Y_{CO2/Glu}$
Xylose uptake	$Y_{X/Xyl}$	0	-1	$Y_{Eth/Xyl}$	0	0	0	0	$Y_{CO2/Xyl}$
Furfural uptake	$\sim 0$	0	0	0	-1	0	0	$Y_{FA/Fur}$	0
Acetate uptake	$\sim 0$	0	0	0	0	-1	0	0	$Y_{CO2/Ac}$
HMF uptake	$\sim 0$	0	0	0	0	$Y_{FA/HMF}$	-1	0	0

Table A2. Process rates for the fermentation process. Note that  $I$  represents an inhibitory term for the fermentation process.

Equation expressed as substrate consumption	
Glu uptake	$v_{Max} X_{bio} \frac{Glu}{K_{SGlu} + Glu + \frac{Glu^2}{K_{IGlu}}} \frac{1}{1 + \frac{Fur}{J_{Fur}}} \frac{1}{1 + \frac{HMF}{J_{HMF}}} \frac{1}{1 + \frac{HAc}{J_{HAc}}} \left( 1 - \left( \frac{Eth}{Eth_{INH}} \right)^\gamma \right) \frac{Glu}{Glu + Xyl}$
Xyl uptake	$v_{Max} X_{bio} \frac{Xyl}{K_{SXyl} + Xyl + \frac{Xyl^2}{K_{IXyl}}} \frac{1}{1 + \frac{Fur}{J_{Fur}}} \frac{1}{1 + \frac{HMF}{J_{HMF}}} \frac{1}{1 + \frac{HAc}{J_{HAc}}} \left( 1 - \left( \frac{Eth}{Eth_{INH}} \right)^\gamma \right) \frac{Xyl}{Glu + Xyl}$
Fur uptake	$v_{Max} X_{bio} \frac{Fur}{K_{SFur} + Fur}$
Ac uptake	$v_{Max} X_{bio} \frac{Ac + HAc}{K_{SAc} + Ac + HAc}$
HMF uptake	$v_{Max} X_{bio} \frac{Fur}{K_{SFur} + Fur}$

Table A3. Estimation statistics: the mean and the standard deviation are given for the absolute estimation error on selected states based on the normalized data. Simulation stands for a simulation with the original plant model (not considering LAB contamination)

Variable → Configuration ↓	$X_{bio}$		Fur		Ac		TIC	
	$\mu \cdot 10^3$	$\sigma \cdot 10^3$						
Scenario 1. Perfect plant model								
1	0.98	1.33	0.73	1.35	1.08	0.87	2.00	6.18
2	0.36	0.50	0.32	0.60	0.39	0.31	0.82	2.22
3	0.36	0.50	0.32	0.60	0.39	0.32	0.82	2.23
Scenario 2. Contamination by lactic acid bacteria (LAB)								
Simulation	96.0	112	21.9	43.2	77.7	73.0	181	286
1	62.0	65.4	2.90	6.70	232	98.7	173	250
2	239	194	19.3	38.7	123	109	117	159
3	27.2	22.0	10.9	21.7	89.0	54.4	66.9	104

## Poster Session

- P1 *Self-tuning of predictive controller based on step response model in real-time framework*  
Dejan Dovzan, Igor Skrjanc  
Faculty of Electrical Engineering, Ljubljana, Slovenia
- P2 *Modeling the Automotive SCR Catalyst*  
Andreas Åberg\*, Anders Widd\*\*, Jens Abildskov\* and Jakob Kjøbsted Huusom\*  
\* DTU, Lyngby, Denmark  
\*\* Haldor Topsøe A/S, Lyngby, Denmark
- P3 *A Trajectory-based Bumpless Switching Control of Multi-Evaporator Air-Conditioning Systems*  
Tushar Jain<sup>1</sup>, Joseph J. Yame<sup>2</sup>  
<sup>1</sup> Aalto University, School of Chemical Technology, Finland  
<sup>2</sup> Université de Lorraine, Vandoeuvre-lès-Nancy, France
- P4 *Active Disturbance Rejection Control of the Newell-Lee forced circulation evaporator – a simulation study*  
Rainer Dittmar, West Coast University of Applied Sciences at Heide, Germany
- P5 *Nonlinear Model Predictive Control of a High-Pressure Polyethylene Tubular Reactor in Stenungsund, Sweden*  
Staffan Skålén and Fredrik Josefsson  
Advanced Process Control group, Borealis AB, Stenungsund, Sweden.
- P6 *Automation experiences during projects in Abu Dhabi*  
Staffan Skålén  
Advanced Process Control group, Borealis AB, Stenungsund, Sweden.
- P7 *Enabling High-Performance Industrial Embedded Model Predictive Control using Code Generation and High-speed Solvers*  
D. K. M. Kufoalor\*, B. J. T. Binder\*, L. Imsland\*, T. A. Johansen\*, G. O. Eikrem\*\*, A. Pavlov\*  
\* Department of Engineering Cybernetics, NTNU, Trondheim, Norway  
\*\* Statoil ASA, Rotvoll & Porsgrunn.
- P8 *Model Selection and Estimation of Neural Networks by Using Weight Dropout*  
Mikael Manngård and Jari M. Böling  
Department of Chemical Engineering, Åbo Akademi University, Finland

- P9 *Using Fluorescence as Control Parameter to Decide Optimal Light Spectrum for Plant Growth*  
Linnéa Ahlman, Torsten Wik and Daniel Bånkestad  
Department of Signals and Systems, Chalmers University of Technology, Göteborg, Sweden
- P10 *Dynamic Effects of Diabatization in Distillation Columns*  
Thomas Bisgaard, Jakob K. Huusom, Jens Abildskov  
CAPEC-PROCESS, Technical University of Denmark, Lyngby, Denmark
- P11 *Fault propagation analysis by merging process causality and plant topology*  
R. Landman, J. Kortela and S-L. Jämsä-Jounela  
Aalto University, Process Control and Automation Research Group, Finland
- P12 *Relative Gain Array Estimation Based on Non-parametric Process Identification for Uncertain Systems*  
Ali M. H. Kadhim\*, Wolfgang Birk and Thomas Gustafsson  
Control Engineering Group, Luleå University of Technology, Sweden
- P13 *Convex optimization as a design tool for feedforward controllers*  
Martin Hast and Tore Hägglund  
Department of Automatic Control, Lund University, Sweden
- P14 *Autotuning Based on Asymmetric Relay*  
Josefin Berner, Karl Johan Åström and Tore Hägglund  
Department of Automatic Control, Lund University, Sweden
- P15 *A reduced observer design for a freezing process*  
Christoph Josef Backi and Jan Tommy Gravdahl  
Department of Engineering Cybernetics, NTNU, Trondheim
- P16 *Decoupling approach in fluidized bed combustor control*  
Szabó, Z.\*, Kovács, J.\*\*\*, Szentannai P.\*  
\* Budapest University of Technology and Economics, Department of Energy Engineering Budapest, Hungary  
\*\*\* University of Oulu, System Engineering Laboratory, Oulu, Finland
- P17 *A performance optimization algorithm in fault tolerant distributed model predictive control*  
Alexey Zakharov, Elena Zattoni, Miao Yu and Sirkka-Liisa Jämsä-Jounela  
Aalto University, Department of Biotechnology and Chemical Technology, Finland
- P18 *Modeling Vapor Compression Cycles for Dynamic Simulation of Supermarket Refrigeration Systems*  
S. N. Mohd. Azam <sup>a</sup>, R. Izadi-Zamanabadi <sup>b</sup>, J. B. Jørgensen <sup>a</sup>  
<sup>a</sup> Department of Applied Mathematics and Computer Science, Technical University of Denmark, Lyngby, Denmark  
<sup>b</sup> Danfoss A/S, Electronic Controllers & Services, DK-6430 Nordborg, Denmark

- P19 *Data Reconciliation method for improving performance and reliability of MPC control strategy for a BioGrate boiler*  
Palash Sarkar, Jukka Kortela, Alexandre Boriouchkine and Sirkka-Liisa Jämsä-Jounela  
Aalto University, Process Control and Automation Research Group, Finland
- P20 *An indirect fuel moisture content estimation approach for BioGrate boilers*  
Alexandre Boriouchkine\*, Miao Yu and Sirkka-Liisa Jämsä-Jounela  
Aalto University, Department of Biotechnology and Chemical Technology, FI-00076 Aalto, Finland.
- P21 *Dynamic Real-Time Optimization for a Reactor, Separator and Recycle Processes*  
Vladimiro Minasidis and Sigurd Skogestad  
Department of Chemical Engineering, NTNU, Trondheim, Norway
- P22 *Non-robustness and limitations of Smith Predictor Control*  
Chriss Grimholt and Sigurd Skogestad  
Department of Chemical Engineering, NTNU, Trondheim, Norway
- P23 *Novel strategies for control of fermentation processes*  
Lisa Mears<sup>1</sup>, Stuart Stocks<sup>2</sup>, Gürkan Sin<sup>1</sup>, Krist V. Gernaey<sup>1</sup>, Kris Villez<sup>3</sup>  
<sup>1</sup> Department of Chemical and Biochemical Engineering, DTU, Denmark  
<sup>2</sup> Novozymes A/S, Pilot plant, Denmark  
<sup>3</sup> Eawag: Swiss Federal Institute of Aquatic Science and Technology, Dübendorf, Switzerland
- P24 *From Tweets to Optimality in the Smart and Sustainable Factory*  
Bengt Lennartson  
Chalmers University of Technology, Göteborg, Sweden
- P25 *Optimal Controller Design for Balancing Input/Output Disturbance Rejection Response with Robust Stability Condition*  
Bo Sun  
School of Electronic Information and Electrical Engineering, Shanghai Jiao Tong University.

# Self-tuning of predictive controller based on step response model in real-time framework

Dejan Dovžan<sup>a</sup>, Igor Škrjanc<sup>b</sup>

*Faculty of Electrical Engineering Tržaška 25, Ljubljana, Slovenia*

<sup>a</sup>*dejan.dovzan@fe.uni-lj.si*

<sup>b</sup>*igor.skrjanc@fe.uni-lj.si*

---

## Abstract

In this paper a self-tuning algorithm for predictive functional controller is presented and applied in a real-time framework. The self-tuning algorithm is based on a step response model. The derived control law was implemented as a part of an in-house real-time C# library called Plug and Play Control Toolbox (PPCT) that is used to tune and control by PID and predictive controllers. The library implements several tuning algorithms for PID controllers and the simple predictive functional controller based on step response model.

The PFC-step is an extension of the predictive functional control algorithm (PFC). The PFC control law is very simple yet effective. The advantage over the PI controller is that it is easier to tune and copes better with dead-times as it incorporates the Smith's predictor principle. The development of control law relies on the process model and this could be sometimes quite difficult to obtain. In this sense the dynamic matrix controller is better since it can cope implicitly with different process orders and is in a way easier to tune since it does not require the identification of the model parameters. It uses recorded step response of the process for tuning. The disadvantage of the DMC is that it requires matrix manipulations in order to calculate the controller output. This is a quite big disadvantage when implementing the controller in a low level hardware. In this paper we tried to merge the good properties from both the DMC and the PFC control approaches. The derivation of the proposed control law is based on the same idea as the PFC: the equality of the process output increment and the model output increment. The first order model in the original derivation of the PFC is replaced by a step-response model, making the presented control algorithm easier to tune and more simple and robust in the case of higher order dynamics.

Two different types of control laws are presented in this paper. The first one is called simple PFC-step. With this control law constant future control is assumed. This means that the assumption is made that the control law will not change in future. With the second presented control law (PFC-step with filtering) the exponential decrease of the future control is assumed. This is especially suitable control law when a lot of noise is present. We also provide an extension of the control law for the processes with dead-time and provide the anti-windup mechanism. During the testing of the algorithm we also found out that when applying the filtering to the calculated controller output difference we can achieve very smooth functioning of the controller even in highly noisy environment. In the Result and Discussion section the performance of the presented

controller is evaluated on a different simulation examples demonstrating the advantages and disadvantages of the proposed algorithm. Also an example of speed control of a DC-motor using the PFC-step controller applied in real-time PPCT framework is shown.

*Keywords:* self-tuning, predictive control, step response model

---

*October 7, 2014*

# Modeling the Automotive SCR Catalyst

Andreas Åberg\*, Anders Widd\*\*, Jens Abildskov\*, Jakob Kjøbsted Huusom\*

\* CAPEC-PROCESS, Department of Chemical and Biochemical Engineering, Technical University of Denmark, Søtofts Plads, Building 229, DK-2800 Kgs. Lyngby, Denmark

\*\* Haldor Topsøe A/S, Nymøllevej 55, 2800 Kgs. Lyngby, Denmark

## Abstract

Diesel engine exhaust gases contain amongst other things nitrous gases such as NO and NO<sub>2</sub> (together abbreviated NO<sub>x</sub>). Reducing the amount of these gases is of great importance due to new legislation, and because of the effect they have on urban air quality [1, 2]. A promising and widely used technology for this is based on selective catalytic reduction (SCR) of the gases, with ammonia (hydrolyzed Urea) as a reducing agent [3, 4, 5]. Challenges with this technology include dosing the right amount of urea to reach maximum NO<sub>x</sub> conversion, while simultaneously minimizing ammonia slip. This requires efficient dosing algorithms, and to this end, model-based control is a promising strategy. Selection of the proper model complexity for the optimization routine and the state estimation is crucial to get a controller able to meet the requirements and is fast enough to handle the transient behavior of the diesel engine. Deriving a model from first principles will give the necessary process understanding to, in the further stages of development, have enough information to make decisions on the required model complexity for control. The model can also be used to try control methods on, before directing experimental effort for validation of the concept.

A high fidelity model has to be able to accurately describe the dynamics of the system. It is important that the NO<sub>x</sub> output and NH<sub>3</sub>-slip from the catalyst can be predicted accurately. To use the model in for example state estimation and control, simulation time has to be measured, and possibly simplifications of the model has to be made.

A high fidelity single monolith channel model has been derived based on underlying physical principles. The model has been combined with a kinetic model taken from literature [6], and adapted to the current system. The kinetic parameters have been calibrated using stationary data from reactor tests with bench-scale equipment, under isothermal conditions. The model has been validated with transient data from a full-scale monolith and a real engine following the European Transient Cycle (ETC) [7]. Results from the NO<sub>x</sub> prediction during a transient test can be seen in Fig. 1.

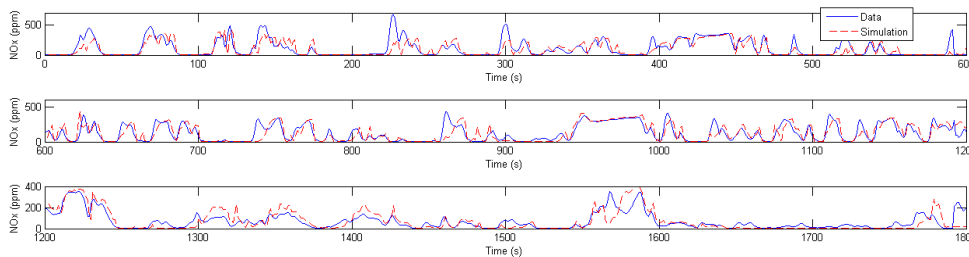


**Figure 1. Model prediction and experimental data for NO<sub>x</sub> during a transient full-scale test. The full line represents the data and the dotted line is the model prediction.**

## References

- [1] A. Fritz, V. Pitchon, The current state of research on automotive lean NO<sub>x</sub> catalysts, *Appl. Catal. B* 13 (1997).
- [2] R. M. Heck, R. J. Farrauto, Automotive exhaust catalysis, *Appl. Catal. A* 221 (2001).
- [3] M. Koebel, M. Elsener, M. Kleeman, Urea-SCR: a promising technique to reduce NO<sub>x</sub> emissions from automotive diesel engines, *Catal. Today* 59 (2000).
- [4] I. E. Wachs, G. Deo, B. M. Wechhuysen, A. Andreini, M. A. Vuurman, M. de Boer, M. D. Amiridis, Selective Catalytic Reduction of NO with NH<sub>3</sub> over Supported Vanadia Catalysts, *J. Catal.* 161 (1996).
- [5] P. Gabrielsson, Urea-SCR in automotive applications, *Top. Catal.* 28 1-4 (2004).
- [6] L. Olsson, H. Sjövall, R. J. Blint, *Appl. Catal. B* 81.
- [7] DieselNet homepage. [Online]. Available: <http://www.dieselnet.com/standards/cycles/etc.php>

# A Trajectory-based Bumpless Switching Control of Multi-Evaporator Air-Conditioning Systems

Tushar Jain<sup>1</sup>, Joseph J. Yame<sup>2</sup>

<sup>1</sup> Aalto University, School of Chemical Technology, P.O. Box 16100, 00076-AALTO, Finland. Email: tushar.jain@aalto.fi

<sup>2</sup> Université de Lorraine, Centre de Recherche en Automatique de Nancy, CNRS, UMR 7039, Vandoeuvre-lès-Nancy 54500, France

## Extended Abstract

Strong requirements on energy saving and the growing end-user demand for air conditioning system that has independent units serving different zones in a building makes multi-evaporator variable refrigerant flow (VRF) system the ideal candidate for many applications such as commercial buildings, offices and hotels. Multiple-evaporator/vapor compression cooling systems are used for air conditioning in multi-zone buildings with a refrigerant supplied to each individual zone-evaporator from a central compressor/condenser unit. Such systems, incorporating controlled electronic expansion valves associated to each evaporator and a variable-speed compressor, allow the overall system to be able to operate in different modes, such as, for example, the modes in which all the indoor units are operating or modes in which selected indoor units are turned off, in order to achieve cooling requirements and energy efficiency. The control scheme of the multi-evaporator cooling system is illustrated in Fig. 1. The controlled VRF system can efficiently distribute cooling capacity to keep up with changing loads with respect to the time of the day, room occupancy, solar loads, etc. Switching between the different modes associated with the cooling demands might give rise to switching transients. Such transients are likely to negatively impact the control performance and consequently the energy efficiency of the overall system. In this paper, a novel technique is proposed for dealing with such transients when switching between control modes in a multiple-evaporator/vapor compression cooling system in order to ensure that the control performance undergoes no degradation. The proposed approach, illustrated in Fig. 2 where plant's model is shaded, is purely a “data-driven” technique using only the plant input/output measurements available in real-time. A simulated experiment with a two-evaporator/vapor compression cooling system shows that the proposed algorithm can achieve a quite satisfactory overall performance under mode switching.

**Keywords:** behavioral system theory, energy efficiency, bumpless switching, multiple evaporator cooling system, data-driven approach.

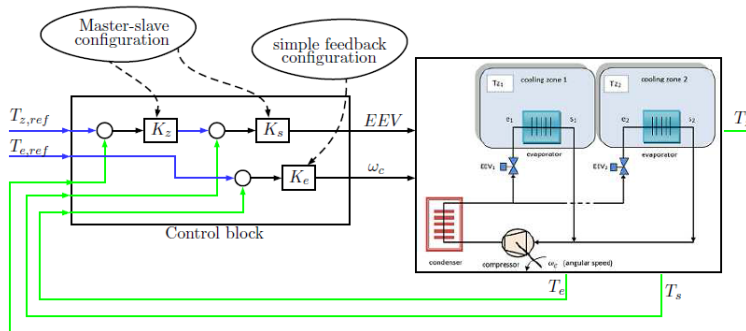


Fig. 1: Control scheme of two-zone VRF system

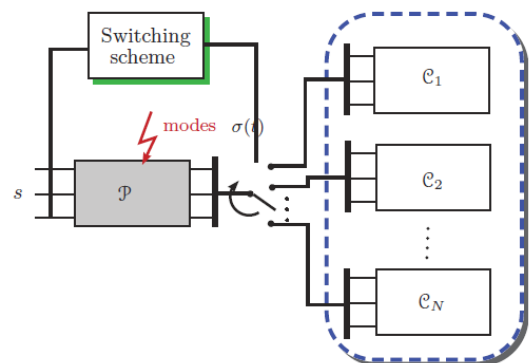


Fig. 2: Schematic view of the mode switching controller architecture

## Suggested Readings

1. T. N. Aynur. Variable refrigerant flow systems: A review. *Energy and Buildings*, 42(7):1106-1112, July 2010.
2. J.-L. Lin and T.-J. Yeh. Mode switching control of dual-evaporator airconditioning systems. *Energy Conversion and Management*, 50:1542-1555, 2009.
3. J. J. Yame and M. Kinnaert. On bumps and reduction of switching transients in multicontroller systems. *Mathematical Problems in Engineering*, 2007:17, 2007.
4. T. Jain. Behavioral System Theoretic Approach to Fault-tolerant Control, PhD. Thesis, Université de Lorraine, 2012.

## **Active Disturbance Rejection Control of the Newell-Lee forced circulation evaporator – a simulation study**

Rainer Dittmar, West Coast University of Applied Sciences at Heide, Germany

As an alternative to both traditional PID control and modern model-based control designs such as Model Predictive Control (MPC), Active Disturbance Rejection Control (ADRC) has gained significant attention in recent years. First industrial applications include motion control, power electronics and web tension control. To our knowledge, very few industrial-scale applications have been realized in process engineering yet (e.g. extrusion control). On the other hand, due to its simple design and tuning, the need of an approximate process model only, and the robustness to process parameter variations, ADRC seems to offer a valuable addition to the toolbox of process control practitioners.

The presentation presents a simulation study of linear ARDC control applied to a forced circulation evaporator, a well-known multivariable/nonlinear benchmark model developed by Newell and Lee [1]. In [2] and [3], either nonlinear ADRC control laws or linear ARDC with feedforward have been studied for chemical reactor control design. Simulations have been carried out using the nominal process model only. Recently, the evaporator benchmark was used to illustrate a simple MPC design methodology [4]. In contrast, a simpler design strategy is chosen here, namely the application of two independent linear SISO ADRC controllers for evaporator pressure and product composition (multi-loop linear ARDC control) using cooling flow rate and steam pressure as controller outputs. The presentation is aimed to answer the question if such a design offers comparable or better results than multi-loop PI and linear MPC control, in terms of control performance, robustness, simplicity of design and tuning, required process model fidelity, and realisability on industrial control systems.

The presentation is organized as follows: (1) the structure, design and tuning of the (linear) extended state observer (ESO) and P/PD controllers required for ADRC are shortly explained, (2) results of the identification of coarse FOPDT/SOPDT models based on PRBS tests are presented; (3) multi-loop linear ADRC closed-loop control simulation results are given, including set-point tracking and disturbance rejection, robustness to heat transfer coefficient changes, and the effect of structural (model) uncertainties such as the approximation of the pressure-to-concentration “hump” step response with an SOPTD model; (4) the comparison of linear ARDC/multi-loop PI/linear MPC controls are summarized; (5) open problems such as the development of ARDC design and simulation tools for practicing control engineers as well as the implementation of ARDC control algorithms on industrial control systems (e.g. DCS) are mentioned.

[1] Newell, R.B., Lee, P.L: Applied Process Control: A case study. Prentice Hall, Englewood Cliffs 1989.

[2] Chen, Z., Zheng, Q., Gao, Z.: Active Disturbance Rejection Control of chemical processes. 16<sup>th</sup> International Conference on Control Applications, Singapore 2007.

[3] Zheng, Q., Chen, Z., Gao, Z.: A practical approach to disturbance decoupling control. Control Engineering Practice 17(2009) 1016 – 1025.

[4] Huusom, J.K., Jorgensen, J.B.: A realistic process example for MIMO MPC based on autoregressive models. 19<sup>th</sup> IFAC World Congress, Cape Town, August 2014.

# Nonlinear Model Predictive Control of a High-Pressure Polyethylene Tubular Reactor in Stenungsund, Sweden

Staffan Skålen and Fredrik Josefsson

Advanced Process Control group, Borealis AB, SE-444 86 Stenungsund, Sweden.

[Staffan.Skalen@borealisgroup.com](mailto:Staffan.Skalen@borealisgroup.com)

*Extended abstract:* A nonlinear model predictive controller (NMPC) is being developed for the high-pressure low-density polyethylene plant in Stenungsund, Sweden. The polyethylene plant is a tubular reactor where the reaction takes place at 2800 bar and 300°C. The plant can produce up to 350 000 ton per year, which is mainly used for cable insulation in Wire & Cable applications. In addition to the reactor there is an extensive purifying and recycle area to reuse the unreacted ethylene.

The NMPC application is developed to control polymer properties such as melt flow rate during operation and during transitions from one grade to another grade. The recycle area provides an extra challenge during the transitions due to the relatively long dynamics of the recycle compared to the dynamics of the reactor. A first-principles model has been developed combined with some empirical components to represent the final properties of the product. The model is then used in a SQP optimization to find the optimal control inputs. A critical point for success is the accuracy of the model, but also a robust state and parameter estimator. Numerous plant measurements are used to estimate the states of the model, used as measured disturbances and finally also used as input to the disturbance estimators to provide integral action. The NMPC has passed the model validation phase and will be commissioned during the fourth quarter of 2014.

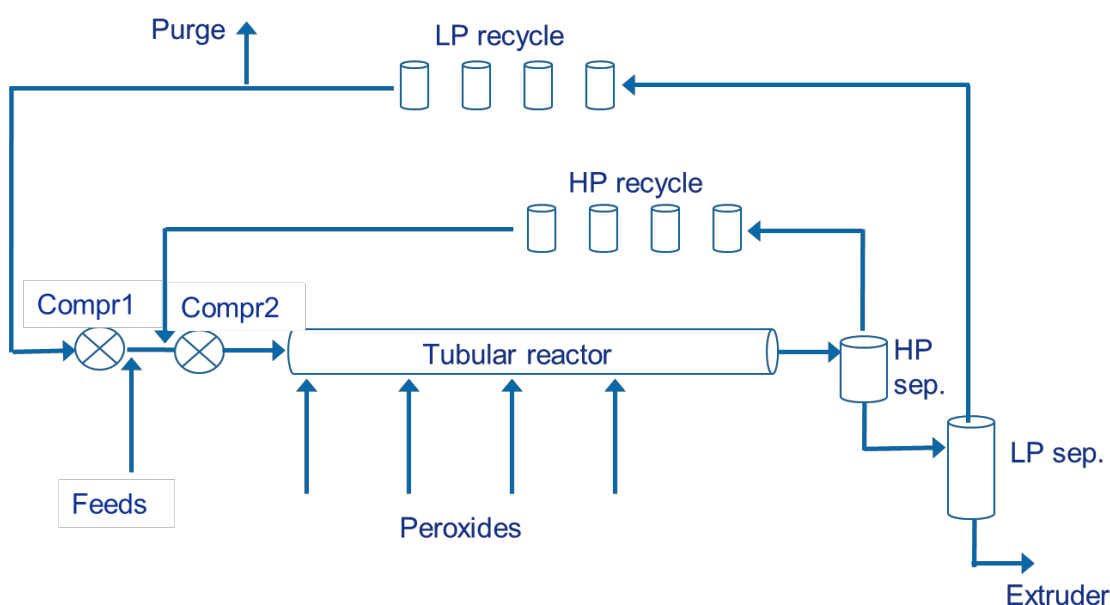


Figure 1: A schematic outline of the LDPE plant in Stenungsund, Sweden.

# Automation experiences during projects in Abu Dhabi

**Staffan Skålen**

*Advanced Process Control group, Borealis AB, SE-444 86 Stenungsund, Sweden.*

*([Staffan.Skalen@borealisgroup.com](mailto:Staffan.Skalen@borealisgroup.com))*

*Extended abstract:* The topic is the automation experiences gained during the \$4.5 billion Borouge3 project, which is being started during 2014. Borouge is a joint venture between Borealis and ADNOC (the national oil company in Abu Dhabi). The number 3 represents the third expansion project within Borouge, where the first complex was built in year 2000.

The Borouge3 project consists of one world-scale ethane cracker, which will produce ethylene to the downstream plants. There are two HDPE, one LDPE and two PP plants. In this case we will focus on the LDPE project.

The learnings can be divided into two parts, non-technical and technical. The non-technical learnings can be how to organize and staff the project or the benefits of a training simulator, whereas the technical learnings can be improved DCS specifications or layout of the control room.

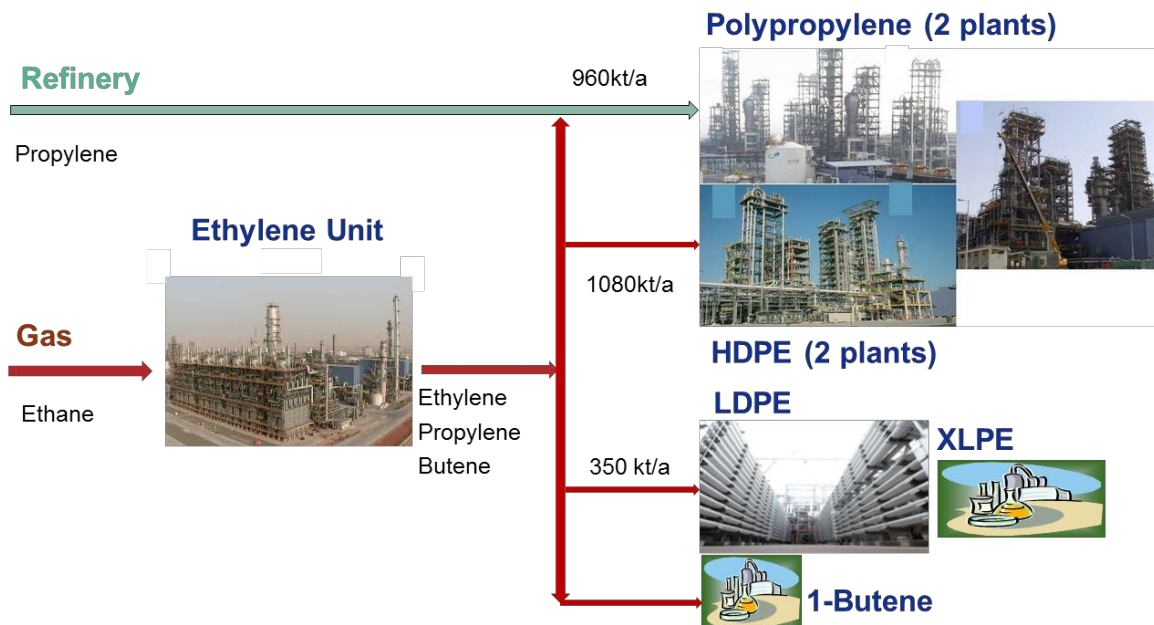


**Figure 1: A schematic outline of the Borouge3 project in Ruwais, Abu Dhabi, UAE.**

# Enabling High-Performance Industrial Embedded Model Predictive Control using Code Generation and High-speed Solvers

D. K. M. Kufoalor\* B. J. T. Binder\* L. Imsland\*  
T. A. Johansen\* G. O. Eikrem\*\* A. Pavlov\*\*

\* *Department of Engineering Cybernetics, Norwegian University of Science and Technology, Trondheim Norway. ([kwame.kufoalor](mailto:kwame.kufoalor@itk.ntnu.no), [benjamin.binder](mailto:benjamin.binder@itk.ntnu.no), [lars.imsland](mailto:lars.imsland@itk.ntnu.no), [tor.arne.johansen](mailto:tor.arne.johansen@itk.ntnu.no))@itk.ntnu.no).*

\*\* *Statoil ASA, Rotvoll & Porsgrunn. ([gise](mailto:gise@statoil.com), [alepav](mailto:alepav@statoil.com))@statoil.com).*

---

**Abstract:** Model Predictive Control (MPC) has proven to be successful in numerous advanced high-level process control applications based on software implementation in PC/server technology. However, for challenging applications offshore and subsea, ultra-reliable industrial embedded hardware, such as Programmable Logic Controllers (PLCs), are usually more suitable. In contrast to high-level onshore or topside process control applications, embedded control applications like subsea processing, automated drilling, and rotating machinery control, tend to be of considerably smaller scale, with much faster dynamics and sampling frequencies. The limited computational resources in *low power* industrial embedded devices, in combination with increased demands for computational speed and system reliability, motivate the development of software tools that enable the use of MPC in industrial embedded real-time applications.

In particular, we incorporate high-speed Quadratic Programming (QP) solvers into an ANSI C code generation framework for embedded MPC. The controllers developed are based on step-response models and MPC design configurations obtained from SEPTIC, Statoil's software tool for MPC. SEPTIC is a field-proven software that has many features used to achieve high control performance in an MPC application. SEPTIC is therefore used to determine the achievable performance targets for the embedded controllers. The embedded MPC code generator produces QP solver configuration files (for generating tailored solver code) or QP data source files (for embedding a more general solver), and supporting files, using a QP problem formulation that is suitable for the particular QP solver used. In order to achieve high online computational efficiency, offline computations/preparations are made at the code generation stage.

We discuss implementation aspects arising when running MPC on an industrial PLC and present results of hardware-in-the-loop simulation tests for two industrial applications. The first application is a case study on Statoil's recently patented subsea compact separation unit, and the second considers the use of an electrical submersible pump in an oil well. The PLC used is the ABB AC500 PM592-ETH, and the high-speed QP solvers considered include the online active set strategy of qpOASES, the primal-dual interior-point method of CVXGEN, and a primal-dual first-order method generated using FiOrdOs, among which qpOASES exhibits superior performance for both applications.

Other high-speed QP solvers are also considered. However, some class of QP solvers cannot be used, while others may become inefficient, when using a standard QP formulation based on step-response models. We discuss why some QP solver approaches are more suitable for MPC based on state-space models, and propose problem reformulation and offline preprocessing strategies that will enable the use of several state-of-the-art high-speed solvers for embedded MPC based on step-response models and configurations typically used in industrial MPC software packages.

*Keywords:* Embedded systems, Model Predictive Control, Code generation, Fast QP solvers.

---

# Model Selection and Estimation of Neural Networks by Using Weight Dropout

Mikael Manngård\*, Jari M.Böling

*Department of Chemical Engineering, Åbo Akademi University, Biskopsgatan 8, FIN-20500 Åbo, Finland*

---

## Extended Abstract

Model selection and identification is a fundamental task in many fields of science and engineering. Neural networks provide a non-linear way of mapping relations between inputs and outputs, and are hence often used as black-box models for systems where the underlying dynamics are either unknown or complex. Single-hidden-layer neural networks have been shown to approximate any continuous function to arbitrary accuracy, provided that the number of nodes is sufficiently large. Since a sufficiently large neural network can exactly implement an arbitrary training set, is the risk of overfitting to measurement noise also high. It is hence important to keep the network size possibly small, and the interest in finding the smallest possible sparsely connected network, which can describe the data well enough, is high. Sparse connectivity in neural networks allow input-output relations of different complexity levels, which will result in less black-box models compared to fully connected neural networks.

A simple way of finding sparse network structures is through weight dropout, or so called weight pruning. A Bayesian approach for model reduction and weight estimation, which utilizes tools such as: maximum a posteriori estimation, importance sampling and weight dropout, has been proposed. Sparse network structures of minimal order are obtained by removing weights iteratively. Such networks are expected to generalize well, and will in other words show little overfitting.

The proposed algorithm have been implemented for non-linear black-box system identification of waste heat recovery in marine vessels. The obtained models are used for forecasting of heat flows, which will allow more efficient scheduling of on-board tasks. A few example of such tasks are: fresh water evaporation, air conditioning and general heating. The use of additional heating can be reduced by scheduling tasks at times when waste heat is available. This will result in an overall improvement in energy efficiency. The research has mainly been carried out in the Efficient Energy Use (EFEU) research programme, which is coordinated by CLEEN Ltd. The programme aims to build knowledge, and to provide tools for improving energy optimization and efficiency at a system level instead of for single components.

*Keywords:* Weight dropout, Neural Networks, System identification

---

---

\*Corresponding author.

*Email address:* mikael.manngard@abo.fi (Mikael Manngård)

# Using Fluorescence as Control Parameter to Decide Optimal Light Spectrum for Plant Growth

Linnéa Ahlman\*, Daniel Bånkestad\*\*, and Torsten Wik\*

\*Department of Signals and Systems, Chalmers University of Technology,  
Göteborg, Sweden

\*\*Heliospectra AB, Göteborg Sweden

## 1 Introduction

Modern greenhouses having lighting systems are large consumers of electricity. In Europe alone, the lighting consumption is estimated to 150 TWh per year. High pressure sodium (HPS) lamps are still dominating and the illumination is in general controlled manually by on/off control. Changing to light emitting diodes (LED) gives the possibility of adapting the spectrum (i.e. changing the power split to diodes of different colours) and to gradually changing the intensity, which implies an energy saving potential. The optimal spectrum might depend on a number of factors, for example plant species, required characteristics and energy use efficiency on the diodes.

Using LEDs with different blue to red (B:R) ratios, as a supplement to sunlight, have been investigated for growing of cucumber seedling [Hernández and Kubota, 2014] and tomato seedling [Hernández and Kubota, 2012]. Their conclusion was that 100% red LED is preferred, indicating that the blue light in the sunlight is sufficient (B:R in sunlight is about 4:3 on *photons/m<sup>2</sup>/s* basis [ASTM, 2012]).

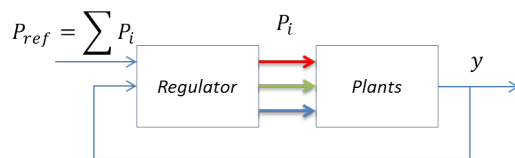


Figure 1: In order to find an optimal spectrum, i.e. how to distribute the power  $P_{ref}$  among the different diode groups by feedback control, one needs to find a parameter of plant growth that could be measured remotely and online. In this study we investigate if chlorophyll fluorescence F740 could be a candidate.

The experiments in this study were performed on basil plants in a closed environment with no sunlight. We aim to find a way of changing the spectrum as a function of some growth measure. Figure 1 shows the basic idea; for a given amount input power  $P_{ref}$ , how should it be distributed among the different diodes in order

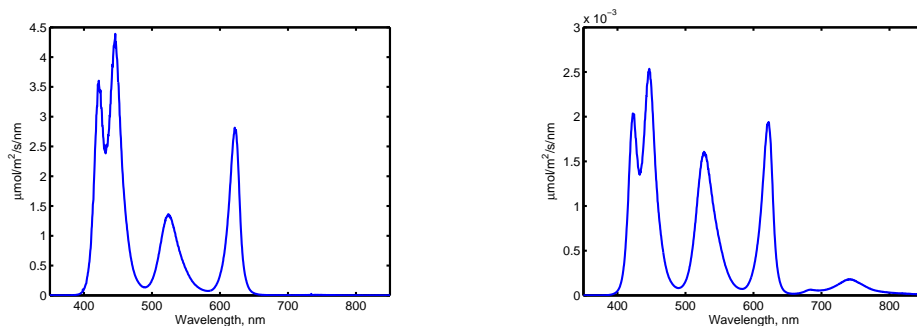


Figure 2: Spectrum when using four diode groups in a LED lamp. Left plot: incident light, i.e. light detected by a spectrometer facing the lamp. Right plot: reflected and fluorescent light, i.e. detected by a spectrometer facing the plants. There are two fluorescent peaks, at 685 and at 740 nm.

to optimize the plant performance,  $y$ , such as growth rate, leaf thickness etc. Having a remotely measured plant performance parameter, a self optimizing controller could be sought to find the optimal spectrum. A candidate signal investigated here is steady state chlorophyll fluorescence. The fluorescence signal originates from chlorophyll  $a$  in photosystem I and II and is an emission of absorbed light energy, with peak wavelengths at 685 and 740 nm. Figure 2 shows a spectrum using four different diode groups. The left plot is the spectrum detected by a spectrometer facing the lamp, i.e. the incident light to the plants. The right plot is the spectrum detected in a spectrometer facing the plants. The same four peaks as for the incident light can be identified, i.e. the reflected light, but also two additional peaks (at 685 and 740 nm) which is the fluorescence. The F740 peak gives the strongest signal, since the F685 is partly reabsorbed by the chlorophyll  $a$ , and was found to be best suited for our purpose.

The hypothesis in this study was that there is a positive correlation between the amount of absorbed light, the amount of fluorescent light and photosynthetic rate under present conditions (well-irrigated and fertilized crops under normal light conditions). This relation has been observed on both leaf level [Flexas et al., 2002] and canopy level [Guantera et al., 2014], but is dependent on plant health since chlorophyll fluorescence is used to remove excess energy. We want to distribute the total incident light  $I_{tot}$  among the available diode groups to reach maximal photosynthetic rate. With our hypothesis this is equal to maximizing the total fluorescence for a given  $I_{tot}$ .

Assume we have two diodes,  $a$  and  $b$ , and assess the changes in fluorescence (with peak at 740 nm,  $F_{740}$ ) when increasing the light by  $\Delta a$  or  $\Delta b$  (where  $|\Delta a| = |\Delta b|$ ). If  $\Delta F_{740}(\Delta a) > \Delta F_{740}(\Delta b)$  the conclusion is that increasing the power to diode group  $a$  increases the performance more than increasing the power to diode group  $b$ . With this argument, the optimal spectrum will be the one where  $\Delta F_{740}(\Delta a) = \Delta F_{740}(\Delta b)$ . This can, formally, be extended to the case of several diode groups with the result that the optimal spectrum will then be the one where all derivatives are equal.

## 2 Experiments and preliminary results

Experiments were performed on basil plants in a closed environment. Two Heliospectra LED lamps were placed 0.9 m above the plants. Two spectrometers were used to detect the light, one detecting the incident light and one detecting the reflected and fluorescent light. In addition, an infrared gas analyzer (IRGA) was used for measuring photosynthetic rate based on carbon dioxide uptake on a single leaf.

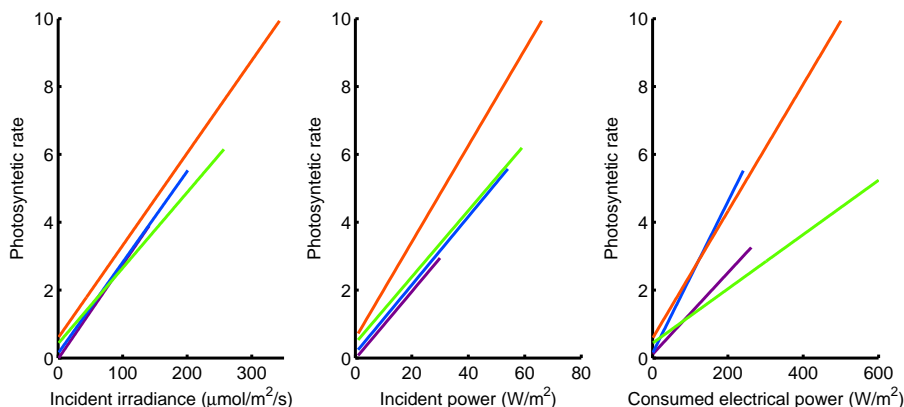


Figure 3: Photosynthetic rate (PN) versus (a) incident irradiance, (b) incident power, (c) consumed electrical power. Four diode groups are tested, one at a time, corresponding to the four lines in each subplot.

### 2.1 One diode group lighting at a time

In the first setup only one diode group was used at a time. The results showed that there is a high correlation ( $R^2 = 0.95$ ) between photosynthetic rate (PN) and fluorescence F740 at low light intensity and they increase linearly with light intensity (Figure 3). PN as a function of photon irradiance (Figure 3a) indicates slightly higher PN using red diodes, possibly due to nonlinearities at light intensities close to zero. The derivatives slightly change if PN is investigated with respect to incident power (Figure 3b); relatively higher derivatives for long wavelength light (red) and relatively lower derivatives for short wavelength light (purple), since light energy is inversely proportional to wavelength. The derivatives for all lines are almost equal, except for the red group clearly having higher derivatives. Taking the efficiency of the different diodes into consideration (Figure 3c) further changes the derivative. The highest derivative, corresponding to the most efficient use of energy, is then the blue group.

### 2.2 Background light

In the second setup different background lights were tested; one regime with blue to red (B:R) ratio 3:1 and with B:R ratio 1:3. Four different light intensity levels were tested for each regime. For a given background light one diode group was changed at a time, in order to measure the fluorescence changes as a function of incident light ( $dF740/dI$ ), at the given operating point. Figure 4 shows the results for

dominating blue background light (B:R 3:1) and Figure 5 shows the same information for dominating red background light (B:R 1:3).

The results are similar to those presented in Section 2.1. To reach the optimal spectrum (based on photon irradiance, not energy) the amount of red light should increase and the amount of green light should decrease; no matter if the B:R ratio is 1:3 or 3:1.

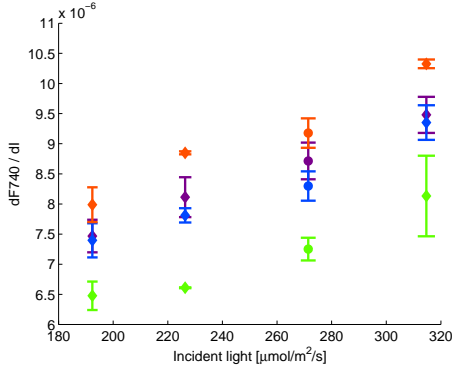


Figure 4: Derivative  $F740$  vs incident light at four operating points with dominating blue background light (B:R 3:1).

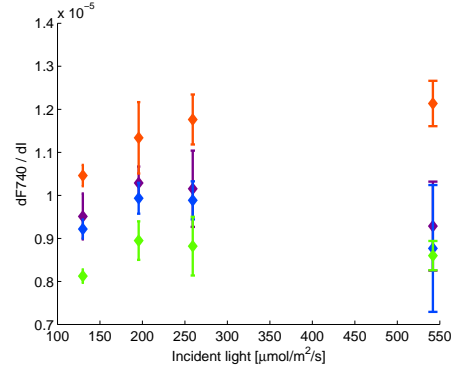


Figure 5: Derivative  $F740$  vs incident light at four operating points with dominating red background light (B:R 1:3).

### 3 Final conclusions

Under present conditions photosynthetic rate and fluorescence 740 correlates well, and therefore, it seems reasonable to use  $F740$  as a control parameter to find optimal spectrum for plant growth. The results indicate that the optimal spectrum with respect to short term photosynthetic growth (not taking efficiency of diodes into consideration) has less blue light than B:R 1:3. If using the control strategy suggested here, it is likely that some boundary conditions are needed (for example maximum and minimum B:R ratio) to ensure long term healthy plants.

## References

- [ASTM, 2012] ASTM (2012). Standard tables for reference solar spectral irradiances: Direct normal and hemispherical on 37° tilted surface. [http://enterprise.astm.org/filtrexx40.cgi?+REDLINE\\_PAGES/G173.htm](http://enterprise.astm.org/filtrexx40.cgi?+REDLINE_PAGES/G173.htm).
- [Flexas et al., 2002] Flexas, J., Escalonaa, J. M., Evainb, S., Gulíasa, J., Moyaa, I., Osmond, C. B., and Medranoa, H. (2002). Steady-state chlorophyll fluorescence (Fs) measurements as a tool to follow variations of net CO<sub>2</sub> assimilation and stomatal conductance during water-stress in C<sub>3</sub> plants. *Physiologia Plantarum*, 114:231–240.
- [Guantera et al., 2014] Guantera, L., Zhanga, Y., Jungb, M., Joinerc, J., Voigta, M., Berryd, J. A., Frankenberge, C., Huetef, A. R., Zarco-Tejadag, P., Leeh, J.-E. M., Morani, S., Guillermo Ponce-Camposi, Christian Beerj, G. C.-V. N. B. D. G. K. K., Cescattio, A., Bakerp, J. M., and Griffisq, T. J. (2014). Global and time-resolved monitoring of crop photosynthesis with chlorophyll fluorescence. *Proceedings of the National Academy of Sciences*, pages 1327–1333.
- [Hernández and Kubota, 2012] Hernández, R. and Kubota, C. (2012). Tomato seedling growth and morphological responses to supplemental led lighting red:blue ratios under varied daily solar light integrals. *Acta Horticulturae*, 956:187–194.
- [Hernández and Kubota, 2014] Hernández, R. and Kubota, C. (2014). Growth and morphological response of cucumber seedlings to supplemental red and blue photon flux ratios under varied solar daily light integrals. *Scientia Horticulturae*, 173:92–99.

Abstract for 19th Nordic Process Control Workshop (NPCW)

## Dynamic Effects of Diabatization in Distillation Columns

Thomas Bisgaard, Jakob K. Huusom, Jens Abildskov ([ja@kt.dtu.dk](mailto:ja@kt.dtu.dk))

CAPEC-PROCESS, Technical University of Denmark, Soltofts Plads Bld. 229, DK-2800 Kgs. Lyngby, Denmark

**Keywords:** dynamic simulation, hidic, distillation

**Preferred type of presentation:** Oral

In diabatic distillation, heat transfer occurs on one or several stages in contrast to adiabatic (conventional) distillation, where the column is considered to be insulated. The heat-integrated distillation column (HIDiC) is an example of a diabatic distillation column. Herein, gradual condensation occurs along the rectifying section and gradual boil-up occurs along the stripping section as heat is exchanged between the sections. This is realized by operating the rectifying section at a higher pressure by introducing a compressor above the feed stage.

Various studies concern benchmarking of the HIDiC against conventional and heat-pump assisted distillation columns. Yet the overall conclusions are contradictory due to numerical and model dissimilarities and different basis of comparisons. This issue has also been addressed by others<sup>1,2,3,4</sup>: It appears that the economic advantage of any configuration is a complex function of mixture identity, whereas correlations between optimality and relative volatility have been shown for ideal mixtures. Furthermore, several studies have already proven the operability of the HIDiC by simulation<sup>5,6</sup> and experimentally in bench-scale experiments<sup>7</sup>, but more work has to be done for real industrial applications. However, a truly feasible optimal, heat-integrated configuration is a trade-off between economical and operational<sup>8</sup> concerns.

Based on a previously developed model framework<sup>9</sup>, the trade-off in diabatization between operability and various performance indicators including total annualised cost is investigated, by gradually converting a conventional distillation column into a HIDiC. A near-optimum feasible HIDiC design is obtained by a knowledge-based design algorithm currently under development. The trade-off evaluation is carried out in terms of open-loop responses, dynamic relative gain array matrices, and dynamic condition numbers.

In addition, simulations using a simple model with linearized tray hydraulics and the constant molar overflow assumption, are compared with the proposed (more) rigorous model.

---

<sup>1</sup> Harwardt A, Marquardt W. (2012), *AIChE Journal* 58(12):3740-3750

<sup>2</sup> Shenvi AA, Herron DM, Agrawal R (2011), *Ind Eng Chem Res* 50(1):119-130

<sup>3</sup> Suphanit B (2011), *Energy* 36(7): 4171-4181

<sup>4</sup> Gutiérrez-Guerra R, Murrieta-Dueñas R, Cortez-González J, Segovia-Hernández JG, Hernández S, Hernández-Aguirre A (2014), *Distillation Absorption 2014*: 655-660.

<sup>5</sup> Huang K, Wang S, Iwakabe K, Shan L, Zhu Q (2007), *Chem Eng Sci* 62(22):6486-6491.

<sup>6</sup> T. Ho, C. Huang, J. Lin, L. Lee (2009), *Comput Chem Eng* 33(6):1187-1201.

<sup>7</sup> Naito K, Nakaiwa M, Huang K, Endo A, Aso K, Nakanishi T, Nakamura T, Noda H, Takamatsu T (2000), *Comput Chem Eng* 24(2-7): 495-499.

<sup>8</sup> Miyazaki A, Alcántra-Avila JR, Sotowa K-I, Horikawa T, *ADCONP 2014*: 426-431

<sup>9</sup> Bisgaard T, Huusom JK, Abildskov J (2013), *NPCW18*

# Fault propagation analysis by merging process causality and plant topology

R. Landman. J. Kortela. S.-L. Jämsä-Jounela

*Aalto University, School of Chemical Technology, Process Control and Automation  
Research Group, P.O Box 16100, 00076 Finland (Tel: 358-(0)50-4382296; e-mail:  
rinat.landman@aalto.fi)*

---

## Abstract

Disturbances in large-scale industrial systems can easily propagate through the process units and thereby adversely affect the overall process performance. Identifying the propagation paths of disturbances can expedite the process recovery and disclose the process units of concern which should be closely monitored. This paper presents a technique for integrating process causality and topology which can ultimately determine the propagation path of disturbances using a dedicated search algorithm. The algorithm validates the quantitative results of the causal analysis using the connectivity matrix which contains the information on the plant topology in a form of a binary matrix. The algorithm has two functionalities: finding feasible propagation paths between two elements and determining whether each path which was found is direct or indirect. The outcome is an enhanced causal model which depicts the propagation path. The underlying aim is to implement the analysis soon after a fault is detected and provide a display of the propagation path so that the proper maintenance can be undertaken before the product quality is severely deteriorated. The analysis is demonstrated on an industrial paperboard machine with multiple oscillations in its drying section due to valve stiction. First the connectivity matrix is extracted from a Piping & Instrumentation Diagram (P&ID) diagram, then, the causal analysis is presented followed by demonstration of the search algorithm. We applied the Granger causality (GC) method to obtain the initial causality matrix while the connectivity matrix was captured from an AutoCAD P&ID as an XML schema. Finally, the causal model illustrating the propagation path is given and the results are evaluated.

*Keywords:* plant topology, causal analysis, control loops

---

## 1. Introduction

In large-scale chemical processes, disturbances can easily propagate through the process units and thereby adversely affect the overall process performance. In particular, oscillations in control loops are very common in industrial processes and lead to poor control performance, low product quality and excessive energy consumption [16]. In large-scale systems with a high degree of connectivity, it is a difficult task to determine the most probable propagation path. In recent years, capturing causality between different process variables has become a vital tool in the diagnosis of faulty systems due to its ability to identify the propagation path of disturbances [14].

Causality can be captured from process knowledge and/or process data. Models which are based on the physical layout of the process are typically referred to as topology-based models or process connectivity models [2]. Several techniques for extracting plant connectivity information from piping and instrumentation diagrams (P&IDs) have been developed in recent years [15, 12, 13]. On the other hand, data-driven causal analysis utilizes historical process data in the form of time series and measures to what extent the time series corresponding to specific variables influence each other.

The main difficulty in data-driven causal analysis is in establishing the statistical significance of the results, hereby eliminating redundant links from the causal model. Consequently, several attempts have been made in recent years to combine data-driven causal analysis with topology-based models [13, 14]. However, in cases where the system has a high degree of connectivity among the process units, finding feasible propagation paths among the process components might not be sufficient to capture precisely the causal topology.

The present study was designed to identify the propagation path of oscillations in control loops by utilizing a dedicated search algorithm which validates each entry in the causality matrix obtained from the data-driven analysis using the connectivity matrix extracted from the P&ID. The search algorithm has two main functionalities: finding feasible propagation paths between two control elements and determining whether a path is direct or indirect. The outcome is a refined causality matrix which contains the structural information of the propagation path. The efficiency of the analysis is successfully demonstrated on an industrial board machine utilizing the Granger causality (GC) while the connectivity matrix was captured from an AutoCAD P&ID as an XML schema.

This paper is organized as follows. Section 2 describes how to generate a topology-based model. Section 3 presents the fault propagation analysis including the data-driven analysis and the search algorithm. Section 4 describes the process case study and the results of the fault propagation analysis. The paper ends with concluding remarks in Section 5.

## **2. Generation of topology based models**

There are two types of topology-based models: causal digraph and connectivity matrix which can be considered as a graphical and a numerical representation of the process schematics, respectively. The digraph reflects physical or signal flows between the equipment and instruments based on the physical layout of the components it represents. Similarly to the digraph, the connectivity matrix indicates the relationships between process components in the form of a binary matrix whose elements are assigned according to the existence of a directional connection from the row header component to the column header component [11, 13].

In this study, topology data was extracted from an electronic P&ID which is drawn by the specialized Autodesk AutoCAD P&ID drafting application that has been developed based on Autodesk AutoCAD. In the developed application, the topology data is exported in the format of ISO 15926-compliant XML scheme XMpLant [8].

The automated generation of topology information includes the following tasks. First, the schematic information on the initial component and the terminal component of every line segment, such as pipes and control signals is included in the drawing. Secondly, this information is attained through the database object of the drawing which includes all the topology information, namely, the names of the process components, the coordinates of the components and the connections among them. Finally, this data is further processed by MATLAB program and converted into connectivity information which includes the tags, coordinates, and the connectivity between process components [11].

## **3. Fault propagation analysis**

This section first provides an overview on the Granger causality method and then proceeds by describing the search algorithm which is utilized in order to combine the connectivity information with the results of the causal analysis.

### 3.1. Granger causality

Granger causality has received great attention in many areas due to its ease of implementation and efficiency when investigating causal relationships [9, 16]. Moreover, the method has been extended to multivariate (MV) time series analysis [3] which makes it highly beneficial when investigating large-scale systems.

The basic notion of the GC is that if one time series affects another series, then the knowledge of the former series should help to predict the future values of the latter one [5]. To illustrate the concept of the method, consider two time series  $X_1(t)$  and  $X_2(t)$  and their corresponding autoregressive (AR) model:

$$\begin{aligned} X_1(t) &= \sum_{j=1}^p A_{11,j} X_1(t-j) + \sum_{j=1}^p A_{12,j} X_2(t-j) + \epsilon_1(t) \\ X_2(t) &= \sum_{j=1}^p A_{21,j} X_1(t-j) + \sum_{j=1}^p A_{22,j} X_2(t-j) + \epsilon_2(t) \end{aligned} \quad (1)$$

where  $p$  is the model order and  $\epsilon_1, \epsilon_2$  are the residuals for each series. (1) is typically referred to as the *unrestricted model* [1]. The GC from  $X_2$  to  $X_1$  is defined as:

$$F_{x_2 \rightarrow x_1} = \ln \left[ \frac{\text{var}(\epsilon'_1)}{\text{var}(\epsilon_1)} \right] \quad (2)$$

where  $\epsilon'_1$  is obtained from (1) by omitting all  $A_{12}$  coefficients for all  $j$  [10]. The model after omitting all  $A_{12}$  coefficients is typically referred to as the *restricted model* [1]. The statistical significance of the GC can be determined via the  $F$ -statistic test [6] :

$$F = \frac{RSS_r - RSS_{ur}}{RSS_{ur}} \times \frac{T - 2p - 1}{p} \quad (3)$$

where  $RSS_r$  and  $RSS_{ur}$  are the residual sum of squares of the *restricted* and *unrestricted* models respectively and  $T$  is the total number of observations. For MV processes, the MV (conditional) GC [7], which is based on the expansion of a univariate Auto Regressive (AR) model to a Multivariate Auto Regressive (MAR) model to include all measured variables can be used. The method requires that the time series are stochastic and wide sense stationary (WSS). Otherwise, the AR model can produce spurious results [4].

### 3.2. Refinement of the causality matrix

The refinement of the causality matrix is based on the process connectivity information. The aim of this operation is to eliminate all the values in the causality matrix which do not represent direct causal interactions. The realization of the refinement procedure of  $n \times n$  causality matrix  $X$  is obtained according to the following implementation:

- In matrix  $X$ , select the next non-zero  $(i,j)^{\text{th}}$  element that has not been tested.
- Check if there is a direct physical path from controller  $(i)$  to controller  $(j)$  using the search algorithm.
- If there is no direct path from controller  $(i)$  to  $(j)$ , set  $X(i,j)$  to zero.

Note that we define a direct path from controller  $(i)$  to controller  $(j)$  if it does not transverse any other controller other than  $(j)$ . The search algorithm first finds if a physical path between two control elements exists. It is performed using a generic algorithm which is based on a graph traversal which searches a series of nodes, ensuring that each node is only traversed once [13]. Once a physical path between the 'cause' variable and the 'effect' variable is found, an additional unique algorithm is employed to find if it is direct or not. The algorithm checks the type of each element in each physical path that had been found in the previous step. If it finds a control element (i.e., valve, controller or sensor) which belongs to a control loop that is neither the 'cause' nor the 'effect', the corresponding path is considered as indirect. Otherwise, if the component belongs to the 'effect' control loop, the path is considered as direct.

## 4. Process case study

In this section, we first provide the process description. Next, spectral analysis is applied to identify the variables associated with the fault. Finally, the fault propagation analysis is applied to obtain the causal model depicting the propagation path.

#### 4.1. Process description

The process case study is a large-scale board machine (BM) which produces a three-layer liquid packaging boards and board cups. The analysis is focused on the drying section of the BM where the remains of excess water in the web are evaporated to achieve the desirable moisture content in the board using steam-filled drying cylinders. The condensing steam in the cylinders releases latent heat which is used to evaporate the bound water in the web. The condensate from the cylinders is collected by siphons to condensate tanks where steam and condensate are separated. Steam is then delivered back to the process and condensate is returned to a power plant. A scheme of the drying section and its control loops can be seen in Fig 1. The cylinders in the drying section are divided into six steam groups (SG). Each SG and its corresponding condensate tank (CT) form a single drying group (DG). Each DG has its own controllers to control the steam pressure, the steam pressure difference between steam and condensate headers and the level of the condensate. The pressure controllers (PCs) are used to control steam pressure in each SG using 5 and/or 10 bar pressurized steam headers (denoted as the red arrows at the top of Fig. 1. The pressure difference control between the steam headers and the condensate tanks is achieved by manipulating the control valves in the steam outlet of the condensate tanks (CTs) using pressure difference controllers. The level of the condensate tanks is controlled by regulating their outlet flow valves using level controllers (LCs). The present case study entails a valve stiction in the pressure controller PC1652 and its effect on the interacting loops of the drying section of the board machine. The stiction diagnosis is based on the long-term maintenance records of the plant.

The power spectra of the series were examined in order to detect measurements with similar dynamic behavior. The power spectra of the controlled variables (*PVs*) are shown in Fig. 2 where the measurement of PC1652 is colored in red. The loops oscillating at a common frequency are: PC668, PC1653, PC651, PC652, PC653, PC670, LC652, PC1652, PC671, LC653, PC672 and PC673. Thus, the disturbance is mainly affecting SG1, SG2 and SG3.

#### 4.2. The results of the GC analysis

The GC method was applied by evaluating the influences of the controllers outputs (*OPs*) on the process controlled variables (*PVs*) and included only the control loops which were found to be oscillating at the same frequency

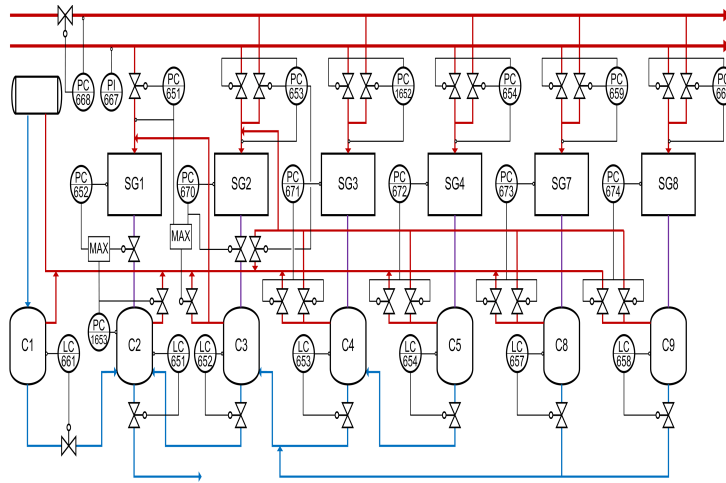


Figure 1: The drying section of a board machine

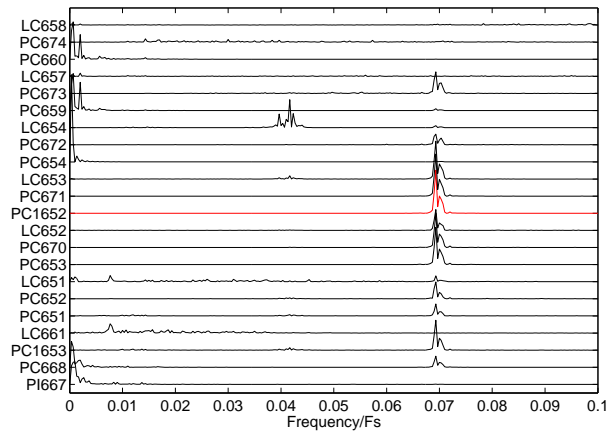


Figure 2: The power spectra of the time series

based on the spectral analysis. The time domain MV (conditional) GC analysis was applied according to [7]. The MAR model estimation was performed using the least squares method and model order was chosen based on the AIC criteria ( $p=10$ ). The statistical significance was determined via the F-statistic test [5] and the results were corrected using the Bonferroni correction for multiple comparisons with a p-value of 0.01 [10]. The initial causality matrix is shown in Fig.3.

	PC1653	PC651	PC652	PC653	PC670	LC652	PC1652	PC671	LC653	PC673
PC1653	-	0	0.072	0	0	0	0	0	0.028	0
PC651	0.039	-	0.056	0	0	0	0	0	0	0
PC652	0.065	0.016	-	0	0	0	0	0	0	0
PC653	0.014	0.019	0.017	-	0.017	0	0.024	0.018	0	0
PC670	0.018	0.029	0.031	0	-	0	0.018	0	0	0
LC652	0	0	0	0	0	-	0	0	0	0
PC1652	0.024	0.013	0	0.016	0.018	0	-	0.113	0.044	0.032
PC671	0	0	0	0.016	0.029	0	0.144	-	0.074	0.031
LC653	0.105	0.013	0.014	0.015	0	0.068	0.019	0.021	-	0.012
PC673	0	0	0	0	0	0	0	0	0	-

Figure 3: The initial causality matrix

#### 4.3. The refined causality matrix and the causal model

The refined causality matrix is shown in Fig. 4. All the GC values which correspond to non-direct interactions based on the process connectivity have been set to zero. The causal model based on the refined causality matrix is shown in Fig. 5. The search algorithm was able to eliminate most of the redundant results from the GC analysis, however the model was still assumed to have few redundant arcs (denoted by the dashed arcs in Fig. 5 and the highlighted values in Fig. 4) based on process knowledge. Those types of ambiguous results are sometimes inevitable and in-depth process knowledge is needed to detect them. Nonetheless, the search algorithm was able to eliminate approximately 88% of the spurious results obtained from the GC analysis, herewith affirming the efficacy of the refinement procedure.

	PC1653	PC651	PC652	PC653	PC670	LC652	PC1652	PC671	LC653	PC673
PC1653	-	0	0	0	0	0	0	0	0	0
PC651	0	-	0.056	0	0	0	0	0	0	0
PC652	0.065	0.016	0	0	0	0	0	0	0	0
PC653	0	0	0	-	0.017	0	0	0	0	0
PC670	0	0.029	0.031	0	-	0	0	0	0	0
LC652	0	0	0	0	0	-	0	0	0	0
PC1652	0	0	0	0	0	0	-	0.113	0.044	0
PC671	0	0	0	0.016	0.029	0	0.144	-	0.074	0
LC653	0	0.013	0.014	0	0	0.068	0	0	-	0
PC673	0	0	0	0	0	0	0	0	0	-

Figure 4: The refined causality matrix

## 5. Summary and Conclusions

This paper introduced a fault propagation analysis by the virtue of the automatic consolidation of data-driven causal analysis with topology-based model using a dedicated search algorithm. This combination results in an

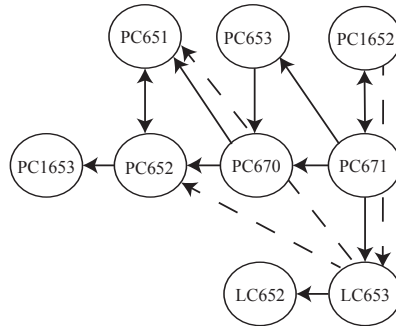


Figure 5: The causal model based on the refined causality matrix

enhanced causal model due to the ability of the search algorithm to eliminate indirect interactions from the causality matrix. Yet, several redundant links remained in the causal model in spite of the refinement procedure, thus, process expert knowledge was essential in eliminating those. Alternatively, numerous data-driven methods can be employed in order to construct the causality matrix prior to the refinement procedure, particularly, in cases where the system is with a high degree of connectivity among variables. In the future, the proposed fault propagation analysis can be used to study how different types of faults propagate in a system and accordingly select the critical variables for monitoring.

## References

- [1] Bressler, S. L., & Seth, A. K. (2010). Wiener-granger causality: A well established methodology. *NeuroImage*, 58, 323–329. doi:10.1016/j.neuroimage.2010.02.059.
- [2] Di Geronimo Gil, G. J., Alabi, D. B., Lyun, O. E., & Thornhill, N. F. (2011). Merging process models and plant topology. In *The 2011 4th International Symposium on Advanced Control of Industrial Processes* (pp. 15–21). Thousand Islands Lake, Hangzhou, China: IEEE.
- [3] Geweke, J. (1982). Measurement of linear dependence and feedback between multiple time series. *Journal of The American Statistical Association*, 77, 304–313.
- [4] Granger, C., & Newbold, P. (1974). Spurious regression in econometrics. *Journal of Econometrics*, 2, 111–120.

- [5] Granger, C. W. J. (1969). Investigating causal relations by econometric models and cross-spectral methods. *Econometrica*, *37*, 424–438.
- [6] Greene, W. H. (2002). *Econometric Analysis*. (5th ed.). Upper Saddle River, NJ, USA: Prentice-Hall.
- [7] Guo, S., Seth, A. K., Kendrick, K., Zhou, C., & Feng, J. (2008). Partial granger causality : eliminating exogenous inputs and latent variables. *Journal of Neuroscience Methods*, *172*, 79–93.
- [8] Noumenon (2008). Ximplant overview. URL: <http://www.noumenon.org.uk/background.html>.
- [9] Seth, A. K. (2005). Causal connectivity of evolved neural networks during behavior. *Network:Computation in Neural Systems*, *16*, 35–54.
- [10] Seth, A. K. (2010). A matlab toolbox for granger causal connectivity analysis. *Journal of Neuroscience Methods*, *186*, 262–273.
- [11] Sun, Q. (2013). *Generation of process topology-based causal models*. Msc thesis Espoo, Finland.
- [12] Thambirajah, J., Benabbas, L., Bauer, M., & Thornhill, N. F. (2007). Cause and effect analysis in chemical processes utilizing plant connectivity information. In *The IEEE Advanced Process Control Applications for Industry Workshop* (pp. 1–6). Vancouver, Canada.
- [13] Thambirajah, J., Benabbas, L., Bauer, M., & Thornhill, N. F. (2009). Cause-and-effect analysis in chemical processes utilizing xml, plant connectivity and quantitative process history. *Computers and Chemical Engineering*, *33*, 503–512.
- [14] Yang, F., Shah, S. L., & Xiao, D. (2012). Signed directed graph based modeling and its validation from process knowledge and process data. *International Journal of Applied Mathematis and Computr Science*, *22*, 387–392.
- [15] Yim, S., Ananthakumar, H., Benabbas, L., Horch, A., Drath, R., & Thornhill, N. F. (2006). Using process topology in plant-wide control loop performance assessment. *Computers and Chemical Engineering*, *31*, 86–99.

- [16] Yuan, T., & Qin, S. J. (2013). Root cause diagnosis of plant-wide oscillations using granger causality. In *The 8th IFAC Symposium on Advanced Control of Chemical Processes* (pp. 160–165). Singapore: The international Federation of Automatic Control.

# Relative Gain Array Estimation Based on Non-parametric Process Identification for Uncertain Systems

Ali M. H. Kadhim\*, Wolfgang Birk and Thomas Gustafsson

Control Engineering Group, Luleå University of Technology, Luleå, Sweden  
(e-mail: {ali.kadhim, wolfgang.birk, tgu}@ltu.se).

\*Corresponding author.

**Abstract:** Since the introduction of the Relative Gain Array (RGA) by Bristol in 1966, it has become a widely used practical tool for solving the input-output pairing problems in decentralized control. In order to remove the dependency of this tool on a parametric description and accurate knowledge of a nominal model, this work proposes a method to estimate the RGA directly from a non-parametric frequency response matrix (FRM) derived from a frequency domain system identification approach. The proposed method reduces the influence of model uncertainties on the calculation of the RGA and derives the RGA at frequencies of interest. The results are exemplified using a  $2 \times 3$  LTI systems and a  $2 \times 2$  uncertain system.

## 1. INTRODUCTION

The RGA is calculated using the frequency response of a process model, which is usually obtained from either first principles or parametric identification algorithms. In both cases, the choice of the model structure and model order has a great influence on the quality of process representation and consequently on the RGA results as in Chen [2002]. In Kadhim [2014], a non parametric frequency response identification using a random excitation was used to estimate the RGA results from the input-output measurements directly. Since this approach does not depend on neither choosing model structure nor order their influence on RGA calculation will be reduced. The main points in Kadhim [2014] are briefly introduced in the next section with an example. A step forward to what has been given in Kadhim [2014], an example to uncertain  $2 \times 2$  system is investigated. At the end a conclusion and ongoing work is presented.

## 2. FRM AND RGA ESTIMATION USING RANDOM EXCITATION

The simplicity of generating noise excitation makes this excitation type very popular in system identification. However, as it is not a periodic signal, the identification results suffer from leakage. A typical solution to this problem is to divide the data into  $M$  blocks which are averaged.

So, for a general  $m \times n$  system,

$$\mathbf{G}(k) = \begin{bmatrix} G_{11}(k) & \cdots & G_{1n}(k) \\ \vdots & \ddots & \vdots \\ G_{m1}(k) & \cdots & G_{mn}(k) \end{bmatrix}$$

the non parametric measurement of transfer function at frequency  $k$  (FRM) excited by noise is given by Schoukens [2012]:

$$\hat{\mathbf{G}}(k) = \frac{\hat{S}_{YU}(k)}{\hat{S}_{UU}(k)} \quad (1)$$

where  $\hat{S}_{YU}$  and  $\hat{S}_{UU}$  are the cross- and auto power spectrum respectively and are given by:

$$\hat{S}_{YU}(k) = \frac{1}{M} \sum_{s=1}^M \begin{bmatrix} Y^{[1,s]}(k) \\ \vdots \\ Y^{[m,s]}(k) \end{bmatrix} \begin{bmatrix} \bar{U}^{[1,s]}(k) & \cdots & \bar{U}^{[n,s]}(k) \end{bmatrix} \quad (2)$$

and

$$\hat{S}_{UU}(k) = \frac{1}{M} \sum_{s=1}^M \begin{bmatrix} U^{[1,s]}(k) \\ \vdots \\ U^{[n,s]}(k) \end{bmatrix} \begin{bmatrix} \bar{U}^{[1,s]}(k) & \cdots & \bar{U}^{[n,s]}(k) \end{bmatrix} \quad (3)$$

where  $X^{[p,q]}(k)$  is the Discrete Fourier Transform of the  $p^{\text{th}}$  input or output of block  $q$  at frequency  $k$ .

Once  $\hat{\mathbf{G}}(k)$  is found, then the RGA can be easily estimated using:

$$\hat{\Lambda}(k) = \begin{bmatrix} \hat{\lambda}_{11}(k) & \cdots & \hat{\lambda}_{1n}(k) \\ \vdots & \ddots & \vdots \\ \hat{\lambda}_{m1}(k) & \cdots & \hat{\lambda}_{mn}(k) \end{bmatrix} = \hat{\mathbf{G}}(k) \otimes \hat{\mathbf{G}}(k)^{-T} \quad (4)$$

where  $\otimes$  denotes the element-by-element product and  $-T$  is the inverse transpose.

The mean and the variance of the  $\hat{\Lambda}(k)$  are calculated over repeating the (1)-(4) for several trials.

*Example 1 ( $2 \times 3$  system):*

Consider the distillation column process given in Glad [2000]:

$$\begin{bmatrix} y_1 \\ y_2 \end{bmatrix} = \begin{bmatrix} 4.05e^{-27s} & 1.77e^{-28s} & 5.88e^{-27s} \\ 50s+1 & 60s+1 & 50s+1 \\ 5.39e^{-18s} & 5.72e^{-14s} & 6.9e^{-15s} \end{bmatrix} \begin{bmatrix} u_1 \\ u_2 \\ u_3 \end{bmatrix} + \begin{bmatrix} 1.44e^{-27s} \\ 40s+1 \\ 1.83e^{-15s} \\ 20s+1 \end{bmatrix} d$$

For  $M = 150$  and 100 trials, the exact  $\Lambda$ , the mean of  $\hat{\Lambda}$ , and  $\pm\sigma_{\Lambda}$  bounds for  $SNR = 10$  are depicted in Fig. 1

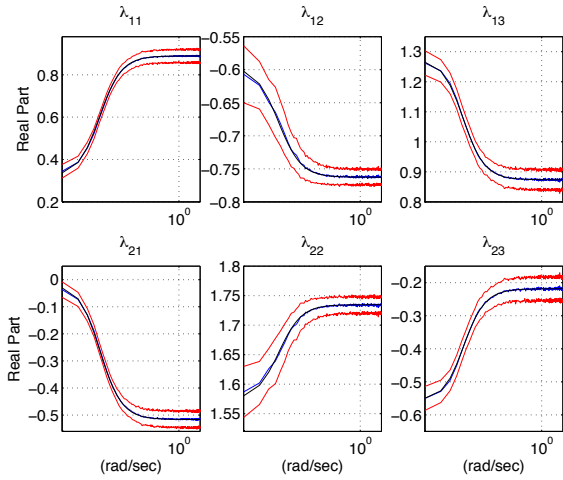


Fig. 1.  $\Lambda$  results. Black: Exact  $\Lambda$ . Blue: Mean of  $\hat{\Lambda}$ . Red:  $\pm\sigma_{\Lambda}$  bounds.

Fig. 1 shows that the mean of  $\hat{\Lambda}$  coincides well with the exact  $\Lambda$ . The pairing selection of  $y_1 - u_3$  and  $y_2 - u_2$  in Glad [2000] is confirmed by taking into consideration the bound of  $\pm\sigma_{\Lambda}$ .

*Example 2 ( $2 \times 2$  uncertain system):*

Consider the quadruple tanks process given in Johansson [2000]:

$$\mathbf{G}(s) = \begin{bmatrix} \frac{3.807\gamma_1}{23.32s+1} & \frac{1.142}{(23.32s+1)(6.99s+1)} \\ \frac{2.379(1-\gamma_1)k_2}{(23.32s+1)(6.99s+1)} & \frac{1.665k_2}{23.321s+1} \end{bmatrix}$$

where

$$\gamma_1 = 0.7 + 0.1 |\delta_\gamma|, \quad |\delta_\gamma| \leq 1 \quad \text{and} \quad k_2 = 1.6 + 0.5 |\delta_k|, \quad |\delta_k| \leq 1$$

To capture the system dynamics, 30 input-output data sets are measured, each with  $M = 50$ . The nominal  $\Lambda$ , the mean of  $\hat{\Lambda}$ , and  $\pm\sigma_{\Lambda}$  bounds are depicted in Fig. 2

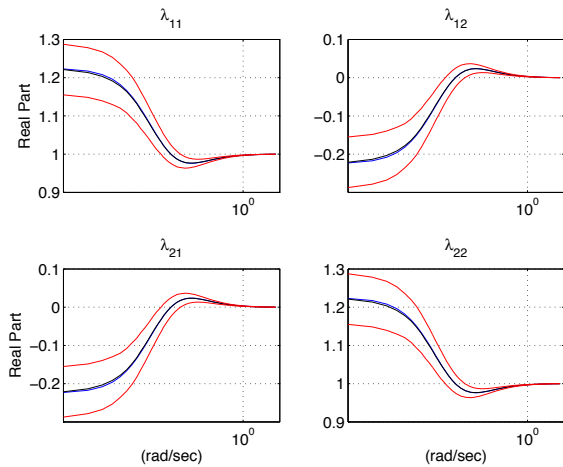


Fig. 2.  $\Lambda$  results. Black: Nominal  $\Lambda$ . Blue: Mean of  $\hat{\Lambda}$ . Red:  $\pm\sigma_{\Lambda}$  bounds.

Fig. 2 shows that the mean of  $\hat{\Lambda}$  coincides well with the nominal  $\Lambda$  even when measurement sets and  $M$  have been reduced. Taking  $\pm\sigma_{\Lambda}$  bounds into account, diagonal pairing is suggested safely for this system.

### 3. CONCLUSION AND ONGOING WORK

Considering the systems as black boxes in a non-parametric identification gives an easy and rather accurate insight to the RGA pairing decision. Choosing a model structure and order is not needed in this method which would reduce their influence on the RGA results. A drawback of using noise excitation is that the results will suffer a leakage. Taking a multi-sine excitation as well as systems structure into consideration is intended in an ongoing work.

### REFERENCES

- Chen, Dan, and Dale E. Seborg. "Relative gain array analysis for uncertain process models." *AICHE journal* 48.2 (2002): 302-310.
- Kadhim, Ali, Wolfgang Birk, and Thomas Gustafsson. "Relative Gain Array Estimation Based on Non Parametric Frequency Domain System Identification." In *Proceedings of 2014 IEEE Multi-Conference on Systems and Control*, Antibes, France .
- Schoukens, Johan, Rik Pintelon, and Yves Rolain. "Mastering system identification in 100 exercises." John Wiley and Sons, 2012.
- Glad, Torkel, and Lennart Ljung. "Control theory." CRC press, 2000.
- Johansson, Karl. "The Quadruple Tank Process: A Multivariable Laboratory Process with an Adjustable Zero." *IEEE Transactions On Control Systems Technology*, Vol.8, NO.3, 2000.
- Hägg, Per. "On Structure System Identification and Nonparametric Frequency Response Estimation." *Doctoral Thesis in Automatic Control*, KTH, Stockholm, 2014.

# Convex optimization as a design tool for feedforward controllers

*Martin Hast, Tore Hägglund*

*Department of Automatic Control, Lund University, Box 118 SE-22100, Lund, Sweden (e-mail: martin.hast@control.lth.se).*

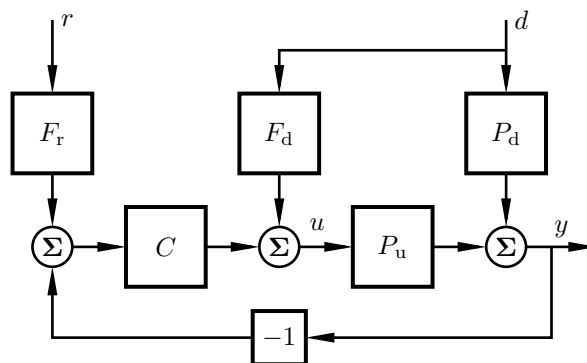
Feedforward control action, either from the reference or a measurable disturbance, can greatly increase the performance in a control structure. By augmenting a control structure with feedforward controllers, the feedback controller can be tuned focusing on robustness and attenuation of unmeasurable disturbances.

In this work we propose a structure of the feedforward controllers that enables designing the controller by solving a convex optimization problem. A number of easy-to-use tools have emerged that makes the procedure of formulating and solving the problems straight-forward. The feedforward controllers consist of two parts, a fixed prefilter and an appropriate number of numerator coefficients or zeros. From this it follows that all the relevant transfer functions and time responses, such as the error, control signal and even the control signal derivative are affinely dependent on the numerator coefficients.

Using the coefficients as optimization variables an optimization problem can be formulated. By sampling the functions and responses the semi-finite optimization problem can be put on a numerically tractable form. With the proposed controller structure many of the commonly used performance measures and constraints are easily formulated using convex functions of the sampled quantities since the functions and responses are affine in the optimization variables. Any convex function of them can therefore be used as either cost function or constraints in the optimization problem. This means for instance, that for a specific reference trajectory or disturbance, bounds on the control signal and/or control signal derivative can be introduced. Also, the error signal can be constrained to a specified envelope.

The convex optimization problems arising when using this method can be solved fast, often in matter of seconds. This can be utilized to design a number of controllers using different prefilters in order to find the best one.

The method has been illustrated in several examples. These examples covers both different aspects of how an appropriate cost function and constraints can be chosen and used, and how the prefilters can be designed to obtain a good feedforward controller.



# Autotuning Based on Asymmetric Relay <sup>★</sup>

Josefin Berner, Karl Johan Åström, Tore Hägglund

*Department of Automatic Control, Lund University, Lund,  
Sweden (e-mail: josefin.berner@control.lth.se)*

---

**Abstract:** The relay autotuner has been widely used since its introduction in the 1980's. Its functionality is based on the idea of finding the process dynamics from a relay oscillation and determining the parameters of a PID controller using simple tuning rules. The main advantages of the relay method is that it does not need any a priori information, it keeps the experiment time short and does not disturb the process much, and it automatically gives you information in the interesting frequency interval close to the critical frequency where the phase is  $-180^\circ$ .

Some modifications of the original autotuner are proposed in this work. One is that we want to find a low-order model from the relay experiment instead of a single point on the Nyquist curve, which was what you got from the original version. Another change is that we use a relay with asymmetric amplitudes. This has the benefit of better excitation and enables us to find the static gain of the process. A third change is that we want to use the normalized time delay as a parameter for the decision-making in the autotuner algorithm.

In this work we show that the normalized time delay can be easily determined from an asymmetric relay experiment since there is a relation between the normalized time delay and the time intervals between switches of the relay. An equation describing this relation that also depends on the ratio between the relay amplitudes is tested and verified on a test batch consisting of more than 100 process models that are common in process industry.

Once the normalized time delay is known decisions on how to continue can be made. It has previously been shown that derivative action is mainly beneficial if the normalized time delay is small. It has also been shown before that a first order model with time delay is usually a sufficient process description if the normalized time delay is large, while higher order models can improve the results for processes with lower values of the normalized time delay. If the normalized time delay is close to zero the process can be modeled as an integrating process. The information on what model structure and which controller type that should be used is relevant to the continuation of the autotuning procedure.

In this work we describe how a first order time delayed model, as well as an integrating model with time delay can be obtained from the asymmetric relay experiment. In a simple version of the autotuner you could also find a second order time delayed model with equal time constants for the case of intermediate values of the normalized time delay. If you want a higher order model with more parameters a more advanced version of the autotuner will provide you with the possibility to make an additional experiment in order to get better excitation of your process. When the model is obtained an appropriate tuning method is used to find the PI or PID controller parameters.

*Keywords:* Autotuning, asymmetric relay, normalized time delay, low-order modeling.

---

---

<sup>★</sup> The authors are members of the LCCC Linnaeus Center and the ELLIIT Excellence Center at Lund University.

# A reduced observer design for a freezing process in plate freezers

Christoph Josef Backi\* Jan Tommy Gravdahl\*

\* *Department of Engineering Cybernetics, Norwegian University of Science and Technology, O.S. Bragstads plass 2D, 7034 Trondheim, Norway (e-mail: christoph.backi@itk.ntnu.no, jan.tommy.gravdahl@itk.ntnu.no)*

---

**Abstract:** In this work we present a reduced observer design for a freezing process. The model underlying the observer represents the dynamics of temperature  $T(t, x, y)$  in a block of foodstuff and is based on a partial differential equation (PDE). In the following we leave out the explicit dependency of  $T$  on  $t, x$  and  $y$ .

The PDE is the diffusion equation with temperature-dependent parameters

$$c(T)\rho(T)T_t = \left(\lambda(T)T_x\right)_x + \left(\lambda(T)T_y\right)_y,$$

where  $c(T) > 0$  denotes the specific heat capacity,  $\rho(T) > 0$  indicates the density and  $\lambda(T) > 0$  represents the thermal conductivity of the good to be frozen. We can rewrite the diffusion equation into

$$T_t = \kappa(T)\left(T_x^2 + T_y^2\right) + k(T)\left(T_{xx} + T_{yy}\right),$$

which represents a nonlinear heat equation with the two parameters

$$\kappa(T) = \frac{\lambda_T(T)}{c(T)\rho(T)} \text{ and } k(T) = \frac{\lambda(T)}{c(T)\rho(T)}.$$

In phase change problems, here in particular for freezing, the phenomenon of *thermal arrest* caused by the presence of *latent heat of fusion* has to be regarded. This means that at the freezing point  $T_F$  the temperature remains constant until the *latent heat of fusion* is removed from the good to be frozen. Only then the temperature can drop below the freezing point. Since the nonlinear heat equation does not model this phenomenon, it has to be imposed to the model. We do this by using the so called *apparent heat capacity method*, which basically overestimates the specific heat capacity  $c(T)$ . This has the effect that heat transfer in a neighbourhood around the freezing point  $T_F \pm \Delta T$  becomes very low, leading to a very slow decay in temperature as well.

In an earlier work we have designed an observer for the aforementioned nonlinear heat equation as an Extended Kalman Filter (EKF). The results showed good transient behavior and that inner-domain temperatures can be correctly estimated. However, real-time applicability could not be guaranteed.

In the present work we show that by designing a reduced observer based on an EKF the states of the process modelled by the nonlinear PDE still can be correctly estimated for the chosen set of measurements. The reduced design is obtained by defining parameters such that the nonlinear part  $\kappa(T)\left(T_x^2 + T_y^2\right)$  becomes zero for the observer model. This represents a first step towards real-time applicability, as the computational effort is reduced.

Robustness is indicated by explicitly adding white Gaussian noise to the measurement signals. In addition, the observer parameters  $\kappa(T)$  and  $k(T)$  and the region around the freezing point  $T_F \pm \Delta T$  are chosen to be double the size compared to those of the process running in parallel to the observer.

Furthermore we show that performance can be improved by introducing temperature-dependent, quasi-adaptive observer covariance matrices. These matrices, however, are not temperature-dependent over the whole temperature range, but change values after a set of measured temperatures crosses a lower bound close to the freezing point (switching).

All theoretical results are highlighted by numerical computations, where we conduct comparative studies between the earlier developed EKF based on the nonlinear PDE and the reduced observer design.

# Decoupling approach in fluidized bed combustor control

Szabó, Z. \*, Kovács, J. \*\*, Szentannai P. \*

\* *Budapest University of Technology and Economics, Department of Energy Engineering  
Budapest, Hungary*

*(e-mail: [szabo@energia.bme.hu](mailto:szabo@energia.bme.hu), [szentannai@energia.bme.hu](mailto:szentannai@energia.bme.hu)).*

\*\* *University of Oulu, System Engineering Laboratory, Oulu, Finland  
(e-mail: [jeno.kovacs@oulu.fi](mailto:jeno.kovacs@oulu.fi))*

---

**Abstract:** Basic behaviors and characteristics of the fluidized bed combustion (FBC) technique differ from those of other traditional combustion techniques. That's why some of the well proven classical combustion control methods cannot be used effectively for FBCs. In this paper an interaction between two traditional control loops was examined, the O<sub>2</sub> concentration control loop and the bed temperature control loop. The bed temperature controller regulates the fuel inlet and the O<sub>2</sub> concentration controller makes changes on the secondary air inlet. The reason of the cross-effect is that the changes in fuel inlet affect also the oxygen level, and the air inlet changes have impact also on the bed temperature. The used control method was based on independently tuned PID controllers while the cross-effect was occurred. To avert that phenomenon, a decoupling controller was designed and tested.

The tests were carried out at the System Engineering Laboratory at University of Oulu on a validated one dimensional dynamic hot-loop model developed at the Lappeenranta University of Technology (LUT) in corporation with Foster Wheeler Energia and modified at the University of Oulu. This work will provide the basics for my PhD work at University of Oulu.

*Keywords:* fluidized bed combustion, decoupling approach, bed temperature control

---

# A performance optimization algorithm in fault tolerant distributed model predictive control <sup>★</sup>

Alexey Zakharov <sup>a</sup>, Elena Zattoni <sup>b</sup>, Miao Yu <sup>a</sup>,  
Sirkka-Liisa Jämsä-Jounela <sup>a</sup>

<sup>a</sup>*Aalto University School of Chemical Technology, Department of Biotechnology and Chemical Technology, P.O. Box 16100, 00076 Aalto, Finland*

<sup>b</sup>*Department of Electrical, Electronics and Information Engineering “G. Marconi”, Alma Mater Studiorum · University of Bologna, 40136 Bologna, Italy*

---

## Abstract

This paper presents a performance optimization algorithm for controller reconfiguration in fault tolerant distributed model predictive control for large-scale systems. After the fault has been detected and diagnosed, several controller reconfigurations are proposed as candidate corrective actions for the fault compensation. The solution of a set of constrained optimization problems with different actuator and setpoint reconfigurations is derived by means of an original approach that exploits the information on the active constraints in the non-faulty subsystems, so as to split the global optimization problem into two optimization subproblems, which enables the on-line computation burden to be greatly reduced. Subsequently, the performances of different candidate controller reconfigurations are compared, and the better performing one is selected and then implemented to compensate the fault effects. Efficacy of the proposed approach has been shown by applying it to the benzene alkylation process, which is a benchmark process in distributed model predictive control.

*Key words:* Distributed model predictive control; fault tolerant control; controller reconfiguration; constrained optimization; alkylation of benzene.

---

---

<sup>★</sup> This work is supported by Academy of Finland Project under Grant No. 13138194.  
*Email addresses:* alexey.zakharov@aalto.fi (Alexey Zakharov), elena.zattoni@unibo.it (Elena Zattoni), miao.yu@aalto.fi (Miao Yu), sirkka-liisa.jamsa-jounela@aalto.fi (Sirkka-Liisa Jämsä-Jounela).

## 1 Introduction

Advanced control strategies, such as model predictive control (MPC), have made it possible to run processes close to the quality and safety limits thereby increasing profitability, whilst ensuring better end product quality and enhancing safety in plants (Qin and Badgwell, 2003). In the engineering practice, one centralized MPC usually cannot handle the whole large-scale process; instead, several MPCs may work together in a distributed manner to exchange the information of each system to achieve the control objectives. To this end, highly efficient distributed control methods have been developed over the past decades. For instance, Scheu and Marquardt (2011) have developed a distributed model predictive control (DMPC) methodology based on a distributed optimization algorithm, which relies on a coordination mechanism using the first-order sensitivities of the objective functions of neighboring systems. This proposed DMPC can effectively reduce the computation burden and overcome possible communication limitations of the centralized MPC. Several other DMPC schemes have been designed based on cooperative game theory (Maestre et al., 2011), bargaining game theory (Alvarado et al., 2011), and serial decomposition of the centralized problem (Negenborn et al., 2008). DMPCs are more and more widely applied to various control systems, such as reactor-separator processes (Liu et al., 2009), alkylation of benzene (Liu et al., 2010), accelerated cooling process test rig (Zheng et al., 2011), and transportation networks (Negenborn et al., 2008). Thus, it has become common practice to utilize DMPC strategy in the large-scale processes (Camponogara et al., 2002; Scattolini, 2009; Negenborn and Maestre, 2014).

Conventional control schemes are developed under the assumption that sensors and actuators are free from faults; however, the occurrence of faults causes degradation in the closed-loop performance and also has an impact on safety, productivity and plant economy. As a result, the research focus is shifting towards advanced management of abnormal situations, such as process disturbances and faults, which still provides great possibilities for further improvement of the process efficiency. To this end, fault tolerant control (FTC) has attracted much attention in the area of engineering practice in recent years (see, e.g., Blanke et al., 1997; Mahmoud et al., 2003; Zhang and Jiang, 2008).

Lately, fault tolerant model predictive control, which incorporates fault tolerance property into MPC, has been extensively studied (Maciejowski, 1999; Sourander et al., 2009). The corrective actions of FTC can be categorized into two types: fault accommodation and controller reconfiguration, whose difference lies in whether the controller setting will change for the compensation of fault effects. In (Kettunen et al., 2008) and in (Kettunen and Jämsä-Jounela, 2011), a data-based fault-tolerant MPC with fault accommodation was proposed and tested in a complex dearomatization process.

Despite being an attractive approach, fault accommodation is infeasible in many cases, especially when the ability to control the system degrades because of an actuator fault. As a result, an actuator reconfiguration approach was proposed aiming to replace the “dropped out” actuator using redundant ones. For example, Gani et al. (2007) developed two alternative SISO controls for a polyethylene reactor, by manipulating different actuators: the temperature of a feed flow and a catalyst flow rate. In the case of an actuator failure, the control relying on the healthy actuator was applied. Similarly, Chilin et al. (2012a) considered two actuator faults and developed two back-up controls which can be applied when the respective fault is discovered. In large-scale systems, it is difficult or impossible to develop back-up control strategies for all possible faults, that is why it is an important issue to ensure plant stability under an on-line reconfigured control, while selecting among the candidate reconfigurations. In particular, Gani et al. (2007) determined the stability regions of the alternative controls when an actuator fault occurs, and Chilin et al. (2012a) utilized a modification of MPC to ensure its stability.

As most of the FTC systems in the literature are based on a centralized MPC for the whole process, there have been only a few attempts to establish a FTC strategy based on DMPC for complex industrial systems (Gandhi and Mhaskar, 2009; Chilin et al., 2012b, 2010). In order to bridge the gap between FTC and DMPC, a framework for the design of a fault tolerant distributed model predictive control (FTDMPC) strategy is presented herein. After the fault has been detected and diagnosed, the key element of the FTDMPC is the performance optimization algorithm that provides the solution of a set of constrained optimization problems with different possible actuator and setpoint reconfigurations. The performance optimization algorithm utilizes the information on the active constraints in the non-faulty subsystems and tackles the global MPC optimization problem by splitting it into two nested sub-problems. In this way, the on-line computation burden is greatly reduced. Subsequently, the performances of the different candidate controller reconfigurations are compared, and the best performing controller is selected and then implemented to compensate the fault effects.

*Notation:* The symbols  $\mathbb{R}$ ,  $\mathbb{Z}_0^+$ , and  $\mathbb{Z}^+$  stand for the sets of real numbers, non-negative integer numbers, and positive integer numbers, respectively. Matrices and linear maps are denoted by capital letters, like  $A$  or  $\Psi$ . The transpose of  $A$  is denoted by  $A^\top$ . The Moore-Penrose inverse of  $A$  is denoted by  $A^\dagger$ . The symbol  $v = \text{vect} \{v_1, v_2, \dots, v_r\}$  denotes a vector  $v$  obtained by concatenating the vectors  $v_1, v_2, \dots, v_r$ , in order. The symbol  $M = \text{diag} \{M_1, M_2, \dots, M_s\}$  denotes a block-diagonal matrix  $M$ , whose blocks on the main diagonal are the matrices  $M_1, M_2, \dots, M_s$ , in order. The symbols  $I_n$  and  $O_{m \times n}$  stand for an  $n$ -dimensional identity matrix and an  $m \times n$  zero matrix, respectively (subscripts are omitted when the dimension can be inferred from the context).

## 2 Distributed MPC problem for the faultless large-scale system

The aim of this section is to introduce the distributed MPC problem for the large-scale faultless system. The finite-horizon optimal control problem subject to input and output constraints within the prediction horizon is reduced to a constrained algebraic optimization problem (Marro et al., 2003; Zattoni, 2008). The large-scale system consists of the interconnection of a set  $\{\Sigma_i, i \in \mathcal{I}\}$ , with  $\mathcal{I} = \{1, 2, \dots, N\}$ , of discrete-time linear time-invariant dynamical systems described by

$$\Sigma_i \equiv \begin{cases} x_i(k+1) = \sum_{j=1}^N A_{ij} x_j(k) + B_i u_i(k), \\ y_i(k) = C_i x_i(k), \end{cases} \quad i \in \mathcal{I}, \quad (1)$$

where  $k \in \mathbb{Z}_0^+$  is the time variable,  $x_i \in \mathbb{R}^{n_i}$  is the state,  $u_i \in \mathbb{R}^{p_i}$  is the control input, and  $y_i \in \mathbb{R}^{q_i}$  is the to-be-controlled output, respectively, with  $p_i, q_i \leq n_i$  for all  $i \in \mathcal{I}$ . The matrices  $A_i, B_i$ , and  $C_i$  are assumed to have constant real entries. The following notation is introduced.  $k_p \in \mathbb{Z}^+$  denotes the prediction horizon. The initial state  $x_i(0)$  of  $\Sigma_i$  is denoted by  $\xi_i$ , with  $i \in \mathcal{I}$ , and  $\xi \in \mathbb{R}^n$ , with  $n = \sum_{i=1}^N n_i$ , is used to denote the vector of all the initial states: i.e.,  $\xi = \text{vect} \{\xi_1, \xi_2, \dots, \xi_N\}$ . For any  $\Sigma_i$ , with  $i \in \mathcal{I}$ , the symbols  $\mathbf{u}_i$  and  $\mathbf{y}_i$  respectively denote the vectors collecting the sequences of the control inputs and the corresponding outputs over the prediction time interval, for the given initial states  $\xi_i$ , with  $i \in \mathcal{I}$ : i.e.,

$$\mathbf{u}_i = \text{vect} \{u_i(0), u_i(1), \dots, u_i(k_p - 1)\}, \quad i \in \mathcal{I}, \quad (2)$$

$$\mathbf{y}_i = \text{vect} \{y_i(1), y_i(2), \dots, y_i(k_p)\}, \quad i \in \mathcal{I}. \quad (3)$$

The dynamic equations (1) are equivalent to the algebraic equations

$$\mathbf{y}_i = \sum_{j=1}^N T_{i,j} \mathbf{u}_j + V_i \xi, \quad i \in \mathcal{I}, \quad (4)$$

where  $T_{i,j} \in \mathbb{R}^{k_p q_i \times k_p p_j}$  and  $V_i \in \mathbb{R}^{k_p q_i \times n}$  are respectively defined by

$$T_{i,j} = \begin{bmatrix} \tilde{C}_i \tilde{B}_j & O & \dots & O \\ \tilde{C}_i \tilde{A} \tilde{B}_j & \tilde{C}_i \tilde{B}_j & \dots & O \\ \vdots & \vdots & \ddots & \vdots \\ \tilde{C}_i \tilde{A}^{k_p-1} \tilde{B}_j & \tilde{C}_i \tilde{A}^{k_p-2} \tilde{B}_j & \dots & \tilde{C}_i \tilde{B}_j \end{bmatrix}, \quad i, j \in \mathcal{I}, \quad (5)$$

$$V_i = \left[ (\tilde{C}_i \tilde{A})^\top, (\tilde{C}_i \tilde{A}^2)^\top, \dots, (\tilde{C}_i \tilde{A}^{k_p})^\top \right]^\top, \quad i \in \mathcal{I}, \quad (6)$$

with

$$\tilde{A} = \begin{bmatrix} A_{1,1} & \dots & A_{1,i-1} & A_{1,i} & A_{1,i+1} & \dots & A_{1,N} \\ \vdots & \ddots & \vdots & \vdots & \vdots & \ddots & \vdots \\ A_{i-1,1} & \dots & A_{i-1,i-1} & A_{i-1,i} & A_{i-1,i+1} & \dots & A_{i-1,N} \\ A_{i,1} & \dots & A_{i,i-1} & A_{i,i} & A_{i,i+1} & \dots & A_{i,N} \\ A_{i+1,1} & \dots & A_{i+1,i-1} & A_{i+1,i} & A_{i+1,i+1} & \dots & A_{i+1,N} \\ \vdots & \ddots & \vdots & \vdots & \vdots & \ddots & \vdots \\ A_{N,1} & \dots & A_{N,i-1} & A_{N,i} & A_{N,i+1} & \dots & A_{N,N} \end{bmatrix}$$

$$\tilde{B}_i = \left[ O_{p_i \times n_1}, \dots, O_{p_i \times n_{i-1}}, B_i^\top, O_{p_i \times n_{i+1}}, \dots, O_{p_i \times n_N} \right]^\top, \quad i \in \mathcal{I},$$

$$\tilde{C}_i = \left[ O_{q_i \times n_1} \dots O_{q_i \times n_{i-1}} C_i O_{q_i \times n_{i+1}} \dots O_{q_i \times n_N} \right], \quad i \in \mathcal{I}.$$

Furthermore, (4) can be written in matrix form as

$$\mathbf{y}_i = T_i^* \mathbf{u}^* + V_i \xi, \quad i \in \mathcal{I}, \quad (7)$$

where  $T_i^* \in \mathbb{R}^{k_p q_i \times k_p p}$  and  $\mathbf{u}^* \in \mathbb{R}^{k_p p}$ , with  $p = \sum_{i=1}^N p_i$ , are defined by

$$T_i^* = \left[ T_{i,1} \ T_{i,2} \ \dots \ T_{i,N} \right], \quad i \in \mathcal{I}, \quad (8)$$

$$\mathbf{u}^* = \text{vect} \{ \mathbf{u}_1, \mathbf{u}_2, \dots, \mathbf{u}_N \}, \quad (9)$$

with  $T_{i,j}$  as in (5) and  $\mathbf{u}_j$  as in (2), for  $j \in \mathcal{I}$ .

The cost functional over the prediction time is defined by

$$J = \sum_{i=1}^N \sum_{k=0}^{k_p-1} \left\{ (y_i(k+1) - \eta_i)^\top Q_i (y_i(k+1) - \eta_i) + u_i(k)^\top R_i u_i(k) \right\}, \quad (10)$$

where  $\eta_i \in \mathbb{R}^{q_i}$  is the set point for the output  $y_i$ , while  $Q_i \in \mathbb{R}^{q_i \times q_i}$  and  $R_i \in \mathbb{R}^{p_i \times p_i}$  are positive-definite symmetric matrices, with  $i \in \mathcal{I}$ . With the notation introduced in (2) and (3), (10) can be written as

$$J = \sum_{i=1}^N \left\{ (\mathbf{y}_i - \boldsymbol{\eta}_i)^\top Q_i^* (\mathbf{y}_i - \boldsymbol{\eta}_i) + \mathbf{u}_i^\top R_i^* \mathbf{u}_i \right\}, \quad (11)$$

where  $\boldsymbol{\eta}_i \in \mathbb{R}^{k_p q_i}$ ,  $Q_i^* \in \mathbb{R}^{k_p q_i \times k_p q_i}$ , and  $R_i^* \in \mathbb{R}^{k_p p_i \times k_p p_i}$ , with  $i \in \mathcal{I}$ , are respectively given by  $\boldsymbol{\eta}_i = \text{vect} \{ \eta_i, \eta_i, \dots, \eta_i \}$ ,  $Q_i^* = \text{diag} \{ Q_i, Q_i, \dots, Q_i \}$ , and  $R_i^* = \text{diag} \{ R_i, R_i, \dots, R_i \}$ . Furthermore, taking (7)–(9) into account, (11) can

be written as

$$J = \sum_{i=1}^N \left\{ (T_i^* \mathbf{u}^* + V_i \xi - \boldsymbol{\eta}_i)^\top Q_i^* (T_i^* \mathbf{u}^* + V_i \xi - \boldsymbol{\eta}_i) + \mathbf{u}^{*\top} S_i^* \mathbf{u}^* \right\}, \quad (12)$$

where  $S_i^* = \text{diag} \{ O_{k_p p_1 \times k_p p_1}, \dots, O_{k_p p_{i-1} \times k_p p_{i-1}}, R_i^*, O_{k_p p_{i+1} \times k_p p_{i+1}}, \dots, O_{k_p p_N \times k_p p_N} \} \in \mathbb{R}^{k_p p \times k_p p}$ . First, note that, by means of simple algebraic manipulations, (12) can be written as

$$J = \sum_{i=1}^N \left( \mathbf{u}^{*\top} \Psi_i \mathbf{u}^* + \varphi_i^\top \mathbf{u}^* + \rho_i \right), \quad (13)$$

where  $\Psi_i \in \mathbb{R}^{k_p p \times k_p p}$ ,  $\varphi_i \in \mathbb{R}^{k_p p}$ , and  $\rho_i \in \mathbb{R}$ , with  $i \in \mathcal{I}$ , are respectively defined as follows

$$\Psi_i = T_i^{*\top} Q_i^* T_i^* + S_i^*, \quad i \in \mathcal{I}, \quad (14)$$

$$\varphi_i = 2(V_i \xi - \boldsymbol{\eta}_i), \quad i \in \mathcal{I}, \quad (15)$$

$$\rho_i = \xi^\top V_i^\top Q_i^* V_i \xi - 2\xi^\top V_i^\top Q_i^* \boldsymbol{\eta}_i + \boldsymbol{\eta}_i^\top Q_i^* \boldsymbol{\eta}_i, \quad i \in \mathcal{I}. \quad (16)$$

Then, by collecting  $\mathbf{u}^*$  from each term in (13), one gets

$$J = \mathbf{u}^{*\top} \Psi \mathbf{u}^* + \varphi^\top \mathbf{u}^* + \rho, \quad (17)$$

where  $\Psi \in \mathbb{R}^{k_p p \times k_p p}$ ,  $\varphi \in \mathbb{R}^{k_p p}$ , and  $\rho \in \mathbb{R}$  are respectively defined by  $\Psi = \sum_{i=1}^N \Psi_i$ ,  $\varphi = \sum_{i=1}^N \varphi_i$ , and  $\rho = \sum_{i=1}^N \rho_i$ .

The control inputs and the to-be-controlled outputs are subject to constraints described by the set of inequalities

$$G_i \mathbf{u}^* + L_i \xi + \ell_i \leq 0, \quad i \in \mathcal{I}, \quad (18)$$

where  $G_i \in \mathbb{R}^{k_p(v_i+w_i) \times k_p p}$ ,  $L_i \in \mathbb{R}^{k_p(v_i+w_i) \times n}$ , and  $\ell_i \in \mathbb{R}^{k_p(v_i+w_i)}$ . Finally, the set of inequalities (18) can be recast as

$$G \mathbf{u}^* + L \xi + \ell \leq 0, \quad (19)$$

where  $G \in \mathbb{R}^{k_p z \times k_p p}$ ,  $L \in \mathbb{R}^{k_p z \times n}$ , and  $\ell \in \mathbb{R}^{k_p z}$ , with  $z = \sum_{i=1}^N (v_i + w_i)$ .

Hence, to summarize, the optimization problem over the prediction time consists in finding  $\mathbf{u}^*$  so as to minimize the cost functional  $J$ , defined by (17), under the constraint (19). Since in model predictive control the optimization is performed within a receding horizon, which implies that the stated problem is to be solved at each time step with the new initial conditions and, in addition, since the systems addressed herein are large-scale systems, which may imply the manipulation of matrices of huge dimensions, ad-hoc algorithms have been developed, like, e.g., that presented in (Scheu and Marquardt, 2011), which, in particular, will be employed in Section 4.

### 3 The distributed MPC problem for the faulty large-scale system, with actuator and setpoint reconfiguration

The aim of this section is to show how the approach to the MPC problem presented in Section 2 is modified when an actuator fault is detected in one of the interconnected systems described by (1). In fact, the detection of the fault triggers the so-called reconfiguration process: namely, faulty actuators are replaced by back-up actuators in the faulty system, the setpoints of the to-be-controlled outputs are redetermined, and a new model predictive controller is derived by solving a different optimization problem.

As was pointed out by Skogestad (2004), in industrial processes, the optimization is generally subject to constraints and, at the optimum, many of these are usually “active”. In this circumstance, if the fault is detected early after the occurrence, the perturbation caused by the fault to the constraints in non-faulty systems is not significant. In other words, the active constraints in these systems remain the same as they were in the nominal operating conditions. In light of these considerations, we will henceforth consider the unknown inputs  $\mathbf{u}^*$  introduced in Section 2 as displacements with respect to their optimal values in the nominal conditions (this can be made by suitably redefining the origin of the input space) and we will split the original problem into two sub-problems, the former of which is focused on the sole inputs of the faultless systems and takes into account only the active constraints in these systems.

Assume that the detected fault has occurred in the system  $\Sigma_i$ , for a known  $i \in \mathcal{I}$ . The fault tolerant approach developed in this work provides the reconfiguration of the control inputs and the redefinition of the output setpoints in the faulty system. As to the reconfiguration of the control inputs, it is assumed that the control input  $u_i$  consists of a set of control inputs which are manipulable when the system is faultless and a set of back-up control inputs which are redundant (hence, not used) in the absence of faults. However, when an actuator fault occurs, some of the manipulable inputs are not available anymore and, therefore, they are replaced by some of the back-up control inputs. In order to avoid notation clutter, it is assumed henceforth that the constraint equation (19) has been redefined according to the considerations above. As to the redetermination of the output setpoints, this is required whenever the original setpoints cannot be reached anymore, due to the occurrence of the fault, not even with the available redundant actuators. The redetermination of the output setpoints affects the weighting parameters  $\varphi$  and  $\rho$  of the cost functional (17). Likewise, it is assumed henceforth that the cost functional (17) has been redefined according to these arguments.

First, the control inputs collected in the vector  $\mathbf{u}^*$ , defined by (9), are reordered in such a way that the inputs of  $\Sigma_i$ , the faulty system, are placed in the last

$k_p p_i$  positions, which allows a convenient partition to be introduced in the cost functional and the constraint equations, as is shown in the following. Let the similarity transformation  $W \in \mathbb{R}^{k_p p \times k_p p}$  be defined by

$$W = \begin{bmatrix} I_{r_1} & O & O \\ O & O & I_{r_2} \\ O & I_{r_3} & O \end{bmatrix}, \quad (20)$$

with  $r_1 = k_p \sum_{j=1}^{i-1} p_j$ ,  $r_2 = k_p \sum_{j=i+1}^N p_j$ , and  $r_3 = k_p p_i$ . It is worth noting that  $W = W^{-1} = W^\top$ . Let  $\mathbf{u}^{*'}$  denote the input vector with respect to the new coordinates, so that

$$\mathbf{u}^* = W \mathbf{u}^{*'}. \quad (21)$$

Then, in light of (21), the cost functional (17) can be written as

$$J = \mathbf{u}^{*'\top} \Psi' \mathbf{u}^{*'} + \varphi'^\top \mathbf{u}^{*'} + \rho, \quad (22)$$

where  $\Psi' = W \Psi W$  and  $\varphi' = W \varphi$ . Thus, if  $\Psi$  and  $\varphi$ , partitioned according to (20), are given by

$$\Psi = \begin{bmatrix} \Psi_{11} & \Psi_{12} & \Psi_{13} \\ \Psi_{12}^\top & \Psi_{22} & \Psi_{23} \\ \Psi_{13}^\top & \Psi_{23}^\top & \Psi_{33} \end{bmatrix}, \quad \varphi = \begin{bmatrix} \varphi_1 \\ \varphi_2 \\ \varphi_3 \end{bmatrix}, \quad (23)$$

with respect to new coordinates,  $\Psi'$  and  $\varphi'$  are given by

$$\Psi' = \begin{bmatrix} \Psi_{11} & \Psi_{13} & \Psi_{12} \\ \Psi_{13}^\top & \Psi_{33} & \Psi_{23}^\top \\ \Psi_{12}^\top & \Psi_{23} & \Psi_{22} \end{bmatrix}, \quad \varphi' = \begin{bmatrix} \varphi_1 \\ \varphi_3 \\ \varphi_2 \end{bmatrix}. \quad (24)$$

With respect to the new coordinates, the last  $k_p p_i$  components of the input  $\mathbf{u}^{*'}$  concern the faulty system  $\Sigma_i$ , while the former components concern the faultless systems  $\Sigma_j$ , with  $j \in \mathcal{I}$ ,  $j \neq i$ . According to this, let

$$\mathbf{u}^{*'} = \begin{bmatrix} \mathbf{u}_h^* \\ \mathbf{u}_f^* \end{bmatrix}. \quad (25)$$

Accordingly,  $\Psi'$  and  $\varphi'$  in (24) can be written in more compact form as

$$\Psi' = \begin{bmatrix} \Psi_{hh} & \Psi_{hf} \\ \Psi_{hf}^\top & \Psi_{ff} \end{bmatrix}, \quad \varphi' = \begin{bmatrix} \varphi_h \\ \varphi_f \end{bmatrix}. \quad (26)$$

With the notation introduced in (25) and (26), the cost functional (22) can be written as

$$J = \mathbf{u}_h^{*\top} \Psi_{hh} \mathbf{u}_h^* + 2 \mathbf{u}_f^{*\top} \Psi_{hf}^\top \mathbf{u}_h^* + \mathbf{u}_f^{*\top} \Psi_{ff} \mathbf{u}_f^* + \varphi_h^\top \mathbf{u}_h^* + \varphi_f^\top \mathbf{u}_f^* + \rho. \quad (27)$$

A similar reasoning can be applied to the constraint (19). In fact, taking (21) into account, one can write (19) as

$$G' \mathbf{u}^* + L \xi + \ell \leq 0, \quad (28)$$

where  $G' = GW$  and, according to the partition (25), (28) can be written as

$$G_h \mathbf{u}_h^* + G_f \mathbf{u}_f^* + L \xi + \ell \leq 0. \quad (29)$$

Then, at first, the assumption of taking into account only active constraints in non-faulty systems is introduced, which means that (29) is replaced by

$$F_h \mathbf{u}_h^* + F_f \mathbf{u}_f^* + E \xi + d = 0, \quad (30)$$

where  $F_h$ ,  $F_f$ ,  $E$ , and  $d$  have been respectively extracted from  $G_h$ ,  $G_f$ ,  $L$ , and  $\ell$  by only considering equality constraints in the faultless systems. Moreover, the cost functional (27) is minimized with respect to the control inputs  $\mathbf{u}_h^*$  of the sole faultless systems. Namely, the first problem which is tackled is finding  $\mathbf{u}_h^*$  such that  $J$ , given by (27), is minimized under the constraint (30).

The Lagrangian function for the problem stated above is defined by

$$\mathcal{L}(\mathbf{u}_h^*, \lambda) = \mathbf{u}_h^{*\top} \Psi_{hh} \mathbf{u}_h^* + 2 \mathbf{u}_f^{*\top} \Psi_{hf}^\top \mathbf{u}_h^* + \mathbf{u}_f^{*\top} \Psi_{ff} \mathbf{u}_f^* + \varphi_h^\top \mathbf{u}_h^* + \varphi_f^\top \mathbf{u}_f^* + \rho + \lambda^\top (F_h \mathbf{u}_h^* + F_f \mathbf{u}_f^* + E \xi + d),$$

where  $\lambda$  denotes the vector of the Lagrange multipliers. Then, according to the Lagrangian multiplier approach, the solution of the following system of equations is sought:

$$\begin{cases} 2 \mathbf{u}_h^{*\top} \Psi_{hh} + 2 \mathbf{u}_f^{*\top} \Psi_{hf}^\top + \varphi_h^\top + \lambda^\top F_h = 0, \\ F_h \mathbf{u}_h^* + F_f \mathbf{u}_f^* + E \xi + d = 0. \end{cases} \quad (31)$$

Since  $\Psi_{hh}$  is symmetric positive-definite, the unknown  $\mathbf{u}_h^*$  can be made explicit from the first of (31) and replaced in the second. Thus, (31) provide

$$\begin{cases} \mathbf{u}_h^* = -\Psi_{hh}^{-1} \Psi_{hf} \mathbf{u}_f^* - \frac{1}{2} \Psi_{hh}^{-1} \varphi_h - \frac{1}{2} \Psi_{hh}^{-1} F_h^\top \lambda, \\ \lambda = 2 \Theta (F_f - F_h \Psi_{hh}^{-1} \Psi_{hf}) \mathbf{u}_f^* - \Theta F_h \Psi_{hh}^{-1} \varphi_h + 2 \Theta E \xi + 2 \Theta d, \end{cases} \quad (32)$$

where  $\Theta = (F_h \Psi_{hh} F_h^\top)^\dagger$ . Then, by replacing the second of (32) in the first, one gets the optimal value for  $\mathbf{u}_h^*$  as

$$\mathbf{u}_h^* = \Gamma \mathbf{u}_f^* + \gamma, \quad (33)$$

where

$$\Gamma = -\Psi_{hh}^{-1} \left( \Psi_{hf} + F_h^\top \Theta (F_f - F_h \Psi_{hh}^{-1} \Psi_{hf}) \right), \quad (34)$$

$$\gamma = -\Psi_{hh}^{-1} \left( -\frac{1}{2} (I + F_h^\top \Theta F_h \Psi_{hh}^{-1}) \varphi_h - F_h^\top \Theta (E \xi + d) \right). \quad (35)$$

Furthermore, by replacing (33) in (27), one gets

$$J = \mathbf{u}_f^{*\top} \Phi \mathbf{u}_f^* + 2 \sigma^\top \mathbf{u}_f^* + \kappa, \quad (36)$$

where

$$\Phi = \Gamma^\top \Psi_{hh} \Gamma + \Psi_{hf}^\top \Gamma + \Psi_{ff}, \quad (37)$$

$$\sigma = \Gamma^\top \Psi_{hh} \gamma + \Psi_{hf}^\top \gamma + \Gamma^\top \varphi_h, \quad (38)$$

$$\kappa = \gamma^\top \Psi_{hh} \gamma + \varphi_h^\top \gamma + \rho. \quad (39)$$

Moreover, by replacing (33) in (29), one gets

$$\Lambda \mathbf{u}_f^* + L \xi + \mu \leq 0, \quad (40)$$

where

$$\Lambda = G_h \Gamma + G_f, \quad (41)$$

$$\mu = G_h \gamma + \ell. \quad (42)$$

Hence, the second optimization problem consists in minimizing  $J$ , given by (36), with respect to  $\mathbf{u}_f^*$  under the constraint (40). Here the unknown variable  $\mathbf{u}_f^*$  consists of a subvector of the unknown  $\mathbf{u}^*$  of the original problem. So, a substantial reduction of the computation complexity has been obtained by the devised approach.

In order to better highlight the impact of the reduction of the computation burden achieved by the proposed approach, it is worthwhile stressing that the optimization problem considered above has to be solved for different choices of the actuator and setpoint reconfiguration, so that a set of candidate reconfigured controllers is obtained. Moreover, as is required in MPC, this algorithm has to be iterated at each step of the prediction horizon. As to the selection of the better performing reconfigured controller, this can be straightforwardly done by comparing the optimal values of the cost functionals obtained for each of the candidate reconfigured controllers.

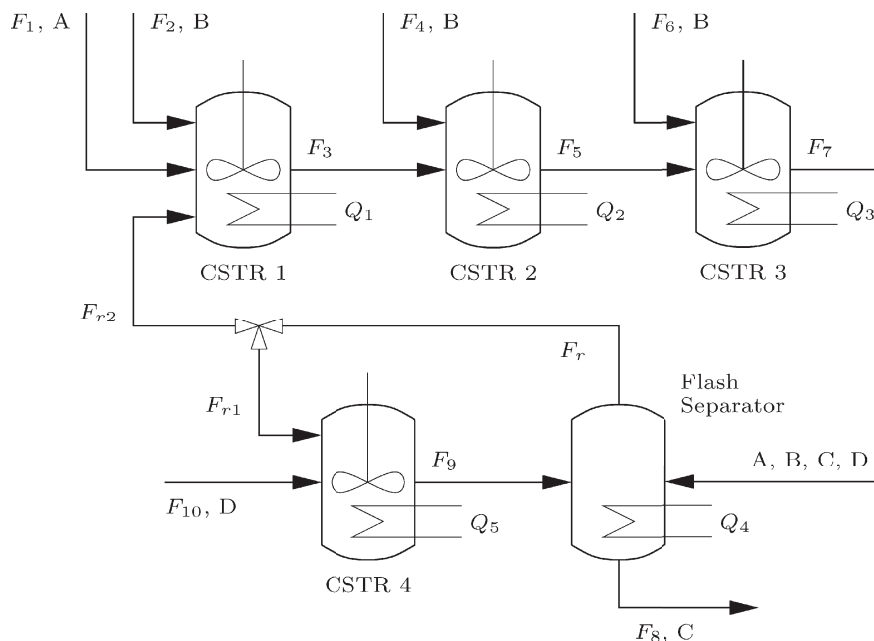


Fig. 1. Process flow diagram for alkylation of benzene (Scheu and Marquardt, 2011)

## 4 Simulation results

This section illustrates the main results obtained by testing the fault tolerant distributed model predictive control scheme devised in this work on the benzene alkylation process.

### 4.1 Process description

The alkylation of benzene is a benchmark process which has been extensively studied with DMPC (Scheu and Marquardt, 2011; Liu et al., 2010; Chilin et al., 2012a). We consider the simulated chemical process for the alkylation of benzene from (Scheu and Marquardt, 2011) — also depicted in Fig. 1 — to illustrate the performance of the proposed FTDMPC scheme. The plant consists of five units: i.e., four continuous stirred-tank reactors (CSTR) and one flash separator. The purpose of the plant is to produce ethylbenzene (C) by the reaction of the raw materials benzene (A) and ethene (B). Benzene and ethene are fed into the cascaded CSTR 1, 2, and 3, where ethylbenzene is produced. In addition, the by-product diethylbenzene (D) is produced. The stream  $F_7$  is fed into the flash separator, where unreacted benzene is separated from the product. The vapor stream is recycled; one part goes directly to CSTR 1, the other to CSTR 4. There, additional diethylbenzene (D) is fed and a transalkylation process leads to the reaction of benzene and diethylbenzene into ethylbenzene. The effluent of CSTR 4 is fed to the flash separator.

The mathematical model consists of material balances for each component and an energy balance for each unit of the plant, which results in a system model that includes a total of 25 states. The states of the process consist of the concentrations of A, B, C and D in each of the five units and the temperatures

Table 1  
Steady-State Inputs and Temperatures

$u_{1s} = -2.0 \times 10^6 J/s$	$u_{7s} = 8.697 \times 10^{-4} m^3/s$
$u_{2s} = -2.0 \times 10^6 J/s$	$T_{1s} = 472.32K$
$u_{3s} = -2.0 \times 10^6 J/s$	$T_{2s} = 472.35K$
$u_{4s} = 4.1 \times 10^6 J/s$	$T_{3s} = 472.39K$
$u_{5s} = -0.01 \times 10^6 J/s$	$T_{4s} = 472.00K$
$u_{6s} = 8.697 \times 10^{-4} m^3/s$	$T_{5s} = 472.49K$

of the units. In addition, the model includes nonlinear reaction kinetics as well as a nonlinear description of the phase equilibrium in the flash separator, leading to a total of approximately 100 equations. The state is assumed to be available continuously to the controllers. Each of the units has an external heat/coolant input. In the normal condition, the manipulated inputs to the process are the heat injected to or removed from the five units,  $Q_1$ ,  $Q_2$ ,  $Q_3$ ,  $Q_4$  and  $Q_5$  ( $u_1$ ,  $u_2$ ,  $u_3$ ,  $u_4$  and  $u_5$ , respectively). The feed stream flow rates to CSTR 2 and CSTR 3,  $F_4$  and  $F_6$ , are the back-up manipulated variables ( $u_6$  and  $u_7$ ) which are activated for the controller reconfiguration when a fault is detected. The steady-state inputs,  $u_{is}$ ,  $i = 1, \dots, 7$ , as well as the steady-state temperatures in the five units are shown in Table 1.

The nonlinear model is linearized (by a finite-difference approach) at this operating point to resulting in the following linear time-invariant model:

$$\Delta \dot{x} = A\Delta x + B\Delta u, \quad \Delta x(0) = x_0 - x_s, \quad (43)$$

where  $\Delta x = x - x_s$  and  $\Delta u = u - u_s$  indicate the deviations of state and input variables from the steady values ( $x_s$ ,  $u_s$ ), and  $x_0$  indicates the initial condition of the plant. The linearized model is used as the internal model of the controller, while the nonlinear model is used to simulate the plant.

#### 4.2 Distributed MPC strategy

In this work, the sensitivity-driven DMPC in Scheu and Marquardt (2011) is utilized as the base controller for the alkylation of benzene process. The whole system is divided into two groups, one includes CSTR 1, CSTR 2 and CSTR 3, the other contains CSTR 4 and the flash separator. Thus, the process is under the control of two distributed controllers, and information is exchanged between them. In the non-faulty situation, only inputs  $u_1$ ,  $u_2$ ,  $u_3$ ,  $u_4$  and  $u_5$  are actuated, which means the first distributed controller (DMPC 1) controls the values of  $Q_1$ ,  $Q_2$  and  $Q_3$ , and the second distributed controller (DMPC 2) controls the values of  $Q_4$  and  $Q_5$ . When the inputs  $u_6$  and  $u_7$  are actuated in the faulty situation, they are used to replace the corresponding faulty actuators.

Table 2  
Constraints of Manipulated Inputs and Temperatures

$ u_1  \leq 0.75MJ/s$	$ u_7  \leq 2 \times 10^{-3}m^3/s$
$ u_2  \leq 0.5MJ/s$	$471K \leq T_1 \leq 474K$
$ u_3  \leq 0.5MJ/s$	$471K \leq T_2 \leq 474K$
$ u_4  \leq 0.6MJ/s$	$471K \leq T_3 \leq 474K$
$ u_5  \leq 0.6MJ/s$	$471K \leq T_4 \leq 474K$
$ u_6  \leq 2 \times 10^{-3}m^3/s$	$471K \leq T_5 \leq 474K$

For each unit  $i$  of the plant, the following conventional objective function is considered:

$$\Phi_i = \frac{1}{2} \int_{t_0}^{t_f} (\Delta y_i^T Q_i \Delta y_i + \Delta u_i^T R_i \Delta u_i) dt \quad (44)$$

with  $Q_i$  and  $R_i$  are positive definite weights. The inputs  $\Delta u_i(t)$  are discretized as a piecewise constant with sampling time  $t = 10s$ . The control horizon is  $N = 5$ , and the prediction horizon is  $P = 20$ . The constraints of manipulated inputs and temperatures are shown in Table 2. In addition to the input constraints, the temperatures in the five units were also bounded to keep the process conditions close to the nominal point.

#### 4.3 Fault detection and diagnosis approach

In this work, we utilize the approach in Chilin et al. (2012a) for the fault detection and diagnosis in actuators. For each state associated with a filter, the fault detection residual can be defined as:

$$r_k(t) = |\hat{x}_k(t) - x_k(t)|,$$

where  $k = 1, \dots, 25$ .  $\hat{x}_k$  is known for all  $t$  and the state measurement  $x_k$  is also available for all  $t$ . If no fault occurs, the filter states track the system states, so  $r_k(t) = 0$  for all times. When there is a fault in the system, filter residuals affected directly by the fault will deviate from zero soon after the occurrence of the fault.

In order to avoid false alarms due to the process and sensor measurement noise, thresholds are necessary in the filters. Since the inputs  $u_1, u_2, u_3, u_4$  and  $u_5$  correspond to the temperatures  $T_1, T_2, T_3, T_4$  and  $T_5$  directly, the following thresholds in the five state filters are set:

$$r_i(t) = |\hat{T}_i(t) - T_i(t)| < 1K, \quad i = 1, \dots, 5.$$

When the difference of the filter and real state exceeds  $1K$ , the actuator corresponding to the unusual temperature value can be easily identified as faulty. After that, the fault parameter estimation approach outlined in Chilin et al. (2012a) can be applied to estimate the magnitude of faults.

#### 4.4 Testing of the performance optimization-based FTDMPC

In this part, two case studies are provided: the first one is to evaluate the candidate reconfigured actuators, and the second one is to check the newly defined operating point.

##### 4.4.1 Case study 1: evaluating candidate actuator reconfigurations

Firstly, the current operating point is checked to determine if it is feasible under the original control strategy when a fault is diagnosed. Subsequent to this the performance of the candidate actuator reconfigurations is evaluated.

We consider an actuator fault occurs at  $t = 300s$  (sample 30):  $u_2$  is blocked at 95% of its steady-state value, that is,  $u_2 = -1.9 \times 10^6 J/s$ . Obviously, the temperature in CSTR 2 will be increasing from that time if no FTC is implemented. (sample 31), the residual for  $T_2$  exceeds the threshold  $1K$ , therefore it can be concluded there is an actuator fault in  $u_2$ . At first, we want to check whether current operating point is feasible under existing control configuration. That means, DMPC 1 controls the actuators  $u_1$  and  $u_3$ , DMPC 2 controls the actuators  $u_4$  and  $u_5$ , while  $u_2$  is blocked at  $-1.9 \times 10^6 J/s$ ,  $u_6$  and  $u_7$  stay the same as steady-state values. Figure 2 shows the test result with existing actuators and current operating point. At time  $t = 310s$  (sample 31), the performance optimization algorithm is implemented to give the predictions of temperature trajectory for the future 20 steps. It shows directly that the current operating point is not feasible without changing the controller configuration, which is verified by the result under DMPC.

Since the current operating point is not feasible with existing actuators, one possible solution is to activate another actuator in order to compensate for the efficiency loss in  $u_2$ . Two back-up actuator reconfigurations are investigated. The first is to activate the feed stream flow rates to CSTR 2,  $u_6$ , and the second is to activate the feed stream flow rates to CSTR 3,  $u_7$ . In the first case, DMPC 1 controls the actuators  $u_1$ ,  $u_3$  and  $u_6$ , DMPC 2 controls the actuators  $u_4$  and  $u_5$ , while  $u_2$  is blocked at  $-1.9 \times 10^6 J/s$ ,  $u_7$  stays the same as steady-state values. In the second case, DMPC 1 controls the actuators  $u_1$ ,  $u_3$  and  $u_7$ , DMPC 2 controls the actuators  $u_4$  and  $u_5$ , while  $u_2$  is blocked at  $-1.9 \times 10^6 J/s$ ,  $u_6$  stays the same as steady-state values. Figure 3 and Figure 4 depict the test result with activating  $u_6$  and  $u_7$  under the current operating point respectively. From the trajectories under performance optimization algorithm shown in Figure 3, it is clear to see that the temperatures can be driven to setpoint after 12 steps under the effect of  $u_6$ . While the trajectories under performance optimization algorithm shown in Figure 4 demonstrates irrefutably that activating  $u_7$  does not make much difference compared with Figure 2. After the comparison, it can be decided to implement the first control reconfiguration at  $t = 310s$  (sample 31), which will result in the temperatures converging to setpoint with reconfigured controller at  $t = 430s$  (sample 43).

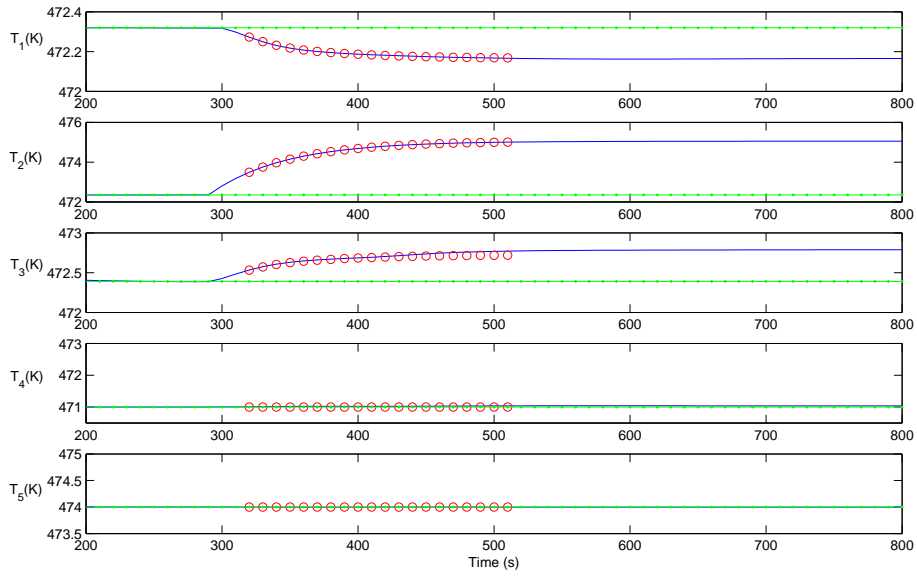


Fig. 2. Test results with existing actuators and current operating point (green dot dash line: setpoint; blue solid line: temperature variations under DMPC; red dot line: trajectories under performance optimization algorithm)

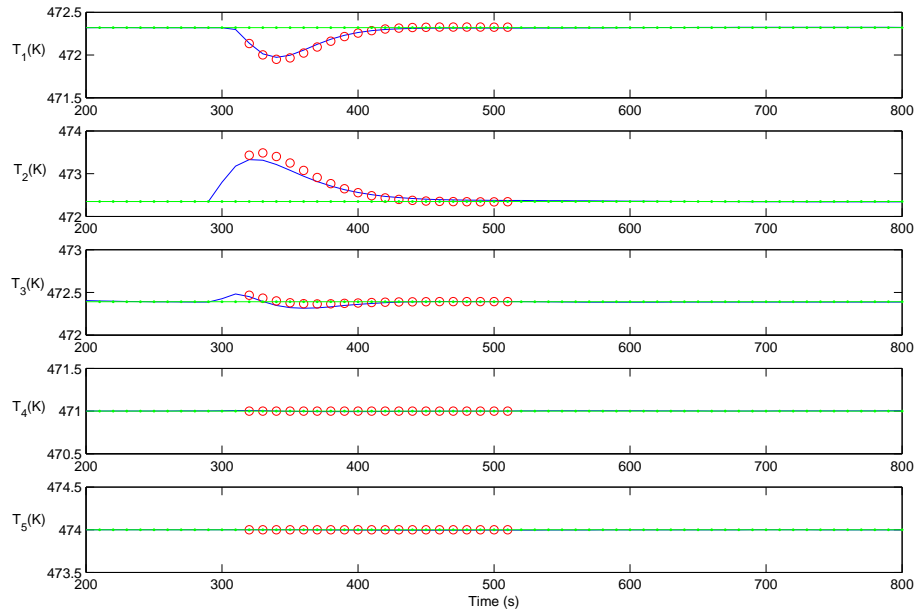


Fig. 3. Test results with activating  $u_6$  and current operating point (green dot dash line: setpoint; blue solid line: temperature variations under DMPC; red dot line: trajectories under performance optimization algorithm)

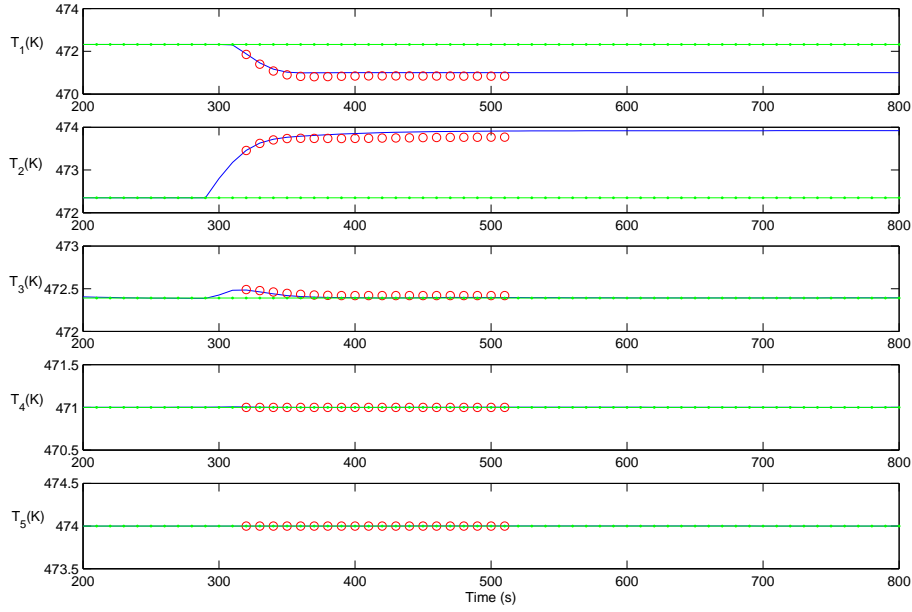


Fig. 4. Test results with activating  $u_7$  and current operating point (green dot dash line: setpoint; blue solid line: temperature variations under DMPC; red dot line: trajectories under performance optimization algorithm)

#### 4.4.2 Case study 2: checking newly defined operating point

In this part, a case study where the current operating point is not feasible with either original control strategy or any reconfigured actuators is outlined. Hence, another operating point must be designed based on the characteristics of the fault. We consider an actuator fault occurs at  $t = 300s$  (sample 30):  $u_1$  is blocked at 97.5% of its steady-state value, that is,  $u_1 = -1.95 \times 10^6 J/s$  and obviously, the temperature in CSTR 1 will be increasing from that time. At time  $t = 320s$  (sample 32), the residual exceeds the threshold  $1K$ , thus, it can be concluded that there is an actuator fault in  $u_1$ . It is clear that the fault in  $u_1$  in CSTR 1 cannot be compensated by current control strategy or activating  $u_6$  and  $u_7$  in CSTR 2 and 3. The trajectories under performance optimization algorithm for the future 20 steps at time  $t = 320s$  (sample 32) has verified our supposition as in Figure 5. Three different control configurations were utilized to carry out the test:

- the first controller uses the current control configuration, that is, DMPC 1 controls the actuators  $u_2$  and  $u_3$ , DMPC 2 controls the actuators  $u_4$  and  $u_5$ , while  $u_1$  is blocked at  $-1.95 \times 10^6 J/s$ ,  $u_6$  and  $u_7$  stay the same as the steady-state values;
- the second controller is to activate the feed stream flow rates to CSTR 2,  $u_6$ , that is, DMPC 1 controls the actuators  $u_2$ ,  $u_3$  and  $u_6$ , DMPC 2 controls the actuators  $u_4$  and  $u_5$ , while  $u_1$  is blocked at  $-1.95 \times 10^6 J/s$ ,  $u_7$  stays the

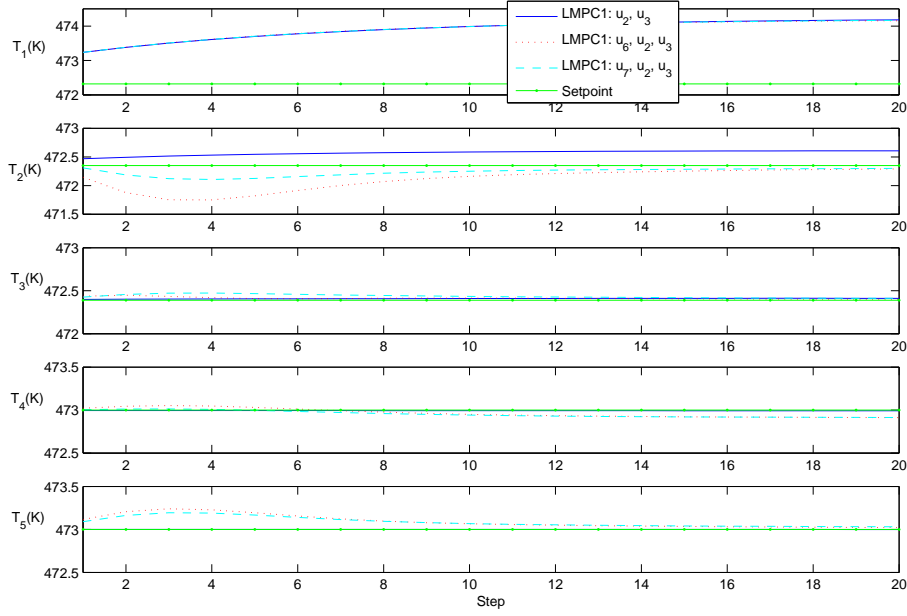


Fig. 5. The trajectories under performance optimization algorithm for the future 20 steps with current setpoint at time  $t = 320s$  (sample 32)

same as the steady-state values;

- the third controller is to activate the feed stream flow rates to CSTR 3,  $u_7$ , that is, DMPC 1 controls the actuators  $u_2$ ,  $u_3$  and  $u_7$ , DMPC 2 controls the actuators  $u_4$  and  $u_5$ , while  $u_1$  is blocked at  $-1.95 \times 10^6 J/s$ ,  $u_6$  stays the same as the steady-state values.

As can be seen from Figure 5 that all the three control configurations cannot drive the temperature in CSTR 1,  $T_1$ , to the current setpoint as it inevitably increases with the loss of efficiency in  $u_1$ . Thus, one possible solution is to increase the setpoint for  $T_1$  within the constraints detailed in Table 2. Another choice is to decrease the setpoint for the temperature in the flash separator,  $T_4$ . Since the recycled vapor stream goes from flash separator to CSTR 1, the cooling of this stream can also lead to the decreasing of  $T_1$ . The new operating point is designed as follows:  $T_{1s} = 473.36K$ ,  $T_{2s} = 472.35K$ ,  $T_{3s} = 472.39K$ ,  $T_{4s} = 471.00K$ ,  $T_{5s} = 473.00K$ . Figure 6 shows the trajectories under performance optimization algorithm for future 20 steps with newly designed setpoint at time  $t = 320s$  (sample 32). It can be clearly seen that both second and third controllers can obtain very good performance. After checking the difference between predicted trajectory and setpoint, it was found that the third controller performs slightly better than the second one and as a result,  $u_7$  is activated at time  $t = 320s$  (sample 32). The test result with activating  $u_7$  and newly designed operating point is shown in Figure 7. The temperature trajectory tracks newly designed setpoint very well and trajectories under performance optimization algorithm is close to actual temperature.

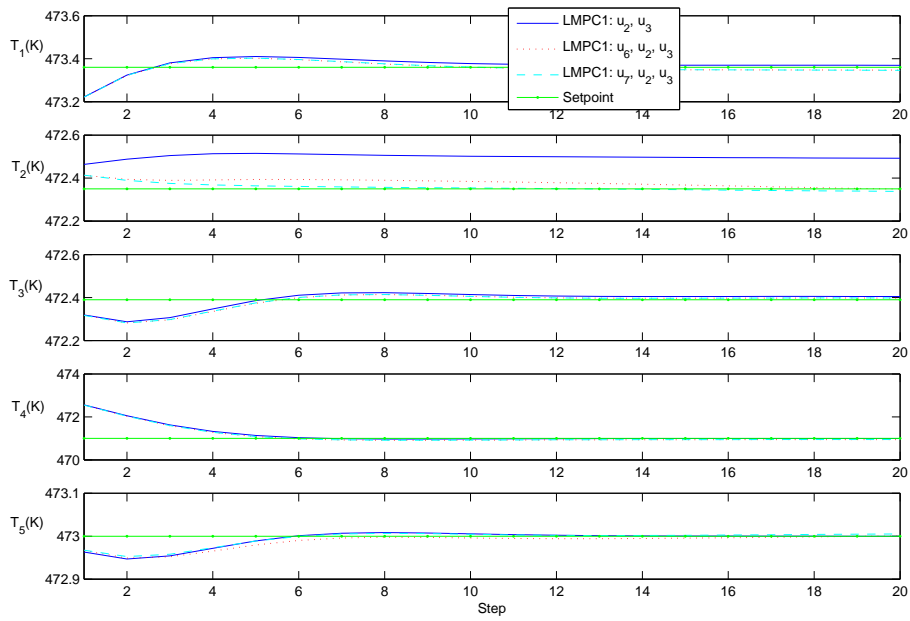


Fig. 6. The trajectories under performance optimization algorithm for the future 20 steps with newly designed setpoint at time  $t = 320s$  (sample 32)

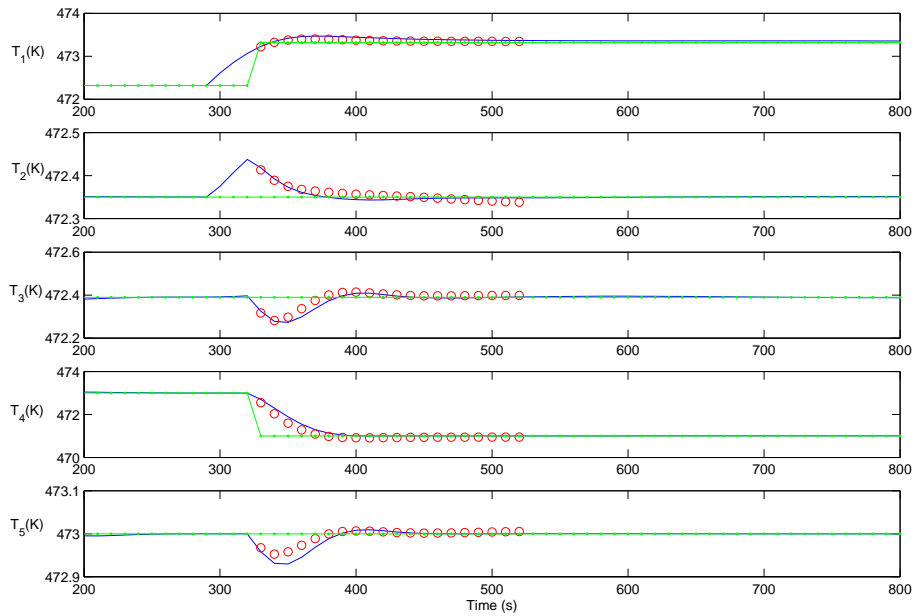


Fig. 7. Test results with activating  $u_7$  and newly designed operating point (green dot dash line: setpoint; blue solid line: temperature variations under DMPC; red dot line: trajectories under performance optimization algorithm)

## 5 Conclusions

This paper presents a performance optimization algorithm for controller reconfiguration in FTD MPC of large-scale systems. The performance optimization algorithm aims to check the ability and performance of the candidate reconfigured controllers in driving the process variables to the newly defined operating conditions. Under the assumption that the active constraints in non-faulty systems remain the same as they are at the nominal operating conditions, the global DMPC is split into two subproblems, which achieves the objective of rendering the computational burden compatible for on-line processing. The efficacy of the proposed performance optimization algorithm for controller reconfiguration has been demonstrated with two case studies on the alkylation of benzene process.

## References

- Alvarado, I., Limon, D., Muñoz de la Peña, D., Maestre, J., Ridao, M., Scheu, H., Marquardt, W., Negenborn, R., De Schutter, B., Valencia, F., Espinosa, J., 2011. A comparative analysis of distributed mpc techniques applied to the hd-mpc four-tank benchmark. *Journal of Process Control* 21 (5), 800–815.
- Blanke, M., Izadi-Zamanabadi, R., Bøgh, S., Lunau, C., 1997. Fault-tolerant control systems - a holistic view. *Control Engineering Practice* 5 (5), 693–702.
- Camponogara, E., Jia, D., Krogh, B., Talukdar, S., 2002. Distributed model predictive control. *IEEE Control Systems Magazine* 22 (1), 44–52.
- Chilin, D., Liu, J., Chen, X., Christofides, P., 2012a. Fault detection and isolation and fault tolerant control of a catalytic alkylation of benzene process. *Chemical Engineering Science* 78, 155–166.
- Chilin, D., Liu, J., Davis, J., Christofides, P., 2012b. Data-based monitoring and reconfiguration of a distributed model predictive control system. *International Journal of Robust and Nonlinear Control* 22 (1), 68–88.
- Chilin, D., Liu, J., de la Peña, D., Christofides, P., Davis, J., 2010. Detection, isolation and handling of actuator faults in distributed model predictive control systems. *Journal of Process Control* 20 (9), 1059–1075.
- Gandhi, R., Mhaskar, P., 2009. A safe-parking framework for plant-wide fault-tolerant control. *Chemical Engineering Science* 64 (13), 3060–3071.
- Gani, A., Mhaskar, P., Christofides, P., 2007. Fault-tolerant control of a polyethylene reactor. *Journal of Process Control* 17 (5), 439–451.
- Kettunen, M., Jämsä-Jounela, S.-L., 2011. Data-based, fault-tolerant model predictive control of a complex industrial dearomatization process. *Industrial and Engineering Chemistry Research* 50 (11), 6755–6768.
- Kettunen, M., Zhang, P., Jämsä-Jounela, S.-L., 2008. An embedded fault detection, isolation and accommodation system in a model predictive con-

- troller for an industrial benchmark process. *Computers and Chemical Engineering* 32 (12), 2966–2985.
- Liu, J., Chen, X., De la Peña, D., Christofides, P., 2010. Sequential and iterative architectures for distributed model predictive control of nonlinear process systems. *AIChE Journal* 56 (8), 2137–2149.
- Liu, J., De la Peña, D., Christofides, P., 2009. Distributed model predictive control of nonlinear process systems. *AIChE Journal* 55 (5), 1171–1184.
- Maciejowski, J., 1999. Modelling and predictive control: Enabling technologies for reconfiguration. *Annual Reviews in Control* 23, 13–23.
- Maestre, J., Muñoz De La Pea, D., Camacho, E., 2011. Distributed model predictive control based on a cooperative game. *Optimal Control Applications and Methods* 32 (2), 153–176.
- Mahmoud, M., Jiang, J., Zhang, Y., 2003. Active fault tolerant control systems: stochastic analysis and synthesis. Vol. 287. Springer.
- Marro, G., Prattichizzo, D., Zattoni, E., 2003. A nested computational approach to the discrete-time finite-horizon LQ control problem. *SIAM Journal on Control and Optimization* 42 (3), 1002–1012.
- Negenborn, R., De Schutter, B., Hellendoorn, J., 2008. Multi-agent model predictive control for transportation networks: Serial versus parallel schemes. *Engineering Applications of Artificial Intelligence* 21 (3), 353–366.
- Negenborn, R., Maestre, J., 2014. Distributed model predictive control: An overview and roadmap of future research opportunities. *IEEE Control Systems* 34 (4), 87–97.
- Qin, S., Badgwell, T., 2003. A survey of industrial model predictive control technology. *Control Engineering Practice* 11 (7), 733–764.
- Scattolini, R., 2009. Architectures for distributed and hierarchical model predictive control – a review. *Journal of Process Control* 19 (5), 723–731.
- Scheu, H., Marquardt, W., 2011. Sensitivity-based coordination in distributed model predictive control. *Journal of Process Control* 21 (5), 715–728.
- Skogestad, S., 2004. Control structure design for complete chemical plants. *Computers & Chemical Engineering* 28 (1), 219–234.
- Sourander, M., Vermaasvuori, M., Sauter, D., Liikala, T., Jämsä-Jounela, S.-L., 2009. Fault tolerant control for a dearomatisation process. *Journal of Process Control* 19 (7), 1091–1102.
- Zattoni, E., 2008. Structural invariant subspaces of singular Hamiltonian systems and nonrecursive solutions of finite-horizon optimal control problems. *IEEE Transactions on Automatic Control* 53 (5), 1279–1284.
- Zhang, Y., Jiang, J., 2008. Bibliographical review on reconfigurable fault-tolerant control systems. *Annual Reviews in Control* 32 (2), 229–252.
- Zheng, Y., Li, S., Li, N., 2011. Distributed model predictive control over network information exchange for large-scale systems. *Control Engineering Practice* 19 (7), 757–769.

# Modeling Vapor Compression Cycles for Dynamic Simulation of Supermarket Refrigeration Systems

S. N. Mohd. Azam<sup>a</sup>, R. Izadi-Zamanabadi<sup>b</sup>, J. B. Jørgensen<sup>a\*</sup>

<sup>a</sup> *Department of Applied Mathematics and Computer Science, Technical University of Denmark, DK-2800 Kgs Lyngby, Denmark*

<sup>b</sup> *Danfoss A/S, Electronic Controllers & Services, DK-6430 Nordborg, Denmark*

Received 22 October 2014; accepted XXXX

---

## Abstract

In this paper, we develop a numerical simulation model that can be used to simulate supermarket refrigeration systems in a smart grid with variable electricity prices. The simulation model can be used to design and evaluate control and optimization algorithms for commercial refrigeration operations. The dynamics of the vapor compression cycle is much faster than the dynamics of the cooling room in the refrigeration system. Therefore, we model the vapor compression cycle as a static system. The thermodynamic properties needed for simulation of the vapor compression cycle are computed using CoolProp. CoolProp is an open-source, cross-platform free property database that includes pure fluids, pseudo-pure fluids, and humid air-properties. CoolProp has interfaces to many languages including C, C++, Python, Modelica, Labview, Matlab, Octave, Microsoft Excel, C#, Mathcad, Java, and Javascript. We use the Matlab interface of CoolProp. The resulting static model for the vapor compression cycle in supermarket refrigeration is nonlinear and provides the cooling duty as function of the power to the compressor, the ambient temperature, and the specified operating point of the vapor compression cycle. The temperature of the food items in the cold room of the supermarket refrigeration system is modeled as a linear second order model with the cooling duty, the external heat load, and the temperature of the supermarket as the main input variables. We document and motivate the equations describing the model and illustrate their implementation in Matlab. Furthermore, we illustrate the use of the software in simulation studies.

*Keywords: Mathematical Model, Numerical Simulation, Vapor Compression Cycle, Supermarket Refrigeration, Simulation for Control and Optimization*

---

\* Corresponding author. Tel: +45-45253088; E-mail: jbj@dtu.dk

# Data Reconciliation method for improving performance and reliability of MPC control strategy for a BioGrate boiler

Palash Sarkar\*, Jukka Kortela, Alexandre Boriouchkine, Sirkka-Lisa Jämsä-Jounela

\*Aalto University, School of Chemical Technology, Process Control and Automation Research Group, P.O. Box 16100, 00076 Finland (email: [palash.sarkar@aalto.fi](mailto:palash.sarkar@aalto.fi))

---

## Extended Abstract

Environmental concerns such as global warming and the limited availability of fossil fuels have led to an increase in the demand for biomass as a renewable energy source. One promising technology, the BioGrate boiler, utilizes biomass as the raw material for power production. The BioGrate boiler was primarily designed for the combustion of biomass fuel with high moisture content. These boilers are, however, often affected by undesirable power production variations that result in economic losses. Such disturbances arise due to variations in both the moisture content of the biomass fuel and the fuel feeding system, thus complicating the operation of BioGrate boiler. Thus, elimination of power fluctuations is a prime objective of power industries and can be achieved with the introduction of an advanced control strategy such as the Model Predictive Control (MPC). Kortela *et al.* [1] developed an MPC control strategy for the BioGrate boiler which utilizes a biomass combustion model and controls combustion power by estimating the moisture content in the fuel and the thermal decomposition of dry fuel. In this control strategy, the combustion power is calculated from the measurements of oxygen content in the flue gas. The flue gas oxygen content is thus a critical process variable in the control strategy of the BioGrate boiler. Its measurements are however, frequently corrupted due to sensor faults, thus making the measurements less reliable. The reduced reliability of the corrupt measurements leads to incorrect estimations of combustion power which subsequently leads to sub-optimal control performance of the MPC. Thus, it is important to reconstruct the corrupt measurements of oxygen content before the measurements are utilized for control action.

The aim of this study is to improve the performance of the MPC control strategy developed by Kortela *et al.* [1] by introducing a data reconciliation method based on mass and energy balances of the boiler. The data reconciliation method reconstructs the corrupt measurements and improves the MPC performance through the minimization of power losses caused by the oxygen content sensor fault. The performance of the MPC with the data reconciliation algorithm was evaluated.

The results show that the inclusion of the data reconciliation method to the MPC control strategy significantly improved the performance and reliability of MPC. The performance of MPC with and without the data reconciliation method is compared in terms of total power loss in Table 1. It was found that the power loss was significantly minimized with the introduction of reconciliation

# P19

algorithm. The inclusion of data reconciliation method proved its efficiency in eliminating the effects of faults in flue gas oxygen measurements, thus improving the overall performance of the MPC.

Table 1. Comparison of the MPC control strategy performance with and without the data reconciliation algorithm.

<b>Month</b>	<b>Power Loss (MPC)</b>	<b>Power Loss (MPC + Data Reconciliation)</b>
<b>January</b>	1.1 MW	0.1 MW
<b>February</b>	43.0 MW	6.7 MW

## Reference

1. Kortela, J., Jämsä-Jounela, S.L., Model predictive control utilizing fuel and moisture soft-sensors for BioPower 5 combined heat and power (CHP) plant, Appl. Energy 131 (2014) 189-200.

# An indirect fuel moisture content estimation approach for BioGrate boilers

Alexandre Boriouchkine<sup>\*a</sup>, Miao Yu<sup>a</sup>, Sirkka-Liisa Jämsä-Jounela<sup>a</sup>

<sup>a</sup>School of Chemical Technology, Aalto University, P.O. Box 16100, 00076 Aalto, Finland  
alexandre.boriouchkine@aalto.fi

---

## Abstract

The utilization of biomass for power production is continuously increasing as the renewable fuel allows to reduce net CO<sub>2</sub> emissions. However, biomass can create challenges in energy generation due to its inhomogeneity and, most importantly, high moisture content. The mass fraction of moisture varies from 20 w% up to 70 w% largely affecting the calorific value of the fuel. Variation in the calorific value is especially problematic for small and medium sized boilers. Due to their moderate capacity, variations in the energy content of the fuel will induce large fluctuations in power production decreasing its reliability and efficiency.

This study presents a novel approach for the indirect fuel moisture content estimation for grate boilers. The approach is based on monitoring the furnace pressure measurement that is strongly affected by the vapor formed from the fuel moisture evaporation. The estimation approach utilizes negative pressure inside the furnace which under normal operation of a boiler is kept constant to avoid flue gas leakages. However, in the case of wet biomass fuel, the volume of the gases is largely dependent on the fuel moisture content. Consequently, the variation of the fuel moisture content significantly affects the furnace pressure and causes large disturbances to the pressure control loop. Thus, the moisture content can be estimated by monitoring furnace pressure measurement of a boiler. Compared with other methods measuring the fuel moisture content, the approach has three advantages. Firstly, the method does not require any new devices or expensive equipment for the measurements. Secondly, the relationship between the moisture content and the furnace pressure is relatively simple and direct, and therefore, the complex modeling and complicated derivations are not required. Finally, the estimation procedure is fast, thus it can facilitate the early compensation in the control loops. In this study the moisture estimation is based on three commonly used monitoring methods: dynamic principal component analysis, CUSUM method and a method based on probability distribution of the measurements. The results obtained indicate the feasibility of this approach and a good estimation ability of the method.

---

# Dynamic Real-Time Optimization for a Reactor, Separator and Recycle Processes

Vladimiros Minasidis, Sigurd Skogestad

*Department of Chemical Engineering,  
Norwegian University of Science and Technology (NTNU),  
Trondheim, Norway*

---

**Abstract:** A conventional approach, for devising an economically optimal, safe and stable chemical plant operation, is to hierarchically decompose into several layers all the necessary operational decisions, based on the time-scale of the horizon on which they are being considered. For example, the hourly optimal decision making is often coordinated by a Static Real-Time Optimization (SRTO) layer, attaining a clear separation between control and economic objectives, but this may impose economic performance limitations if the economic disturbances occur on a faster time scale than SRTO's and/or if there are dynamic degrees of freedom that could be utilized to improve the process economics e.g. plants with long settling times. The alternative is to use a Dynamic Real-Time Optimization based coordination. In this work, we exemplify the performance of a DRTO coordinated optimal operation of chemical process plant consisting of a reactor, a distillation column and a recycle stream. The particular process flow has been selected mainly because this type of plants often have large settling times due to mass and energy integration, thus limiting the potential of SRTO coordinated schemes. To carry out our investigation, we have implemented a dynamic optimization algorithm, that can be briefly described as follows: the dynamic optimal control problem is discretized and formulated as a Non-Linear Programming (NLP) problem based on orthogonal collocation on finite elements, then it's solved using an interior-point NLP solver IPOPT with exact 1<sup>st</sup> and 2<sup>nd</sup> order gradient information provided by an algorithmic differentiation tool CASADI. As a first step, we have tested the algorithm on a high purity distillation column, based on a dynamic nonlinear first-principle model with ideal VLE and non-linear liquid holdup hydrodynamics, and successfully identified the optimal input trajectories under a range of different economic scenarios. Next, the algorithm was modified to include the size of the finite elements, as additional decision variables for the NLP problem, in order to detect accurately the breakpoints in control profiles and increase the resolution for the parts of the state profile trajectories that largely vary, without requiring additional finite elements. This modification was successfully tested by accurately locating the optimal switching points for a batch distillation operation. Finally, moving to the main investigation of this work, where we have accurately and in timely manner determined the economically optimal input trajectories of a RSR plant for a long control horizon, subject to heavy feed flow and composition variations. In this paper, we present the results for all three case studies and reveal that the economically optimal transient responses were obtained for economic objective function formulations without enforcing any terminal constraints or terminal penalties. We discuss the advantages of flexible size finite elements, that allow the formulation of economically optimal control of RSR process with substantially long control time horizons using only a small number of finite elements, and thus offering significant computational savings. We conclude that, a careful formulation of the economic optimal control problems in combination with efficient state-of-the-art numerical algorithms, appears to be highly promising for a DRTO controlled flexible economic operation of chemical plants.

*Keywords:* Economic Plantwide Control, Dynamic Real-Time Optimization, Advanced Process Control, Reactor-Separator-Recycle Process

---

# Non-robustness and limitations of Smith Predictor Control

Chriss Grimholt and Sigurd Skogestad

## Abstract

Smith Predictor (SP) are one of the most popular solutions for dealing with processes that have long time delays. It is generally known that a properly tuned SP will give significantly better set-point response than ordinary proportional-integral-derivative controller (PID control). However, structural limitations of the SP severely limits the controllers performance for disturbance rejection for processes with large time constants. In addition, the SP is quite sensitive to modelling errors, especially with respects to time delay. For a tightly tuned SP, the controller can actually become unstable for both increasing and *decreasing* time delays. Thus, an accurate model is required with a fairly constant time delay. In contrast the PID controller only becomes unstable for increasing time delays.

With this list of drawbacks, is the increased performance sufficient justification for using SP compared to PI and PID control? To test this, we compared optimal SP with optimal PI and PID controllers for different first order plus time delay processes for specified levels of robustness ( $\max\{M_S, M_T\}$ ). Optimality (performance) was defined in terms of the integrated absolute error for combined step changes in load output and load input disturbances.

The SP and PI controller had comparable performance, while PID had clearly best performance in the robust region (Figure 1). In the low robustness region where SP performs best, the delay margin is too small to be of practical use. The low margin results from multiple crossover frequencies of the loop-function of the SP. Thus, a properly tuned PID controller will outperform the SP. Even for pure time delay processes, where the SP should clearly be the fastest controller, the performance between SP and PID is comparable.

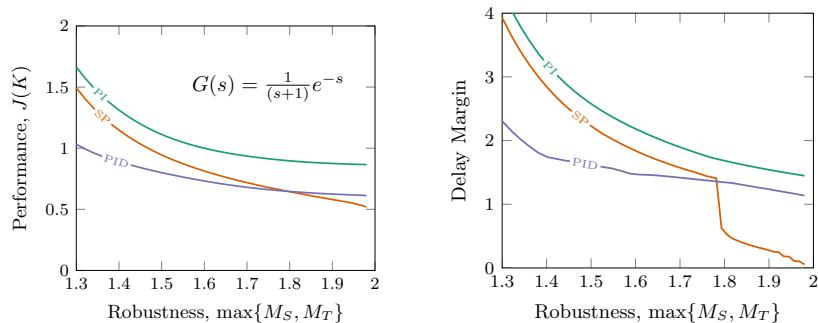


Fig. 1: Comparison of optimal trade-off between Smith predictor, PI and PID control (left) and the resulting delay margin (right).

# NOVEL STRATEGIES FOR CONTROL OF FERMENTATION PROCESSES

**Lisa Mears<sup>1</sup>, Stuart Stocks<sup>2</sup>, Gürkan Sin<sup>1</sup>, Krist V. Gernaey<sup>1</sup>, Kris Villez<sup>3</sup>**

- 1. Department of Chemical and Biochemical Engineering,  
Technical University of Denmark, Building 229, 2800 Lyngby, Denmark*
- 2. Novozymes A/S, Pilot plant, Krogshøjvej 36, 2880 Bagsværd, Denmark*
- 3. Eawag: Swiss Federal Institute of Aquatic Science and Technology,  
Dübendorf, Switzerland*

Bioprocesses are inherently sensitive to fluctuations in processing conditions and must be tightly regulated to maintain cellular productivity. Industrial fermentations are often difficult to replicate across production sites or between facilities as the small operating differences in the equipment affect the way the batches should be optimally run. In addition, batches run in the same facility can also be affected by batch variations in the growth characteristics of a specific cultivation. There is demand therefore to identify key monitoring parameters and to continually monitor the performance of a fermentation.

Industrial fermentation processes are typically operated in fed batch mode, which also poses specific challenges for process monitoring and control. This is due to many reasons including non-linear behaviour, and a relatively poor understanding of the system dynamics. It is therefore challenging for the process engineer to optimise the operation conditions, due to a lack of available process models, and complex interactions between variables which are not easy to define, especially across scales and equipment. There is however a vast amount of batch process data generated, which can be investigated with the aim of identifying desirable process operating conditions, and therefore areas of focus for optimising the process operation. This requires multivariate methods which can utilise the complex datasets which are routinely collected, containing online measured variables and offline sample data. This is interesting, since the process dynamics are governed by the combination of process variables, and cannot be fully characterised by individual variables alone.

A 30 batch dataset from a production process operating at Novozymes A/S is analysed by multivariate analysis with the aim of predicting the final product concentration, which is measured offline at the end of each batch. By creating a model for product concentration, it is possible to analyse the model results and interpret this to guide process optimisation efforts towards achieving a greater product concentration. By analysis of the variable contributions to the prediction, and the variable trends, it may be possible to develop improved control strategies for these variables.

# From Tweets to Optimality in the Smart and Sustainable Factory

Bengt Lennartson *Member, IEEE*, Kristofer Bengtsson, and Oskar Wigström

**Abstract**—Operations and sequences of operations (SOPs) are key components in the design, control and monitoring of smart production units. In this paper SOPs for multi product systems are modeled as modular Petri nets with shared variables (PNSVs), which are formally represented as predicate transition models. To update these models by online information, an event-based information system architecture, the “tweeting factory”, is proposed. Simple messages (tweets) from all kinds of equipment are stored and combined into high-level knowledge, based on formalized transformation patterns and stream-based aggregation. This knowledge add information to the modular SOPs, which are then used for performance and energy optimization. Performance and energy are related to time and continuous-time state behavior. Therefore, the predicate transition model is generalized to include continuous dynamics, resulting in a modular hybrid predicate transition model. It is finally shown how this hybrid model can be optimized based on abstractions and integrated optimization, combining results from operation research and constraint programming.

**Note to practitioners**— Operations and operation sequences are well known in the design of production and automation systems. In this paper these concepts are formalized and extended to include multi-product systems based on a new type of Petri nets. These nets include the option to represent logical conditions not only graphically but also by variables that are shared among a number of local Petri nets. The result is a more readable and understandable model. To support this operation model with online information, an event- and service-based information architecture, the “tweeting factory”, is also proposed. Simple messages (tweets) from all kinds of devices are stored and combined into high-level knowledge to be used for online monitoring, control, optimization, and reconfiguration. For optimization a hybrid model including continuous-time dynamics is also included. By this model and its approximations especially energy consumption can be optimized for complex systems such as robot cells, where individual robots need to be synchronized to avoid collisions. Integrating the tweeting factory with optimal sequences of operations results in a *smart factory*, characterized by flexibility, scalability, efficiency, reusability and sustainability in terms of minimal energy consumption. This concept has already been partly evaluated in industrial environment, and the next plan is to make complete implementations especially in vehicle companies that have contributed to the initial development of the tweeting factory concept.

**Index Terms**—event-based information, high-level knowledge, operation sequences, optimization, hybrid systems

This paper is based on a *keynote* given by the first author at CASE2014 in Taipei. The work was carried out within the Wingquist Laboratory VINN Excellence Centre within the Area of Advance - Production at Chalmers, and supported by VINNOVA and the Swedish Science Foundation. The support is gratefully acknowledged.

B. Lennartson, Kristofer Bengtsson, and Oskar Wigström are all with the Automation Research Group, Department of Signals and Systems, Chalmers University of Technology, SE-412 96 Göteborg, Sweden, e-mail: bengt.lennartson@chalmers.se

## I. INTRODUCTION

Growing demands on product quality, cost and energy reduction, and short product life cycle ask for increased flexibility and concurrent development of new products and manufacturing systems. A key issue to obtain this flexibility and concurrent development is to have a unified information flow from early product and process design to the final control and monitoring of a manufacturing plant. In [1] it was shown that operations and sequences of operations (SOPs) are common elements that interconnect product, process and control information.

*Modeling of operations and SOPs:* A formal model for self-contained operations was also introduced in [1] based on preconditions, that must be fulfilled to execute an operation, and postconditions that are guaranteed to be satisfied when an operation is completed. This model was defined by modular automata extended with shared variables, called extended finite automata (EFAs). Predicates on the current and next value of variables may then be added as additional transition conditions. Compared to automata, Petri nets (PNs) have the additional strength of graphically showing discrete part flows, more specifically flows of multiple parts where the number of parts is essential, not the individual identity. However, complicated logical conditions related to mutual exclusion, synchronization and precedence relations often result in complex graphical descriptions. Therefore, modular Petri nets with shared variables (PNSVs) were also recently introduced as a complement to EFAs, [2]. Both EFAs and PNSVs were then formally defined by predicate transition models (PTMs), a unified modeling framework for discrete event systems. In this paper it is illustrated how the shared variables in PNSVs have a potential to greatly simplify the modeling of part flows including logical constraints, compared to ordinary PNs. Furthermore, SOPs for multi product systems are shown to be naturally represented by PNSVs.

*Operation information based on tweets:* Operations and SOPs give a flexible and unified information structure. For online adaption, monitoring, optimization and reconfiguration of this information, an event- and service-based information system architecture, the “tweeting factory”, is proposed. Every device (machine, PLC, robot, operator HMI, truck, RFID-reader, measuring sensor, etc) should be able to connect to a message bus, either by itself or via a virtual device that is connected to the hardware. These devices send simple messages (tweets), or events, when they change state, for example when a product is moved, when a machine breaks down, when a button is pushed, or when a robot completes a

sequence.

All these tweets are published on the message bus. Then it is up to other devices to listen for tweet events that are interesting for them. However, these device events only include data that is hard to understand like a list of bytes, a specific identifier number, a couple of strings or a boolean value. Therefore, a number of transformation services are transforming events by adding extra information and structure to them, and publish them back to the bus. In this way, a dynamic chain of services creates knowledge about the behavior of the factory from these simple and unstructured tweets. The more devices that tweet, the better the knowledge will be. Furthermore, higher-level systems do not need to know anything about the detailed structure of the devices, the layout, timing problems, etc. This makes all parts of the architecture very loosely coupled, and therefore flexible in handling changes and updates.

The unique feature of this architecture is the bottom-up and industrially oriented approach, starting from specific industrial and knowledge enhancement needs, implementation of the architecture at several levels in the interested organizations, development, test and validation of the services directly on the shop-floor. The implementation is to a large extent based on established off-the-shelf software, and it has shown to be applicable for discrete manufacturing. An automotive company that has been involved in the development of the architecture is currently installing it in their new body-in-white plant. It has also been evaluated successfully on historical data from another automotive manufacturer.

*Optimization of hybrid systems:* Modular SOPs, including online information adaption, are the basis for performance and energy optimization. Performance and energy are related to time and continuous-time state behavior. Therefore, the predicate transition model, which is the basis for modular SOPs, is generalized to include continuous dynamics, resulting in a modular hybrid predicate transition model (HPTM). This hybrid model is then the input to the optimization problem. Performance criteria such as makespan and linear cost are preferably optimized by Constraint Programming (CP), cf. [3], compared to more classical Mixed Integer Linear Programming (MILP) solvers, [4]. Our formulation based on PNSV is also shown to have a structure that makes it extremely simple to convert to a CP model.

Energy minimization results in a Mixed Integer Nonlinear Programming (MINLP) formulation. Different ways to abstract the continuous-time part of the dynamics are proposed and illustrated. Finally, an *integrated optimization method* combining CP and NLP is proposed as a strong alternative to classical MINLP solvers. The strength of CP is its ability to detect infeasible solutions without evaluating the continuous part by the NLP solver. Especially for systems with tight final time, the number of feasible solutions are reduced, resulting in a significantly faster solution for the integrated method compared to state of the art MINLP methods.

*Summary of contributions:* The strength of using PNSVs is illustrated, both its readability compared ordinary PNs, its relation to SOPs for multiple instances of products, and its strong relation to CP models for performance optimization. An event- and service-based information architecture is proposed,

based on simple tweet messages and service transformations. A recent modular predicate transition model is generalized to modular hybrid predicate transition systems. For optimization of such systems, different abstractions of the continuous-time part are presented and an integrated CP/NLP solver is proposed for optimization of hybrid systems.

*Outline:* In Section 2 the PTM and PNSVs are briefly introduced, followed by a summary of operations and SOPs in Section 3. The tweet based information architecture is presented in Section 4, while the generalized PTM including hybrid systems is formulated in Section 5. Finally, optimization of hybrid systems presented in Section 6, followed by conclusions and future work in Section 7.

## II. MODELS FOR DISCRETE EVENT SYSTEMS

The three main issues in this paper, formal operations, an event- and service-based information architecture, and optimal operation sequences, are all related to events and discrete event systems. When a system changes from one discrete state to another, a state *transition* takes place. Such transitions are associated with *events* and are assumed to happen instantaneously.

This type of discrete event behavior is often modeled by automata, formal languages or Petri nets (PNs) [5]. Three different discrete event models for a buffer with limited capacity are presented in the following example.

*Example 1 (Limited capacity buffer):* A buffer with a given limited capacity can store a number of elements. Assume a capacity of  $n$  elements. In Fig. 1 (a) and (b) an automaton and a PN are shown for capacity  $n = 4$ , where the event  $a$  models the arrival of an element, as long as there is space in the buffer, while the event  $b$  models the removal of an element as long as there is at least one element left in the buffer. This behavior is also modeled by an EFA in Fig. 1(c) for an arbitrary capacity  $n$ . The variable  $x$  models the current number of elements in the buffer, while  $\hat{x}$  represents the value of  $x$  after the next state transition.  $\square$

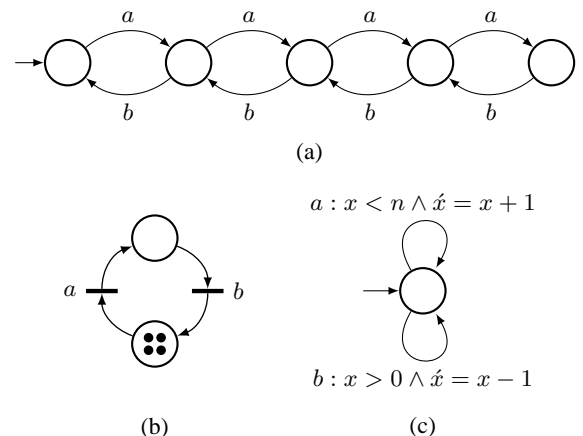


**Fig. 1** Discrete event models for a limited buffer with capacity  $n$ , (a) automaton ( $n = 4$ ), (b) PN ( $n = 4$ ), and (c) EFA.

### A. Predicate Transition Model

The EFA in Fig. 1(c) is an example of a model including predicates on variables. The PTM, which is also based on predicates on variables, is able to formally represent all three models in Example 1, as well as other extensions such as colored PNs and PNSVs. This modeling framework was recently presented in [2] as state-vector transition models. Some of the benefits of PTMs are further highlighted in this paper, and the model is generalized including mixed continuous and discrete event behavior, also known as hybrid systems.

Before a brief introduction to PTMs is given, we observe that a subset  $W$  of a set  $X$  also can be defined by the *predicate* mapping  $\mathcal{W} : X \rightarrow \mathbb{B}$  as  $\mathcal{W}(x) = 1$  iff  $x \in W$  and  $\mathcal{W}(x) = 0$  iff  $x \notin W$ .

Now, consider a universal ordered set (tuple) of discrete variables  $(x_1, \dots, x_n)$ , where the domain of definition for each variable  $x_j$  is  $X_j$ . A subset of these variables are included in a tuple  $x$ , for which the PTM model is defined.

*Definition 1 (Predicate Transition Model):* A predicate transition model  $G$  is a 6-tuple

$$G = \langle \Omega_x, X, \Sigma, T, \mathcal{X}_i, \mathcal{X}_m \rangle \quad (1)$$

where:

- (i)  $\Omega_x = \{j_1, \dots, j_n\}$  is the index set for the tuple  $x = (x_{j_1}, \dots, x_{j_n})$ .
- (ii)  $X = X_{j_1} \times \dots \times X_{j_n}$  is the domain of definition for  $x$ .
- (iii)  $\Sigma$  is a finite set of events.
- (iv)  $T$  is a finite set of transitions. Each transition is a tuple  $(\sigma, \mathcal{C})$ , where  $\sigma \in \Sigma$  and  $\mathcal{C} : X \times X \rightarrow \mathbb{B}$  is a predicate on the current value  $x$  and the next value  $\hat{x}$ .
- (v)  $\mathcal{X}_i : X \rightarrow \mathbb{B}$  is a predicate, defining possible initial values of  $x$ .
- (vi)  $\mathcal{X}_m : X \rightarrow \mathbb{B}$  is a predicate, defining desired marked values of  $x$ .  $\square$

The reason to introduce the index set  $\Omega_x$  is that variables will later be arbitrarily shared between different local models. Generally, the domain of the variables may be infinite, as for unbounded PNs, but for computational reasons a finite domain is normally assumed. The predicates are generated by boolean expressions, including conjunction  $\wedge$ , disjunction  $\vee$ , and negation  $\neg$ , while relations between variable values involve the operators  $=$ ,  $\neq$ ,  $<$ ,  $>$ ,  $\leq$ , and  $\geq$ .

A transition  $(\sigma, \mathcal{C})$  is *enabled* when the predicate  $\mathcal{C}(x, \hat{x})$  is true. When the enabled transition is executed the event  $\sigma$  occurs. Also note the condition on the next value  $\hat{x} \in X$ . In Example 1, assuming that  $X = \{0, 1, \dots, n\}$ , this means that the conditions  $\hat{x} = x + 1$  and  $\hat{x} = x - 1$  implicitly include the additional guards  $x < n$  and  $x > 0$ , respectively. These guards on the current value of  $x$  do not need to be explicitly introduced, since they are achieved by the domain of definition for  $\hat{x}$ . Thus, the set of transitions  $T$  in the PTM for the limited buffer in Example 1 is simplified to

$$T = \{(a, \hat{x} = x + 1), (b, \hat{x} = x - 1)\}$$

*Keep-current-value semantics:* When no condition on  $\hat{x}_j$  is included in  $\mathcal{C}(x, \hat{x})$ , it is assumed that  $x_j$  keeps its current value. Therefore, consider the index set

$$\Omega_{\mathcal{C}} = \{j \mid \text{condition on } \hat{x}_j \text{ in } \mathcal{C}(x, \hat{x})\}$$

Any expression involving  $\hat{x}_j$ , such as  $\hat{x}_j = x_j + 2$  or  $\hat{x}_j < 3$ , implies that  $j \in \Omega_{\mathcal{C}}$ . No condition on  $\hat{x}_j$  in  $\mathcal{C}(x, \hat{x})$  yields  $j \in \Omega_x \setminus \Omega_{\mathcal{C}}$ , and the variable  $x_j$  will be assumed to keep its current value, i.e.  $\hat{x}_j = x_j$ . Introducing the keep-current-value predicate

$$\mathcal{C}_{cv}(x, \hat{x}) \equiv \bigwedge_{j \in \Omega_x \setminus \Omega_{\mathcal{C}}} \hat{x}_j = x_j, \quad (2)$$

the *complete transition predicate* for transition  $(\sigma, \mathcal{C})$  becomes  $\Phi(x, \hat{x}) \equiv \mathcal{C}(x, \hat{x}) \wedge \mathcal{C}_{cv}(x, \hat{x})$ . This results in the following set of explicit state transition relations  $\{(x, \sigma, \hat{x}) \in X \times \Sigma \times X \mid \exists (\sigma, \mathcal{C}) \in T : \Phi(x, \hat{x})\}$ .

### B. Synchronous Composition

The synchronous composition of PTMs is defined based on Hoare's full synchronous composition [6], but extended to include shared variables.

*Definition 2 (Synchronous composition of PTMs):* Let  $G^k = \langle \Omega_x^k, X^k, \Sigma^k, T^k, \mathcal{X}_i^k, \mathcal{X}_m^k \rangle$ ,  $k = 1, 2$ , be two PTMs, including their individual tuple of variables  $x^k$ . The synchronous composition of  $G^1$  and  $G^2$  is then defined as

$$G^1 \parallel G^2 = \langle \Omega_x^1 \cup \Omega_x^2, X, \Sigma^1 \cup \Sigma^2, T, \mathcal{X}_i^1 \wedge \mathcal{X}_i^2, \mathcal{X}_m^1 \wedge \mathcal{X}_m^2 \rangle$$

where the domain of definition  $X$  and the corresponding tuple of variables  $x$  are defined based on the index set  $\Omega_x^1 \cup \Omega_x^2$ , according to Definition 1. The transition  $(\sigma, \mathcal{C}) \in T$  is defined for each combination of  $(\sigma, \mathcal{C}^k) \in T^k$ ,  $k = 1, 2$ , such that

$$\mathcal{C}(x, \hat{x}) \equiv \begin{cases} \mathcal{C}^1(x^1, \hat{x}^1) \wedge \mathcal{C}^2(x^2, \hat{x}^2), & \sigma \in \Sigma^1 \cap \Sigma^2 \\ \mathcal{C}^1(x^1, \hat{x}^1), & \sigma \in \Sigma^1 \setminus \Sigma^2 \\ \mathcal{C}^2(x^2, \hat{x}^2), & \sigma \in \Sigma^2 \setminus \Sigma^1 \end{cases} \quad (3) \quad \square$$

The reason why the keep-current-value predicate  $\mathcal{C}_{cv}$ , is not involved in the synchronization in (3), only the predicate condition  $\mathcal{C}$ , is that shared variables can be updated in different PTMs. The keep-current-value predicate is therefore a global property that can be determined first after all local models have been synchronized. Then the set  $\Omega_{\mathcal{C}}$  for the global model and the complete transition predicate  $\Phi(x, \hat{x})$  are determined.

### C. Automata and PNs with shared variables

The relation between the proposed PTM and other well known discrete event models is now briefly surveyed. Especially, the benefit of PNSVs is illustrated, see further details in [2].

*Finite automata:* An ordinary finite automaton (FA) is modeled by one variable  $x$ , taking symbolic values from a discrete set  $X = \{q_1, \dots, q_n\}$ . A transition from a state  $q_i$  to a state  $q_j$  is determined by the predicate  $\mathcal{C}_{FA}(x, \hat{x}) \equiv x = q_i \wedge \hat{x} = q_j$ .

*Extended finite automata:* An EFA is an automaton extended with a tuple of variables  $v$  with domain  $V$ , and a location variable  $\ell$ , with domain  $L = \{\ell_1, \dots, \ell_n\}$ . Hence, the total tuple of variables is  $x = (\ell, v)$ , and  $X = L \times V$ . The condition predicate  $\mathcal{C}$  is often specialized into a guard condition  $g$  on the current value of  $v$ , and an action function that updates  $v$  to a new value  $\hat{v} := a(v)$ , cf. [7]. A transition from location  $\ell_i$  to location  $\ell_j$  is then represented by the PTM predicate  $\mathcal{C}_{EFA}(x, \hat{x}) \equiv \ell = \ell_i \wedge \hat{\ell} = \ell_j \wedge g_{ij}(v) \wedge \hat{v} = a_{ij}(v)$ .

*Petri nets:* In a PTM, the marking vector  $m$  for a PN is the tuple of variables, and the transition predicate for a transition  $t$  can be formulated as

$$\mathcal{C}_{PN}(m, \hat{m}) \equiv \bigwedge_{i=1}^n \left( m_i \geq \text{Pre}(p_i, t) \right. \\ \left. \wedge \hat{m}_i = m_i + \text{Post}(p_i, t) - \text{Pre}(p_i, t) \right). \quad (4)$$

where  $\text{Pre}(p_i, t) = w$  ( $\text{Post}(p_i, t) = w$ ) means that there is an arc from place  $p_i$  (transition  $t$ ) to transition  $t$  (place  $p_i$ ) with weight  $w$ .

*Petri nets with shared variables (PNSVs):* In the same way as variables can be added to ordinary automata, resulting in EFAs, shared variables and related guards and actions can be added also to a Petri net, resulting in a PNSV. Extra variables in a tuple  $v$  then results in the total tuple of variables  $x = (m, v)$ . Additional guards and actions on the transitions in an ordinary PN are then included in a predicate  $\mathcal{C}_V$ , which results in the PNSV transition predicate  $\mathcal{C}_{PNSV}(x, \hat{x}) \equiv \mathcal{C}_{PN}(m, \hat{m}) \wedge \mathcal{C}_V(x, \hat{x})$ .

The following example illustrates how a PN can be simplified by introducing shared variables in modular PNSVs.

*Example 2 (From PN to PNSVs):* Consider the PN in Fig. 2, where two common resources  $R_1$  and  $R_2$  are shared between three straight sequences. The places and arcs between these sequences model the mutual exclusion conditions for the two resources, as well as the precedence condition  $c_1$

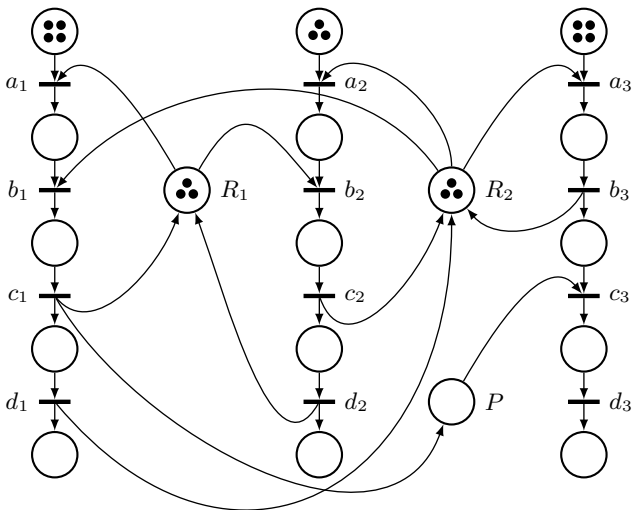


**Fig. 2** Petri net including two shared resources  $R_1$  and  $R_2$  and a precedence token place  $P$ .

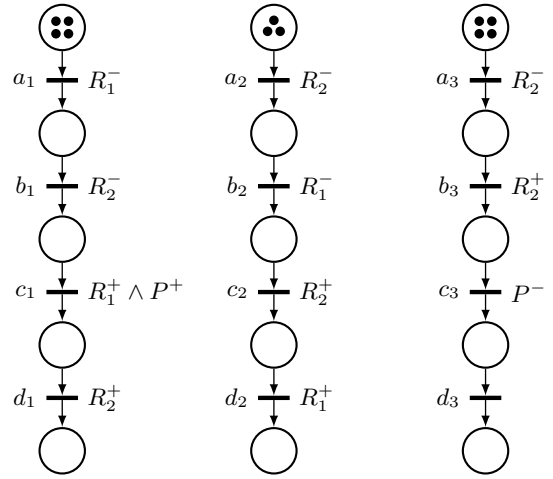


**Fig. 3** Three PNSVs with shared variables  $R_1$ ,  $R_2$  and  $P$ , increased and decreased by the short-cut condition (5).

before  $c_3$  for each individual token. In Fig. 3 three PNSVs are presented, where the two shared resource places are replaced by the shared variables  $R_1$  and  $R_2$ , and the precedence condition is modeled by the shared variable  $P$ . The domain of the variables  $R_1$  and  $R_2$  models their capacity, and with the short cut notation

$$R^\pm \equiv \dot{R} = R \pm 1 \quad (5)$$

for a variable  $R$ , the resources are booked (-) and unbooked (+) in an equivalent way in the ordinary PN in Fig. 2 and the PNSVs in Fig. 3. The precedence condition based on  $P$  has also an equivalent behavior. The PNSVs are easily expressed as three synchronized PTMs. Note that the transition conditions on the shared variables are exactly those that are given on  $R_1$ ,  $R_2$  and  $P$  in Fig. 3.  $\square$

In this example the predicates on the shared variables belong to  $\mathcal{C}_V$ . Generally,  $\mathcal{C}_V$  may include guards and actions on both the number of tokens in  $m$  and the variables in  $v$ . An example of an action on  $m$  is the reset of tokens.

A clear benefit of PNSVs is that graphical modeling can be used where it has its strength, typically showing flows of items between places in a PN. Complicated logical conditions related to mutual exclusion, synchronization, and precedence relations are preferably expressed by logical conditions. This is clear already in the simple PN models in Fig. 2 and Fig. 3, but even more obvious for larger systems. Logical conditions between places far away from each other generate complex graphical models. These models may be much harder to understand than modularized PNSVs with added explicit transition predicates, where variable names can be assigned to clearly express the meaning of for instance resource booking, as in Fig. 3.

#### D. Supervisor Guards

Since the resources  $R_1$  and  $R_2$  are booked in opposite order in the PNs in Fig. 2 and Fig. 3, a deadlock may occur. In the PNSV, this is avoided by replacing the predicate  $R_1^-$  at the event  $a_1$  with  $R_1^- \wedge (R_1 > 1 \vee (R_2 + m_2^3) > 0)$  and the predicate  $R_2^-$  at the event  $a_2$  with  $R_2^- \wedge (R_1 > 0 \vee (R_2 + m_2^3) > 1)$ . Here,

$m_2^3$  is the number of tokens in the second place after event  $a_3$  in the right PNSV in Fig. 3. This unsymmetric contribution comes from the fact that a token in this place without any restriction follows by an action  $R_2^+$  at the event  $b_3$ . These guards guarantee that the deadlock state  $R_1 + R_2 + m_2^3 = 0$  never occurs. Hence, they can be considered as supervisor guards, which guarantee a correct behavior without adding unnecessary restrictions. Thus, these supervisor guards generate a nonblocking and minimally restrictive supervisor, see [8]. Guards added to PNSVs is an attractive alternative to implement such supervisors, cf. [2].

### III. OPERATIONS AND OPERATION SEQUENCES

Operations can be used as a common notion for activities in a factory, related to both products, manufacturing processes and automation solutions. In this section EFAs and PNSVs will be used to formally represent such operations and SOPs.

#### A. Product, Process and Transportation Operations

Typical product operations are machining and assembly operations, where no specific resources to perform these operations are defined. Logical precedence relations between operations are introduced to obtain desired product functionality and quality. These product operations and resulting SOPs are determined in the product design.

To implement these operations, resources such as machines, humans and robots are required. These resources must have the right capability to be able to realize the desired product operations. Combining a product operation with a specific resource results in a process operation. Transportation operations, moving parts to and from resources and buffers, are also required. These process and transportation operations and resulting SOPs are determined in the process and manufacturing design.

Finally, SOPs must be coordinated to obtain a correct but also optimal behavior. This is determined in the automation design, and the resulting optimal SOPs are implemented by control functions such as programmable logic controllers (PLCs). The conclusion is that operations and SOPs can be used as an integrated framework from early product and process design to the final control of a production unit.

#### B. Formal Definition of Operations and SOPs

Motivated by this holistic perspective, a formal model of operations and SOPs was recently proposed [1]. This formulation is now briefly described based on PTMs, and for multi product systems extended, involving both EFAs and PNSVs.

*Definition 3 (Operation):* An operation  $O_k$  is a PTM where its tuple of variables  $x_k$  includes a location variable  $l_k$  with domain  $L_k = \{O_k^i, O_k^e, O_k^f\}$ , the event set  $\Sigma_k = \{e_k^\uparrow, e_k^\downarrow\}$ , the initial predicate  $\ell_k = O_k^i$ , and the set of transition conditions

$$T_k = \{(e_k^\uparrow, l_k = O_k^i \wedge \ell_k = O_k^e \wedge O_k^\uparrow(x_k, \hat{x}_k)), \\ (e_k^\downarrow, l_k = O_k^e \wedge \ell_k = O_k^f \wedge O_k^\downarrow(x_k, \hat{x}_k))\}. \quad \square$$

Since a PTM does not include any graphics, the user is free to use his own favorite, such as EFA or PTSV. An EFA

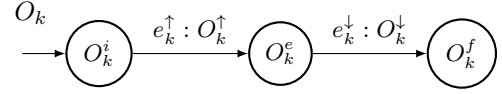


Fig. 4 EFA representing operation  $O_k$  in Definition 3.

representing the operation  $O_k$  is shown in Fig. 4. The transition for operation  $O_k$  from the initial location  $O_k^i$  to the execution location  $O_k^e$  is enabled when the *precondition*  $O_k^\uparrow$  is satisfied, after which the transition can be executed and the start event  $e_k^\uparrow$  occurs. In the same way the completion event  $e_k^\downarrow$  can only occur when the *postcondition*  $O_k^\downarrow$  is fulfilled. The pre- and postconditions include conditions on other operation locations, but also variables representing for instance resources such as  $R_1$  and  $R_2$  in Fig. 3.

*Sequences of operations:* When a number of operations are interacting, our basic assumption is that all operations are running in parallel. This is modeled by the synchronous composition. For a set of  $n$  operations  $O_1, O_2, \dots, O_n$ , where any restrictions between the individual operations are expressed by their pre- and postconditions, a SOP is defined by the composite PTM

$$SO = O_1 || O_2 || \dots || O_n \quad (6)$$

If for instance  $n = 3$  and  $O_1^\uparrow = O_2^\uparrow$  while  $O_3^\uparrow = O_1^\downarrow$  (no further pre- and postconditions), the sequence of operations  $SO$  is the straight sequence  $O_2 \rightarrow O_1 \rightarrow O_3$ .

A graphical syntax similar to the batch control standard IEC 61512-1 (ISA SP88) [9], Grafset [10], and Sequential Function Chart (SFC) [11] was proposed in [1] for this SOP. Thus, the proposed graphical syntax is easily adapted by industry. An efficient algorithm that automatically generates a graphical SOP model based on the PTM (6) is developed in [12], and implemented in the tool Sequence Planner. The following example shows a nontrivial SOP.

*Example 3 (SOP):* Consider the SOP in Fig. 5 where three sequences are given, including additional explicit preconditions. These conditions add further restrictions based on the shared variables  $R_1$ ,  $R_2$ , and  $P$ . For instance, operation  $O_{12}$  has the precondition  $O_{12}^\uparrow \equiv O_{11}^\uparrow \wedge R_2^- \equiv O_{11}^\uparrow \wedge R_2 = R_2 - 1$ . Thus,  $O_{11}$  must be finished, and it must be possible to decrease  $R_2$  one step, to be allowed to start  $O_{12}$ .

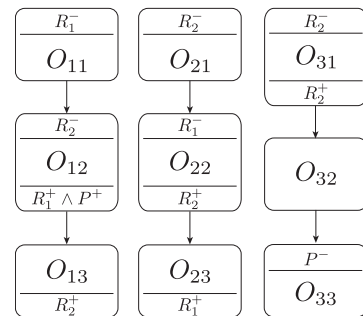


Fig. 5 SOP including preconditions on the shared variables  $R_1$ ,  $R_2$ , and  $P$ .

By joining the finished location for one operation with the initial location for another one, when they are in sequence, the sequences in Fig. 5 generate three corresponding EFAs with the shared variables mentioned above. These can also be considered as PNSVs with only one token in corresponding initial places. Now, a transition without any predicate in the resulting PNSVs, followed by a transition including a predicate, means that the same logical behavior is obtained by removing the first transition in the corresponding PNSV. Doing this, the result is the three PNSVs in Fig. 3 but with only one token in each initial place and renamed event labels. By taking the freedom to update this model with the desired number of parts (initial number of tokens in the first place of every sequence), we have obtained exactly the PTSVs in Fig. 3. This example illustrates the possibility to generate compact formal models from SOPs also for multiple part flows.  $\square$

### C. SOPs for Multiple Parts

Example 3 illustrates that the individual sequences in a SOP can be transformed to EFAs which are equivalently represented by PNSVs with only one token in each input place. If such a model represents a part flow, it is also trivial to extend this model to a multiple part flow, where still mutual exclusion between multiple resources etc are naturally involved by predicates on the transitions. This simple approach is indeed a well defined and novel way to obtain PNSVs from SOPs, which then can be used for various optimization strategies. This extension of earlier results on SOPs illustrates that PNSV is both a simple and powerful modeling concept.

## IV. FROM TWEETS TO KNOWLEDGE

Operations and SOPs give a flexible and unified information structure. For online monitoring, control, optimization, adaptation, and reconfiguration, this information needs to be updated and related to the physical devices acting in a factory. This is however often more complicated than expected. In most factories, there are a large variety of systems, machines and communication protocols. The oldest systems have probably been running for more than 30 years. The traditional integration approach is based on point-to-point communication, where data is directly read from each device. The number of connections can in a fully connected network increase quadratically with the number of devices and systems. This is known as “spaghetti integration” and makes the system rigid and hard to maintain [13].

This paper instead presents an information architecture that let each system and device publish simple tweets or events about their current status. These simple events are transformed and aggregated by multiple services, resulting in a better knowledge about the system behavior and performance. The core of the architecture is service-oriented and event-driven [14], which provides loose coupling among services and devices, as well as a flexible message structure for integration.

### A. Event Based Architecture Based on Tweets

The core components of the architecture are a message bus (currently using ApacheMQ), a simple message format (based

on JSON), and communication and service endpoints (based on Apache CAMEL and AKKA). Every device publishes simple tweets or events onto the message bus. These events are then transformed and aggregated by various services and published back to the bus. In this way, a dynamic chain of services creates knowledge about the behavior of the factory from these simple and unstructured tweet events. The more devices that tweet, the better the knowledge will be.

When something happens, for example, when a machine changes state, a simple event with information about the change can be published. A tweet event can only happen once and is defined as  $e = \langle id, t, AV \rangle$ , where  $id$  is a unique event identifier,  $t$  is a timestamp, and  $AV = \{attr_1 : value_1, \dots, attr_k : value_k\}$  is a set of ordered attribute–value pairs describing the event.

Let us consider an example based on the system represented by SOPs in Fig. 5. The system produces products using a set of resources and a set of operations. Each operation has a dedicated RFID-scanner that reads the unique id of the current product instance when the operation starts. The scanner then publishes an event including that id. When the operation finishes, the id is published again onto the bus. However, this low level data should never be used by other services. If for example some of the scanners are upgraded, the format of these events may change, requiring major changes in service logic. Therefore, multiple transformation services are used to adopt the low level events to a better structure.

### B. Transformation Services

Events can be transformed using three basic types of transformations: *Fill*, *Map* and *Fold*. *Fill* and *Map* add additional data to events and *Fold* transforms event sequences into new events. A service will implement one of these transformations, by first matching and reading events from the bus, then updating them and publish the updated events back onto the bus. A service is matching events by finding patterns in the attribute–value pairs in  $AV$ . These attribute patterns are defined as follows:

*Definition 4 (Attribute pattern):* An attribute pattern  $ap = \langle AV_{ap}, A_{ap} \rangle$  is a tuple including a set of ordered attribute–value pairs  $AV_{ap}$  and a set of attributes  $A_{ap}$ . If  $e_1 = \langle id_1, t_1, AV_1 \rangle$  such that  $AV_{ap} \subseteq AV_1$  and  $A_{ap} \subseteq A_1$ , where  $A_1$  denotes all the attributes found in  $AV_1$ , then  $e_1$  is matched by  $ap$ . This is denoted  $e_1 \leftarrow ap$ . Events matched by  $ap$  are included in  $\Sigma_{ap} = \{e \in \Sigma | e \leftarrow ap\}$ . The pattern is for simplicity denoted  $ap = \{attr_1 : v_1, \dots, attr_n : v_n, attr_k, \dots, attr_l\}$   $\square$

A transformation service transforms an event  $e \leftarrow ap$  to an event  $e' \leftarrow ap'$ . This is generally denoted  $(e' \leftarrow ap') = Service(e \leftarrow ap)$ . Thus, if  $e$  is matched by  $ap$  it will be transformed into  $e'$ , where  $ap'$  defines the additional attributes and values that will be included in the event  $e'$ . In this paper,  $ap'$  only includes new attributes that will be added to the event if not stated otherwise, i.e.  $e' \in \Sigma_{ap'} \implies e' \in \Sigma_{ap}$ . For brevity, from now the shorter notation  $ap' = Service(ap)$  will be used.

A service can also take a set of events, defined by an attribute pattern  $ap$ , and generate a single event, which is denoted  $ap' = Service(\Sigma_{ap})$ . Some services also need to listen for other events that support the transformation process, but will not trigger the publishing of a new event. These are given as a second input, i.e.  $ap' = Service(ap, ap^{others})$ .

*Fill transformations:* Fill transformations update the matched event with static data, usually fetched from a database. If applied to the same event, the result will always be the same. In the example system, the RFID events include a product id as well as the sender IP-address, i.e.  $e^{rfid} \leftarrow \{prodID, IP\}$ . A Fill service,  $ap^{fill} = FillOp(\{prodID, IP\})$ , where  $ap^{fill} = \{opType, prodType\}$ , matches RFID events and updates them with the correct operation type,  $opType$ , and product type,  $prodType$ . The operation type is related to the IP-address of RFID-scanner, and the product type is connected to the product ID read by the scanner.

*Map transformations:* Often, an event also needs information that depends on the current system state. This is added to events by map transformations. In the example system, a map service listens to events from the resources and updated events in  $\Sigma_{ap^{fill}}$ , to get which resource each product instance uses. A resource publishes an event when it is allocated to a specific product instance and re-send the same information when it is deallocated. These resource events,  $e^r \leftarrow \{prodID, res\}$  are used by the Map service,  $ap^{map} = MapResource(ap^{fill}, ap^r)$ , where  $ap^{map} = \{prodID, IP, opType, prodType, resources\}$  and  $ap^r = \{prodID, res\}$ . Which resources that are currently allocated to a specific product id is kept in memory by the service. The service will add this information to every event in  $\Sigma_{ap^{fill}}$ . Observe that the value of attribute  $resources$  is a list of resources, i.e. an operation may use multiple resources.

Fill and Map can be used to transform events in multiple steps, to simplify the implementation and to increase the flexibility. However, they do only update current events and do not aggregate multiple events into higher-level events.

*Fold transformations:* The final transformation service, Fold, can be used to bundle a set of events. It can also implement advanced event pattern identification algorithms like Complex Event Processing (CEP) [15] or other real-time languages [16]. CEP tries to formalize how patterns and knowledge are identified from a flow of low-level events, which results in high-level events [17]. These types of languages and algorithms are for example used in algorithmic trading [18].

Fold services do not update an event, but rather collect multiple events of a specific type and create a new event based on them. In the example system, a fold transformation service that creates operations based on  $\Sigma_{ap^{map}}$  events is defined as  $ap^{foldOp} = FoldOp(\Sigma_{ap^{mapID}})$ , where  $\Sigma_{ap^{mapID}} \subseteq \Sigma_{ap^{map}}$ ,  $ap^{mapID} = \{prodID : i, opType : j, prodType, resources\}$ , and  $ap^{foldOp} = \{prodID : i, opType : j, prodType, resources, start, stop\}$ . The service listens on the events in  $\Sigma_{ap^{map}}$  and merges each pair of events with the same  $prodID$  and  $opType$  and produces a new event representing one unique

operation. The first time an event matches for example  $e \leftarrow \{prodID : 123, opType : o_{11}\}$ , the start event, the service stores it and then waits for the next occurrence of  $e$ . The second time  $e$  arrives, the finish event, the service makes the new event and publishes it. Based on the two events, operation  $O_{11} \leftarrow \{prodID : 123, opType : o_{11}, prodType : A, resources : [R_1], start : 11 : 35 : 01, stop : 11 : 35 : 15\}$  can be created.

### C. Implementation

These examples of fill, map and fold transformation services are easy to implement. They do not know anything about the current layout, the resources, or the operations. When a new product type is introduced, everything will keep on working. The fold services do not know any details about the scanner, making it easy to change the scanners only by updating the fill and map transformations. The result from the transformation layer is used by other services for analysis or even more transformation steps.

The architecture does not persist the current state as most information system do. Instead only the low level events are stored in a fast journal database. This makes it possible to easily change and add services in a later stage and then replay also historical events to be updated and to make everything consistent. This is called event sourcing [19]. The events, as well as the result from other services are also stored in a search database called Elasticsearch in memory [20], which enables fast free-text search and is used for rapid visualisation and KPI calculations on higher levels.

*Industrial evaluations:* The architecture has been developed with the objective to be industrially applicable. It is to a large extent based on international standards and established off-the-shelf solutions, for example, ActiveMQ. It has been shown to be applicable for discrete manufacturing, for example in the automotive industry, where processes are running asynchronously and the product flow is non-linear. An automotive company that has been involved in the development of the architecture is currently installing it in their new body-in-white plant. It has also been evaluated on historical data from another automotive manufacturer.

The architecture is based on a set of powerful concepts. Still, this approach is not used in most industries. The architecture together with the industrial implementations has shown a great potential in using an event-driven and service oriented architecture in the automotive industry. The next step to really show the full potential of the architecture, is to implement smart services that utilizes the generated knowledge for optimization, prediction, validation and control. The optimization procedures presented below include data that preferably is generated and updated by this kind of services.

## V. HYBRID SYSTEMS

The final step in this paper is to present performance and energy optimization methods for SOPs. Performance and energy are related to time and continuous-time state behavior. Therefore, the predicate transition model in Def. 1 is now

generalized to include continuous dynamics, resulting in a modular *hybrid predicate transition model* (HPTM).

**Definition 5 (Hybrid Predicate Transition Model):** A hybrid predicate transition model  $G$  is an 8-tuple

$$G = \langle \Omega_x, X, \Sigma, T, \mathcal{X}_c, \mathcal{X}_i, \mathcal{X}_m, \mathcal{X}_{inv} \rangle \quad (7)$$

where  $\Omega_x$ ,  $X$ ,  $\Sigma$ ,  $T$ ,  $\mathcal{X}_i$ , and  $\mathcal{X}_m$  are defined in Definition 1 and

- (i)  $\mathcal{X}_c : X \times X \rightarrow \mathbb{B}$  is a predicate on the current value  $x$  and the time derivative  $\dot{x}$ .
- (ii)  $\mathcal{X}_{inv} : X \rightarrow \mathbb{B}$  is a predicate, defining desired invariants of  $x$  that must always be satisfied.  $\square$

The time derivative of a state has a meaning only if the state has a continuous domain of definition. Assume for simplicity that those states are collected in the vector  $x_c$ . Then, even a differential inclusion such as  $\dot{x}_c \geq f_1(x_c) \wedge \dot{x}_c \leq f_2(x_c)$  may determine the continuous part of the trajectory. In the same way as keep-current-value is the normal assumption for those variables that are not updated in a discrete transition, the default time derivate of a variable  $x_j$  is  $\dot{x}_j = 0$  for those variables that are not assigned any specific time derivative in  $\mathcal{X}_c$ . Since all discrete variables are only updated at the discrete transitions defined by the transition relation  $T$ , these variables are constant in-between. Thus, the time-derivate  $\dot{x}_j = 0$  can also be defined for discrete variables  $x_j$ , and we take the freedom to include all variables in the tuple  $x$  in the predicate  $\mathcal{X}_c(x, \dot{x})$

A synchronization of local HPTMs is also naturally achieved, applying the same rules for  $G^1 \parallel G^2$  as in Definition 2, adding the rules

$$\begin{aligned} \mathcal{X}_c(x, \dot{x}) &= \mathcal{X}_c^1(x^1, \dot{x}^1) \wedge \mathcal{X}_c^2(x^2, \dot{x}^2) \\ \mathcal{X}_{inv}(x) &= \mathcal{X}_{inv}^1(x^1) \wedge \mathcal{X}_{inv}^2(x^2) \end{aligned}$$

This formulation makes it easy to formulate modular representations of hybrid systems that is illustrated in the following example.

**Example 4 (Two robots with shared zone):** Consider two 1-DOF robots with identical continuous dynamics

$$\begin{bmatrix} \dot{x}_1^k \\ \dot{x}_2^k \end{bmatrix} = \begin{bmatrix} x_2^k \\ -d \cos(x_1^k) + u^k \end{bmatrix} \stackrel{\text{def}}{=} \begin{bmatrix} f_1(x_1^k, x_2^k, u^k) \\ f_2(x_1^k, x_2^k, u^k) \end{bmatrix} \quad (8)$$

where  $d$  is the distance to the center of gravity, and  $k = 1, 2$  for the two robots. Also, suppose that these robots are to move through a shared zone. The robots are in this shared zone when  $|x_1^k| \leq \pi/4$  and outside otherwise. The first robot starts out pointing upwards,  $x_1^1 = \pi/2$ , moves through the zone and ends pointing downwards,  $x_1^1 = -\pi/2$ , the second robot does the converse.

Each robot will obviously have to pass the shared zone and as such, each of the robots have two mode switches, moving into, and out of the zone. To avoid collision between the two robots, the shared zone is considered as a common resource that needs to be booked to be allowed to access the zone. This is easily represented by a shared discrete variable  $R$ , where  $R = 0$  means that the zone is booked, and  $R = 1$  the opposite, cf. (5). The hybrid system involving the two robots and the

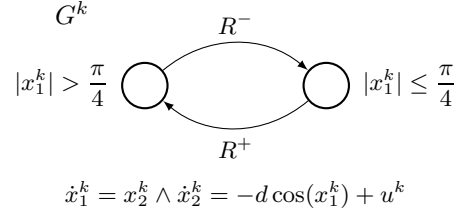


**Fig. 6** Local HPTM for a 1-DOF robot with a shared zone  $R$ , where the discrete part is represented as an EFA.

shared resource  $R$  is modeled as two local HPTMs  $G^k$ . In Fig. 6 the local  $G^k$  is graphically represented as an EFA for the discrete part, including the continuous state invariants. The common continuous-time dynamics is given by the continuous state predicate  $\dot{x}_1^k = x_2^k \wedge \dot{x}_2^k = -d \cos(x_1^k) + u^k$ . Also observe that the local tuple of variables  $x^k = (x_1^k, x_2^k, u^k, R)$ . Thus, it includes both the continuous state variables  $x_1^k$  and  $x_2^k$ , the input signal  $u^k$ , and the shared resource variable  $R$  that is common for  $G^1$  and  $G^2$ . The total hybrid system  $G = G^1 \parallel G^2$  will in the next section be optimized concerning the energy consumption by introducing suitable abstractions of the continuous-time behavior.  $\square$

Compared to the well established hybrid automaton, see [21], this HPTM is more clean, general and flexible. The logical behavior can be expressed not only by transitions between specific locations, but also by combining locations with discrete variables, in this example the shared resource  $R$ . This is the same generalization as going from automata to EFAs and from PNs to PNSVs. Also note the modular formulation, where most variables are local except for the shared variable  $R$ . The graphical representation is free to adapt, but our experience shows that focusing on the discrete part including shared discrete variables in the graphical model is often preferable. The continuous part can often be given by a common set of differential equations, where mode specific details are handled by adding local discrete variables that are updated in the discrete transitions. Note that continuous variables can also be updated at the transitions, often called state jumps. A classical example is the reset of clocks.

## VI. OPTIMIZATION OF HYBRID SYSTEMS

The objective in optimization of hybrid systems is to compute optimal or sub-optimal trajectories for the systems. In the context of hybrid systems, a trajectory can be regarded as a sequence of discrete modes, as well as a set of continuous trajectories describing the continuous dynamics for each discrete mode. The combinatorial explosion in the discrete decision space, combined with the infinite dimensional continuous trajectories in each mode makes the hybrid optimal control problem very difficult to solve [22].

There are several approaches to the problem. These fall into two categories, indirect and direct methods. The field of indirect methods include several approaches based on variations of Dynamic Programming (DP), e.g. [23], [24], [25]. While these approaches guarantee a globally optimal trajectory, they also suffer from the 'curse of dimensionality'. In this paper, direct methods are considered, where local optimality is sufficient.

In direct methods, the problem is split into two parts, searching the discrete mode sequence search space, and computing the optimal continuous trajectories for each candidate sequence. Take for example, the Hybrid Maximum Principle (HMP), in which a set of necessary conditions for optimality is posed [26], [27], [28]. For very simple cases, it may be possible to analytically derive an optimal solution, but in general, numerical methods must be used. That is, within a neighbourhood of mode trajectories a combinatorial algorithm searches for the optimal sequence, and for each mode trajectory, the optimal continuous-time state trajectories are determined using numerical methods. These numerical methods generally do not guarantee global optimality. In the case of a single hybrid system, the continuous optimization problem is a multi-phase optimal control problem, which may be solved using a multiple-shooting method [29] or collocation.

#### A. Mode sequence optimization in hybrid systems

There are several frameworks available for searching a set of discrete mode sequences. If we can derive a minimum time spent in each mode, then we can add time to our discrete problem, making it a scheduling problem. In a scheduling problem, not only do we have to make sure that the model is feasible with regard to the discrete dynamics, but we need also make sure that the discrete sequence is feasible with regards to timing constraints. Also, we could include a maximum final time constraint, which may reduce the number of feasible solutions. Adding minimum times to the sequencing problem is particularly important because it may allow the elimination of infeasible trajectories already during the mode sequence search, before a continuous problem is posed.

In the HMP papers mentioned above, a neighbourhood of sequences is defined and explicitly enumerated. Similarly, the discrete search space may be modeled using mixed integer constraints. In combination with the continuous dynamics, this results in a monolithic non-convex Mixed Integer Nonlinear Program (MINLP) [30], [22] or a Generalized Disjunctive Program [31].

In the case of synchronized modular hybrid systems, as introduced in Section V, the combinatorial explosion becomes even more of a problem. Enumerating a neighbourhood of meaningful size is simply not tractable. In the case of mixed integer programming, the bounds provided by relaxations solved at each node are not very tight. The relaxation of a mutual exclusion constraint marks the entire search space as feasible, thus, we may unnecessarily visit a large number of nodes in a branch before detecting infeasibility.

If the reason for infeasibility stems from the scheduling part of the problem, we consider the computations in such branches particularly wasteful. When multiple systems are synchronized, this may often be the case. In [32], we suggest putting more focus into the discrete mode sequence optimization, in an effort to reduce the number of sequences necessary to evaluate. Our approach is to use Constraint Programming to model the discrete parts of the decision space, and Nonlinear Programming methods for the continuous problem.

#### B. Constraint Programming

Constraint programming uses a branch and bound search, much like that of mixed integer programming. But in each node, where mixed integer programming solves a relaxed version of the problem with the hopes of finding a lower bound or proving infeasibility, constraint programming takes a slightly different approach. Instead of looking at the entire problem, each constraint is examined separately, and a local constraint specific algorithm tries to either shrink the search space, or prove infeasibility. This is called propagation, and is performed in each node until no further domain reduction is achieved or some other stopping criteria are met. Thus, each constraint may be propagated more than once in each node.

Because CP uses a localized algorithm for each constraint, it is straight forward to implement new ones, as long as one has a strategy for reducing the domain. The PNSV model in Figure 3 is directly translated to a CP model. The solution, although just an example, demonstrates the principles how this can be done for an arbitrary number of local PNSVs, communicating by discrete shared variables.

*Example 5 (CP model for PNSVs):* We will need three types of constraints to model the PNSVs in Fig. 3, precedence constraints, a maximum constraint and a cumulative constraint. Each combination of token and transition timing is instantiated as a variable. The flow of tokens may be described by precedence constraints on transition timings. These constraints also include the minimum execution time.

Introduce the following bounded set of integers  $I^n = \{1, \dots, n\}$  and  $Z^n = \{0\} \cup I^n$ . For each token  $j \in I^{m_0^k}$  in task  $k \in I^3$  and place  $i \in I^{N^k}$  the execution time is  $T^k(i)$ . Execution is assumed to occur in all places except the first and the last one. Hence, the first execution place ( $i = 1$ ) is the second place in each straight sequence in Figure 3.

Given the continuous transition times  $t^k(i, j)$  for each token  $j \in I^{m_0^k}$ , the precedence constraints are

$$t^k(i, j) + T^k(i) \leq t^k(i + 1, j), \quad \forall i \in I^{N^k - 1}$$

where we note that the total duration time in each place may be larger than the execution time. A single constraint expresses the makespan

$$T_f = \max_{k \in I^3, j \in I^{m_0^k}} t^k(N^k, j),$$

which may simply act as a bound or be the objective for minimization, depending on which is desired.

The shared variables  $R_1 \in Z^3$ ,  $R_2 \in Z^3$  and  $P \in Z^4$  generate restrictions by the use of cumulative constraints. A cumulative constraint can be regarded as a function expressing the utilization of a resource over time. A cumulative constraint is feasible if the utilization is within an allowed span for all time instances. The cumulative constraint for the  $R_1$  resource may be expressed as

$$\begin{aligned} \text{cum}(R_1) = & R_1^0 - \sum_{j=1}^{m_0^1} \text{step}(t^1(1, j), 1) + \sum_{j=1}^{m_0^1} \text{step}(t^1(3, j), 1) \\ & - \sum_{j=1}^{m_0^2} \text{step}(t^2(2, j), 1) + \sum_{j=1}^{m_0^2} \text{step}(t^2(4, j), 1) \end{aligned}$$

with initial value  $R_1^0 = 3$ . The other resources may be expressed in a similar fashion. The function  $\text{step}(t, \ell)$  denotes a step function of magnitude  $\ell$  at time  $t$  and  $\text{cum}(R)$  specifies that the expression must be within the domain of definition for variable  $R$  at all time instances. The step function can also be regarded as a resource booking interval of infinite length, see [33] for details on the cumulative constraint.  $\square$

It is clear from this example that it is very easy and natural to express PNSVs as a CP model, where the precedence relations between the tokens in each local PNSV are determined by their transition and execution times. What is more interesting is the easy way the integer variables  $R_1$ ,  $R_2$  and  $P$  are updated, representing the logical constraints of the token flow. All incremental updates of a variable say  $R$ , by expressions  $R^+$  and  $R^-$ , are in the CP model determined by the corresponding step function. This function specifies at which time the corresponding discrete variable will be updated. Then the optimization algorithm distributes the transition times such that the desired criterion is minimized satisfying the necessary constraints.

The flexibility of CP makes the discrete modeling straight forward. Dynamics such as shared events occurring multiple times in one system may be treated using alternatives. Since CP revolves around specialized constraints, many of these are available as standard functions in the different solvers.

### C. Constraint programming propagators

In the previous section we mentioned propagators. These are small algorithms designed to compute how changes to a variables domain affects other variables through constraints. The following will provide an explanation of the propagation of precedence constraints, maximum constraints, and mutual exclusion constraints. The mutual exclusion constraint can be regarded as a special case of the cumulative constraint used in the previous example, where the resource capacity is one. Furthermore, an event which allocates the resource must be paired with another event which deallocates the resource. We call these pairs intervals, as the resource is considered booked during the time span (interval) between two such events.

*Propagation of the Precedence constraint:* Consider a precedence constraint,  $t_1 + d_1 \leq t_2$ , where  $t_1$  and  $d_1$  are the start time and duration of the preceding operation, and  $t_2$  is the start time of the following operation. The duration is constant in this case. If a change occurs in the domain of  $t_1$  then  $t_2.\text{min} = t_1.\text{min} + d_1$ , and similarly, if a change occurs in  $t_2$ , then  $t_1.\text{max} = t_2.\text{max} - d_1$ .

In summary, changes to the minimum of  $t_1$  will shrink the domain of  $t_2$  from below, while changes to the maximum of  $t_2$  will shrink the domain of  $t_1$  from above.

For example, take the propagation of  $t_1 + 5 \leq t_2$ , where the two start times initially have the same domain  $t_1, t_2 \in [0..15]$ . Application of the first rule reduces  $t_2$  to  $[5..15]$ , and using the second rule we reduce  $t_1$  to  $[0..10]$ .

*Propagation of the Maximum constraint:* Consider the maximum constraint,  $x = \max_{t \in T} t$ , which expresses  $x$  being equal to the maximum element  $t \in T$ . In the case of changes to elements  $t \in T$ , the propagator for this constraint will simply

set lower bound on  $x$  to the maximum lower bound of all  $t \in T$ . Similarly the upper bound on  $x$  is the maximum upper bound on all  $t \in T$ .

*Propagation of the Mutual exclusion constraint:* The propagation of a no-overlap (mutex) constraint used in constraint programming is somewhat more intricate. First, let us define no-overlap( $s, d$ ), where  $s$  is a vector of variables representing start times and  $d$  is a vector of durations. The durations are here assumed to be constant.

In essence, the propagation constitutes a local search for infeasibility in the constraint. This local search aims to find proof of precedence relations, implied by the constraint and the current variables domains.

There are several algorithms available which try to find this type of proof. The start times and durations form intervals during which the resource is booked. One technique, *edge finding*, will for a specific interval, try to find sets of intervals which must precede or follow the specific interval.

For example, consider three starting times  $t_1, t_2, t_3$ , all with constant duration 10. Also suppose that other constraints have reduced the domain of the variables to  $t_1 \in [0..9]$ ,  $t_2 \in [0..30]$  and  $t_3 \in [0..30]$ . Obviously,  $t_1$  must come before  $t_2$  and  $t_3$ , but we need a way to prove this. Therefore, we consider  $t_1$  as the specific interval, and  $t_2$  and  $t_3$  as the set of intervals which we would like to prove occurs after  $t_1$ . By evaluating the following sequences, we find that  $t_2 \rightarrow t_3 \rightarrow t_1$  and  $t_3 \rightarrow t_2 \rightarrow t_1$  are infeasible, while  $t_1 \rightarrow t_2 \rightarrow t_3$  is feasible. Thus, we may conclude that no permutation of  $t_2$  and  $t_3$  occurring before  $t_1$  is feasible. Also, because at least one permutation is feasible if it follows  $t_1$ , we may also conclude that  $t_1$  must occur before  $t_2$  and  $t_3$ . The example might seem trivial, but at the lower branches of a larger problems, what is left may very well look like this example.

### D. The continuous problem

As previously mentioned, the evaluation of a mode sequence for one hybrid system corresponds to solving a multi stage optimal control problem, where each stage corresponds to a mode in the sequence. If there are several hybrid systems, each will have a multi stage optimal control problem. In the case of synchronization between systems, the synchronization takes the form of precedence constraints on the transition timings.

For a moment, let us consider a hierarchical view of the problem. Assume that we are given a set of mode sequences and timing conditions, the latter resulting from synchronization. The objective is at the high level to decide the optimal switching times such that a criterion is minimized. The switching times will affect the boundary conditions between each stage in the sequences. Finally, the boundary conditions will affect the trajectories inside each stage. The contribution to the minimization criterion generated by these trajectories is then propagated upwards in the hierarchy, via the boundary conditions, up to the transitions timings.

*Collocation and shooting methods:* The highest level of detail is to encode the complete hierarchy into a single NLP. Both the timing constraints and boundary conditions take the form of linear inequalities/equalities. The system dynamics are then modeled using collocation [34] or a shooting method [29].

In collocation, the continuous states and inputs are approximated as polynomials. These polynomials are differentiated and at selected points, the continuous dynamics is then enforced at these points using nonlinear equalities. Another approach is shooting methods, where the integration of the dynamics is approximated using numerical methods. It is also possible to compute the sensitivity functions for these approximations. In summary, the collocation methods result in a large sparse NLP for which the second order information is readily available. The shooting methods are much smaller in size, but it is somewhat harder to compute the second order information.

Let us take a closer look at collocation. Thus, let  $L_\ell(t)$ , ( $\ell = 0, \dots, N$ ), be a basis of Lagrange polynomials, on the interval  $[-1, 1]$  given by

$$L_\ell(t) = \prod_{\substack{i=0 \\ i \neq \ell}}^N \frac{t - t_i}{t_\ell - t_i}, \quad \ell = 0, \dots, N.$$

We see that

$$L_\ell(t_i) = \begin{cases} 1 & \text{if } \ell = i \\ 0 & \text{if } \ell \neq i \end{cases} \quad (9)$$

and the continuous state vector  $x_c(t)$  is approximated by  $X_c(t)$  as

$$x_c(t) \approx X_c(t) = \sum_{\ell=0}^N L_\ell(t)x_c(t_\ell). \quad (10)$$

Recall that the polynomial is defined on the interval  $[-1, 1]$ . As such, the interpolation points used are the boundary point,  $-1$ , and the  $N$  Gaussian quadrature points,  $t_\ell$ ,  $\ell = 1, \dots, N$ . Thus, by (9)

$$X_c(t_\ell) = x_c(t_\ell), \quad \ell = 0, \dots, N. \quad (11)$$

Differentiation of (10) yields the following expression for the approximated continuous state derivatives  $\dot{X}_c(t_i)$

$$\dot{x}_c(t_i) \approx \dot{X}_c(t_i) = \bar{D}_i x_c(-1) + \sum_{\ell=1}^N D_{i\ell} x_c(t_\ell), \quad (12)$$

where  $\bar{D}_i = \dot{L}_0(t_i)$  and  $D_{i\ell} = \dot{L}_\ell(t_i)$ . This model approximation is now applied to the optimization of the simple two robot system in Example 4.

*Example 6 (Robot trajectory optimization):* Consider the 1-DOF robots in Example 4. Recall that each robot performs a series of three stages. We will start at the lowest level with the stages. In an attempt to keep the number of indices low, we consider the equations for a single stage for one robot. Thus, the system superscript on the variables are dropped.

First we approximate the dynamics of  $x_1$  in (8) using (12) as

$$\bar{D}_i X_1(t_k) + \sum_{\ell=1}^N D_{i\ell} X_1(t_\ell) = \frac{(t_{k+1} - t_k)}{2} \dot{X}_2(t_i), \quad \forall i \in [1, \dots, N]$$

where  $t_k$  and  $t_{k+1}$  denote the initial and final time of the stage, the initial is  $X_1(t_k) = x_1(t_k)$ . However, because  $t_\ell$

is defined on  $[-1, 1]$ , we need to transform the problem onto  $[t_k, t_{k+1}]$ . Thus,  $X_p(t_\ell) = x_p(t_k + \Delta_\ell)$ ,  $p \in [1, 2]$ , where  $\Delta_\ell = (t_i + 1)(t_{k+1} - t_k)/2$ . The term  $\frac{(t_{k+1} - t_k)}{2}$  on the right hand side comes from transforming the problem from  $t \in [-1, 1]$  into  $[t_k, t_{k+1}]$ . Similarly, the dynamics of the second state  $x_2$  is

$$\begin{aligned} \bar{D}_i X_2(t_k) + \sum_{\ell=1}^N D_{i\ell} X_2(t_\ell) = \\ \frac{(t_{k+1} - t_k)}{2} (-d \cos(X_1(t_i)) + U(t_i)), \\ \forall i \in [1, \dots, N] \end{aligned}$$

where  $U(t_\ell)$  is an  $N - 1$  degree approximation of the controls collocated at the Gaussian points.

The terminal states are enforced by quadrature approximation of the dynamics as

$$\begin{aligned} X_p(t_{k+1}) = X_p(t_k) + \frac{(t_{k+1} - t_k)}{2} \\ \sum_{\ell=1}^N w_\ell f_p(X_1(t_\ell), X_2(t_\ell), U(t_\ell)), \quad p = 1, 2, \quad (13) \end{aligned}$$

where  $w_\ell$  are the Gaussian weights. It is (13) which connects the continuous states in the sequence of stages for each robot.

A contribution to the cost functions from the current stage is expressed in much the same way, using a Gaussian quadrature. In this example the energy is minimized by considering the squared control  $u^2(t)$  as a normalized measure of the power consumption.

$$c = \int_{t_k}^{t_{k+1}} u^2(\tau) d\tau \approx \frac{(t_{k+1} - t_k)}{2} \sum_{\ell=1}^N w_\ell U(t_\ell)^2.$$

Now that the lower level parts are modeled, we may move up in the hierarchy and specify the boundary constraints more closely. Recall our example, each robot shifts from one stage into another at specific positions, namely at,  $x_1 = \pi/4$  and  $x_1 = -\pi/4$ . We solve this by using linear equalities acting on the boundary points, that is  $X_1(t_k)$ .

Finally, the mutual exclusion constraint is posed such that both robots cannot be in the second stage at the same time. The transition timings are available as variables, suppose  $t_2^j$  indicates the time of transition into stage 2 and  $t_3^j$  is the time of transition into stage 3, for Robot  $j$ . Posing the mutual exclusion constraint is simply a matter of indicating that these intervals in time may not overlap. Another way to view this is

$$(t_3^1 \leq t_2^2) \vee (t_3^2 \leq t_2^1),$$

where either Robot 1 performs stage two first, or Robot 2 does so. Once we explore and fix these alternatives, the synchronization takes the form of linear inequalities.

Exploring one alternative using a fixed final time  $t_f = 2$  takes less than 0.2 [s] on a home computer using an initial guess of all zeros and a relatively high grid resolution,  $N = 15$ . The problem includes 460 variables and 375 constraints and is very sparse. The resulting sum of squared control for the two robots as a function of time is illustrated in Figure 7.

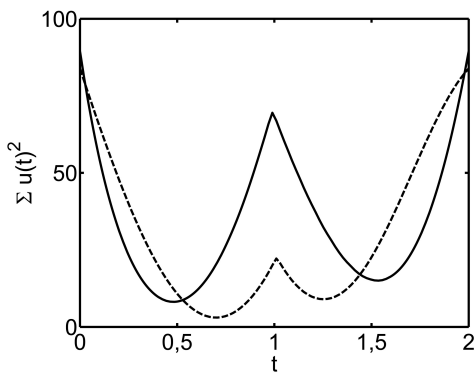


**Fig. 7** The optimal sum of squared controls as a function of time for the two robots: Robot 1 moves first through the zone (solid); Robot 2 moves first through the zone (dashed).

In this example, the total cost (normalized energy) is 12% less when Robot 2 moves up first through the zone.  $\square$

*Abstraction:* It is also possible to reduce the complexity of the continuous problem by abstraction of the continuous state space as in [35]. Consider a robot with a single stage in which it is to move from  $x_0$  to  $x_f$  in time  $t_f$ . If the robot has a large number of joints and a realistic cost function, the problem becomes non-convex and is generally difficult to solve. In a lot of robotic applications however, the path through joint space is actually fixed before hand. One such example is a joint movement, where the joints all move synchronously from  $x_0$  to  $x_f$ .

In [35], Dynamic Programming is used to solve the reduced problem when the path is given, which results in a mesh describing the optimal cost as a function of  $x_0$  and  $t_f$ , for one specific point in  $x_f$ . If the initial and final velocities are known, for example to be zero, we can enter a polynomial approximation of the optimal cost directly into our NLP. The resulting NLP now has a simple polynomial evaluation at the lowest level of the hierarchy. Because the boundary conditions are known, only the switching times with respect to the polynomial cost approximations must be decided.

The requirement on stopping between each stage in [35] may of course be too restrictive for many systems. However, it is also a possibility to solve the problem using DP for a range of  $x_f$ , yielding a mesh of the optimal cost as a function of  $x_0$ ,  $x_f$  and  $t_f$ . This allows for a sequence of modes for which the boundary conditions are parameterized by the velocity at the switching point.

### E. Integrated optimization

Since 2001, methods integrating mathematical programming with CP have been used for scheduling problems [36]. For a recent and extensive survey, see [37]. A generalized approach to integrate optimization techniques is SIMPL (Programming Language for Solving Integrated Models) [38]. In SIMPL, the problem is specified using its own modeling language, the solver then decides which CP and mathematical programming techniques should be used to solve the problem.

Most of these integrated methods are used to solve problems traditionally solved by CP or MILP. While the inclusion

---

### Algorithm 1 Integrated Algorithm

---

```

1:  $UB \leftarrow \infty$ 
2: set  $\mathcal{N} \leftarrow$  root node
3: while  $0 < |\mathcal{N}|$  do ▷ While any nodes left
4:    $n \leftarrow \mathcal{N}$  ▷ Get the next node
5:    $n \leftarrow$  Inference( $n$ ) ▷ Use CP for inference
6:   if  $n$  is feasible then
7:      $s \leftarrow$  CreateNLP( $n$ )
8:      $cost \leftarrow$  SolveNLP( $s$ ) ▷ Optimal control problem
9:     if  $cost < UB$  then
10:      if  $n$  is branch node then
11:         $\mathcal{N} \leftarrow$  Branch( $n$ )
12:      end if
13:      if  $n$  is leaf node then
14:         $UB = cost$  ▷ New best found
15:      end if
16:    end if
17:  end if
18: end while

```

---

of nonlinear programming is briefly mentioned in [38], it is not discussed in any detail. In [39], we showed how integrated methods could be successfully used for certain MINLP problems. In a MINLP solver, each node consists of solving an NLP, or possibly an LP in the convex case. Thus, the performance gained for each node that CP may reduce is much higher in a MINLP than in a MILP, where each node is always an LP.

The pseudocode Algorithm 1 describes our integrated algorithm. The algorithm begins by initializing the set of nodes yet to be explored  $\mathcal{N}$  with the root node. Next the main program loop will remove and process one node at a time. First, all constraints are propagated. This step reduces the domains of variables and may fix some of the decisions yet to be made. If the node is still feasible the corresponding optimal control problem is generated and solved. If the solution is bounded by the current upper bound we stop and continue with the next node in  $\mathcal{N}$ . Otherwise, depending on if the node is a branch or leaf node, we branch or update the upper bound respectively.

Implementation in existing constraint programming solvers is rather straight forward and utilizes the fact that user defined constraints and propagators are simple to add. Recall that in a CP algorithm, decisions are branched upon just like in a branch and bound MINLP algorithm, but instead of solving a relaxation, constraints are propagated in each node until a criterion is satisfied. By adding a specialized cost constraint, and forcing it to be propagated last, we can use existing constraint programming solvers to get the behavior described by Algorithm 1.

In [39] we evaluated the integrated approach using a job shop style problem with nonlinear costs on the durations. Benchmarks show that when the number of feasible solutions is small in a problem, for example due to a tight final time, the integrated method performs significantly faster than state of the art MINLP methods. When the final time is larger and the number of feasible solutions increase, the time to optimal solutions becomes roughly the same. The time to optimality

proof on the other hand is still much better for the integrated methods.

The good performance of the integrated approach compared to classic MINLP is mainly due to CP's ability to rule out infeasible branches at a much earlier stage. Additionally, if a branch is feasible, the propagation may still speed up the search by inferring and fixating decisions otherwise handled by branching.

In [32], we combine CP for the discrete dynamics with NLP for the synchronized multi stage optimal control problem. The continuous states are approximated by the collocation method in Section VI-D. Applied to an example where four AGVs are to move through an intersection without collisions, the integrated algorithm managed to reduce the number of NLPs by more than a factor 4. The added time of running the CP routines was less than 10% of the running time for the algorithm. Thus, an integrated CP/NLP approach is a strong candidate for solving MINLP problems that results when hybrid systems are optimized by numerical methods and nonlinear criteria.

## VII. CONCLUSIONS AND FUTURE WORK

Formal models for self-contained operations and operation sequences has in this paper been extended to include multi-product systems. The model is based on modular Petri nets with shared variables, which are formally represented as predicate transition models. To support this operation structure with online information, an event- and service-based information architecture, the "tweeting factory", is also proposed. Simple messages (tweets) from all kinds of devices are stored and combined into high-level knowledge to be used for online monitoring, control, optimization, and reconfiguration. Since optimization of performance and energy is related to a systems continuous-time behavior, a hybrid extension of the predicate transition model is also formulated. Based on this model, efficient strategies for optimization of modular hybrid systems are presented, including continuous-time abstractions and integrated constraint programming and operation research methods.

Integrating the tweeting factory with self-contained operations and optimal sequences of operations results in a *smart factory*, characterized by flexibility, scalability, efficiency, reusability and sustainability in terms of minimal energy consumption. This concept is now developed and implemented together with industry, especially for generating flexible information and knowledge systems, and energy optimization of robots cells. Future steps is to include the whole framework in a software called Sequence Planner, which can be used both stand-alone and as a plug-in together with established industrial software.

## REFERENCES

- [1] B. Lennartson, K. Bengtsson, C. Yuan, K. Andersson, M. Fabian, P. Falkman, and K. Åkesson, "Sequence planning for integrated product, process and automation design," *Automation Science and Engineering, IEEE Transactions on*, vol. 7, no. 4, pp. 791–802, Oct. 2010.
- [2] B. Lennartson, F. Basile, S. Miremadi, Z. Fei, M. N. Hosseini, M. Fabian, and K. Åkesson, "Supervisory Control for State-Vector Transition Models - A Unified Approach," *IEEE Transaction on Automation Science and Engineering*, vol. 11, no. 1, pp. 33–47, 2014.
- [3] P. Baptiste, C. L. Pape, and W. Nuijten, *Constraint-based scheduling: applying constraint programming to scheduling problems*. Springer, 2001, vol. 39.
- [4] A. S. Manne, "On the job-shop scheduling problem," *Operations Research*, vol. 8, no. 2, pp. 219–223, 1960.
- [5] C. G. Cassandras and S. LaFortune, *Introduction to Discrete Event Systems*, 2nd ed. Chapter 3, pp. 133–221, Springer, 2008.
- [6] C. A. R. Hoare, *Communicating sequential processes*, ser. Series in Computer Science. ACM, Aug. 1978, vol. 21.
- [7] M. Sköldstam, K. Åkesson, and M. Fabian, "Modeling of discrete event systems using finite automata with variables," in *46th IEEE Conference on Decision and Control*, 2007, pp. 3387–3392.
- [8] P. Ramadge and W. Wonham, "Supervisory control of a class of discrete event processes," *SIAM Journal of Control and Optimization*, vol. 25, no. 1, pp. 635–650, 1987.
- [9] IEC, *61512-1: Batch Control Part 1: Models and Terminology*. International Electrotechnical Commission, 1998.
- [10] IEC 60848 Ed. 2.0 b:2002, "Grafset specification language for sequential function charts," International Electrotechnical Commission, Tech. Rep., 2002.
- [11] IEC 61131-3:2003, "Programmable controllers—part 3: Programming languages," International Electrotechnical Commission, Tech. Rep., 2003.
- [12] K. Bengtsson, P. Bergagård, C. Thorstensson, B. Lennartson, K. Åkesson, C. Yuan, S. Miremadi, and P. Falkman, "'sequence planning using multiple and coordinated sequences of operations'," *IEEE Transactions on Automation Science and Engineering*, vol. 9, no. 2, pp. 308–319, 2012.
- [13] A. Boyd, D. Noller, P. Peters, D. Salkeld, T. Thomasma, C. Gifford, S. Pike, and A. Smith, "Soa in manufacturing guidebook," *MESA International, IBM Corporation and Capgemini Co-Branded White Paper*, 2008.
- [14] B. M. Michelson, "Event-driven architecture overview," *Patricia Seybold Group*, vol. 2, 2006.
- [15] D. Luckham, *The Power of Events: An Introduction to Complex Event Processing in Distributed Enterprise Systems*. Addison-Wesley Professional, 2002.
- [16] J. Perez, J. Jimenez, A. Rabanal, A. Astarloa, and J. Lazaro, "FTL-CFree: A fuzzy real-time language for runtime verification," *Industrial Informatics, IEEE Transactions on*, 2014.
- [17] G. Cugola and A. Margara, "Processing flows of information: From data stream to complex event processing," *ACM Comput. Surv.*, vol. 44, no. 3, pp. 15:1–15:62, 2012.
- [18] D. Luckham, *The power of events*. Addison-Wesley Reading, 2002, vol. 204.
- [19] R. Kuhn and J. Allen, *Reactive Design Patterns*, MEAP 2 ed. Manning Publications, 2014.
- [20] R. Kuc and M. Rogozinski, *Elasticsearch Server*. Packt Publishing Ltd, 2013.
- [21] R. Alur, C. Courcoubetis, T. Henzinger, and P. Ho, "Hybrid automata: An algorithmic approach to the specification and verification of hybrid systems," in *Lecture Notes in Computer Science*. Springer Berlin / Heidelberg, 1993, vol. 736, pp. 209–229.
- [22] P. I. Barton and C. K. Lee, "Modeling, simulation, sensitivity analysis, and optimization of hybrid systems," *ACM Transactions on Modeling and Computer Simulation (TOMACS)*, vol. 12, no. 4, pp. 256–289, 2002.
- [23] M. Branicky, V. Borkar, and S. Mitter, "A unified framework for hybrid control: model and optimal control theory," *Automatic Control, IEEE Transactions on*, vol. 43, no. 1, pp. 31–45, Jan 1998.
- [24] S. Hedlund and A. Rantzer, "Optimal control of hybrid systems," in *Decision and Control, 1999. Proceedings of the 38th IEEE Conference on*, vol. 4. IEEE, 1999, pp. 3972–3977.
- [25] —, "Convex dynamic programming for hybrid systems," *Automatic Control, IEEE Transactions on*, vol. 47, no. 9, pp. 1536–1540, 2002.
- [26] H. J. Sussmann, "A maximum principle for hybrid optimal control problems," in *Decision and Control, 1999. Proceedings of the 38th IEEE Conference on*, vol. 1. Ieee, 1999, pp. 425–430.
- [27] B. Passenberg, P. Caines, M. Sobotka, O. Stursberg, and M. Buss, "The minimum principle for hybrid systems with partitioned state space and unspecified discrete state sequence," in *Decision and Control (CDC), 2010 49th IEEE Conference on*, Dec 2010, pp. 6666–6673.
- [28] M. Shahid Shaikh and P. Caines, "On the hybrid optimal control problem: Theory and algorithms," *Automatic Control, IEEE Transactions on*, vol. 52, no. 9, pp. 1587–1603, Sept 2007.
- [29] P. Riedinger, J. Daafouz, and C. Iung, "About solving hybrid optimal control problems," *IMACS05*, 2005.

- [30] M. Avraam, N. Shah, and C. Pantelides, "Modelling and optimisation of general hybrid systems in the continuous time domain," *Computers & chemical engineering*, vol. 22, pp. S221–S228, 1998.
- [31] J. Oldenburg and W. Marquardt, "Disjunctive modeling for optimal control of hybrid systems," *Computers and Chemical Engineering*, vol. 32, no. 10, pp. 2346 – 2364, 2008.
- [32] O. Wigström and B. Lennartson, "An integrated CP/OR method for optimal control of modular hybrid systems," in *12th IFAC - IEEE International Workshop on Discrete Event Systems*, 2014.
- [33] A. Aggoun and N. Beldiceanu, "Extending chip in order to solve complex scheduling and placement problems," *Mathematical and Computer Modelling*, vol. 17, no. 7, pp. 57–73, 1993.
- [34] D. Benson, "A gauss pseudospectral transcription for optimal control," Ph.D. dissertation, Massachusetts Institute of Technology, 2005.
- [35] O. Wigström, B. Lennartson, A. Vergnano, and C. Breitholtz, "High level scheduling of energy optimal trajectories," *IEEE Transactions on Automation Science and Engineering*, 2013.
- [36] V. Jain and I. E. Grossmann, "Algorithms for hybrid milp/cp models for a class of optimization problems," *INFORMS J. on Computing*, vol. 13, no. 4, pp. 258–276, Sep. 2001.
- [37] M. Lombardi and M. Milano, "Optimal methods for resource allocation and scheduling: a cross-disciplinary survey," *Constraints*, vol. 17, pp. 51–85, 2012.
- [38] I. D. Aron, J. N. Hooker, and T. H. Yunes, "Simpl: A system for integrating optimization techniques," in *Integration of AI and OR Techniques in Constraint Programming for Combinatorial Optimization Problems, First International Conference, CPAIOR 2004, Nice, France, April 20-22, 2004, Proceedings*, ser. Lecture Notes in Computer Science, J.-C. RÅ©gin and M. Rueher, Eds., vol. 3011. Springer, 2004, pp. 21–36.
- [39] O. Wigstrom and B. Lennartson, "Integrated or/cp optimization for discrete event systems with nonlinear cost," in *Decision and Control (CDC), 2013 IEEE 52nd Annual Conference on*, Dec 2013, pp. 7627–7633.

# Optimal Controller Design for Balancing Input/Output Disturbance Rejection Response with Robust Stability Condition

Sun Bo

*Department of Chemical Engineering,  
Norwegian University of Science and Technology (NTNU),  
Trondheim, Norway*

---

*Abstract:* The paper is concerned with the problem of the optimal controller design for balancing input/output disturbance responses. For a given linear time-invariant plant with time delay, our attention is focused on the optimal control strategy in terms of the synthesis performance criterion which takes into account both input load disturbance rejection performance and output load disturbance rejection performance. Firstly, the synthesis input/output disturbance performance criterion is given. The weights of both the input disturbance and the output disturbance on the system can be tuned by an adjustable parameter. Then, by combining the optimal control theory with the inner-outer factorization method, we present the optimal controller for the proposed criterion. Specially, for a class of first order processes widely adopted in industry, the paper introduces the analytical inner-outer factorization solution. Finally, the analysis and simulations are given to illustrate the superiority of the method. For the plants with slow dynamics, the tuning formula based on the proposed method is provided to effectively cope with the inevitable trade-off brought by the existence of the dominant poles. The results show that the proposed controller effectively improves the system performance.

---